ÖAW
Österreichische Akademie
der Wissenschaften

IBN
INSTITUTE OF BIOPHYSICS AND
NANOSYSTEMS RESEARCH

ANNUAL REPORT
2006

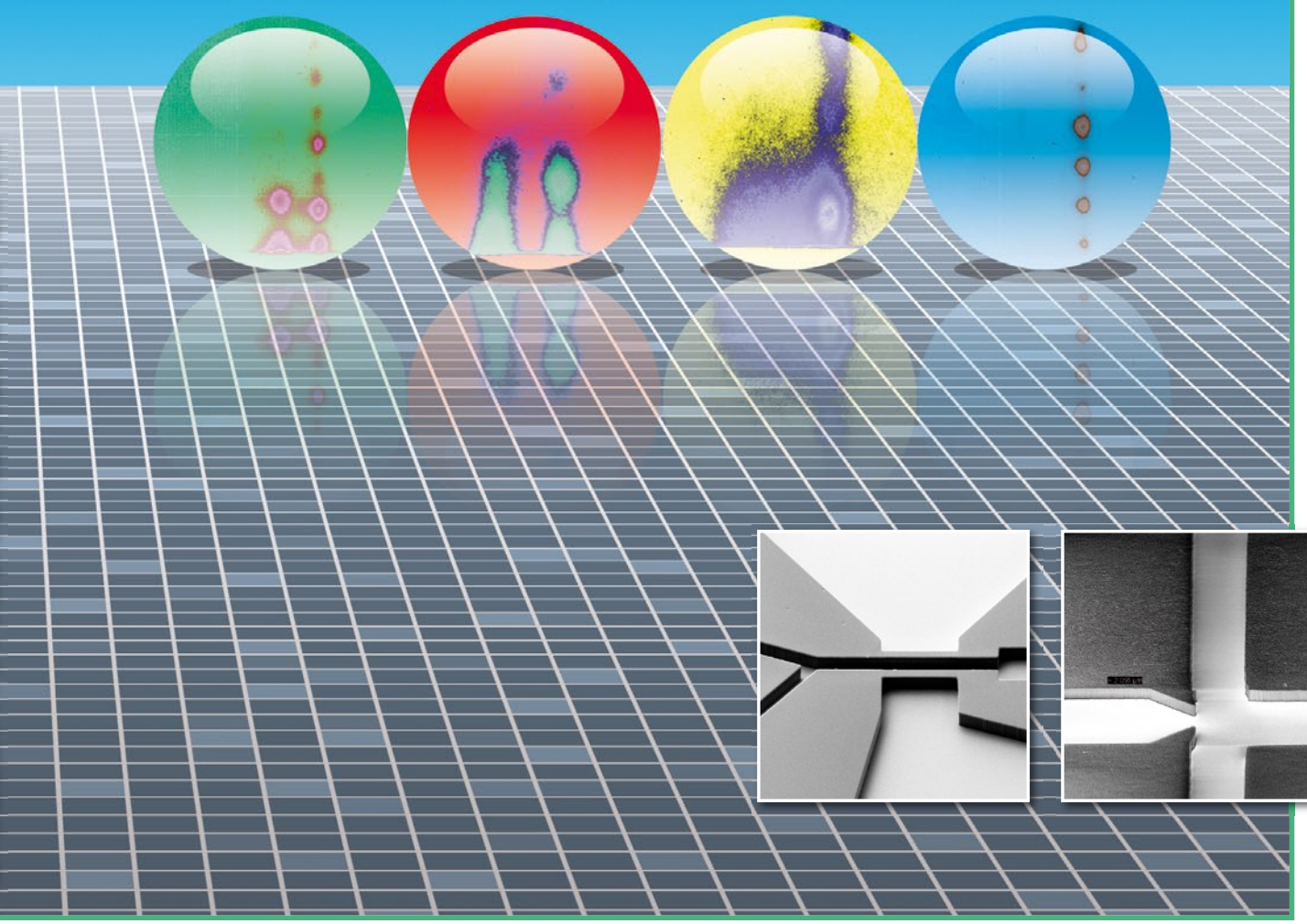

AUSTRIAN SAXS BEAMLINE AT elettra

Austrian Small Angle X-ray Scattering (SAXS) Beamline at ELETTRA

Annual Report 2006

Compiled by the SAXS-Group:

- for IBN: B. Sartori, M. Rappolt & H. Amenitsch
- for ELETTRA: S. Bernstorff

Table of Contents

Preface

Peter Laggner
Director
Institute of Biophysics and Nanosystems Research
Austrian Academy of Sciences

Science flies – and so does the Austrian SAXS Station at Elettra. As this report is being compiled, the festivities on the 10th anniversary of SAXS beamline operation in November 2006 with the fine symposium are already history. But the momentum persists thanks to internal and external factors. Internally, the infrastructure upgrade projects at Elettra, with the installation of a booster system, promise a very competitive increase in source quality which will doubtlessly further enhance the attractivity. Externally, the collaboration between five of the strongest synchrotron SAXS groups in Europe aiming at cutting-edge development in new techniques such as microfluidics and single-particle handling, has taken up full speed in the framework of the EU-SAXIER project. Here, the scientists and technicians of our SAXS Station are once again groundbreaking pioneers, and users are invited to take advantage of these developments at the early stage – for the benefit of their science and for the necessary feedback for further improvement.
It is in these new technological frontiers, where synchrotron SAXS is at its best, as classical SAXS experiments are increasingly being served by convenient and powerful home-laboratory equipment.
I want to thank the many useres of our facility, the management and staff of Elettra, and last but not least our team at the SAXS Station for their great efforts and achievements.

Peter Laggner

Alfonso Franciosi
Director, ELETTRA Laboratory
Chief Executive Officer, Sincrotrone Trieste S.C.p.A.

We are pleased to welcome the publication of the 2006 Annual Report of the SAXS Beamline of the Austrian Academy of Sciences. In 2006 we celebrated two anniversaries, namely the 10th year of user operation of the SAXS beamline at Elettra and the 20th anniversary of the foundation of Sincrotrone Trieste S.C.p.A., the managing company of the Elettra Laboratory. The high point of the festivities was the symposium "SAXS Nanosystems-Science and Technology", that took place at the International Center for Theoretical Physics in Trieste immediately following the Elettra Users' Meeting, and saw the participation of highly qualified experts from many European, Asian and U.S. Research Facilities. During the Elettra's Users' Meeting itself the partnership between Sincrotrone Trieste S.C.p.A. and the SAXS Beamline of the Austrian Academy of Sciences was highlighted by the award of the Fonda-Fasella award to Dr. Giulio Caracciolo for experiments performed by means of the SAXS beamline in close collaboration with the beamline staff. The award, in memory of Professors Luciano Fonda and Paolo Maria Fasella, is assigned every year to a young scientist for outstanding research accomplishments at Elettra, and Dr. Caracciolo was awarded the prize for SAXS studies of the structural stability of transfection-efficient cationic liposome/DNA complexes.

The year 2006 has seen the launch of a number of major activities at Elettra, following the solution of the financial crisis that plagued most development activities in the two previous years and the success of several ambitious project-financing initiatives with the Italian government and the European Investment Bank. A new 5-year plan was approved by the Board of Directors of Sincrotrone Trieste S.C.p.A, on October 31, 2006. The plan, available on the Elettra web site, presents the mission, vision and core values of our organization, defines our strategic objectives and develops a project-oriented operational structure to better pursue our objectives. Major infrastructure projects have begun. Elettra, that was one of the first two medium-energy third-generation synchrotron radiation sources in the world, is being upgraded with a full-energy injector, a substantial increase in the available rf power, and the introduction of an advanced global orbit feedback system. The combination of these should give rise to a substantial increase in beamtime available to user, average brilliance and source stability.

We have begun mapping a strategy - in collaboration with our key partners and users - regarding future insertion devices so that maximal advantage can be taken of the upgraded Elettra storage ring with top-up filling mode. A first important step in this direction has been taken with the successful workshop “New Frontiers in Insertion Devices” that was held in conjunction with the Elettra Users’ meeting November 20-21, 2006. The scope of the workshop was to review insertion devices operating or planned at synchrotron radiation facilities worldwide.

Some of the world's foremost experts attended the workshop and gave their views on short period-small gap undulators (including in-vacuum undulators) based on permanent magnets, cryo-permanent magnets, superconducting magnets, etc and how these can be optimized in the top-up mode of operation. The program and copies of the talks are available on Elettra's homepage. This was the first in a series of three workshops, which was completed in 2007. The second one focused on 2.0 vs. 2.4 GeV mode of top-up operation and the third one (planned for April 2007) will be a reviewed the different straight sections available, including SAXS, and discussed the related upgrade plans.

The Conceptual Design Report (CDR) of FERMI, one of the first free electron lasers (FEL) of its kind in the world, and construction has started through extensive national and international collaborations. FERMI is expected to provide femtosecond pulses of unparalleled brilliance at nanometer wavelengths starting in 2009. Strength of our Laboratory in the foreseeable future will include the availability of Elettra+FERMI at the same site, small-angle x-ray scattering, microscopies, VUV/soft x-ray spectroscopies, x-ray medical imaging, tailor-made materials and structures, and theoretical in-house support. Challenges that we will have to meet include rebuilding the structural biology program, as well as the lithography and nanofabrication program, expand our offer toward harder x-ray applications, and - above all - building FERMI while fully exploring Elettra's upgrade.

To exploit our strengths and meet our challenges we will need the support of our key partners, such as the Austrian Academy of Sciences, and of our user community worldwide. The SAXS beamline is an essential facility for the users' community in the life sciences, materials chemistry and materials physics, thanks to the competence and dedication of the beamline management and staff. We at Sincrotrone Trieste look forward to increased collaboration with the Austrian Academy of Sciences in the exploration of the frontiers that the new Elettra and FERMI will open for us.

Alfonso Franciosi

Events

"SAXS on Nanosystems - Science and Technology" Meeting, Trieste, 2006

On the occasion of the 10-years anniversary of the Austrian small-angle X-ray (SAXS) beamline in Trieste, renowned SAXS experts came from all important centers of Europe, Asia and the USA in order to participate at the symposium "SAXS on Nanosystems-Science and Technology". At the International Center of Theoretical Physics of the UNESCO in Trieste (November 23rd, 24th 2006), the progress of nanomaterials research at SAXS beamlines worldwide was discussed.

The IBN-outstation at the Trieste synchrotron radiation facility ELETTRA is subject to a continuous change and upgrading, and over the past years it developed into a real centre of excellence. The constant engagement in novel research fields such as the study of self-assembling materials on surfaces, the high knowledge transfer from the researchers to the industry, as well as the education of young scientists form the basis for the innovative and lively scientific work on-site. This gets confirmed not only by the high demand for beamtime at the Austrian SAXS station (compare page 24), but also by the fact, that the scientific director of the Trieste synchrotron, Alfonso Franciosi, recently mentioned that eventually a second X-ray small angle scattering station should be planned.

The research landscape at the Austro-SAXS-station has been mainly coined by numerous key experiments on nanomaterials and biostructural complexes. Here, the intense and brilliant light source ELETTRA not only permits a glimpse at the fascinating world of molecules, but allows also to record whole molecular processes, i.e. structural changes of matter with nanometer resolution. Whether basic- or applied research, the list of promising technological fields which profit from the Austro-SAXS-station is long: production of nanoparticles for pharmaceutical applications, improvement of food standards, creation of custom-made materials for catalysis, design of innovative types of solar cells and the development of new safety techniques are just some of several promising research topics. Further, also the efficiency of new antibiotics are studied in real time.

Development and innovation are always kept high at the IBN outstation, and this is reflected also in the impressive total number of 465 published projects, which were performed during the first 10 years in cooperation with 255 research teams from 27 countries. In addition, the IBN group from Trieste participates in the European collaboration project SAXIER (budget 7. 2 million Euro), which has the goal to develop innovative and new SAXS-methods. This initiative is now fully under way and has a duration until the end of 2009.

A special thanks to all our 414 users!

ÅGREN Patrik, *AICHMAYER Barbara,* ALBOUY Pierre-Antoine, *ALDABE Sara,* ALEKSANDROVIC Vesna, *ALEXE Gabriela,* ALFREDSSON Viveka, *ALLAIS Celile,* AMENITSCH Heinz, *AMITESH Paul,* ANGELONI Massimo, *ARNOLD Donna C.,* ARUMUGAM Mahendrasingam, *ASHLEY Christopher Charles,* ASWAL Vinod Kumar, *AUSILI P.,* BABONNEAU Florence, *BACCILE Niki,* BAGNI Maria Angela, *BALDRIAN Josef,* BALKENENDE A. Ruud, *BALOGH Levente,* BAUER Guenther, *BENES Ludvík,* BERNSTORFF Sigrid, *BESCH Hans-Juergen,* BIERMANN Horst, *BINDER Wolfgang H.,* BISBANO Stefania, *BLANCHARD Juliette,* BOISSIÈRE Cédric, *BOLLER H.,* BONARSKI Jan T., *BONGAERTS Karin,* BORBÉLY Andras, *BORVANOVIC Vesna,* BOURGAUX Claudie, *BOYD Ben,* BRANDHUBER Doris, *BREZESINSKI Torsten,* BULJAN Maya, *BUSINARO Luca,* BUSSIA Patrik, *CACHO Fernando,* CAELLES BALCELLS Jaime, *CAMINITI Ruggero,* CAMPI Gaetano, *CARACCIOLO Giacomo,* CARACCIOLO Giulio, *CARRARA Sandro,* CARRERA ALTARRIBA Immaculada Concepcion, *CARSUGHI Flavio,* CASTAGNA Riccardo, *CAUDA Valentina Alice,* CECCHI Giovanni, *CESÀRO Attilio,* CHATTOPADHYAY Soma, *CHAUDARY Suresh Manohar,* CHMIELEWSKA Dagmara, *CHOLEWA Marian ,* CINELLI Stefania, *CLAUSEN Torben,* CÓCERA Mercèdes, *COJOC Danut-Adrian,* CÖLFEN Helmut, *COLOMBINI Barbara,* COPLEY Mark P., *COSTACURTA Stefano,* COUPÉ Aurélie, *CREPALDI Eduardo,* CRNJAK-OREL Zorica, *CROCE Gianluca,* CUREDDA Daniele, *DANNER Sabine,* DARHUBER Anton, *DE LA MAZA A.,* DEL PIERO Gastone, *DESNICA Uroš,* DESNICA-FRANKOVIC Ida-Dunja, *DEUTSCH Günter,* DI FABRIZIO Enzo, *DI GREGORIO Giordano M.,* DI STASIO Stefano, *DONG Charlie Yao Da,* DUBČEK Pavo, *DUFAU Natalie,* EDLUND Hakan , *ERDEMIR Deniz,* EROKHIN Viktor, *EVANS James M.B.,* FALCARO Paolo, *FALTA Jens,* FANTINI Marcia C. A., *FARKAS Ödön,* FARNIK Dominique, *FEDERICONI Francesco,* FERNANDEZ-VIDAL Monica, *FERRACINI Elena,* FERRARI Enrico, *FERRERO Adele,* FEUCHTER Michael, *FIORILLI Sonia,* FLEGE Jan-Ingo, *FLODSTRÖM Katarina,* FORSTNER Michael, *FRANCESCANGELI Oriano,* FRANCIS Timothy, *FRATZL Peter,* FRITSCHER Christina, *FROEBA Michael,* FULLER Watson, *FUNARI Sergio,* GAJOVIC A., *GAMINI Amelia,* GANGODADYHAY Subhashis, *GARAB Gyozo,* GARBIN Valeria, *GEBHARDT Ronald,* GEHL Bernhard, *GEIST Steffi,* GESERICK Jasmin, *GHISLETTI Danila,* GIESENHENG Thomas, *GIOVINE Marco,* GOYAL Prem Sagar, *GRABNER Barbara,* GRACIN Davor, *GRENCI Gianluca,* GRIFFITHS Peter John, *GRIGORIEW Helena,* GRÖHN Franziska, *GROSSO David,* GUENNADY Evmenenko, *GUGLIELMI Massimo,* GUPTA Ajay , *GUPTA Himadri Shikhar,* GUPTA Mukul, *GUPTA Ratnesh,* GUTBERLET Thomas, *GYENES Tamás,* HAHN Andreas, *HANAK Peter,* HANRAHAN John P., *HARTMANN Sarah, HAUBENBERGER Ulrike,* HÄUßLER F., *HEERKLOTZ Heiko,* HERNANDO-MANERU Antonio, *HEUMANN Hermann,* HICKEL Andrea, *HIRAGI Yuzuru,* HODZIC Aden, *HOLMES Justin D.,* HOLZAPFEL Gerd A., *HORKY Martin,* Horvath Gyoezoe, *HUESING Nicola Karola,* IBRAHIMKUTTY Shyjumon, *IDE Semra,* INNOCENZI Plinio, *JAKSIC Milko,* JAKUBIAK Patrycya, *JONGEN Nathalie,* JOSIPOVIC Marina, *JURAIC' Krunoslav,* KALNIN Daniel, *KANCLER Aljosa ,* KARNTHALER H.P., *KASPAROVA J.,* KATSARAS John, *KAUCIC V.,* KECKES Josef, *KELLER Gerhard,* KENESEI Peter, *KERBER Michael,* KICKELBICK Guido, *KIDCHOB Tongjit,* KLAUSHOFER Klaus, *KLEPPINGER Ralf,* KLOSE GOTTHARD, *KLUGER Christian,* KOCH Thomas, *KOGLER Franz Re'ne,* KOHLBRECHER J., *KOPACZ Ireneusz,* KORNOWSKI Andreas, *KOSCHUCH Richard,* KOVACEVIC Ivana, *KRAL Robert,* KRIECHBAUM Manfred, *KRUNO Jurajic,* KUEMMEL Monika , *KÜHNE Christian,* KUMAR Dileep, *KUNZ Michael J.,* LA CARRUBA Vincenzo, *LA MESA Camillo,* LAGGNER Peter, *LAUER Iris,* LéONE Philippe, *LICHTENEGGER Helga,* LINARI Marco, *LIND Anna,* LINDÉN Mika, *LINDSAY J.G.,* LISKA Robert, *LO CELSO Fabrizio,* LOHNER Karl, *LOIDL Dieter,* LOMBARDI Vincenzo, *LOMBARDO Domenico,* LOPES Pedro, *LOPEZ Christelle,* LÓPEZ Olga, *LUCIANI Paola,* LUCIC LAVCEVIC Magdy, *LUCII Leonardo,* MACCHEGIANI Stefania, *MACCIONI Elisabetta,* MACHL Doris, *MADDALENA Amadeo,* MÄDLER BURGHARD, *MAIER Guenther,* MAJEROWICZ Monika, *MAJOR S.S.,* MALFATTI Luca, *MANAKOVA Elena,* MANCINI Giovanna, *MARANGONI Alejandro,* MARCHESE L., *MARCHESINI Augusto,* MARIANI Paolo, *MARMIROLI Benedetta,* MAROHNIC Zeljko, *MARTINS Tereza,* MARTOIU Sorin, *MARTORANA Antonino,* MARTUCCI Alessandro, *MAVROMOUSTAKOS Thomas,* MAXIMILIAN Cornelius, *MAZAJ Matjaz,* MAZUMDER Subhasish, *MELÁNOVÁ Klára,* MENK Ralf, *MILANESIO Marco,* MILAT Ognjen, *MISCHENKO Nicolai,* MISOF Klaus, *MOCELLA Vito,* MORELL Juergen, *MORELLO Christian,* MORETTI Luigi, *MUELLER Gudrun,* MYERSON A. S., *NAWROTH Thomas,* NAYAK Pradipta Kumar, *NICOLINI Claudio,* NOVAK TUSAR Natasa, *NYILAS Krystian,* O'CALLAGHAN J. M., *OLLIVON Michel,* ONORI Giuseppe, *ORTHEN Andre',* ORTNER Balder, *ORTORE Maria Grazia,* OVCAR Silvester , *PABST Georg,* PACCAMICCIO Lydia, *PADUANO L.,* PALOMARES F. Javier, *PAOLETTI Sergio,* PARADOSSI Gaio, *PARIS Alfred,* PARIS Oskar, *PAVLOVIC Mladen,* PEREIRA LACHATAIGNERAIS Joedmi, *PERSSON Gerd,* PETERLIK Herwig, *PETKOV Nikolay,* PETRARU Laura, *PHASE D. M.,* PIAZZESI Gabriella, *PICCAROLO Stefano,* PIFFERI Augusto, *PILI Barbara,* PISANI Michela, *PISERI Paolo,* PIVAC Branko, *PLESTIL Josef,* PONS Ramon, *POSPÌSIL Herman,* POZO-NAVAS Beatriz, *POZZI Daniela,* PRASSL Ruth, *PREGETTER Magdalena,* PRESSL Karin, *PRINCIPI Giovanni,* PUCHEGGER Stephan, *RAAB Christina,* RADIC Nikola, *RAJEWSKA Aldona,* RAJPUT Parasmani, *RANDJELOVIC Igor,* RAPPOLT Michael, *REBBIN Vivian,* RECONDITI Massimo, *REDDY Raghavendra Varimalla,* RENNHOFER Harald, *RESEL Roland,* RHEYNAERS Harry, *RIBARIK Gabor,* RIELLO Pietro, *RINNERTHALER Susanne,* RIZZO Roberto, *ROESSLE Manfred,* ROSCHGER Paul, *ROSENHOLM Jarl B.,* RUSTICHELLI Franco, *SABOLEK Stjepan,* SACHSENHOFER Robert, *SAIANI Alberto,* SALAMON Krešo, *SANCHEZ Clément ,* SANTRA Pralay, *SAPRA Sameer,* SARAIYA Amit, *SARMA Dipankar Das,* SARTORI Barbara, *SARVESTANI Amir,* SATURNI Letizia, *SCHAFER Olivier,* SCHAFLER Erhard, *SCHMID Fabian,* SCHMIDT Thomas Jr., *SCHMIDT Wolfgang,* SCHULER Peter, *SCHULZE-BAUER Christian A. J.,* SCHURTENBERGER Peter, *SCHUSTER Bernhard,* SCHÜTH Ferdi, *SCHWARZENBACHER Robert,* SEN Debasis, *SEVCSIK Eva,* SHAH Jitendra, *SHARMA Pooja,* SIAPI Eleni, *SIKORA Antonín,* SIMON Kornel, SINIBALDI Raffaele, *SINKO Katalin,* SMARSLY Bernd , *SMOLLE Michaela,* SOLER-ILLIA Galo J. de A. A., *SOMMER Gerhard,* SPAGNOLI Rachele P., *SPINOZZI Francesco,* SPITZBART Manfred, *SRINIVASA Raman,* STACHOWIAK Christian, *STANGL Julian,* STANIC Vesna, *STAUDEGGER Erich,* STEINER G., *STEINHART Milos,* STELZER Franz, *STEPANEK Petr ,* STRANCAR Janez, *STROBL Marlene,* SUPPLIT Ralf, *SUSSICH Fabiana,* TAVIOT-GUÉHO Christine, *TEIXEIRA Cilaine Veronica,* TESCH Walter, *THEUNISSEN Elisabeth,* TIEMANN Michel, *TITOVA Svetlana,* TORMA Viktoria, *TRIOLO Alessandro,* TRIOLO Roberto, *TURKOVIC Aleksandra,* UNGÁR Tamas, *VALENTA Angelika,* VALKOVA Larissa, *VAN OUYTSEL Kristel,* VINCK Liesel, *VISWANATHA Ranjani,* VITERBO Davide, *VITTA Satish,* VITTUR Franco, *VOLPE Luigia,* VOLTOLINA Francesco, *WAGNER Hendrik,* WALENTA Albert Heinrich, *WEBER Markus,* WEISS Oezlem, *WELLER Horst,* WENNERSTRÖM Haken, *WILHELM Harald,* WINTER Ingrid, *WOO David,* WRIGHT Anthony, *WURZINGER Harald,* YOLANDA GESTRO Martin, *ZABUKOVEC LOGAR Natasa,* ZANELLA Giovanni, *ZANONI Roberto,* ZEHETBAUER Michael, *ZEIPPER Leonhard,* ZIDANSEK Alexander, *ZIMA Vitezslav,* ZIZAK Ivo, *ZOEFRE Bayraun,* ZOUMPOULAKIS Panagiotis, *ZWEYTICK Dagmar.*

The SAXS-Group

HEAD OF PROJECT: Peter Laggner [1)]

e-mail: peter.laggner@oeaw.ac.at

SCIENTISTS: Heinz Amenitsch [1), 3)]

e-mail: amenitsch@elettra.trieste.it

Sigrid Bernstorff [2])

e-mail: bernstorff@elettra.trieste.it

Michael Rappolt [1), 3)]

e-mail: michael.rappolt@elettra.trieste.it

POST DOCS: Fernando Cacho [1), 3)] (since January 2007)

e-mail: fernando.cacho@elettra.trieste.it

Shyjumon Ibrahimkutty [1, 3)] (since April 2006)

e-mail: shyju.ibrahimkutty@elettra.trieste.it

Benedetta Marmiroli [1, 3)] (since March 2006)

e-mail: benedetta.marmiroli@elettra.trieste.it

PHD-STUDENT: Fabian Schmid [1), 3)]

e-mail: fabian.schmid@elettra.trieste.it

CHEMICAL ASSISTANT: Barbara Sartori [1, 3)]

e-mail: barbara.sartori@elettra.trieste.it

TECHNICIAN: Christian Morello [2)]

e-mail: christian.morello@elettra.trieste.it

1) Institute for Biophysics and Nanosystems Research, Austrian Academy of Sciences, Schmiedlstraße 6, 8042 Graz, Austria.
Tel 0043-316-4120 302
Fax 0043-316-4120 390

2) Sincrotrone Trieste, Strada Statale 14, km 163.5, 34012 Basovizza (TS), Italy.
Tel 0039-040-375 81
Fax 0039-040-938 0902

3) Institute for Biophysics and Nanosystems Research, Austrian Academy of Sciences
c/o Sincrotrone Trieste

The SAXS-Beamline in General

Small Angle X-ray Scattering has become a well known standard method to study the structure of various objects in the spatial range from 1 to 1000 Å, and therefore instruments capable to perform such experiments are installed at most of the synchrotron research centers. The high-flux SAXS beamline at ELETTRA is mainly intended for time-resolved studies on fast structural transitions in the sub-millisecond time region in solutions and partly ordered systems with a SAXS-resolution of 10 to 1400 Å in real-space.
The photon source is the 57-pole wiggler whose beam is shared and used simultaneously with a Macromolecular Crystallography beamline. The wiggler delivers a very intense radiation between 4 and 25 keV of which the SAXS-Beamline accepts 3 discrete energies, namely 5.4, 8 and 16 keV. The beamline optics consists of a flat double crystal monochromator and a double focusing toroidal mirror.
A versatile SAXS experimental station has been set-up, and an additional wide-angle X-ray scattering (WAXS) detector monitors simultaneously diffraction patterns in the range from 1 to 9 Å. The sample station is mounted move-able onto an optical table for optimising the sample detector distance with respect to SAXS resolution and sample size.
Besides the foreseen sample surrounding the users have the possibility to install their own specialised sample equipment. In the design phase, besides technical boundary conditions, user friendliness and reliability have been considered as important criteria.
The optimisation of the beamline with respect to high-flux and consequently high flux density, allows to perform the following experiments:

- Low Contrast Solution Scattering
- Grazing Incidence Surface Diffraction
- Micro-Spot Scanning
- X-ray Fluorescence Analysis
- Time-Resolved Studies ≥ 11 μs
- Simultaneously Performed Small- and Wide-Angle Measurements (SWAXS) on:
    - Gels
    - Liquid Crystals
    - (Bio) Polymers
    - Amorphous Materials
    - Muscles

Furthermore, using 5.4 and 16 keV energies, the beamline is widely applicable also to very thin, e.g. single muscle fibers, and optically thick (high Z) specimen, as often used in e.g., material science and solid state physics.

THE INSERTION DEVICE

The wiggler for the SAXS beamline consists of three 1.5 m long segments, each having 19 poles. The device can work with a minimum gap of 20 mm, which corresponds to K=20 at 2 GeV. The main parameters of the wiggler are:

- Critical Energy 4.1 keV
- Radiation Power 8.6 kW
- Flux 3.5×10^{14} ph/s/mrad/0.1%BW (at 400 mA)

The wiggler radiation cone has a horizontal width of 9 mrad. From this the SAXS-beamline accepts vertically 0.3 mrad, and horizontally +/-0.5 mrad at a 1.25 mrad off-axis position. The resulting source size for 8 keV photons is 3.9 x 0.26 mm^2 (horiz. x vert.).

THE OPTICS

The optics common with the diffraction beamline consists of:

- C-Filter and Beryllium window assembly to reduce the power load on the first optical elements by a factor of 2 and to separate the beamline vacuum from the storage ring.
- Beam defining slit chamber which allows to define the SAXS beam on three sides before the monochromator in order to reduce the straylight in the downstream beamline sections.

The SAXS beamline optics consists of:

- A double-crystal monochromator consisting of four individual chambers, in which three interchangeable asymmetric Si(111) crystal pairs are used to select one of three fixed energies. Each of the crystal pairs is optimised for the corresponding energy to accomplish a grazing angle of 2°. The energy resolution $\Delta E/E$ of the monochromator is in the range of $0.7 - 2.5\ 10^{-3}$.
- A baffle chamber after the monochromator is used as an adjustable straylight fenditure.
- A segmented toroidal mirror focuses the light in horizontal and vertical direction with a 1/2.5 magnification onto the SAXS-detector.
- An aperture slit reduces the straylight after the monochromator and the toroidal mirror.
- A guard slit defines the illuminated region around the focal spot. The spot size on the detector is 1.6 mm horizontally and 0.6 mm vertically. The calculated flux at the sample is in the order of 10^{13} ph/s at 400 mA. For a maximum sample size of 5.4 x 1.8 mm^2 correspondingly a flux density of 10^{12} ph/s/mm^2 has been calculated.

SAMPLE STAGE

The multipurpose sample stage allows to perform fast time-resolved relaxation studies based on temperature- or pressure-jumps as well as stopped flow experiments. Shear jump relaxation experiments are planned. Specifically, T-jumps can be induced by an infra-red light pulse (2 ms) from an Erbium-Glass laser, raising the temperature about 20 °C in an aqueous sample volume of 10 µl. A hydrostatic pressure cell with a maximal accessible angular range of 30° for simultaneous SAXS and WAXS measurements is available. P-jumps are realised by switching fast valves between a low and a high pressure reservoir, increasing or decreasing the hydrostatic pressure in the range from 1 bar to 2.5 kbar within a few ms. A Differential Scanning Calorimeter (DSC) allows for DSC-scans simultaneously to SWAXS measurements. In an overview, the following sample manipulations are possible (further details, see page 32-38):

- Temperature Manipulations: Ramps, Jumps and Gradient Scans
- Pressure Manipulation: Scan and Jumps
- Stopped Flow Experiments
- SWAXS Measurements Applying Mechanical Stress
- Calorimetric measurements

Scientific Applications	Low Contrast Solution Scattering, Grazing Incidence Surface Diffraction, Micro-Spot Scanning, X-ray Fluorescence Analysis, Time-Resolved Studies ≥ 11 µs and Simultaneously Performed Small- and Wide-Angle Measurements (SWAXS) on: Gels Liquid Crystals (Bio) Polymers Amorphous Materials Muscles
Source characteristics	Wiggler (NdFeB Hybrid): Period 140 mm No. full poles 57 Gap 20 mm B_{max} 1.607 T Critical Energy ε_c 4.27 keV Power (9 mrad) 8.6 kW Effective source size FWHM 3.9 x 0.26 mm^2(HxV)
Optics	Optical elements: Double crystal monochromator: Si (111) asym. cut, water cooled. Mirror: two–segment,toroidal, Pt coated. Distance from source: 18.4 m 26.5 m Acceptance 1 mrad/0.3 mrad (HxV) Energy (3 selectable) 5.4, 8, 16 keV (0.77, 1.54, 2.3 Å) Energy resolution $\Delta E/E$ 0.7-2.5 x 10^{-3} Focal spot size FWHM 1.2 x 0.6 mm^2 (HxV) Spot at Sample FWHM 5.4 x 1.8 mm^2(HxV) Flux at sample 5 x 10^{12} ph s^{-1}(2 GeV, 200 mA, 8 keV)
Experimental apparatus	Resolution in real space: 10-1400 Å (small-angle), 1- 9 Å (wide-angle) Sample stage: temperature manipulations: ramps, jumps and gradient scans, pressure manipulation: scan and jumps, stop flow experiments, SWAXS measurements applying mechanical stress, SWAXS measurements applying magnetic fields. In-line calorimetric measurements simultaneously with SWAXS. Detectors: 1D gas-filled detectors for simultaneous small- and wide-angle (Gabriel type), 2D CCD-detector for small-angle.
Experiment control	Beamline control: Program-units written in LabView for Windows 1 D detector control: PC-card and software from Hecus X-ray Systems GmbH, Graz. 2 D detector control: Software from Photonic Science, Oxford.

CURRENT STATUS

The beamline has been built by the Institute for Biophysics and Nanosystems Research (IBN), Austrian Academy of Science in collaboration with staff members from Sincrotrone Trieste, and is in user operation since September 1996. The set-up of the beamline started at the beginning of January 1995 with the installation of the support structure. Until the end of 1995, the 8 keV single energy system had been realised. The upgrade to the full three energy system was finished in spring 1998. Time resolved experiments require fast X-ray detectors and data acquisition hard- and software. Depending on the desired resolution in time and in reciprocal space, on isotropic or anisotropic scattering of the sample, one-dimensional position sensitive (delay-line type) or two-dimensional CCD detectors are employed.

In August 2002 our new chemistry and X-ray laboratory went into operation. The chemistry unit serves mainly for sample preparation and analysis for both, in house research and external user groups, whereas the X-ray laboratory allows on-site testing of samples before moving on to the SR beamline (see page 31).

In conclusion, due to wide versatility of the beamline and the highly flexible sample stage, there are nearly no limits for the realisation of an experiment, and you are welcome by our team to propose any interesting and highlighting investigation for the benefit of material and life sciences.

Application for Beamtime at ELETTRA

1. Beamtime Policy at SAXS beamline

According to the agreement from March 2001 regarding the co-operation between the Austrian Academy of Sciences and Sincrotrone Trieste, at the Austrian SAXS-beamline the available beamtime of about 5000 hours/year is distributed as follows:

- 35% for Austrian Users, type: "CRG" (Collaborating Research Group)
- 35% for Users of Sincrotrone Trieste (General Users (GU))
- 30% is reserved for beamline maintenance and in-house research

In both user beamtime contingents also any industrial, proprietary and confidential research can be performed according to the "General User Policy" of Sincrotrone Trieste.

To apply for CRG and GU user beamtime proposals must be submitted according to the rules of Sincrotrone Trieste. The international review committee at ELETTRA will rank the proposals according to their scientific merit assessment. Based on this decision beamtime will be allocated according to the specific quotes for the beamtimes (CRG/GU) either for the following semester ("normal application") or for the next two years ("long term application"). However, at the moment no more than a maximum of 10% of the beamtime will be assigned to "long term" projects.

2. How to apply for beamtime

There are two deadlines each year for proposals, namely August 31st and February 28th. Accepted proposals will receive beamtime either in the then following first or second half year period, respectively. The Application Form must be completed on-line according to the following instructions.

ELETTRA USERS OFFICE
Strada Statale 14 - km 163.5
34012 Basovizza (Trieste), ITALY
Tel: +39 040 375 8628 - fax: + 39 040 375 8565
e-mail: useroffice@elettra.trieste.it

INSTRUCTIONS GIVEN BY THE USERS OFFICE
(see also http://www.elettra.trieste.it/UserOffice/)

1. Read carefully the General Guidelines.

2. Connect to the Virtual Unified Office: https://vuo.elettra.trieste.it/pls/vuo/guest.startup using your favorite browser with JavaScript enabled.

3. Select the Virtual Unified Office link.

4. When prompted, insert your ID and password. If you are a new user fill in the registration form with your data and choose your institution with the search button; in case your institution does not appear in the list, please contact useroffice@elettra.trieste.it giving all the details about it. When registered, you will receive an acknowledgment with your ID and password. You can change your password, if you wish. In case you forget your password, please don't register again but contact useroffice@elettra.trieste.it. At any moment you can select the help button and view more detailed instructions. By inserting your ID and password you will be able to continue.

5. Select the proposals button in the User functions group.

6. Select add and fill in on-line the proposal form. Please, type your proposal in English. Repeat this procedure for each proposal you intend to submit.

7. In case of continuation proposal: a) attach the experimental report of previous measurements; b) give your previous proposal number.

8. When finished, submit the proposal electronically, selecting the save button.

9. Print the proposal form together with each related safety form.

10. Sign the safety form(s).

11. Mail all signed safety form(s) as printed copy to the Users Office.

NOTE:

For technical questions related to proposals submission or other practical issues contact useroffice@elettra.trieste.it

For scientific questions related to the possibility of performing a given experiment contact bernstorff@elettra.trieste.it or amenitsch@elettra.trieste.it

List of Users and Institutes in 2006

Argentina

Unidad de Actividad Quimica, Centro Atomico Constituyentes, San Martín, Prov. de Buenos Aires
SOLER ILLIA Galo

IN.QUI.M.A.E., Buenos Aires
ALDABE Sara

Australia

Monash University, Dept.of Parmaceutics, Victorian College of Pharmacy, Parkville VIC
BOYD Ben J.
DONG Yao-Da

Austria

Austrian Academy of Science, Institute for Biophysics and Nanosystem Research, Graz
AMENITSCH Heinz
DANNER Sabine
DEUTSCH G.
HODZIC Aden
IBRAHIMKUTTY Shyjumon
KRIECHBAUM Manfred
LAGGNER Peter
LOHNER Karl
MARMIROLI Benedetta
PABST Georg
RAPPOLT Michael
SARTORI Barbara
SCHMID Fabian
SEVCSIK Eva
WURZINGER Harald
ZWEYTICK Dagmar

Institut fuer Werkstoffkunde und Pruefung der Kunststoffe, University of Leoben
FEUCHTER Michael

MCL Leoben and Dep. of Materialphysics, University of Leoben
KECKES Josef
MAIER Guenther

Medical University of Graz, Institute of Pathology, Graz
REGITNIG P.

University of Technology, Institute of Applied Synthetic Chemistry, Vienna
FARNIK Dominique

University of Technology, Institute of Materials Chemistry
BRANDHUBER Doris
HAUBENBERGER Ulrike

University of Technology, Institute of Materials Science & Technology
FRITSCHER Christina
KOCH Thomas
LICHTENEGGER Helga C.
SEIDLER S.

University of Technology, Institute of Structural Analysis-Computational Biomechanics, Graz
CACHO Fernando

University of Vienna, Institute of Materials Physics
KERBER Michael
PETERLIK Herwig
SCHAFLER Erhard
ZEHETBAUER Michael

University of Vienna, Faculty of Physics, Scattering and Spectroscopy
PUCHEGGER S.

Belgium

VITO - Flemisch Institute for Technological Research, MOL
HEYSE Pieter

Brazil

University of Sao Paulo, Institute of Physics, Sao Paulo
FANTINI Marcia C. A.
ARTINS Tereza

Croatia

Institute of Physics, Zagreb
SALAMON Kresimir

"Ruder Boskovic" Institute, Zagreb
BULJAN Maya
CAPAN Ivana
DESNICA-FRANKOVIC Ida-Dunja
DESNICA Uros
DUBČEK Pavo
GAJOVIC A.
GRACIN, Davor
JURAIC Krunoslav
PAVLOVIĆ Mladen
PIVAC Branko
RADIC Nikola

TURKOVIĆ Aleksandra
ZORC H.

University of Split, Faculty of Chemical Technology, Split
LUČIĆ LAVČEVIĆ Magdy

Czech Republic

Czech Academy of Sciences, Institute of Macromolecular Chemistry, Prague
STEINHART Milos
STEPANEK Petr

Finland

Åbo Akademi University, Dept. of Physical Chemistry, Turku
LINDÉN Mika

France

ISMRA-CNRS, Laboratoire Catalyse et Spectrochimie, Caen
THIBAULT- STARZYK F.

University Paris-Sud, Dep. of Physical-chemistry, Pharmacotechnique and Biopharmacy, Paris
BOURGAUX Claudie
COUVREUR P.
FAIVRE Vincent
GLIGUEM Hela
MARANGONI Alejandro
OLLIVON Michel
PILI Barbara
REDDY L. Harivardhan

Université Pierre et Marie Curie, Chimie de la Matière Condensée,, Paris
BOISSIÉRE Cédric
GROSSO David
KUEMMEL Monika

Germany

BASF AG, Ludwigshafen
FRANCIS Timothy
MOREIRA A.
RUELLMANN M.
SCHULER Peter

BASF AG, Ludwigshafen and University of Porto, Portugal
LOPES Pedro

Martin-Luther University Halle-Wittenberg, Institute of

Chemistry / Macromolecular Chemistry, Halle
BINDER Wolfgang H.
JOSIPOVIC Marina
SACHSENHOFER Robert

Max-Planck-Institute for Colloids and Interfaces, Golm / Potsdam
CÖLFEN Helmut

University of Bremen, Institute for Applied and Physical Chemistry
GEHL Bernhard
BÄUMER M.

University of Bremen, Institute of Solid State Physics
FALTA Jens
SCHMIDT Thomas

University of Ulm, Division of Inorganic Chemistry I
HUESING Nicola
HARTMANN Sarah
GEIST Steffi
GESERICK Jasmin

Greece

National Hellenic Research Found - Dept. of Chemistry
MAVROMOUSTAKOS Thomas
SIAPI Eleni
ZOUMPOULAKIS Panagiotis

Hungary

Eötvös University, Department of General Physics, Budapest
BALOGH Levente
NYILAS Krystian)
RIBARIK Gabor
UNGÁR Tamas

India

Indian Institute of Science, Solid State and Structural Chemistry Unit, Bangalore
SANTRA Pralay
SARMA Dipankar Das
VISWANATHA Ranjani

Indian Institute of Technology, Dep. of Metallurgical Engineering and Materials Science, Powai, Bombay
SRINIVASA Raman S.

Indian Institute of Technology, Dep. of Physics, Powai, Bombay
MAJOR S.S.
AYAK Pradipta Kumar

UGC-DAE Consortium for Scientific Research, Indore
GUPTA Ajay
KUMAR Dileep
RAJPUT Parasmani

Ireland

University College Cork (UCC), Dept. of Chemistry, Cork City
ARNOLD Donna C.
HOLMES Justin D.
MORRIS Michael A.
O'CALLAGHAN J. M.
PETKOV Nikolay

Italy

Associazione CIVEN, Nano Fabrication Facility, Venice
FALCARO Paolo

Bruker Optics s.r.l., Milano,
MORINI Pierangelo
SALI Diego

CNR-IMIP and Laboratorio Nazionale TASC, CNR-INFM, Trieste
CORENO Marcello

CNR- IMM sez. di Napoli, Napoli
ANGELONI Massimo
MOCELLA Vito
RENDINA Ivo

CNR - Institute of Crystallography, Monterotondo, Rome
CAMPI Gaetano
PIFFERI Augusto

DIMET- Università Mediterranea, Reggio Calabria
MORETTI Luigi

CNR - Institute of Material Structure, Monterotondo, Rome
SUBER L.

INFM - CNR Laboratori Nazionali di Frascati (Roma)
PICCININI Massimo

INFM - CNR Laboratorio TASC, Trieste
BUSINARO Luca
GRENCI Gianluca

Politecnico di Torino, Dip. Scienze dei Materiali e Ingegneria Chimica, Torino
CAUDA Valentina Alice
FIORILLI Sonia
ONIDA B.

Sincrotrone Trieste, Trieste

BERNSTORFF Sigrid
MORELLO Christian

University of Camerino, Dep. of Molecular Cellular and Animal Biology, Genetic Immunization Laboratory

AMICI A.
MARCHINI C.
MONTANI M.

Università di Padova, Dep. of Mechanical Engineering, Padova

COSTACURTA Stefano
MARTUCCI Alessandro

Università di Perugia, Dipartimento di Fisica, Perugia

CINELLI Stefania

Università del Piemonte Orientale "A.Avogadro", Dip. Scienze e Tecnologie Avanzate (DISTA), Alessandria

CROCE Gianluca
MILANESIO Marco
VITERBO Davide

Università Politecnica delle Marche, Dipartimento di Scienze Applicate ai Sistemi Complessi, Ancona

CARBINI Andrea
MARIANI Paolo
ORTORE Maria Grazia
SINIBALDI Raffaele
SPINOZZI Francesco

Università di Milano, Dip. di Fisica and CIMAINA, Milan

BONGIORNO Gero Antonio
MILANI P.
PISERI Paolo

Università di Roma "La Sapienza", Dip. di Chimica

CAMINITI Ruggero
CARACCIOLO Giulio
POZZI Daniela

Universita' Roma Tre, Dipartimento di Scienze Geologiche, Rome

MARCELLI Augusto

Università di Sassari, Dipartimento di Architettura e Pianificazione, Laboratorio di Scienza dei Materiali e Nanotecnologie, Alghero

COSTACURTA S.
CUREDDA Daniele
INNOCENZI Plinio
KAUČIČ V.
KIDCHOB Tongjit
MALFATTI Luca
PUSCEDDU Fabrizio

Poland

Institute of Nuclear Chemistry and Technology, Warsaw

CHMIELEWSKA Dagmara
GRIGORIEW Helena

Slovenia

Josef Stefan Institute and J. Stefan International Postgraduate School, Ljubljana

KANCLER Aljosa
OVCAR Silvester
ZIDANSEK Alexander

National Institute of Chemistry, Ljubljana

MALI G.
MAZAJ Matjaz
NOVAK TUSAR Natasa
ZABUKOVEC LOGAR Natasa

Spain

Autonomous University of Barcelona, Unity of Biophysics, Faculty of Medicine, Barcelona

TEIXEIRA Cilaine Veronica

Sweden

Royal Institute of Technology, Department of Solid Mechanics, Stockholm

HOLZAPFEL Gerd A.

Switzerland

Particle Technology Laboratory, Swiss Federal Institute of Technology, Zürich

WEGNER K.

USA

Georgia Tech, Department of Chemical and Biomolecular Engineering

BEHRENS S.

University of Cincinnati, Department of Chemical and Materials Engineering, Cincinnati OH

BEAUCAGE G.

List of Performed Experiments

2006 (first half year)

Proposal	Proposer	Institution	Country	Title	Research Area
2005569	HODZIC Aden	IBN, AAS, Graz	Austria	In situ study of antihypertensive drug effects on lipid model membranes	Life Science
2005570	PABST Georg	IBN, AAS, Graz	Austria	Electrostatic Attraction of Coupled Wigner Crystals in Lipid Model Membranes	Life Science
2005606	CAMPI Gaetano	Istitute of Cristallography, Monterotondo Rome	Italy	Ionic liquid crystal template for silver nanoparticle superstructures	Chemistry
2005611	SCHMIDT Thomas, Jr.	Institute of Solid State Physics, Uni. of Bremen	Germany	Lateral ordering of CdSe quantum dot stacks	Materials Science
2005631	GUPTA Ajay	UGC-DAE Consortium for Scientific Research, Indore	India	Depth resolved in-plane diffraction studies of melting of Lnagmuir-Blodgett films using x-ray wave-guide	Materials Science
2005636	INNOCENZI Plinio	Lab. di Scienza dei Materiali e Nanotecnologie, Uni. di Sassari, CR-INSTM, Alghero	Italy	Development of a new multi-techniques analytical approach to study in situ materials processing	Chemistry
2005671	SCHMID Fabian	IBN, AAS, Graz	Austria	2-dimensional Layer Specific Tensile Testing of Human Carotid Arteries	Life Sciences
2005696	MARTUCCI Alessandro	Università di Padova - Dip. Ingegneria Meccanica (Settore Materiali)	Italy	Mesoporous nickel oxide films	Materials Science
2005710	ZWEYTICK Dagmar	IBN, AAS, Graz	Austria	Effect of human host defense derived peptides on lipid model membranes	Life Sciences
2005726	SARMA Dipankar Das	Indian Institute of Science	India	In-situ study of one-dimensional growth mechanism in highly luminescent CdSe nanorods,	Chemistry
2005738	ORTORE Maria Grazia	Dip. di Scienze Applicate ai Sistemi Complessi, Uni. Politecnica delle Marche, Ancona	Italy	Study of the hydrophobic alcohol aggregation under pressure	Life Sciences
2005749	SCHAFLER Erhard	Institute of Materials Physics, University of Vienna	Austria	Enhanced background scattering caused by deformation induced vacancies: In-Situ Synchrotron WAXS, Part II: Body Centered Cubic Metals (bcc)	Materials Science

2005762	KRIECHBAUM Manfred	IBN, AAS, Graz	Austria	Structure of oriented lipids on solid support under hydrostatic pressure	Life Sciences
2005777	LINDEN Mika	Dept. of Physical Chemistry, ÅBO Academi University,	Finland	In-situ synchrotron SAXS/XRD study of the formation of self-assembled multiwalled carbon nanotubes	Chemistry
2005804	HOLMES Justin	Materials and Supercritical Fluids Group, Department of Chemistry, University College Cork	Ireland	Structural Investigations of Mesoporous Thin Films Grown Within Confined Architectures	Chemistry
2005819	FRITSCHER Christina	Institute of Materials Science and Technology, Vienna Uni. of Technology	Austria	Formation of Periodically Ordered Mesostructures in Silica and Organosilica Gels synthesized with Various Novel Polyol-Modified Silanes and Organosilanes	Chemistry
2005840	FRITSCHER Christina	Institute of Materials Science and Technology, Vienna Uni. of Technology	Austria	In-situ investigation of the formation and anisotropic alignment of periodic mesostructures in nanocomposite gels	Chemistry
2005860	ZIDANSEK Aleksander	J. Stefan Institute and J. Stefan International Postgraduate School, Ljubljana	Slovenia	Quenched Disorder in Confined Smectic Liquid Crystals	Chemistry
2005866	AMENITSCH Heinz	IBN, AAS, Graz	Austria	Evaporation induced self assembly of phospholipids into non lamellar phases on solid supports	Life Sciences
2005051 Long Term	FALTA Jens	Institute of Solid State Physics, Uni. of Bremen	Germany	In-situ characterization of self-assembled nanoparticle films under harsh conditions	Materials Science
In-house research	BERNSTORFF Sigrid + PIVAC Branko	Sincrotrone Trieste + Ruđer Bošković Institute, Zagreb	Croatia	Ge nanostructures for memory devices	Materials Science
In-house research	AMENITSCH Heinz + OLLIVON Michael	IBN, AAS, Graz + Physico-Chimie, Pharmacotechnie, Biopharmacie, UMR 8612, Univ. Paris-Sud, Chatenay, France	France	Insertion of cytotoxic anticancer agent in sphingomyelin-cholesterol liposomes: Study of the liquid crystalline structures and phase transitions by coupling of Differential Scanning Calorimetry and High Resolution SAXS	Life Sciences
In-house research	BERNSTORFF Sigrid + MARIANI Paolo	Sincrotrone Trieste + Dip. di Scienze Applicate ai Sistemi Complessi, Uni. Politecnica delle Marche, Ancona	Italy	SAXS and GISAXS studies of proteins immobilised in atmospheric plasma polymerised thin coatings	Life Sciences

In-house research	AMENITSCH Heinz + STEPANEK Petr	IBN, AAS, Graz + Czech Academy of Sciences, Inst. of Macromolecular Chemistry, Prague	Czech Republic	Determination of the phase diagram of diblock copolymers in immiscible selective solvents.	Chemistry
In-house research	BERNSTORFF Sigrid + ANGELONI Massimo	Sincrotrone Trieste + C.N.R. - IMM - sez. di Napoli	Italy	In situ investigation of capillary condensation phenomena in porous silicon nanostructures by means of GISAXS and SAXS measurements	Materials Science
In-house research	BERNSTORFF Sigrid + GRACIN Davor	Sincrotrone Trieste + Ruđer Bošković Institute, Zagreb	Croatia	SAXS on amorphous silicon-carbide alloys	Materials Science
In-house research	BERNSTORFF Sigrid + RADIC Nikola	Sincrotrone Trieste + Ruđer Bošković Institute, Zagreb	Croatia		Materials Science
In-house research	AMENITSCH Heinz + GROSSO David	IBN, AAS, Graz + Uni. Paris 6, Chimie de la Matiere Condensee	France	Morphological characterization of Mesoporous-Nano-Patterns	Chemistry

2006 (second half year)

Proposal	Proposer	Institution	Country	Title	Research Area
2006035	ORTORE Maria Grazia	Dip. di Scienze Applicate ai Sistemi Complessi, Uni. Politecnica delle Marche, Ancona	Italy	Effects of Pressure and Temperature on Protein Equilibria in Solution	Life Sciences
2006057	FRANCIS Timothy	BASF Aktiengesellschaft	Germany	Time-Resolved Nucleation of the Early Stages of Bubble Growth in Foaming Polymers	Chemistry
2006067	BINDER Wolfgang	Martin-Luther Uni. Halle-Wittenberg, Institute of Chemistry, Halle	Germany	Determination of Nanoparticle Location in Block-co-Polymers via GISAXS	Chemistry
2006068	DESNICA Uros	Ruđer Bošković Institute, Zagreb	Croatia	Nanometer-size Germanium Quantum Dots produced by magnetron sputtering	Materials Science
2006120	TURKOVIC Aleksandra	Ruđer Bošković Institute, Zagreb	Croatia	Morphology and crystallization kinetics of solid polymer electrolyte (PEO)8ZnCl2 via combined Time-resolved synchrotron SAXS-WAXD techniques	Materials Science
2006123	MAJOR S S	Indian Institute of Technology Bombay, Powai, Mumbai	India	Study of intralayer Structure and molecular packing in Langmuir-Blodgett Multilayers and related Nanostructures	Materials Science

2006210	KRIECHBAUM Manfred	Institute of Biophysics and Nanosystems Research (IBN), Austrian Academy of Science (AAS), Graz	Austria	Structure of oriented lipids on solid support under hydrostatic pressure.	Life Sciences
2006216	RAPPOLT Michael	IBN, AAS, Graz	Austria	The structural properties of the collageneous membranes containing the antibiotic gentamycin	Life Sciences
2006221	VITERBO Davide	DISTA, Uni. del Piemonte Orientale, Alessandria	Italy	In situ SAXS study of the deposition of ordered mesoporous silica in composite materials for drug delivery	Chemistry
2006241	PISERI Paolo	Dipartimento di Fisica and CIMAINA, Università di Milano, Milano	Italy	Time resolved SAXS on free TiOx nanoparticles in a molecular beam	Materials Science
2006285	HODZIC Aden	IBN, AAS, Graz	Austria	Phosphatidyserine influence biological model membranes the human brain cells.	Life Sciences
2006329	PIVAC Branko	Ruđer Bošković Institute, Zagreb	Croatia	Ge nanostructures in SiO2 multilayers for memory devices	Materials Science
2006364	AMENITSCH Heinz	IBN, AAS, Graz	Austria	Evaporation Induced Self-Assembly of Nanoparticles in the Gasphase.	Materials Science
2006368	AMENITSCH Heinz	IBN, AAS, Graz	Austria	Ultrafast Nucleation and Growth Study of Calcium Carbonate by SAXS	Materials Science
2006374	MAIER Guenther	MCL Leoben and Dep. Materialphysics, Uni. of Leoben	Austria	Size effect in thin metallic films on polymer foils studied by in-situ SAXS/WAXS coupled with tensile tests and reflectance difference spectroscopy	Materials Science
2006389	SCHMID Fabian	IBN, AAS, Graz	Austria	2-dimensional Layer Specific Tensile Testing of Human Aorta	Life Sciences
2006440	TEIXEIRA Cilaine Veronica	Unity of Biophysics, Faculty of Medicine, Autonomous University of Barcelona, Spain	Spain	Study of the kinetics of formation of FDU-1 materials and the antibody loading and unloading in SBA-15.	Chemisty
2005051 LONG TERM	FALTA Jens	Institute of Solid State Physics, Uni. of Bremen	Germany	In-situ characterization of self-assembled nanoparticle films under harsh conditions	Materials Science

In-house research	BERNSTORFF Sigrid + PIVAC Branko	Sincrotrone Trieste + Ruđer Bošković Institute, Zagreb	Croatia	Structural analysis of annealed amorphous SiO/SiO2 superlattice	Materials Science
In-house research	AMENITSCH Heinz + SOLER-ILLIA Galo	IBN, AAS, Graz + Unidad de Actividad Quimica, San Martín, Buenos Aires	Argentina	In-situ SAXS/WAXS for characterisation of nanoparticle growth in mesoporous materials	Chemistry
In-house research	AMENITSCH Heinz + CARACCIOLO Giulio	IBN, AAS, Graz + Department of Chemistry, University of Rome "La Sapienza", Rome	Italy	Multi-component lipid/DNA complexes for gene delivery applications	Life Sciences
In-house research	BERNSTORFF Sigrid + GRIGORIEW Helena	Sincrotrone Trieste + Institute of Nuclear Chemistry and Technology, Warsaw	Poland	The gelation process of low-molecular-weight organic gelators.	Chemistry
In-house research	AMENITSCH Heinz + CARACCIOLO Giulio	IBN, AAS, Graz + Department of Chemistry, Uni. of Rome "La Sapienza", Rome	Italy	Mechanism of formation of lipoplexes	Life Sciences
In-house research	AMENITSCH Heinz, RAPPOLT Michael + BOYD Ben	IBN, AAS, Graz + Department of Pharmaceutics, Victoria College of Pharmacy, Monash University	Australia	Phase transitions in liquid crystalline dispersed particles: Thermodynamics, kinetics and mechanism of phase interconversion	Life Sciences
In-house research	BERNSTORFF Sigrid + GRACIN Davor	Sincrotrone Trieste + Ruđer Bošković Institute, Zagreb	Croatia	SAXS on nanocrystal silicon	Materials Science
In-house research	BERNSTORFF Sigrid + RADIC Nikola	Sincrotrone Trieste + Ruđer Bošković Institute, Zagreb	Croatia	Intergranullar matter in nanocrystalline nickel	Materials Science

User Statistics

1. Number of submitted proposals and assigned shifts from 1995 until December 2007

The Austrian SAXS-beamline at ELETTRA opened to users in September 1996. Since then many experiments have been performed related to the fields of life science, materials science, physics, biophysics, chemistry, medical science, technology and instrumentation.

From September 96 on users gained access to the SAXS-beamline on the basis of the proposals received for the periods shown in Fig. 1. The assignment of beamtime at this beamline is done separately for the group of "General Users" (GU) and the "Collaborating Research Group" (CRG), i.e., the Austrian users. Beamtime was assigned to the proposals of each group in the order of the rating received by the Scientific Committee, and up to the maximum number of shifts available to each group according to the contract between "The Austrian Academy of Sciences" and the "Sincrotrone Trieste". Until December 1997 up to 30 % of the beamtime was given to CRG, up to 55 % to GU, and 15% was reserved for maintenance purposes. From January 98 to June 2001 the quota for beamtime was up to 35 % for CRG, up to 50 % for GU, and again 15% reserved for maintenance purposes. From July 2001 on the two contingents for user proposals from CRG and GU receive up to 35% of the beamtime each. The remaining 30 % of beamtime are used for inhouse research projects as well as for maintenance purposes.

Figure 1 gives an overview of the numbers of received proposals, the numbers of requested and assigned shifts, as well as the percentage between assigned and requested shifts. Included in Fig.1 are also the same data for the period End 1995 - August 1996, during which some beamtime had been given already to users in order to perform first pilot- and test-experiments together with the beamline staff. These first experiments during the commissioning phase were not yet based on proposals, since the goal was mostly to evaluate and improve the performance of the beamline and the equipment of its experimental station. As can be seen in Fig.1, the request for beamtime at the SAXS-beamline increased continuously and strongly until the first half year of 1999 (also during the period Sept.-Dec. 1997, if one takes into account that this period was only 4 instead 6 month long, and that for this reason less proposals were submitted). Then, probably due to the high rejection rates, the number of submitted proposals decreased somewhat during 2001, which resulted in a better ratio of accepted / rejected proposals. This oscillating behaviour of beamtime request can also be seen for the period 2002 – 2007 where after higher numbers of submitted proposals slightly reduced request periods follow. The numbers for the second semester of 2007 reflect also that, due to the long shut-down from 1.10.2007 to 3.03.2008 (for the booster installation) less proposals were submitted, and less beamtime will be available.
In 2006, in total 73 proposals (15 from CRG, and 58 from GU) were submitted. From these 24 proposals (0 from CRG and 24 from GU) were submitted by "new" usergroups, i.e. groups which so far had never beamtime at the SAXS beamline. From these, 2 GU proposals were officially accepted.

Figure 1 (Next page). The statistical information about the beamtime periods since end of 1995 are given for the groups "CRG", and "GU" separately, as well as for both together ("Total"). Shown are, for all beamtime periods (from top to bottom):

- Number of received proposals, ● Number of requested shifts,
- Number of assigned shifts, and ● Relation between assigned and requested shifts

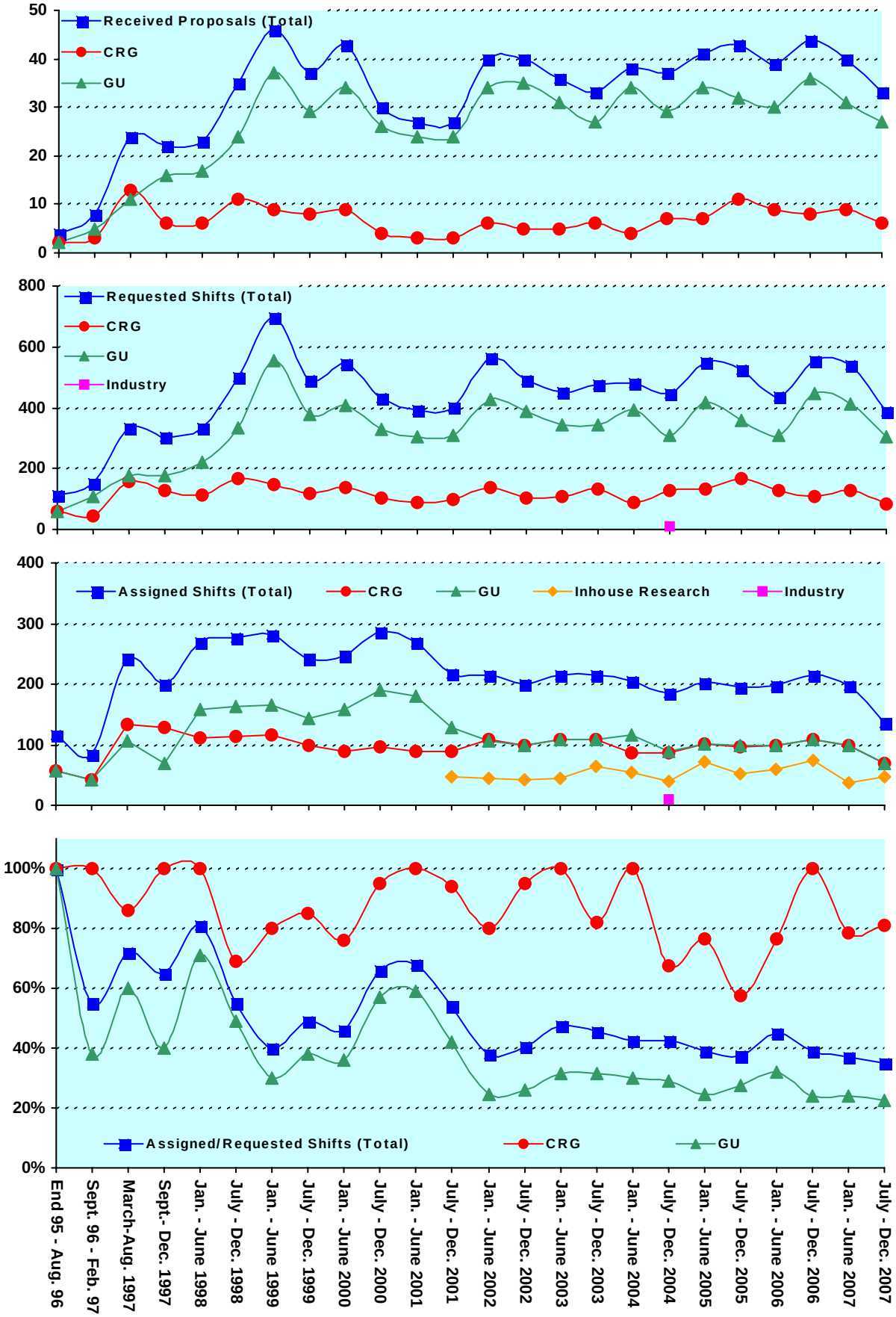
Received Proposals (Total)
CRG
GU
Requested Shifts (Total)
CRG
GU
Industry
Assigned Shifts (Total)
CRG
GU
Inhouse Research
Industry
Assigned/Requested Shifts (Total)
CRG
GU
End 95 - Aug. 96
Sept. 96 - Feb. 97
March-Aug. 1997
Sept.- Dec. 1997
Jan. - June 1998
July - Dec. 1998
Jan. - June 1999
July - Dec. 1999
Jan. - June 2000
July - Dec. 2000
Jan. - June 2001
July - Dec. 2001
Jan. - June 2002
July - Dec. 2002
Jan. - June 2003
July - Dec. 2003
Jan. - June 2004
July - Dec. 2004
Jan. - June 2005
July - Dec. 2005
Jan. - June 2006
July - Dec. 2006
Jan. - June 2007
July - Dec. 2007

2. Provenience of users

During 2006, 169 users from 62 institutes in 21 countries have performed experiments at the SAXS beamline. In Fig. 2 are shown both the provenience of these users, and of their respective institutes. Each user or institute was counted only once, even though many users performed experiments in both beamtime periods of 2006.

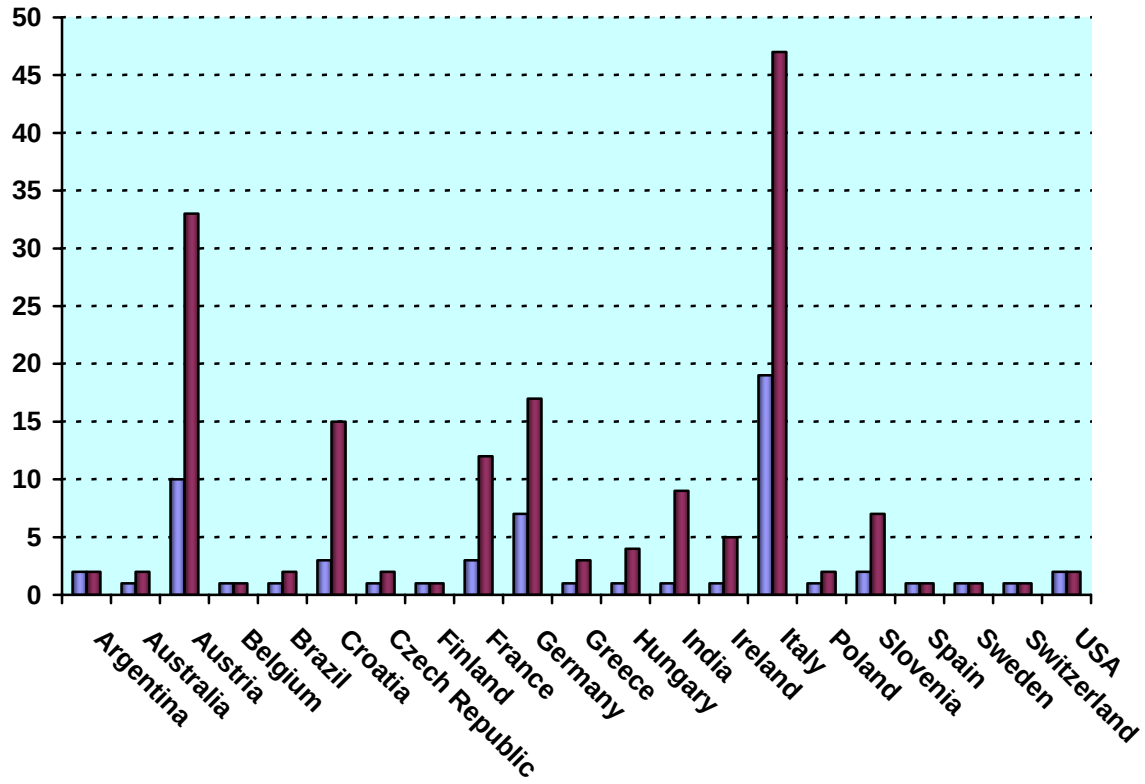

Figure 2. Provenience of users (dark grey) and of their corresponding institutes (light grey).

3. Documentation of experimental results

As could be expected, with the start of user-operation at the SAXS-beamline the number of contributions to conferences started to increase strongly. With a delay of one year - the average time needed for paper publications - also the number of publications increased accordingly, as can be seen in Fig. 3.

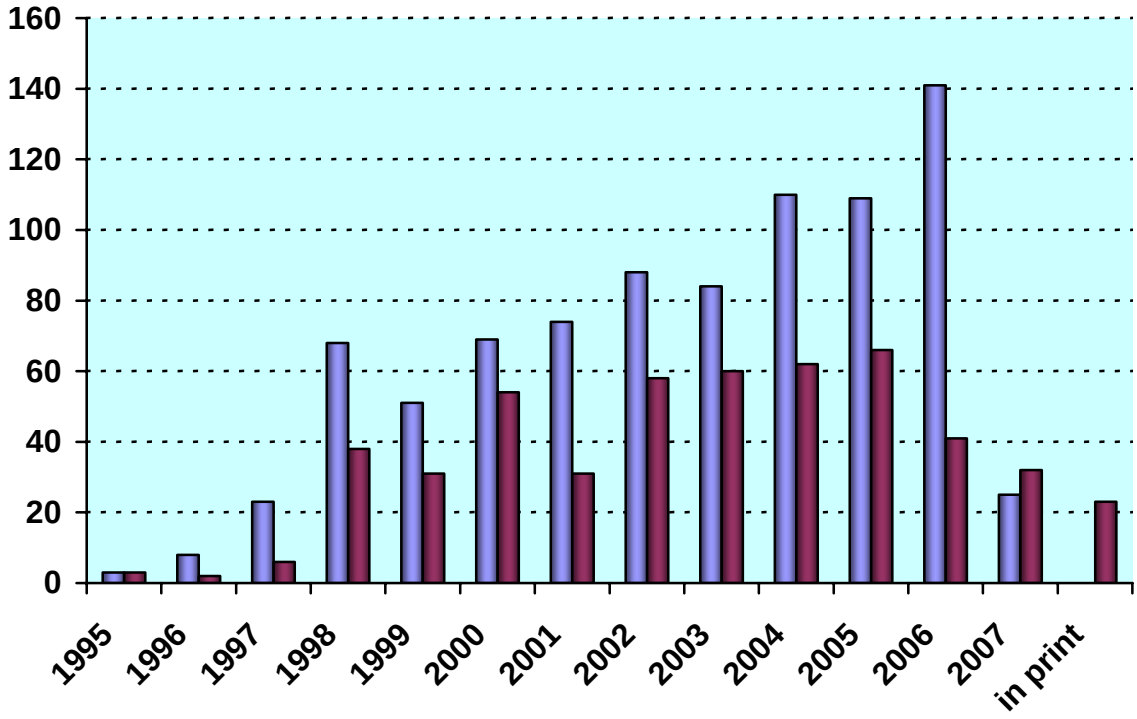

Figure 3. Number of conference contributions (light grey) and of refereed paper publications (dark grey) for the years 1995-2006. Also contributions, which have been published until June 2007 as well as those in print at that time are included.

In addition, from 1995 until June 2007, the following documentations based on instrumentation of the SAXS-beamline, or on data taken with it, have been produced.

Unrefereed publications:

Technical Reports on Instrumentation:	5
Contributions to Elettra Newsletters:	15
Contributions to Elettra Highlights:	24
Habil Thesis:	3
PhD Thesis:	56
Master Thesis :	27

Experimental Possibilities at the SAXS-beamline

1. LATEST DEVELOPMENTS

Vantec Detector

In the beginning of 2007, the SAXS group has purchased a one-dimensional high count rate capable Vantec-1 Detector from BrukerAXS Inc (see Fig. 1). It has a rather large active area of 50 x 16 mm and reaches a spatial resolution of about 50 µm, which is smaller than the resolution obtained by the presently used Gabriel Type Gas detectors. Moreover its new gas amplification principle based on the Microgap technology [1] allows much higher count rates compared to the old system. Now the main limitation is the data acquisition system with its maximum integral count rate of about 1 MHz. First tests have shown that the new detector based on the delay line principle can be directly integrated in the present data acquisition system HCI (Hecus X-ray Systems, Graz, Austria) of the beamline maintaining its performance with respect to time resolution and integral count rate [2].

Minimal time resolution: 11 µs
Maximum No. of frames: 512 (depending on the no. of channels)
Maximum integral count rate: 1 MHz

Fig. 2 is an example of the high count rate performance of the new Vantec-1 detector. In this figure the resulting diffraction pattern of dry rat tail tendon collagen are shown by varying the primary intensity. It has been demonstrated that measurements with an integral count rate of up to 700 kHz cause no distortion of the diffraction pattern. Please note that the maximum count rate of the old system would be 50 kHz.

Figure 1. Photograph of the Vantec 1 detector

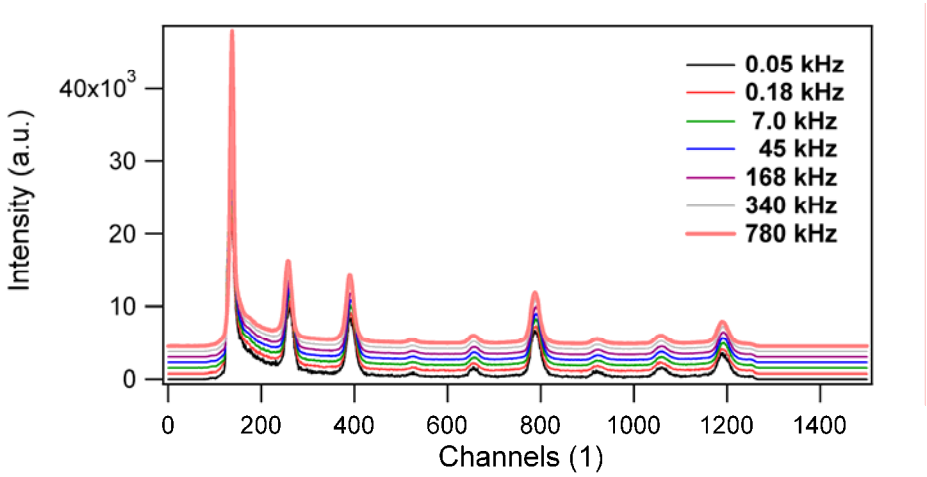

Figure 2. Stacked diffraction pattern of dry rat tail tendon collagen measured at various count rates. No local saturation effects have been detected.

To demonstrate the high time resolution we repeated a chopper experiment from reference 2 applying the new detector. We imprinted a time structure in the primary intensity by using a fast rotating copper wheel (up to 30000 rpm) and triggered the data acquisition system. As test diffraction pattern we used again dry rat tail tendon collagen. The results of the experiments are shown in Figure 3, in which the time resolved diffraction pattern during the passing of two holes of the chopper wheel rotating with 6 kHz are shown. 1000 single experiments have been summed for this figure.

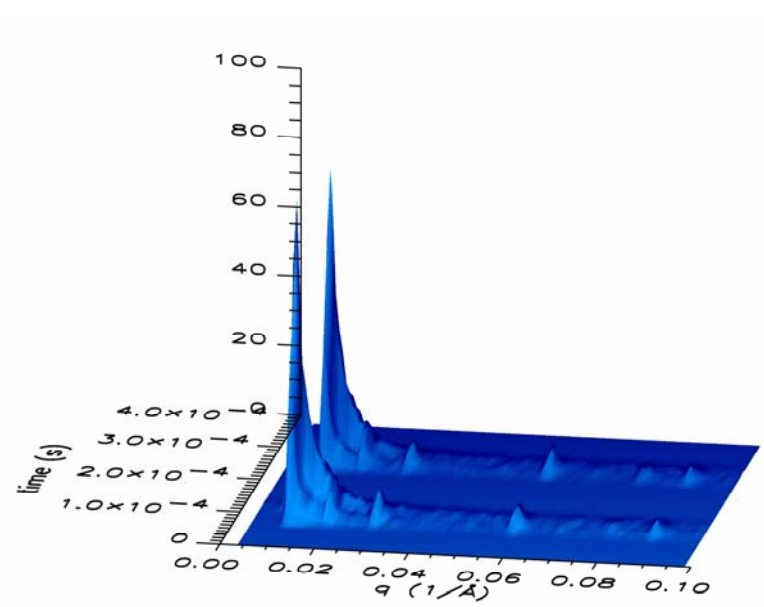

Figure 3. Time resolved results of dry rat tail tendon collagen during the passage of 2 holes of the chopper. The chopper was operated with a 48 hole disc (diameter of 1 mm) with a frequency of 6 KHz.

[1] US Patent US 6,340,819 B1
[2] H Mio et. al., NIMA **392**, (1997), 384

2. ACCESSIBLE SAXS AND WAXS RANGES

Simultaneous SAXS- and WAXS-measurements can be performed using a linear sensitive gas detector (Gabriel type, windows size 8 x 100 mm, active length 86.1 mm with a resolution of 0.135 mm/channel) for the WAXS-range, and either a second linear Gabriel type detector (windows size 10 x 150 mm, active length 134 mm with a resolution of 0.159 mm/channel), or the 2D CCD-system for the SAXS-range. A specially designed vacuum chamber (SWAXS-nose, see Annual Report of 1996/97, p. 32) allows to use both scattering areas below (for SAXS) and above (for WAXS) the direct beam, respectively.

Depending on the photon energy maximum SAXS resolutions of 2000 Å (5.4 keV), 1400 Å (8 keV) or 630 Å (16 keV) are available. The available possible WAXS-ranges are summarised in Table 1. The overall length of the SWAXS-nose in the horizontal direction, measured from the sample position, is 512 mm and the fixed sample to WAXS-detector distance is 324 mm. At the shortest SAXS camera-length an overlap in the d-spacings covered by the SAXS- and WAXS-detectors, respectively, is possible: then, the common regime lies around 9 Å.

Table 1. Possible d-spacing ranges in the WAXS-regime at the SAXS-beamline at ELETTRA. Since the WAXS-detector can be mounted at four different fixed positions on the SWAXS-nose (range 1-4), with the three possible energy choices (5.4, 8 and 16 keV) this results in 12 different d-spacing regimes. In italic the most common choice (8 keV, range 1) is highlighted. This range is suited for experiments, e.g., on lipid-systems and (bio)polymers.

Range	2θ [deg]	d-spacing (Å)		
		8 keV	5.4 keV	16 keV
1	9.4	*9.40*	14.03	4.27
	27.6	*3.23*	4.82	1.47
2	27.4	3.25	4.86	1.48
	45.6	1.99	2.97	0.90
3	45.4	2.00	2.98	0.91
	63.6	1.46	2.18	0.66
4	63.4	1.47	2.19	0.67
	81.6	1.18	1.76	0.54

3. CALIBRATION OF THE S-AXIS AND FLAT FIELD CORRECTION

At the SAXS beamline various standards are used for the angular (s-scale) calibration of the different detectors:

- Rat tail tendon for the SAXS detector - high resolution (rtt*.dat)
- Silver behenate for the SAXS detector – medium and low resolution (agbeh*.dat)
- Para-bromo benzoic acid for the WAXS detector – WAXS range 1 and 2 (pbromo*.dat)
- Combination of Cu, Al foils and Si powder for the WAXS detector – WAXS range 2 and higher

In Figure 2 a typical diffraction pattern of rat tail tendon is shown, depicting the diffraction orders (from the first to the 14th order) measured with a "high" resolution set-up (2.3 m) and the delay-line gas detector. The d-spacing is assumed to be 650 Å, but this value can vary depending on humidity up to 3%. Thus, the rat tail tendon is often used only to determine the position of the direct beam (zero order), while the absolute calibration is performed using the diffraction pattern of Silver behenate powder. Fig. 3 depicts a diffraction pattern of Silver behenate measured with "medium" resolution set-up (1.0 m) from the first to the 4th order (repeat spacing 58.4 Å) [1].

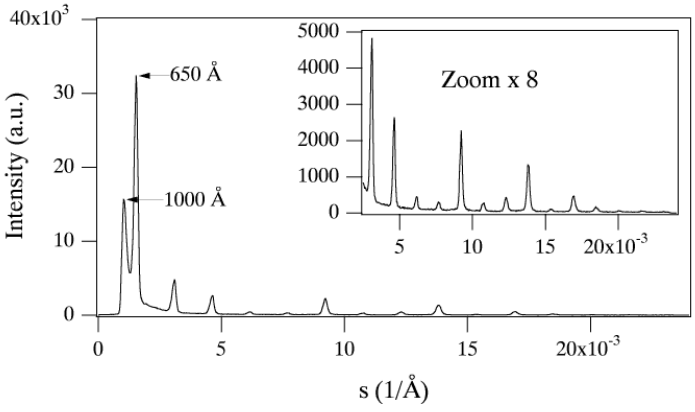

Figure 2. SAXS diffraction pattern of the collagen structure of rat tail tendon fibre at a distance of 2.3 m.

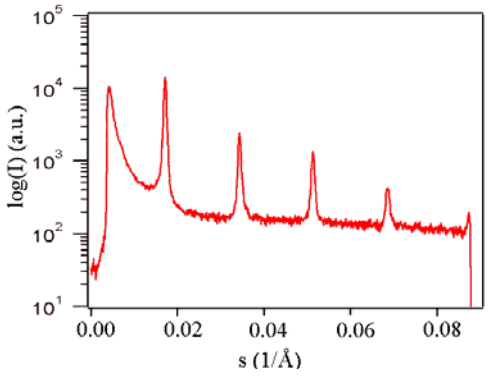

Figure 3. SAXS diffraction pattern of Ag behenate powder at a distance of 1.0 m

In Fig. 4 a typical WAXS pattern of p-bromo benzoic acid is shown. The diffraction peaks are indexed according to the values given in Table 2, taken from [2].

Table 2. d-spacings and relative intensities of p-bromo benzoic acid according to [2].

d-spacing/Å	rel. intensity	d-spacing/Å	rel. intensity
14.72	18000	4.25	490
7.36	1200	3.96	2380
6.02	330	3.84	10300
5.67	980	3.74	26530
5.21	6550	3.68	1740
4.72	26000	3.47	760

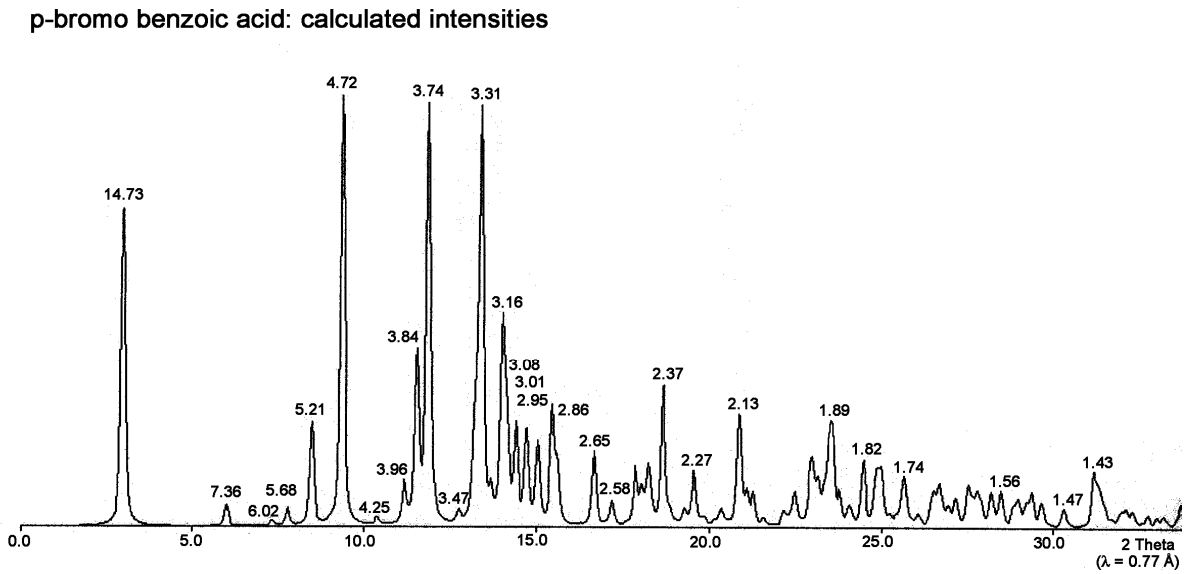

Figure 4. Calculated diffraction pattern of p-bromo benzoic acid. d-spacings are given in Å.

The s-scale for both, the SAXS and the WAXS range, can be obtained by linear regression, i.e., the linear relation between the kown s-values of the calibrant versus the measured peak positions has to be found.

A further correction is regarding the flat field response (efficiency) of the detectors. For this correction, the fluorescence light of various foils are used to illuminate the detectors rather homogeneously:

At 8 keV: iron foil (100 μm thick), fluorescence energy: 6.4 keV K_α, 7.1 keV K_β (effic*.dat)
At 16 keV: copper foil (> 100 μm thick), fluorescence energy: 8.028 keV $K_{\alpha 2}$, 8.048 keV $K_{\alpha 1}$, 8.905 keV K_β (effic*.dat)

The measured scattering pattern are corrected for the detector efficiency simply by dividing them by the fluorescence pattern. Note: The average of the detector efficiency data should be set to unity and a small threshold should be applied to avoid any division by zero.

[1] T.N. Blanton et. al., Powder Diffraction 10, (1995), 91
[2] K. Ohura, S. Kashino, M. Haisa, J. Bull. Chem. Soc. Jpn. 45, (1972), 2651

4. ELETTRA VIRTUAL COLLABORATORY

During 2005, a new possibility for data file sharing between ELETTRA and external laboratories went into operation. The Elettra Virtual Collaboratory (EVC) is a collaborative virtual environment (i.e., a computer system that supports human to human and human to machine communication and collaboration) for X-ray experiments at the Elettra Synchrotron Light Laboratory, Trieste, Italy. The EVC allows a distributed team of researchers to share experimental data, exchange ideas, discuss problems, from data collection to results publication.

Connecting to https://evc.elettra.trieste.it/ with a web browser it is possible to enter the EVC environment. A new user can easily register from any PC workstation at ELETTRA filling in a dedicated form in the EVC web page. An already registered user then can login, open a new project folder, add new members, who will share all the information and files of the project, and operate on all projects he takes part in. However, we note these actions can only be carried out from an ELETTRA intranet workstation.

From home a registered user can download the experimental data via web browser, work on them and perform a data backup in his own PC workstation: thus a researcher can partecipate in an experimental session even if not physically present at ELETTRA. In the near future, it will also be possible to perform the data reduction online, through the web browser.

A system for data backup on DVD is also available on the EVC workstation at the SAXS beamline. For more informations, please have a look at the EVC web page, https://evc.elettra.trieste.it/

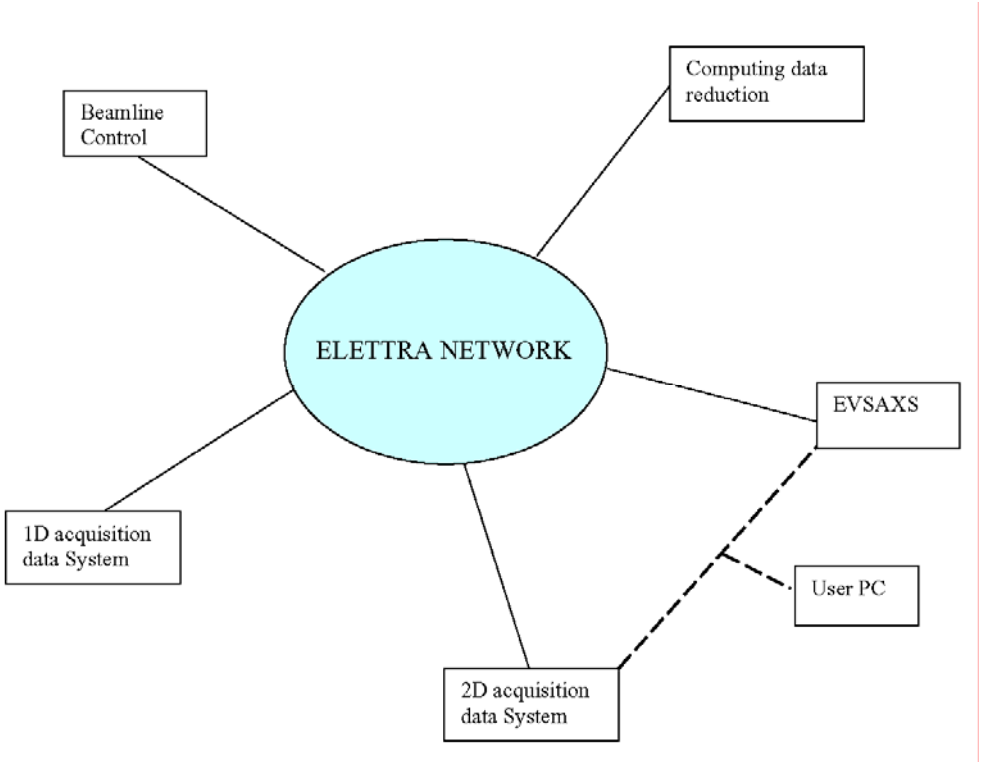

Figure 5. Overview of the local network of the SAXS beamline at ELETTRA

5. SITE LABORATORIES

In August 2002 our new chemistry and X-ray laboratory went into operation. The 70 m^2 big laboratory is divided in two parts, in which the bigger share of 43 m^2 is occupied by the chemistry lab. This unit serves mainly for sample preparation and analysis for both, in house research and external SAXS user groups. In the X-ray laboratory the set-up of a SWAX camera for simultaneous small and wide angle scattering has been completed (Hecus X-ray Systems, Graz, Austria: www.hecus.at), which allows on-site testing of samples before moving on to the SR beamline. The chemistry lab is meanwhile equipped with:

- micro centrifuge (max. 13200 rpm; model 5415D from Eppendorf , Hamburg, Germany)
- chemical fume hood (model GS8000 from Optolab, Concondordia, Italy)
- vacuum drying oven (min. pressure 1 mbar; max. T: 200 °C; Binder WTB, Tuttlingen. Germany)
- balance (min.-max.: 0.001 - 220 g; model 770 from Kern & Sohn, Balingen, Germany)
- magnetic stirrer with heating plate and a vortexer for microtubes (model MR 3001 and REAX; both from Heidolph, Schwabach, Germany)
- two water baths (the model Unistat CC is freely programmable in range from -30 to 100 °C from Huber, Offenburg, Germany; the model M3 from Lauda can only heat; Lauda-Könighofen, Germany)
- ultrasonic bath (VWR International, Milano, Italy)

Further, two working benches (one with a water sink), two fridges and a separate freezer (- 20 °C), standard glassware, syringes and needles of different sizes, µ-pipettes (10 - 50 - 200 - 1000), as well as some standard solutions (e.g., chloroform, ethanol, methanol) and de-ionized water are available.

Figure 6.
Typical lab activity: Barbara Sartori loads the centrifuge (September 2003).

6. AVAILABLE SAMPLE MANIPULATIONS STAGES

1. General

Usually the sample is mounted onto the sample alignment stage which allows the user to place the sample into the beam with a precision of 5 μm (resolution: 1 μm). In Fig. 7 the ranges for vertical and horizontal alignment as well as the maximum dimensions of the sample holders are given. The maximum weight on the sample stage is limited to 10 kg. In case the envelope dimensions of a sophisticated sample station provided by the users are slightly larger than those given in Fig. 7, the user can ask the beamline responsible for a check up of his space requirements. If it does not fit at all to these specifications, user equipment can also be mounted directly onto the optical table, which allows much larger spatial dimensions.

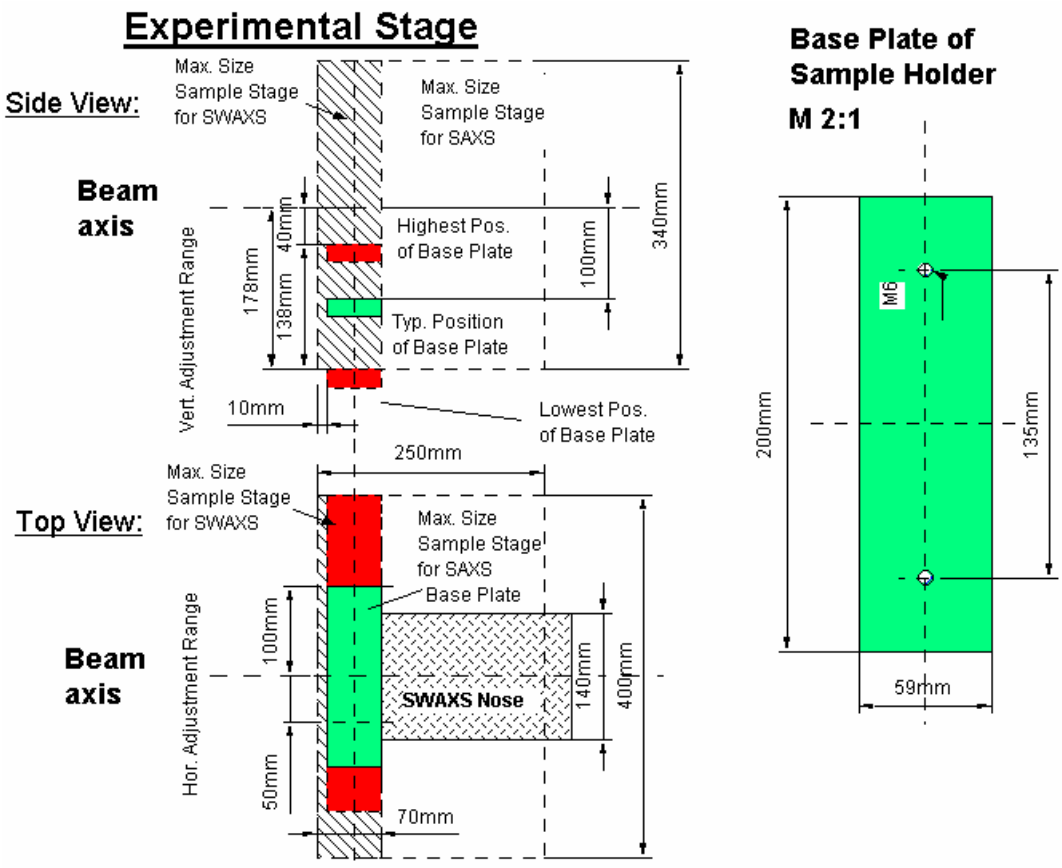

Figure 7. Maximum dimensions and alignment range of the sample holder to be mounted via a base-plate onto the standard alignment stage (left), and dimensions of the base-plate (right).

2. Sample Holders

As standard equipment for liquid samples Paar capillaries (diameter: 1 and 2 mm) are used thermostated with the KHR (electrical heating) or KPR (Peltier heating/cooling) sample holders (Anton Paar, Graz, Austria). For use in these sample holders flow through capillaries and Gel holders are standard equipment. Temperature scans can be performed with KHR (25-300 °C) or KPR (-30-70 °C). Typically the precision and the stability of this systems is 0.1 °C. Additionally thermostats for temperature control or cooling proposes can be used at the

beamline (-40 - 200 °C). Helium and Nitrogen gas bottles are available at the beamline, for other gases please contact the beamline responsible.
Multiple-sample holders can be mounted onto the standard sample manipulator. At present holders are available for measuring in automatic mode up to 30 solid samples at ambient temperature or up to 4 liquid or gel samples in the temperature range 0 – 95 °C.

3. Online Exhaust System

At the experimental station is available a custom-built fume cover and chemical exhaust system for toxic gases. Thus it is possible to e.g. study in-situ chemical reactions, during which toxic gases might develop.

4. Stopped Flow Apparatus

A commercial stopped flow apparatus (manufactured by Bio-Logic, Paris, France), especially designed for Synchrotron Radiation SAXS investigations of conformation changes of proteins, nucleic acids and macromolecules, is available. The instrument consists of a 4 syringe cell with 3 mixer modules manufactured by Bio-Logic. Each syringe is driven independently from the others by an individual stepping-motor, which allows a high versatility of the mixing sequence (flow-rate, flow duration, sequential mixing). For example, injection sequences using one or up to 4 syringes, unequal filling of syringes, variable mixing ratio, reaction intermediate ageing in three- or four-syringe mode etc.. The solution flow can be entirely software-controlled via stepping motors, and can stop in a fraction of a millisecond.

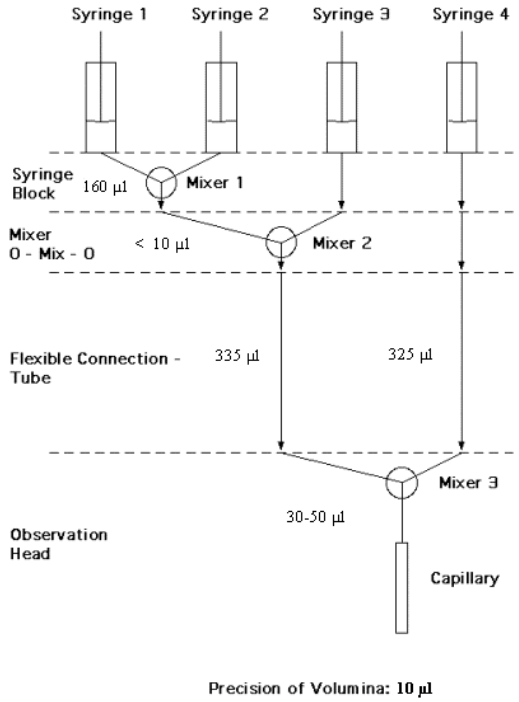

The software allows the set-up of the shot volumes of each of the 4 syringes in a certain time interval. Up to 20 mixing protocols can be programmed. Additionally macros for the repeated execution of individual frames can be defined. Furthermore, the input and output trigger accessible for user operation can be programmed. In the usual operation modus the start of rapid mixing sequence is triggered from our X-ray data-acquisition system (input trigger).

After the liquids have been rapidly mixed, they are filled within few ms into a 1 mm quartz capillary - situated in the X-ray beam- , which is thermostated with a water bath. Depending on the diffraction power of the sample time resolutions of up to 10 ms can be obtained.

Figure 8. Sketch of the stop flow system.

The main parameter of the system are:

- Thermostated quartz capillary (1 mm)
- Temperature stability 0.1 °C
- Total sample used per mixing cycle (shot volume): 100 µl
- Maximum 2θ angle of 45°
- Total Volume 8 ml
- Dead volume 550 µl
- Speed: 0.045 – 6 ml/s
- Duration of flow 1 ms to 9999 ms/Phase
- Dead time: 1 ms
- Reservoir volume: 10 ml each

Further information can be found at the webpage: http://www.bio-logic.fr/

5. Grazing Incidence Small Angle X-ray Scattering

Grazing incidence studies on solid samples, thin film samples or Langmuir-Blodget-films can be performed using a specially designed sample holder, which can be rotated around 2 axes transversal to the beam. Furthermore the sample can be aligned by translating it in both directions transversal to the beam. The precisions are 0.001 deg for the rotations and 5 µm for the translations. Usually the system is set to reflect the beam in the vertical direction. According to the required protocol and the actual assembly of the rotation stages ω, θ, 2θ and φ scans can be performed.

6. Temperature Gradient Cell

A temperature gradient cell for X-ray scattering investigations on the thermal behaviour of soft matter manybody-systems, such as in gels, dispersions and solutions, has been developed. Depending on the adjustment of the temperature gradient in the sample, on the focus size of the X-ray beam and on the translational scanning precision an averaged thermal resolution of a few thousands of a degree can be achieved.

7. Flow-through Cell

The flow through cell works in a simple manner: Special quartz capillaries (Glas Technik & Konstruktion, Schönwalde/Berlin) of 1.5 mm diameter and wide openings of about 3 mm at each end, can be inserted into the standard Anton Paar sample holder, which allows various temperature treatments (T-range 25-300 or –30-70 °C, respectively). Thin tubes are connected directly to the capillary ends and a constanst flow is achieved by a peristaltic pump.

8. IR-Laser T-Jump System for Time-Resolved X-ray Scattering on Aqueous Solutions and Dispersions

The Erbium-Glass Laser available at the SAXS-beamline (Dr. Rapp Optoelektronik, Hamburg, Germany) delivers a maximum of 4 J per 2ms pulse with a wavelength of 1.54 µm onto the sample. The laser-beam is guided by one prism onto the sample, which is filled in a glass capillary (1 or 2 mm in diameter) and Peltier or electronically thermostated in a metal sample holder (A. Paar, Graz, Austria). With a laser spotsize of maximal 7 mm in diameter a sample-volume of maximal 5.5 µl or 22 µl, respectively, is exposed to the laser-radiation. In a water-solutions/dispersions with an absorption coefficient of A = 6.5 cm^{-1} T-jumps up to 20°C are possible.

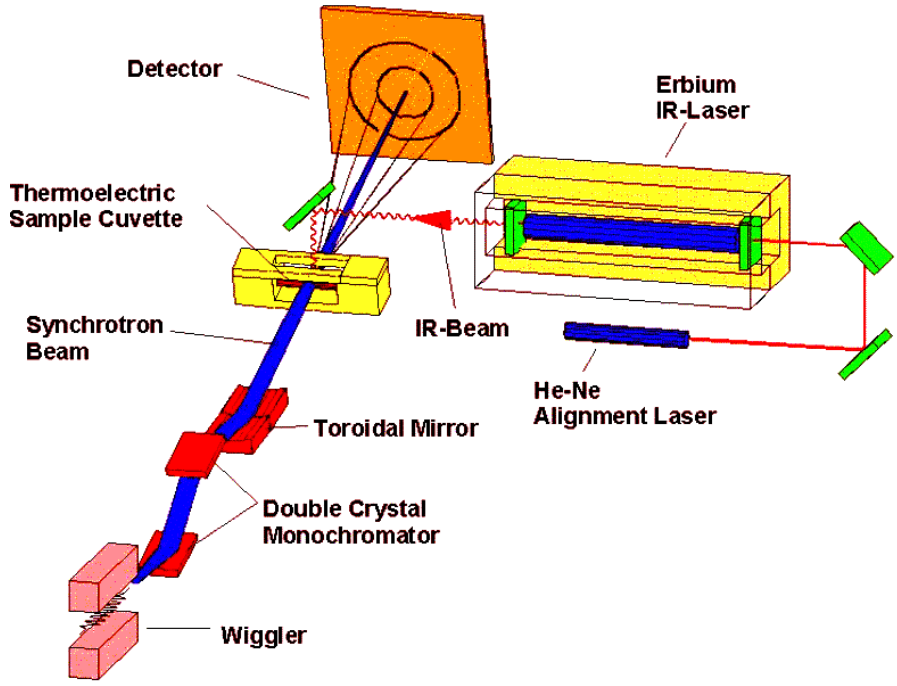

Figure 9. Sketch of the T-jump set-up.

9. High Pressure Cell System

SWAXS measurements of samples under pressure can be performed from 1 to 2500 bar, from 0 to 80 °C in the scattering angle region up to 30 degrees, both in the static or time-resolved mode, e.g. p-jump or p-scan, with a time-resolution down to the ms range. Precise pressure scans of any speed within a broad range (e.g. ca. 1.0 bar/s - 50 bar/s in the case of water as pressurising medium, and a typical sample volume) can be performed. Alternatively, dynamic processes can be studied in pressure-jump relaxation experiments with jump amplitudes up to 2.5 kbar/10ms in both directions (pressurising and depressurising jumps).
In most applications diamond windows of 0.75 mm thickness (each) are used. The transmission of one pair (entrance and exit window) is 0.1 at 8 keV, i.e. lower than 0.3, the value for the originally used 1.5 mm thick Be-windows. However the loss in intensity is more than compensated for by the considerably lower background scattering of diamond thus leading to higher q-resolution in the experiments.
The sample thickness can be 0.6-4.0 mm, with a volume of approximately 0.5-3 mm^3 completely irradiated by pin-hole collimated (< 1.0 mm diameter) X-rays.
The pressure cell system is flexible and can be built according to the needs of the particular experiment. Normally, a liquid (water, ethanol or octanol) is used as pressurising medium.

But in principle, also gaseous media can be employed as well. N_2 has been successfully tested, and measurements in supercritical CO_2 became frequent.
Beside bulk measurements on samples in transmission set-up, also grazing incidence experiments using silicon wafer with highly aligned samples on its surface inserted in the high-pressure cell have been carried out successfully.

10. Oxford Cryostream Cooler

The Cryostream cooler creates a cold environment only a few millimeters from the nozzle position. The temperature and the flow of the nitrogen gas stream is controlled and regulated by a Programmable Temperatur Controller based on an 'in stream' heater and a thermo-sensor before it passes out over the sample.

The system has been especially developed for X-ray crystallography to perform diffraction experiments on e.g. shock frozen bio-crystals. However, the programmable temperature controller allows further implication for SAXS-experiments, e.g., rapid temperature drops in solvents. The design of the Cryostream Cooler facilitates:

- Nitrogen stream temperatures from -190 to 100 °C
- Stability of 0.1 °C,
- Refill without any disturbance of the temperature at the sample
- Temperature ramps can easily be carried out remotely controlled with scan rates up 6 °C/min
- Individual temperature protocols can be cycled
- T-jumps in both directions can be performed by rapid transfer of the sample in a pre-cooled or -heated capillary using an fast syringe driver reaching a minimum temperature of -80 °C. Here, typical scan rates are about 15 °C/sec with a total process time in the order of 10 sec.

Further information can be found at the webpage: http://www.oxfordcryosystems.co.uk/

11. In-line Differential Scanning Calorimeter (DSC)

The in-line micro-calorimeter built by the group of Michel Ollivon (CNRS, Paris, France) allows to take simultaneously time-resolved synchrotron X-ray Diffraction as a function of the Temperature (XRDT) and high sensitivity DSC from the same same sample.
The microcalorimetry and XRDT scans can be performed at any heating rate comprised between 0.1 and 10 °C/min with a 0.01 °C temperature resolution in the range -30/+130 °C. However, maximum cooling rates are T dependent and 10°C/min rates cannot be sustained below 30°C since cooling efficiency is a temperature dependent process. Microcalorimetry scans can be recorded independently, and also simultaniously, of X-ray patterns. The microcalorimeter head can also be used as a temperature controlled sample-holder for X-ray measurements while not recording a microcalorimetry signal. Isothermal microcalorimetry is also possible when a time dependent thermal event such as meta-stable state relaxation or self-evolving reaction, is expected. The sample capillaries have a diameter of 1.5 mm and are filled over a length of 10 mm.

12. The 2D CCD-camera System

The CCD has a 115 mm diameter input phosphor screen made of a gadolinium oxysulphide polycrystalline layer. The screen is coupled by means of a fiber optic to the image intensifier. The image intensifier is coupled again with an additional taper to the CCD itself. The achieved spatial resolution of a pixel is 79 μm for the whole set-up.
The number of pixels is 1024 x 1024 and they can be pinned down to 2 x 2 and 4 x 4. The dynamic range of the CCD is 12 bit. The dark current of the CCD is in the order of 100 ADU (off-set) and the readout noise (read out speed: 10 MHz) is in the order of 6 ADU. (The CCD is cooled by multistage Peltier element for reducing the dark noise.) The intensifier gain is adjustable between 200 and 20000 photons full dynamic range. Typical readout times and exposure times are 150 ms and 100 ms, respectively. The readout times can be reduced down to 100 ms by using the pinning mode of the CCD. Between the frames additional wait times can be programmed e.g. for reducing the radiation damage in the sample or to extend the time for measuring long time processes.
For the external control a TTL trigger signal is provided (active low, when the CCD is accumulating an image), which is used to control the electromagnetic fast shutter of the beamline on one hand. On the other hand this signal can be used also to trigger processes as requested by the user.
The CCD is controlled by Image Pro+, which also includes non too sophisticated data treatment capabilities. The program is featuring a comprehensive set of functions, including:

- flat fielding/background corrections
- enhanced filters and FFT
- calibration utilities (spatial and intensity)
- segmentation and thresholding
- arithmetic logic operations
- various measurements, like surface, intensity, counts, profiles
- advanced macro management

The data are stored in 12 bit – TIFF format. At the present state up to 300 full images (1024 x 1024) can be recorded by the system, but a strict conservation of the timing sequence is maintained only for the first 15 - 17 frames until the RAM memory is full. Afterwards the images are stored in the virtual memory on the hard disk. At present a software development for the CCD readout system is under way to improve the stability of the readout cycles.
For the treatment of the 2D-data the programe FIT2D of Dr. Andy Hammersley is used. It allows to perform both interactive and 'batch' data processing. Furthermore FIT2D supports spatial, flat field and background corrections and elevated data-treatment like circular integration, segment integration and similar can be performed (see also the webpage: http://www.esrf.fr/computing /expg/subgroups/data_analysis/FIT2D/index.html).

13. Tension Cell

Together with the external user group Schulze-Bauer/Holzapfel the research team constructed a general-purpose tension cell. This particular cell was designed for *in-situ* tensile testing with the particular feature that the sample could be completely immersed in a solvent (e.g. physiological solution), which is of particular interest for the blood vessel or collagen fiber testing. The sample container can be attached to a thermal bath to control the temperature in the range from 5 to 95 ºC. A screw with an appropriate opening for the passage of the X-ray beam can adjust the optical thickness of the sample container continuously and optimize the set-up for different sample geometries.
The fully remote controlled system allows to control not only the fiber extension from 0 to 50 mm, but also it records simultaneously the force signal in the range from 0 to 25 N and as an option the optically determined Video extensometer signal to measure the transversal contraction of the sample.

User Contributions

1. Materials Science

SELF-ORGANIZATION OF GERMANIUM QUANTUM DOTS IN MULTYLAYERS PRODUCED BY MAGNETRON SPUTTERING

U.V. Desnica[1], M. Buljan[1], P. Dubcek[1], K. Salamon[2], I.D. Desnica-Frankovic[1], and S. Bernstorff[3]

1.) R. Boskovic Institute, Bijenicka 54, 10000 Zagreb, Croatia
2.) Institute of Physics, 10000 Zagreb, Croatia
3.) Sincrotrone Trieste, SS 14 km163.5, 34012 Basovizza, Italy

Semiconductor materials in the form of Quantum Dots (QDs) display a significant dependence of electronic, optical and other properties on the size of nanoparticles, which opens a large number of potential applications in semiconductor and other industries [1-5]. Specifically, physical properties of nano-Ge material makes it suitable for many electronic, optoelectronic and photonic applications, including integrated opto-couplers in micro-systems in biotechnology, etc [1]. If QDs can be produced to be ordered in 3D dimension (the superlattice, i.e. QDs ordered analogously to atoms in crystal lattice), new very exciting possibilities for designing new materials are obtained [6,7] via combination of versatile geometrical arrangements [7,8] and QDs superlative properties [10].
The samples are prepared by deposition of 20 alternating (Ge+SiO_2) and SiO_2 bi-layers in a multisource magnetron sputtering KJLC CMS-18 system. The molar ratio of Ge: SiO_2 was 40:60 in the mixed layers, while SiO2 layers served as spacers. This report presents a few examples of the most interesting results obtained by the Grazing Incidence Small Angle X-ray Scattering (GISAXS) technique in studying the synthesis of Ge GDs, their properties and self-organization of Ge QDs in SiO2 after co-deposition at various deposition temperature, Td, followed by thermal treatment at Ta = 800^o C.

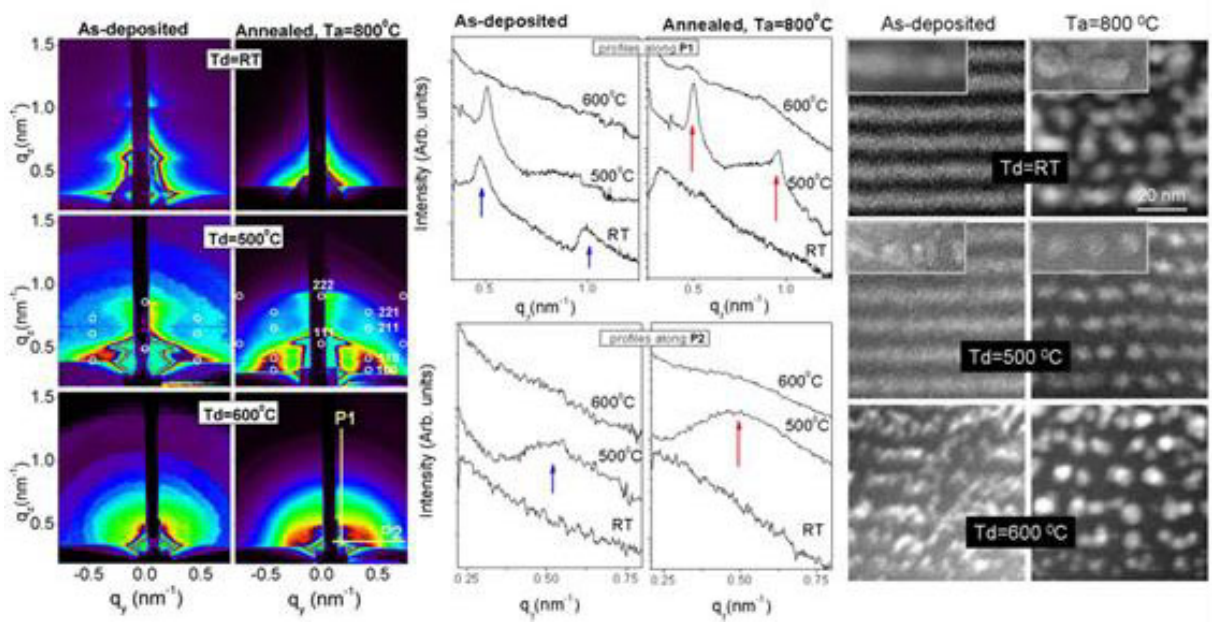

Figure 1. LEFT: 2D GISAXS patterns from the samples with Ge+SiO2 /SiO2 layers (thickness: 8 nm each) co-deposited with magnetron sputtering at different temperatures before (left column) and after subsequent thermal annealing for 1h at 800^{0}C (right column). Open circles denote the positions of Bragg peaks, for rhomobohedral QDs ordering, simulated by the NANOCELL code. MIDDLE: Intensity profiles of GISAXS patterns from the samples shown in the LEFT Figure, taken along the lines indicated by P1 and P2. RIGHT: TEM and HRTEM from the same samples, before (As-deposited), and after annealing.

Figure 1 demonstrates the formation of a QDs superlattice, obtainable under specific experimental conditions. Different characteristics of GISAXS patterns of the as-deposited samples (Fig. 1, left column) show that clustering and ordering of deposited material are very sensitive to the deposition temperature. The sample deposited at RT shows well defined Bragg sheets parallel to the qy axis. This indicates that the Td = RT sample has a layered structure, but with no evidences of cluster formation (weak form-factor contribution) or in-layer ordering. Such result indicates small diffusion rates of deposited material: the deposited Ge atoms are homogenously distributed through the mixed ($Ge+SiO_2$) layers which are separated by SiO_2 layers. Thermal annealing of this sample resulted in formation of Ge clusters within the mixed layers (strong diffuse signal combined with Bragg sheets parallel to the qy axis), but without spatial correlations. Deposition at Td=500 ^{0}C results in formation of the 3D ordered structure of QDs. Regular QDs ordering in this sample is evidenced by the appearance of Bragg diffraction peaks (maxima of interference function) with both q components different from zero. The arrangement of peaks is typical for a rhombohedral ($R\bar{3}m$) structure, as found by the NANOCELL code [11]. Ge QDs are hexagonally ordered in layers, which have a FCC-like ABCABC stacking sequence. The diffuse background (form factor contribution) suggests an elongated shape of the QDs. The period of bi-layers calculated for the Bragg peak positions is (13± 1 nm). After annealing, the initially formed QD superlattice retains its structure, what is reflected in a very similar Bragg peaks arrangement for the annealed sample. Small differences in the shape and precise position of the Bragg peaks reveal changes in the QDs shape (they become spherical) and arrangement, with parameters very close to a rhombohedral unit cell. For Td=600 ^{0}C, the QDs formation is very pronounced already during the deposition. Weakly resolved Bragg peaks in the GISAXS pattern indicate that the formed QDs have a poor in-layer ordering, as well as a disturbance of the layer structure. Annealing at Ta=800^0 C results in spherical QDs in all samples. TEM cross-sections (Fig. 1, RIGHT) support the findings from the GISAXS analysis. We also demonstrated by Raman spectroscopy (not shown) that the Ge QDs phase in obtained superlattices can be tuned from amorphous to crystalline by post-deposition thermal annealing without destroying the superlattice structure.

In summary, the self-ordering growth of 3D Ge QD superlattices in completely amorphous SiO_2 matrix is achieved during deposition at 500^o C. For lower or higher Td the deposited Ge atoms form Ge QDs after annealing but the QDs are randomly distributed. The deposition temperature Td, together with an appropriate thickness of the spacer layers and the Ge/SiO_2 molar ratio, are found essential for achieving the self-organized growth. Td governs the surface and the bulk diffusion dynamics of Ge atoms during the deposition process, influencing the Ge clustering and ordering via surface topology effects. The reported process opens new opportunities in numerous existing and new Ge/SiO_2 system applications, and can be applied more generally for the production of new materials with crystalline QDs in amorphous matrix.

References:

[1] A. P. Alivsatos, Science 271, 933 (1996).
[2] J. Tersoff, C. Teichert and M. G. Lagally, Phys. Rev. Lett. 76, 1675 (1996).
[3] G. Springholz, V. Holy, M. Pinczolits, G. Bauer, Science 282, 734 (1998).
[4] J. Stangl, V. Holy, G. Bauer, Rev. Mod. Phys. 76, 725 (2004).
[5] W. Scorupa, L. Rebohle, T. Gebel, Appl. Phys. A 76 (2003) 1049
[6] M. Elhassan et al. Phys. Rev. B 70, 205341 (2004).
[7] D. V. Talapin and C.B. Murray, Science 310, 86 (2005).
[8] K. Karral et al. Nature 427, 135 (2004).
[9] M. Perrini, S. Barbay, M. Brambilla and R. Kuszelewicz, Appl. Phys. B 81, 905 (2005).
[10] M. Kroutvar et al. Nature 432, 81 (2004).
[11] Tate, M.P. *et al.*, *J. Phys. Chem. B* 110, 9882-9892 (2006)

IN-SITU CHARACTERIZATION OF SELF-ASSEMBLED NANOPARTICLES FILMS UNDER HARSH CONDITIONS

B. Gehl[1], Th. Schmidt[2], S. Bernstorff[3], M. Bäumer[1] and J. Falta[2]

1.) Institute for Applied and Physical Chemistry, University of Bremen, Leobener Str., 28359 Bremen, Germany
2.) Institute of Solid State Physics, University of Bremen, Otto-Hahn-Allee, 28359 Bremen, Germany
3.) Sincrotrone Trieste, Strada Statale 14, km 163.5, 34012 Basovizza/Trieste, Italy

Arrays of metal nanoparticles on oxidic surfaces have become a widely-researched type of materials systems in various disciplines of chemistry and physics. In contrast to techniques in which particles are grown directly on the substrate, the approach of self-assembling layers of colloidal metal particles offers increased flexibility in terms of materials combinations and particle size and structure. Usually, the nanoparticles prepared by wet chemistry are surrounded by a shell of stabilizing and coordinating ligands and then deposited on substrate surfaces by different techniques. To access the properties of the underlying metal particle surface without an interfering organic shell, the latter has to be removed. Among the requirements to be met by a method for stripping the deposited colloids of their ligands is the conservation of particle and layer structure. Within this project the effect of two different techniques, thermal annealing and reactive/sputtering treatment on arrays of bimetallic cobalt-platinum particles [1] were examined with ordering and size distribution as a particular focus.
Since neither plasma nor thermal treatment were possible in-situ in the beamline due to technical restrictions, samples had been prepared ex-situ before GISAXS measurements. The effects of thermal annealing were studied on the basis of a series of samples heated under flowing nitrogen and a second batch annealed under ultra-high vacuum (UHV) conditions varying heating times and maximum temperatures. In parallel, a number of samples had been treated with oxygen and then hydrogen plasma in order to strip them of their ligand shell and then reduce them back to the metallic state.
It was found that samples heated under protective atmosphere or UHV conditions had undergone a thermally induced melting process at elevated temperatures. The more precise measurements on the samples prepared under UHV showed an increasing loss of order with rising temperatures and a clear loss of structural definition above 700 K as can be seen in Figure 1. These findings were complimented well by SEM images which show sintering and agglomeration of distinct particles into larger structures after exposure to the corresponding temperatures.

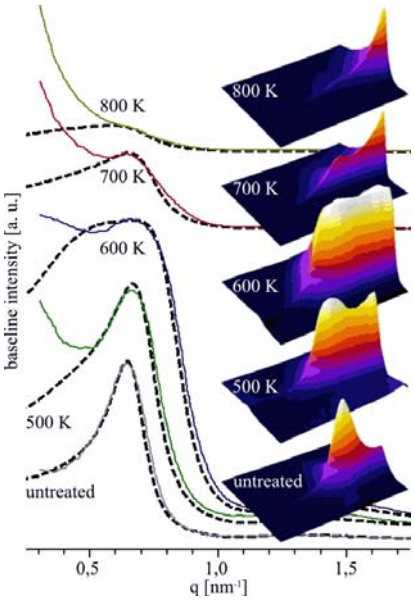

Figure 1. Left: GISAXS baseline intensity measured from nanoparticle arrays annealed at different temperatures for 120 minutes under UHV. Right: 3D representation of the respective spectra.

In a second series of experiments, layers of deposited particles were exposed to oxygen and hydrogen plasmas in a custom built RF plasma source [2] with treatment time, plasma power and the partial pressure of argon in the gas feed as variable parameters. From the GISAXS results it could be seen that while completely removing the ligand molecules from the particles, a plasma treatment at 20 W of 120 min oxygen and 30 min hydrogen with considerably less impact on layer order and particle definition as can be seen in Figure 2. However, a certain reduction of the mean interparticle distance can be deduced from the recorded spectra. Furthermore it turned out that the sputtering effect resulting from a partial pressure of argon in the plasma process gas was of no use to improve ligand stripping but damaged the layer structure.
Due to the exposure of the naked metal particles before and during the treatment to an oxygen-containing and contaminating atmosphere, the oxidation of their cobalt content could not be precluded. However, the corresponding transition of lattice structure of the individual particles was neglected in this case since it affects both methods to the same extent and doesn't distort the results of the comparison. To avoid this possible source of error, it remains the objective of future beamtimes to study the plasma- or heat-induced structural changes in-situ by integrating the treatment into the beamline.

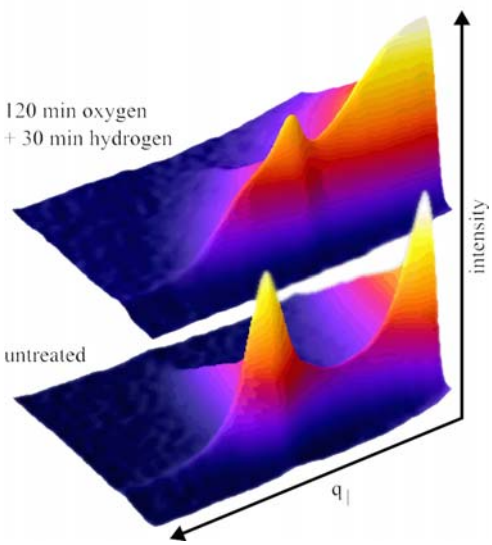

Figure 2. 3D representation of GISAXS spectra measured from nanoparticle arrays before and after exposure to an oxygen plasma at 20 W for 120 min and then to a hydrogen plasma at 20 W for 30 min.

References:

[1] J. I. Flege, T. Schmidt, V. Aleksandrovic, G. Alexe, T. Clausen, B. Gehl, A. Kornowski, S. Bernstorff, H. Weller, J. Falta; Nuclear Instruments and Methods in Physics Research B 246, 25-29 (2006)
[2] B. Gehl, U. Leist, V. Aleksandrovic, P. Nickut, V. Zielasek, H. Weller, K. Al-Shamery, M. Bäumer; Review of Scientific Instruments 77, 083902-1 -083902-7 (2006)

THE INFLUENCE OF SUBSTRATE MORPHOLOGY ON THE GROWTH OF THIN SILICON FILMS: A GISAXS STUDY

D.Gracin, S.Bernstorff[2], P.Dubcek[1], A.Gajovic[1] and K. Juraic[1]

1.) Rudjer Boskovic Institute, Bijenicka 54, 10000 Zagreb, Croatia
2.) Sincrotrone Trieste, SS 14 km 163.5, 34012 Basovizza (TS), Italy

A typical thin film silicon solar cell is deposited on a glass substrate, and covered with a conductive transparent metal oxide. The active part of a solar cell consists of 3 to 6 silicon layers, each with a thickness of ten to several hundred nanometers, deposited subsequently layer by layer by decomposition of silicon hydrides in a high frequency glow discharge. Recently, a lot of effort has been made in order to deposit a combination of amorphous and nano-crystalline material in the same thin film cell. The nano-crystalline structural form enables a broadening of the absorption range in the visible part of the solar radiation due to quantum effects, which increases the solar cell efficiency and improves the material stability. However, the deposition of the crystalline form on the glass substrate, which assumes growth at relatively low temperatures, requires strong plasma surface interactions during the film formation. That is why it is important to study the growth on different substrate structures, in particularly regarding a possible influence of the deposition condition of a new layer onto the interfaces or previously deposited layers.

Thin Si films, with thickness between 100 and 300 nm, were deposited by PECVD (Plasma Enhanced Chemical Vapour Deposition) in silane gas (SiH_4) under various condition and substrates. The nanostructure of deposited films was studied by GISAXS.

The GISAXS pattern of all of the examined samples indicated the presence of not-spherical-like “particles” in the “bulk” of the thin films, with an average "particle" size between 1.5 and 4 nm. These “particles” are most probably voids and their shape indicates columnar growth. By applying the GISAXS technique on samples deposited on different substrates, the borderline deposition conditions between “transport limited growth” and "growth dominantly influenced by plasma surface reactions" was estimated.

A typical example of this type of study is illustrated in Fig.1, where GISAXS patterns are compared which were obtained from three different substrates, and for several samples deposited with different growing conditions on these substrates. In analysis, [1,2] it was discussed that if the nanostructure of a film looks like the substrate, the growth is "transport limited". It means that during the growth particles from the edge of the plasma bond to the surface of the growing film through chemical reaction. In contrary, if the film morphology differs from those of the substrate, "growth is influenced by plasma surface interactions"

The first column corresponds to three different substrates (a: amorphous Si-layer, d: metal oxide layer, and g: bare glass). In the next columns are GISAXS of samples deposited under various deposition conditions. In the first row the discharge power increases from 5 mW/cm^2 (1b) to 10 mW/cm^2 (1 c). The second and third row in Fig.1 show pattern from samples deposited with lower power while the gas dilution increases from Fig 1e to 1f, 1h and 1i corresponding to a silane fraction of 24%, 14%, 7.4% and 5.5%,respectively.

In summary, comparing the presented GISAXS patterns of the samples in Fig. 1, second and third column, with those of the corresponding substrates (first column of Fig.1), it can be concluded that up to a dilution close to 6 % of silane and some 10 mW/cm^2 discharge power density, the sample structure follows the substrate morphology, defining the borders of the transport limited growth for our experimental setup.

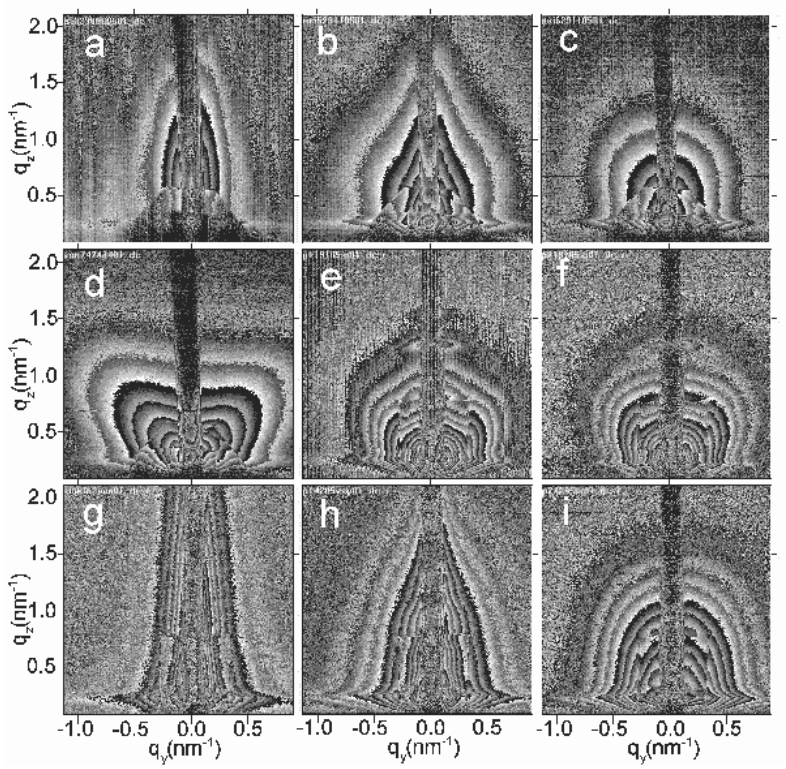

Figure 1. 2D GISAXS pattern obtained from 3 different substrates (a, d, g) and from samples deposited under different growing conditions ("transport limited growth" (b, e, f, h) or "strong plasma surface interactions" (c, i)) on these substrates (see text for detailed description)

References:

[1] D.Gracin, S.Bernstorff, P.Dubcek, A.Gajovic and K.Juraic, J. Appl.Crystalography 40, 373-376 (2007)
[2] D.Gracin, S.Bernstorff, P.Dubcek, A.Gajovic and K.Juraic, Thin Solid Films 515, 5615-6519 (2007)

DEPTH RESOLVED IN-PLANE DIFFRACTION STUDIES OF MELTING OF LANGMUIR-BLODGETT FILMS USING X-RAY WAVEGUIDE

A. Gupta[1], P. Rajput[1], D. Kumar[1], S. Bernstorff[2], and H. Amenitsch[3]

1.) UGC-DAE Consortium for Scientific Research, Khandwa Road, Indore, India
2.) Sincrotrone Trieste, SS 14, Km 163.5, I-34012 Basovizza, Trieste, Italy
3.) Institute for Biophysics and X-ray Structure Research, Austrian Academy of Sciences, A-8010 Graz, Austria

The objective of the proposal was to study melting of cadmium arachidate (CdA) Langmuir-Blodgett (LB) multilayers using depth resolved in-plane diffraction. Depth resolution is achieved using a waveguide structure with the LB film forming the cavity of the waveguide. The structure of multilayer was Si substrate/ Ni (70 nm) / CdA (13 monolayer)/Ni 2nm. When x-rays fall at grazing incidence, various transverse electric modes of such a structure can be excited when the condition $\theta_n = (n+1)\lambda/2d$ is satisfied, where θ_n is the angle at which the x-rays fall at the interfaces of the cavity, λ is the wavelength of x-rays, d is the thickness of the cavity, and n is the order of the mode.

In-plane diffraction measurement are done with angle of incidence corresponding to different waveguide modes so as to obtain selective information from the region of antinodes: While for $\theta=\theta_0$ information is obtained from the centre of the layer, for $\theta=\theta_1$ information is obtained from the regions near both top and bottom interfaces [1]. X-rays of 8 keV were used for simultaneous measurement of reflectivity (using a 1D detector) and in-plane diffraction (using CCD camera) at SAXS beam line of Elettra synchrotron. Figure 1 gives the in-plane diffraction pattern of the multilayer as a function of the angle of incidence. Two strong peaks are observed at $q_x = 1.56$ Å^{-1} and $q_x = 1.68$ Å^{-1} corresponding to $(01+1\bar{1})$ and (10) reflections

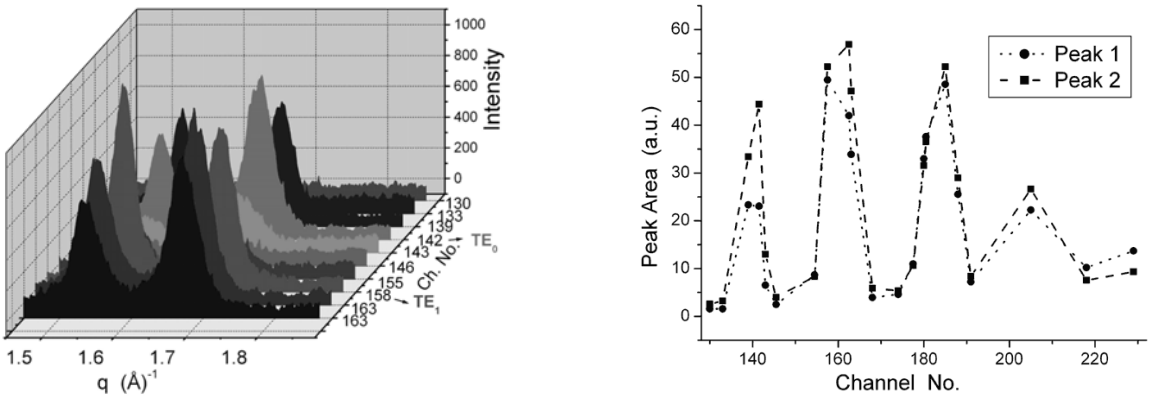

Figure 1. a) In-plane diffraction of CdA multilayer (13 monolayers) embedded in a waveguide structure as a function of the angle of incidence (represented in terms of the channel number of specular spot on forward detector); b) Peak intensities as a function of the angle of incidence (represented in terms of the channel number of specular spot on forward detector). The sharp increase in the intensities corresponding to channel nos. 142, 158 and 185 evidence the excitation of waveguide modes TE_0, TE_1 and TE_2 respectively.

This suggests that in conformity with earlier works [2], the in-plane structure is distorted hexagonal lattice. The overall intensity of the two peaks exhibits strong variation with the angle of incidence (Fig. 1b). Maxima in the peak intensity correspond to the excitation of the waveguide modes in the cavity. Precise values of the angle of incidence corresponding to the excitation of TE_0 and TE_1 modes (θ_0 and θ_1 respectively) were determined by monitoring the intensity of the peaks.

Figure 2 gives the temperature dependent diffraction pattern corresponding to the angle θ_1. One may note that with increasing temperature both the peaks shift to lower angles due to thermal expansion. However the peak corresponding to (10) reflection shifts at a faster rate and finally merge with first peak. The distortion of the lattice from regular hexagonal one can be quantified in terms of parameter $\Delta\gamma = 60°-\gamma$,

where $\gamma = \cos^{-1}\frac{q_2}{2q_1}$, q_1 and q_2 are the positions of the $(01+1\bar{l})$ and (10) reflections respectively.

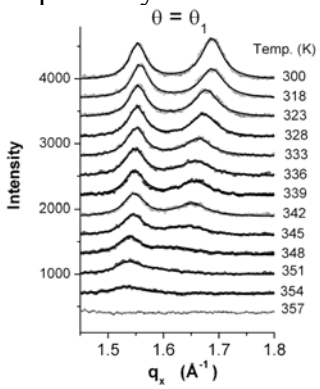

Figure 2. In-plane diffraction of CdA multilayer (13 monolayers) embedded in a waveguide structure at $\theta=\theta_0$, as a function of temperature

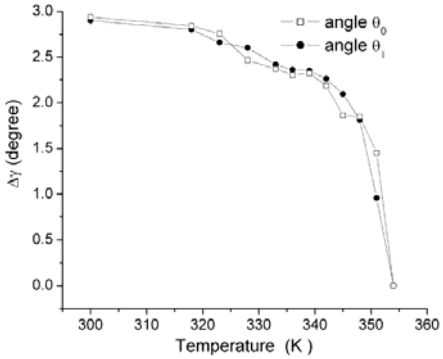

Figure 3. Parameter $\Delta\gamma$ as a function of temperature at the two angles θ_0 and θ_1

Figure 3 gives the parameter $\Delta\gamma$ as a function of temperature at the two angles. In both the cases, initially $\Delta\gamma$ shows a gradual change with temperature, and around 345 K it suddenly drops down, showing rather abrupt decrease in the distortion. Figure 4 gives the width of diffraction peaks at the two angles. At θ_0 , while the width of the peak corresponding to $(01+1\bar{l})$ reflection shows only a small increase with temperature, that of (10) reflection exhibits substantial variation with temperature. On the other hand, at θ_1, width of both the peaks increases simultaneously with temperature.

In conclusion present studies shows that in-plane diffraction using waveguide structures can be used to get depth resolved information about structural transformation occurring in CdA LB multilayer as a function of temperature. Significant differences between the interfacial regions and the center of the layer are observed.

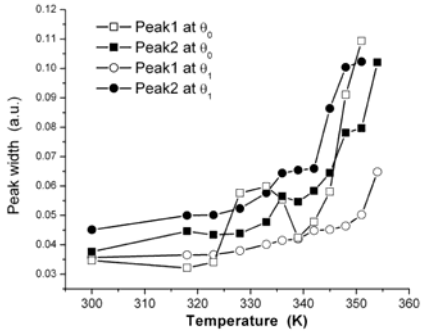

Figure 4. The width of diffraction peaks at the two angles θ_0 and θ_1

References:

[1] A. Gupta, P.Rajput, A. Saraiya, V. R. Reddy, M. Gupta, S. Bernstorff, and H. Amenitsch, Phys. Rev. B 72, 075436 (2005)

[2] M.K. Mukhopadhyay, et al., Phys. Rev. B 70, 245408 (2004)

SAXS STUDY OF AEROSOL AND NANOPARTICLES IN GAS PHASE

S.Ibrahimkutty, M.Rappolt, B.Sartori, P. Laggner, and H.Amenitsch

Institute of Biophysics and Nanosystems Research, Austrian Academy of Sciences, Graz, Austria.

Formation and structural characterisation of nanoparticles using the recently developed method of evaporation induced self-assembly [1] in the field of high end nanotechnology, and the construction of a prototype for gas phase studies of nanoparticles.

Only few experiments are performed with *in situ* SAXS [2, 3, 4], the limiting factor being the particle concentration in the gas phase, which is extremely low (10^7 particles equivalent to 6 µg dry matter per cm^3, for a commercial apparatus). Following the reports in references [5, 6] a fog generator (aerosol generator) was built in-house with a low cost ultrasonic ceramic disc mist maker (300 ml/hr) working at 1.7 MHz, shown in figure 1. A ring gas inlet system is used above the mist maker container, that efficiently en-route the fog to the outlet with minimal turbulence and condensation.

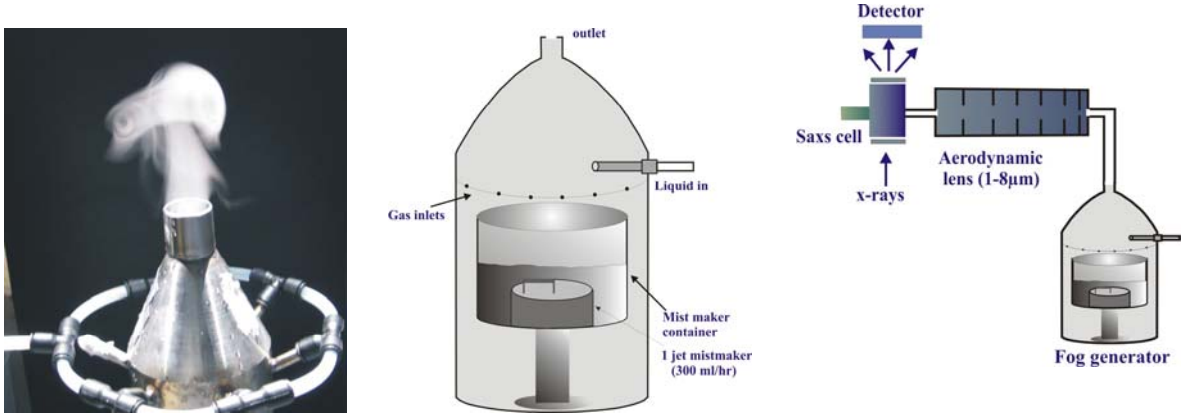

Figure 1. left: picture of fog generator, operating and the schematic; right: in situ set-up for the study of Au nanoparticles (schematic).

Using the in-house built fog generator the first test prototype (figure 1) constructed for the *in situ* SAXS study of nanoparticles. The outlet of the fog generator is connected to an aerodynamic lens that can size select particles or droplets in the range of 1-8 µm [7]. An X-ray transparent SAXS cell is used with an efficient exhaust system for the removal of the fog after the beam. As a first approach to prove the principle of operation we have carried out pilot experiment with Au nanoparticles synthesized by citrate route ($2.5x10^4$ M $HAuCl_4$ + 34 mM sodium citrate, purchased from *Sigma Aldrich*), that give spherical gold nanoparticles of size about 10 nm [8]. This was confirmed by laboratory SAXS experiment to be ca. 13 nm.

Figure 2(a) shows the scattering raw data of gold nanoparticles (Au-NP) with fog and the background. Figure 2(b) gives the extracted data with a universal fit (simultaneous Guinier and Porod fit) for individual particles and additional Porod contribution for large aggregates. The fitting function is explained in equation 1, following the works of Beaucage [9, 10].

$$I(q) = G\exp\left(\frac{-q^2R_g^2}{3}\right) + B\exp\left(\frac{-q^2R_{sub}^2}{3}\right)\left(\frac{1}{q^*}\right)^p + \left(P_c \Big/ q^{p_e}\right) \qquad (1)$$

with, $q^* = \frac{q}{\left[erf\left(kqR_g/\sqrt{6}\right)\right]^3}$, $B = \left(G_p/R_g^p\right)\exp\left(\Gamma\left(p/2\right)\right)$,

where G the Guinier pre-factor, B is a pre-factor specific to the type of power-law scattering and Γ(x) is the gamma function. R_{sub} is the cut-off radius of gyration, k is the constant used to define q^*, p_c the Porod coefficient for the aggregates and p_e the Porod exponent.

Figure 2: (a) - Scattering raw data of Au particles with & without fog, (b) - Reduced data with Porod fit (d ~ 45 nm).

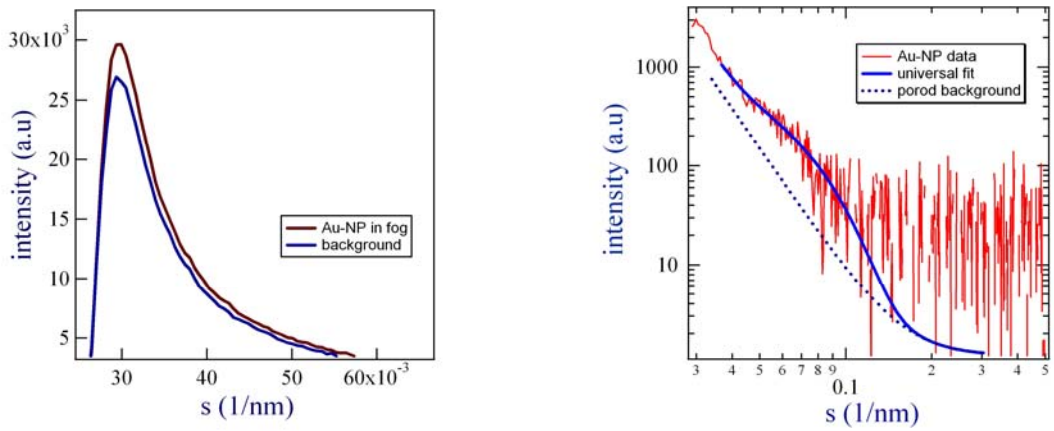

Figure 2. (a) scattering raw data of gold nanoparticles (Au-NP) with fog and background; (b) extracted data with a universal fit (simultaneous Guinier and Porod fit) for individual particles, and Porod contribution for large aggregates.

The fit demonstrates total particle aggregation (d ~ 45 nm) occurred when the particles are trapped in the fog. This pilot experiment demonstrates the working principle for gas phase detection of nanoparticles with the present experimental set-up using SAXS

Reference:

[1]Lu.Y.F, H.Y.Fan, A. Stump, T.L. Ward, T. Rieker, and C.J. Brinker, Nature, 398, 223 (1999).
[2] Boissiere. C, D. Grosso, H. Amenitsch, A. Gibaud, A. Coupe, N. Baccile, and C. Sanchez, Chemical Communications, 2798-2799 (2003).
[3] G. Beaucage et al., Nature materials Vol 3, 370-374 (2004).
[4] S. di Stasio, et al., Carbon 44, 12671279 (2006)
[5] Didenko YT, Suslick KS, J. American Chemical Society, 127(35), 12196-12197 (2005).
[6] J. Shu et al., Rev. Sci. Instrum., 77, 043106 (2006).
[7] Liu. P, Ziemann. P. J, Kittelson. D. B, and McMurry, P. H, Aerosol Sci. Technol. 22(3):293313 (1995).
[8] G. Frens, Nature, 241, 20 (1973).
[9] Beaucage. G, J.Appl. Cryst., 28, 717728 (1995).
[10] Beaucage. G, J.Appl. Cryst., 29, 134146 (1996).

STRESS-STRAIN RELATIONSHIP IN SILVER COATED POLY(ETHYTEREPHTALATE) FILMS

G. Maier[1], J.Keckes[1], M. Feuchter[2] and H. Amenitsch[3]

1.) MCL Leoben and Dep. Materialphysics, University of Leoben, Jahnstrasse 12, 8700 Leoben, Austria
2.) Institut f.Werkstoffkunde und Prüfung der Kunststoffe, University of Leoben, Franz-Josefstrasse 18, 8700 Leoben Austria
3.) Institute of Biophysics and Nanosystems Research, Austrian Academy of Sciences, Graz, Austria

Introduction:

The response of all kind of materials on external load is of crucial importance on the application. Especially coated materials are of high scientifically interest, because of different mechanical properties of the coating material and the substrate. One special class of such materials are metal-coated polymer films. There a soft substrate is covered with a rather stiff metal thin film. When such a coated material is strained, the stress is dissipated in both phases. The high elasticity allows for higher elastic strains in polymer as in metal film. At small-applied strains both materials show a fully elastic strain behavior. At increasing strain, first the metal film is plastically deformed and later on also the polymer films. We have investigated response of the coated material on the applied strain. A nearly one to one dependence of microscopic an applied (macroscopic) strain was found.

Experiment:

The simultaneous SAXS and WAXD experiments were performed on the SAXS beamline at ELETTRA, Trieste, Italy. A wavelength of 0.15 nm was used. SAXS patterns were recorded using a 2D CCD detector (Photonoic Science, Oxford, GB). WAXD data were recorded using a 1D line detector (Braun, Germany). The distance between sample and detector were 960mm and 250mm, SAXS and WAXD respectively. The distance for SAXS was calibrated using silver-behenate powder. Calibration of WAXD detector was performed with corundum powder. The setup is sketched in figure 1. The tensile experiments were performed using a self-constructed tensile tester [1].

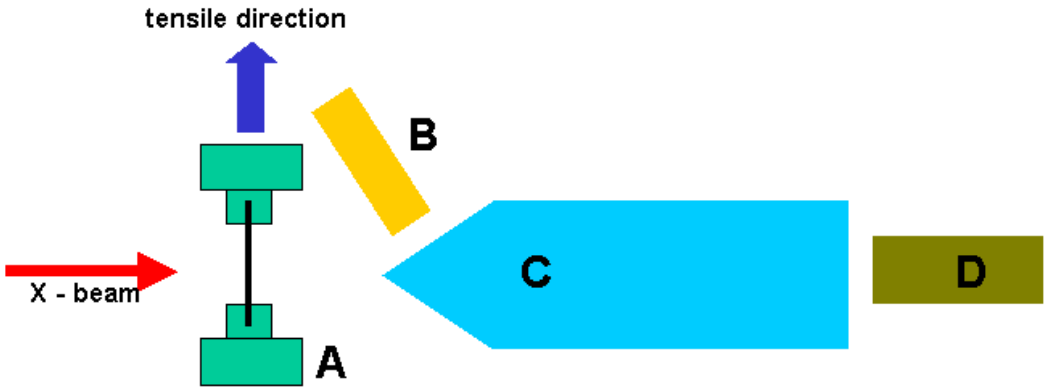

Figure 1. Setup of the experiment. A denotes the tensile machine, B the WAXD detector, C the tube and D the SAXS detector.

The samples were 50µm thick commercial uniaxial oriented semi-crystalline poly(ethyterephtalate) films coated with 100nm silver. Coating was performed using a PVD technique. From sheets of this material samples with a size of 0.9 x 40 mm^2 were cut. Cutting direction was chosen that the main orientation axis was parallel to tensile direction.

Data evaluation:
2D SAXS patterns were reduced to scattering curves by radial integration in arcs with an opening angle of 20 degrees, with the orientation axis being the center. The scattering curves were corrected for background scatter [2,3]. The long period (LP), thickness of lamellae (t) and distance between lamellae (d) were determined using a 1D correlation function approach. A value, describing the volume fraction of crystalline phase (x_{CV}) was calculated with $x_{CV}=t/(d+t)$. The position of the reflections of the Ag-WAXD peaks was determined using a sliding gravity method. The strain ε was calculated by $\varepsilon=(d_M-d_0)/d_0$ with d_0 being the value when no force is applied (long period, lamellae thickness, d-spacing or free length of the sample in the tensile tester) and d_M was the distance (length, lattice spacing…) for a certain macroscopic strain. For calculating the effective strain (ε_{eff}) in the polymer a composite model was used, which weighting the strain fraction from amorphous and crystalline part of the polymer: $\varepsilon_{eff} = \varepsilon_t * x_{CV} + \varepsilon_d * (1-x_{CV})$. ε_t is the strain in lamellae, ε_d the strain in amorphous interlayer.

Results:
The results of one experiment are shown in figure 2. From beginning of the tensile experiment, the applied and effective microscopic strains had the same amount. Also the silver d-spacings showed a clear dependence on the applied strain, with approximately three times lower values. When the macroscopic strain reached a value of 0.01, the silver film was plastically deformed, while the polymer still showed elastic response.

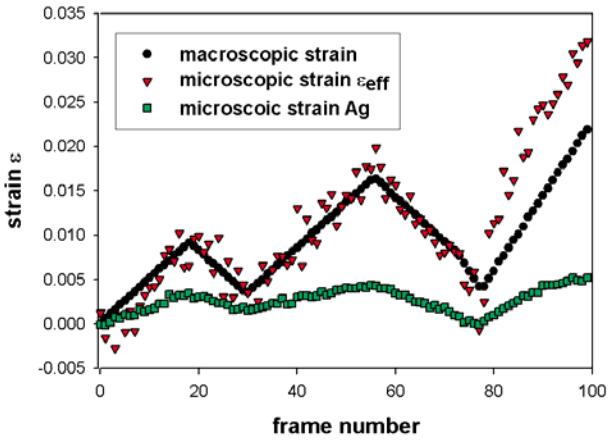

Figure 2. Applied strain, effective strain in polymer and in silver film plotted against frame number.
Around frame 80, the polymer was plastically deformed and the calculated strain values overestimated the applied macroscopic strain. This point is still under investigation.

Conclusion and Outlook:
The experiments performed at SAXS beamline at ELETTRA enabled the calculation of microscopic strain in polymer film out of the SAXS pattern. We were able to collect WAXD pattern from silver coating and calculate also strain in Ag film. For evaluation of effective strain in polymer we used a composite model, showing a very good correspondence with the applied strain. Detailed data analysis is on the way.

References:

[1] J. Keckes, Keckes, J., Burgert, I., Fruhmann, K., Muller, M., Kolln, K., Hamilton, M., Burghammer, M., Roth, S., Stanzl-Tschegg, S. and Fratzl, P., Nature Materials 2 (2003), 810-814
[2] Maier G.A, Wallner G.,Lang R. and Fratzl P, Macromolecules 38 (2005), 6099-6105
[3] Maier G.A., Wallner G., Lang R., Keckes J., Amenitsch H. and Fratzl P., J. Appl. Cryst. 40 (2007), 564 567

ULTRAFAST NUCLEATION AND GROWTH STUDY OF CALCIUM CARBONATE BY SAXS

B. Marmiroli[1], G. Grenci[2], B. Sartori[1], M. Rappolt[1], H.Cölfen[3], L. Businaro[2], P. Laggner[1], and H. Amenitsch[1]

1.) Institute of Biophysics and Nanosystem Research, Austrian Academy of Sciences, Schmiedlstraße 6, Graz, Austria
2.) TASC-INFM-CNR at Elettra Synchrotron, S.S. 14 km 163.5, Trieste, Italy
3.) Max Planck Institute of Colloids and Interfaces, Am Mühlenberg 1, 14476 Potsdam-Golm, Germany

The motivation of our work is to detect by SAXS the early stages of nucleation and growth in the microsecond time regime by means of a free jet micromixer. The time resolution is reached by scanning along the free jet after the mixing and therefore probing different residence times.

First pilot experiments allowed obtaining a highly stable free solution jet using a microfluidic nozzle. As a first control measurement we choose to record the scattering of a gold particle solution (size: 13 nm, 2.5 $*10^{-4}$ M Au) passing through a 100 μm HPLC tube in order to see if it is in principle possible to detect any signal from a free micro jet. The results (shown in figure 1, left) confirm the capability to get sufficient scattering signal with a free micro-jet of 100 μm. Moreover we studied the scattering of the Calcium Carbonate reaction through a mechanically fabricated cross channel device with triangle cross section 100μm high, 200μm wide (figure 1). The length of the mixing channel was 5 mm. However, no signal was detected (right panel, figure 2) as the reaction did not occur.

At present, to circumvent the experimental difficulties like mixing times, long dead times, micromixers of smaller dimensions and higher aspect ratio are projected [2]. In future our plan is to study the chemical reaction using a custom made microfluidic device designed by FE simulations, in order to be able to control the mixing of the reagents and therefore the reaction. The jet flow rate will be 10 m/s, the cross section of the exit nozzle of the micromixer will be 5 μm wide, 100 μm deep, leading to a time resolution of 50μs. The micromixer will be fabricated by deep X-ray lithography. In addition, we intend to apply simultaneous SWAXS detection to follow the formation of crystalline polymorphs, protein solutions, etc.

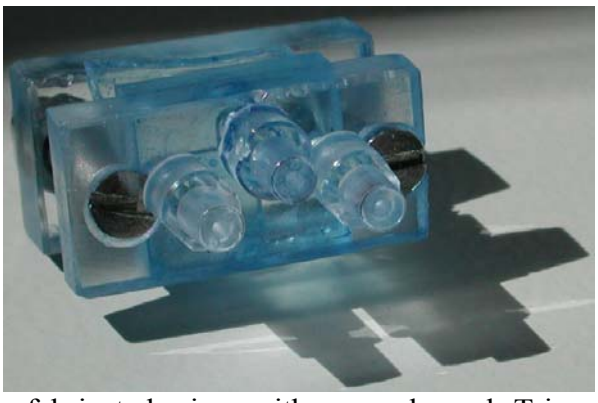

Figure 1. Mechanically fabricated mixer with cross channel. Triangle cross section 100μm high, 200μm wide.

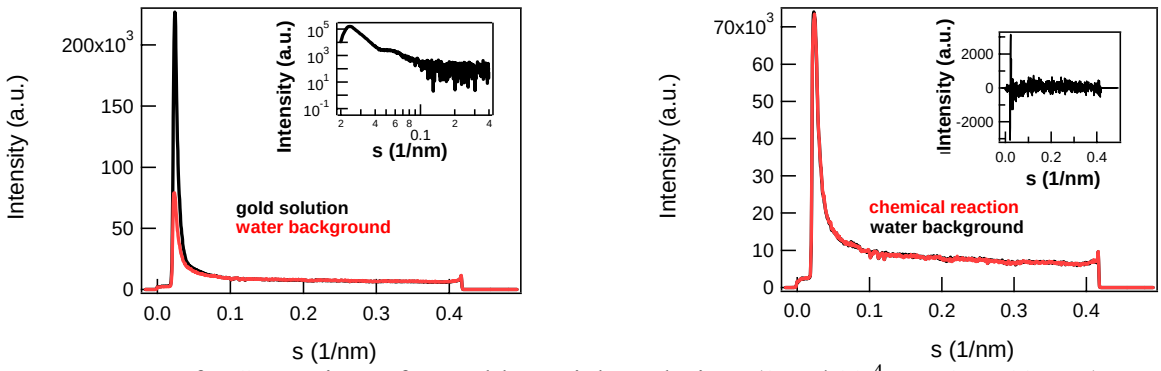

Figure 2. Left: Scattering of a gold particle solution (2.5 *10^{-4} M Au, 13 nm) passing through a 100 µm HPLC tube. Right: Scattering of the $CaCO_3$ crystallization reaction through a mechanically fabricated cross channel device.

References:

[1] H. Haberkorn, D. Franke, T. Frechen, W. Goesele and J.Rieger, J. Colloid Interf. Sci. **259**, 112-126 (2003).
[2] B. Marmiroli, G. Grenci, L. Businaro, D. Cojoc, B. Sartori, M. Rappolt, A. Gosparini, P. Laggner and H. Amenitsch, *SAXS on Nanosystems, Science and Technology Workshop*, Trieste (Italy), 23-24.11.2006

STUDY OF INTRALAYER STRUCTURE AND MOLECULAR PACKING IN LB MULTILAYERS AND RELATED NANOSTRUCTURES

P. K. Nayak[1], R. S. Srinivasa[1], S. S. Major[1] and S. Bernstorff[2]

1.) Indian Institute of Technology Bombay, Powai, Mumbai–400076
2.) Sincrotrone Trieste, I -34012 Basovizza, Trieste, Italy

Long chain fatty acids and their divalent metal salts, such as, those of cadmium arachidate (CdA) and lead arachidate (PbA) are extensively studied LB systems and their three dimensional structure and molecular packing have been investigated using a variety of techniques, including GIXD AND AFM [1]. Their molecular packing usually corresponds to the closed packed structures proposed by Kitaigorodskii [2] for long chain organic compounds. CdA multilayers have molecules packed in an ideal close packed herringbone structure based on an orthorhombic subcell packing. In contrast, zinc arachidate (ZnA) multilayers exhibit polymorphism and their molecular packing depends strongly on the subphase pH at which the monolayers are transferred [3]. The most stable polymorphic phase of the ZnA multilayers possesses a hexagonal layer plane packing, with loosely packed molecules tilted at ~32^{o} with the layer normal. In another recent work, we have shown that the presence of CdA molecules has a strong influence on the structure of CdA-ZnA mixed multilayers and leads to the appearance of new layered structural phases [4]. LB multilayers of divalent fatty acid salts, such as, CdA are also used as precursors for the growth of semiconducting chalcogenide nanoclusters within the layered matrix through post deposition sulphidation treatment [5]. However, inspite of the extensive work, the overall structure of the resulting composite multilayers still remains to be completely understood.

Under the present ELETTRA proposal at the SAXS beamline, we have taken up a detailed characterization of the three dimensional structure of polymorphic ZnA multilayers transferred at different subphase pH and zinc ion concentrations, mixed CdA- ZnA multilayers with varying proportions of the two components and H_2S exposed pure and mixed arachidate multilayers. The effect of heat treatment on the structure of some of the above multilayers was also examined, in-situ. LB multilayers typically consisted of 15 monolayers. GIXD measurements were carried at a fixed angle of incidence ~0.2^{o}, using the 2-D (CCD) detector. The detector was configured so as to cover a Q_{xy} range of ~ 1- 2 Å^{-1} and the Q_z range of 0-1 Å^{-1}, to obtain the rod scans at Bragg peak positions. A heater was arranged on the sample stage to carry out the experiments in a temperature range of 300 - 400K.

Typical results are shown in Fig.1. Fig.1.(a) clearly shows the presence of two low order GIXD peaks, characteristic of orthorhombic subcell based molecular packing [3]. In contrast, the ZnA multilayer transferred at low subphase pH shows a single peak suggesting a one molecule per unit cell type packing, based on hexagonal /monoclinic subcell [3]. More detailed analysis is in progress to understand the nature of subcell as well as determine the molecular tilt from the intensity variation along Q_z. Fig. 1(c) shows that the ZnA multilayer transferred at higher subphase pH has asignificantly different molecular packing. It appears to posses a one molecule per unit cell type packing, but the intensity variation along Q_z is significantly changed, indicating the possibility of the packing of molecules normal to the layer plane, as indicated by X-reflection measurements carried out in laboratory.

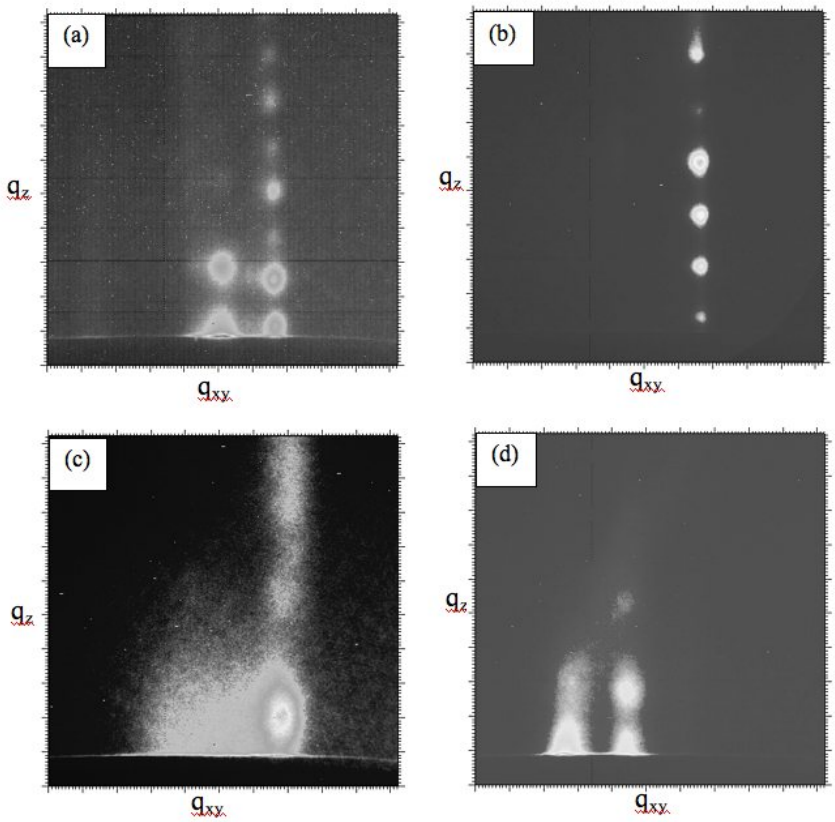

Figure 1. The 2 D patterns of (a) CdA, (b) ZnA transferred at pH 7, (c) ZnA transferred at pH 7.7 and (d) mixed CdA-ZnA (40:60) multilayers.

However, the presence of a diffused background at lower Q_{xy} indicates the coexistence of a weak orthorhombic phase as well, but this aspect needs to be investigated in more detail. Fig. 1(d) shows the influence of incorporating the CdA molecules in the mixed CdA-ZnA multilayers, indicating the presence of a two molecule per unit cell type packing. More detailed analysis is in progress to determine the nature and parameters of the layer cell and molecular tilt angle. These are just few typical results which show interesting molecular packing behaviour of CdA, ZnA and mixed CdA-ZnA systems. Significant changes have also been observed (not shown here) to take place in the 3-dimensional structure of these systems, as a result of heat treatment and sulphidation.

References

[1] D. K. Schwartz, Surface Science Reports 27 (1997) 41
[2] A. I. Kitaigorodskii, *Organic Chemical Crystallography* (Consultant Bureau, New York, 1961)
[3] N. Prasanth Kumar, S. Major, S. Vitta, S.S. Talwar, P. Dubcek, H. Amenitsch, S. Bernstorff, V. Ganesan, A. Gupta and B.A. Dasannacharya, Colloids & Surfaces A 198-200 (2002) 75
[4] P. K. Nayak, S. S. Talwar, S. S. Major and R. S. Srinivasa, Colloids & Surfaces A 284-285 (2005) 187
[5] N. Prasanth Kumar, S. N. Narang, S. Major, S. Vitta, S. S. Talwar, P. Dubcek, H. Amenitsch and S. Bernstorff, Colloids & Surfaces A 198-200 (2002) 59

SAXS CHARACTERIZATION OF TI AND CARBON NANOPARTICLES FROM SUPERSONIC CLUSTER BEAMS

P. Piseri[1], G. Bongiorno[1], P. Milani[1], H. Amenitsch[2], M. Coreno[3], G. Beaucage[4], and K.Wegner[5]

1.) Dipartimento di Fisica and CIMAINA, Università degli Studi di Milano, Via Celoria 16 - 20133, Milano, Italy
2.) Institute of Biophysics and X-ray Structure Research, Austrian Academy of Sciences, Schmiedlstrasse 6, A-8042 Graz, Austria
3.) CNR-IMIP and Laboratorio Nazionale TASC, CNR-INFM, AreaSciencePark, 34012 Trieste, Italy
4.) Department of Chemical and Materials Engineering, University of Cincinnati, Cincinnati OH 45221-0012, USA
5.) Particle Technology Laboratory, Swiss Federal Institute of Technology Zürich, Sonneggstrasse 3, ML F22, CH-8092 Zurich, Switzerland

Supersonic Cluster Beam Deposition (SCBD) is an innovative approach for the synthesis of nanostructred materials by directly assembling nanoparticles from the gas-phase [1]. The particles are first formed e.g. by evaporation-condensation and subsequent coagulation and sitering, and are then accelerated in a carrier gas undergoing a supersonic expansion. Thereby a highly collimated molecular beam of clusters is formed with a particle kinetic energy high enough to form mechanically stable films on a substrate that is intercepted with the beam, but not yet sufficient to substantially modify the particle structure upon landing [1,2]. We exploit this technique utilizing a Pulsed Microplasma Cluster Source (PMCS), that was developed by our group [3] and produces clusters and nanoparticles of refractory metals, metal oxides, and carbon at very high intensity and stability. In SCBD, the formation of aggregates (made up from smaller nanoparticles) inside the cluster source is of high relevance for the kinematic properties of the molecular beam and aerodynamic focusing. Consequently, it strongly influences the formation as well as the performance of the deposited nanostructured film.
We used SAXS with the aim of investigating the particle size distribution, and state of aggregation of titanium and carbon clusters produced by the PMCS. The goal was to characterize the free particles in the beam as well as their organization into nanostructured films after deposition, in order to achieve an understanding of the fundamentals of clusters growth and nanostructured films formation at early stages. The PMCS delivers supersonic cluster beam pulses with duration in the range of 10^{-2} s, repetition rate up to 20 Hz, and with a peak particle density at the nozzle exit of 10^{13} cm^{-3}. With a 1 s accumulation time it was possible to detect the scattered intensity from single-shot PMCS pulses of Ti clusters deposited on thin membranes, and thus to follow the deposit evolution during its growth; nevertheless, a sum over several similar pulses was necessary to accumulate sufficient statistics for data analysis. A Guinier plot as shown in Figure 1 gives a gyration radii of 2.27 nm, 2.45 nm, 2.57 nm for the scatterers after 12, 120 and 1200 pulses respectively, deposited on a biaxially stretched hydrocarbon wax film (Parafilm M®). Similar results were obtained when using a thin Si wafer (thickness 20μm) as a substrate although a minimum deposition time corresponding to approximately 110 pulses was needed in this case (the gyration radii are in this case 2.27 nm, 2.57 nm, 2.88 nm for similar deposited thickness). Figure 2 shows in detail the evolution of R_g with increasing amount of deposited particles for both substrates. A measure of the amount of deposited material is obtained through the average scattered intensity over the whole detection angle and integration time. The two different substrates have been chosen as prototypes of dissimilar cluster sticking and surface mobility properties. A substantially different behaviour on the two different substrates can be recognized. On Parafilm M® the R_g is only slightly variying with thickness and an extrapolation to very thin deposits gives approximately 2.1 nm. On Si there is a substantial increase of R_g at the early stages of film growth, although a considerable number of pulses is necessary to get the same overall scattered intensity that is observed on Parafilm M® after only few PMCS pulses. This

can be interpreted as a selective deposition of only the smaller particles on the fresh Si surface, with an increase of the sticking probability after the first layers of nanostructured material have been deposited.
After deposition of a few hundred pulses a fitting with the unified law as introduced by Beaucage [4] can be attempted. This yields exponents in the range of 2.5-2.7 for the power law term depending on the substrate and on the number of deposited pulses. For larger amounts of deposited material (several hundred shots) better results are obtained if two length-scales are considered; the scattered intensity can be closely reproduced by using a sub-structure with gyration radius in the range 0.9-1.2 nm (depending on the number of pulses) and Porod-like power law behaviour. The larger length-scale shows an increasing R_g with increasing deposit thickness, reaching values of few tens of nanometers after few thousand deposited pulses.
A similar investigation has been performed for carbon clusters deposition and data analysis is currently underway.

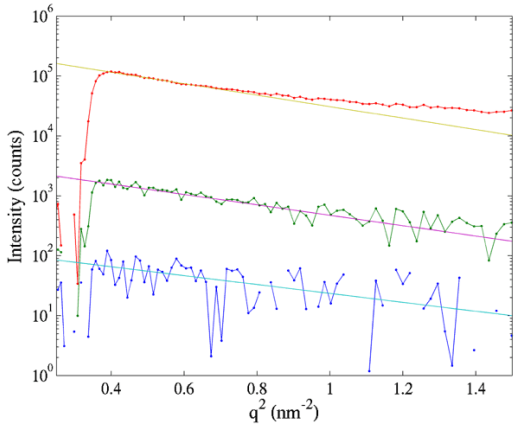

Figure 1. Guinier plots of the scattered intensity for different deposition times. The Guinier law interpolants fitting the data at small q^2 values are also shown.

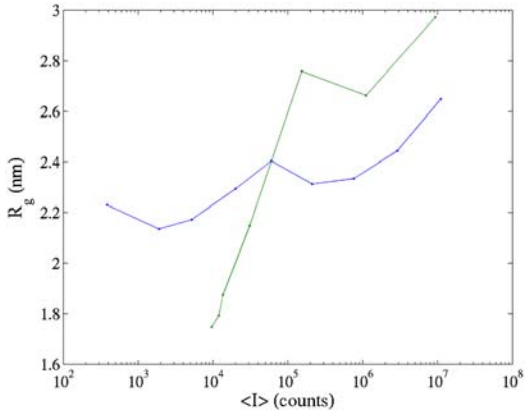

Figure 2. Gyration radius as obtained by Guinier law fitting for different amounts of deposited material and different substrates (blue – Parafilm M®, green – Si wafer).

Even at the high intensity of the cluster source and long accumulation time we could not detect a clear signal from the in-flight measurements of the particles in the gas phase. Considerable effort has been devoted to the reduction of background scattered intensity. A substantial decrease in the background scattered intensity was obtained by the installation of a lead foil asymmetric collimator directly under vacuum, right before the nozzle exit. The reduction of background pressure from the 10^{-1} mbar range typically adopted at the beamline to $4x10^{-4}$ mbar as typical in the expansion chamber in our molecular beam setup provided a further 16% decrease of the scattered background intensity in the angular range of interest. A precise determination of the scattered intensity corresponding to a single PMCS pulse and of the achievable background level with the available setup let us conclude that the gas phase-experiment will be very difficult to perform unless the signal to noise ratio can be improved by at least a factor 100. A possibility can be envisaged in the removal of a couple of polymer windows presently used to insert a ionization cell for X ray beam intensity monitoring before the interaction point.

References:

[1] P.Milani, P. Piseri, E. Barborini, A. Podestà, C. Lenardi; J Vac Sci Tech A 19, 2025-2033 (2001).
[2] L. Ravagnan, F. Siviero, C. Lenardi, P. Piseri, E. Barborini, P. Milani, C. Casari, A. Li Bassi, C.E. Bottani; Physical Review Letters 89, 285506 (2002)
[3] E.Barborini, P.Piseri, P.Milani; J Phys D 32, L105-L109 (1999).
[4] G.Beaucage; J Appl Crystallogr 28, 717 (1995).

STRUCTURAL ANALYSIS OF ANNEALED AMORPHOUS SIO/SIO_2 SUPERLATTICE

B. Pivac[1], P. Dubček[1], I. Capan[1], H. Zorc[1], and S. Bernstorff[2]

1.) R. Bošković Institute, P.O. Box 180, Zagreb, Croatia
2.) Sincrotrone Trieste, SS 14, km 163.5, Basovizza (TS), Italy

It is known that the band structure of silicon based materials can be engineered and adjusted for next generation photovoltaic applications. This engineering is realized in selective fabrication of silicon nanocrystals embedded in either a SiO_2 or Si_3N_4 matrix [1].
The actual research on formation of nanosized Si structures in dielectric matrix is focused on different methods of preparation such as: Si ion implantation in SiO_2, sputtering of Si-rich oxides or reactive evaporation of Si-rich oxides, and on formation of Si/dielectric multilayer. This last method, first suggested by Z.H. Lu et al. [2] was recently intensively studied [3-6]. It has been shown that upon annealing at 1100°C silicon precipitates from supersaturated solid solution to form nanocrystals. But many questions are still open regarding the Si nanoclusters formation in SiO_2 matrix and the influence of the deposition parameters and subsequent annealing on their formation. This work aims to contribute to the clarification of this problem.
Amorphous SiO/SiO2 superlattices were prepared by high vacuum evaporation of alternating films of SiO_2 and SiO, each 4 nm thick (forming a stack of 10 bilayers) on clean Si (100) substrate held at room temperature. After deposition, the samples were annealed from 600°C to 1100 °C for 1h in vacuum better than 10^{-2} Pa to induce Si nanocrystals formation.
Grazing incidence small angle X-ray scattering (GISAXS) experiments were carried out at the synchrotron facilities of Elettra, Trieste, Italy on the SAXS beamline, using synchrotron radiation with wavelength λ=0.154 nm (photon energy of 8 keV).
The details of the scattering intensities obtained for samples treated with different annealing temperatures can be more easily compared when linear scans of intensities are taken at q_y=0.15nm^{-1} and plotted together as has been done in Fig.1. Here, the angular scale has been corrected for the refraction effects.

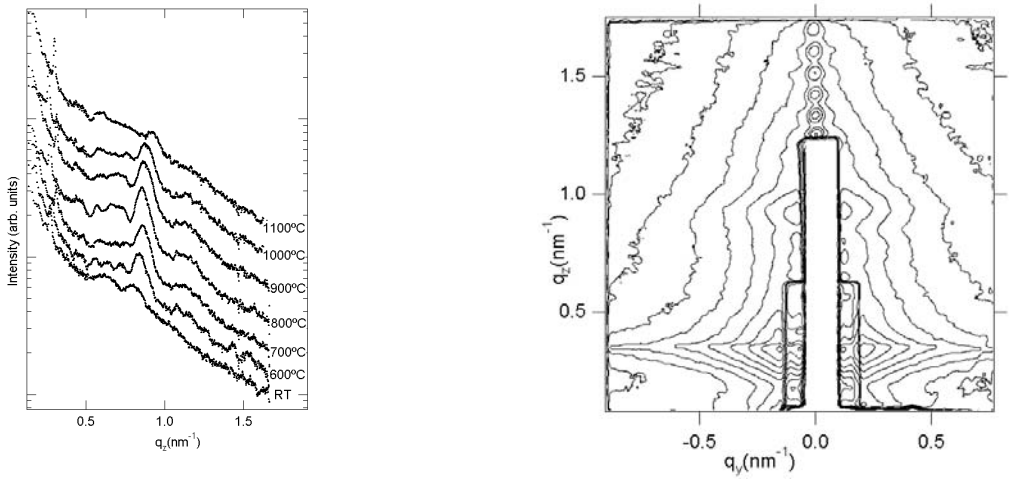

Figure1. left: The scattering intensity in vertical direction taken at q_y = 0.15nm^{-1} vs. q_z and as a function of the annealing temperature as indicated at the corresponding graphs. The intensities were obtained from 2D patterns like the one on the right, and are offset vertically for clarity.

The Bragg peak, corresponding to the repetitive bilayered structure is clearly resolved and will be analyzed in more detail here. First, the peak position (obtained from fitting the Bragg peak shape) is shifting slightly towards higher angles with increasing annealing temperature. It's shifting to wider angles reveals that the thickness of the bilayer is decreasing linearly with the annealing temperature (as can be seen in Fig.2), up to the last point where the thickness reduction is more substantial. Namely at lower temperatures, the structure of the bilayer, which consists of a SiO and a SiO_2 part, is relaxed. At higher temperatures the annealing of the amorphous SiO_x films results in a phase separation.

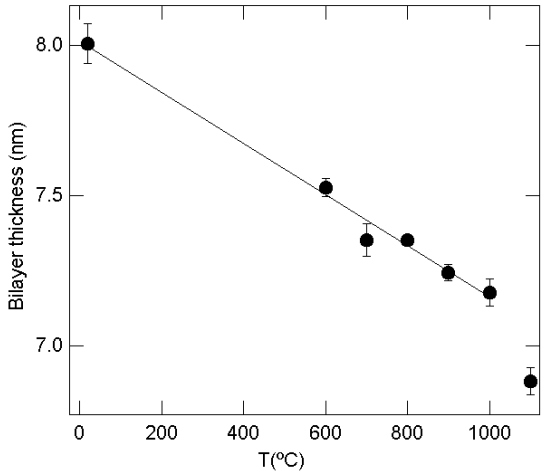

Figure.2 Bilayer thickness obtained from the Bragg peak position vs. the annealing temperature.

In our case x ≈1. Yi et al. [7] have shown that the phase separation process of the annealed SiO/SiO_2 superlattice can be divided into three stages: first up to 600°C it was characterized with infrared (IR) response having a peak at 880 cm^{-1} assigned to a silicon ring configuration and a band at 1039 cm^{-1} due to the Si-O-Si asymmetric stretching mode, both changing only little in this annealing range. The second stage from 600°-900°C according to these authors represents still an amorphous state of the superlattice, characterized by a more pronounced shift of the Si-O-Si stretching mode, which nicely corresponds to our result of the Bragg peak shift describing the compacting of the SiO layer. From our SAXS data we can not exclude also a Si nuclei formation but the evidence is not yet conclusive.

The third stage above 900°C shows a stable IR band at about 1080 cm^{-1}, characterizing the SiO_2 phase. This is again in agreement to our finding of a sudden decrease of the SiO layer thickness at the highest temperature of annealing revealing the formation of a uniform SiO_2 layer. The phase separation seems to be proportional to the temperature up to 1000ºC, but becomes more rapid at 1100°C, where it is expected to finish.

Silicon that results from the separation is diffusing through the ex SiO layer and is expected, under optimal preparation conditions, to aggregate into silicon nanoparticles. In this process, the SiO_2 layer acts as a buffer, blocking the diffusion out of the ex SiO layer, forcing the confined Si to remain in a layered order.

From the profile of the Bragg peaks in Fig. 1, we have calculated the bilayer correlation length in the direction perpendicular to the film, and the result is shown in Fig. 3. The correlation length behavior corresponds to the long range order of the bilayer thickness. Namely, it is increasing linearly with the annealing temperature up to 1000°C, after which it suddenly drops. The relaxation and compacting of the SiO layer with annealing is enhancing the ordering of the layered structure in this temperature range. The separated silicon formed is confined to the position of the ex SiO layer. However, at 1100°C, when the final and the most intensive aggregation into silicon nanoparticles occurs, the correlation suddenly drops. Apparently, the growth of the particles is not controlled well, and their sizes as well as position (with respect to the center of ex SiO layer) is not uniform throughout the layer itself.

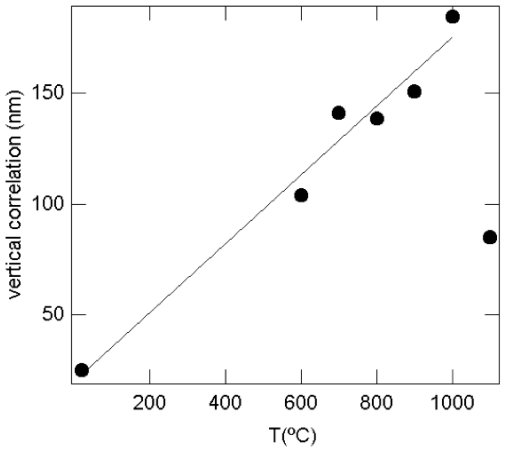

Figure 3. Vertical bilayer position correlation obtained from the width of the Bragg peak vs. the annealing temperature.

The formation of nanoparticles is indicated by a new contribution to the scattering, appearing as an enhancement of the scattering intensity in the range 0.3 $nm^{-1} < q_z < 0.7$ nm^{-1} (below the Bragg peak angle) for the 1100°C scattering intensity curve in Fig. 1. This scattering contribution is due to the particles whose position in the vertical direction is very poorly correlated (missing of the correlation peak). We estimated the size of the particles using a Guinier fit in this range, and the Guinier radius was found to be R_G=1.7nm^{-1}. This value was expected from the SiO layer thickness, which was 4 nm, but the absence of the vertical correlation peak suggests that the formed particles were largely scattered both in vertical and horizontal direction.

References

[1] G. Conibeer et al., Thin Solid Films, 511-512 654-659 (2006)
[2] Z.H.Lu, D.J.Lockwood and J.M.Baribeau, Nature 378 258-259 (1995)
[3] M. Zacharias, P. Streitenberger, Phys. Rev. B 62 8391-8396 (2000)
[4] I. Kovačević, B. Pivac, P. Dubček, N. Radić, S. Bernstorff, A. Slaoui, Thin Solid Films, 511-512 463-467 (2006)
[5] I. Kovačević, P. Dubček, S. Duguay, H. Zorc, N. Radić, B. Pivac, A. Slaoui, S. Bernstorff, Physica E, 38 50-53 (2007
[6] S. Bernstorff, P. Dubček, I. Kovačević, N. Radić, B. Pivac, Thin Solid Films, 515 5637-5640 (2007)
[7] L.X. Yi, J. Heitman, R. Scholz M. Zacharias, Appl. Phys. Lett. 22 4248-4250 (2002)

GISAXS STUDY OF NANOCRYSTALLINE NICKEL THIN FILMS

N. Radić[1], P. Dubček[1], S. Bernstorff[2]

1.) Rudjer Boskovic Institute, HR-10000, Zagreb, Croatia
2.) Sincrotrone Trieste, I-34012 Basovizza (TS), Italy

Nanocrystalline nickel (nc-Ni) is a very interesting material due to its enhanced mechanical, corrosion, and catalytic properties. Apart from the nanocrystals of different sizes which are present in the nc-Ni films, a considerable fraction of the films consists of a non-homogenous, disordered part mixed with nanocrystals. We have employed the GISAXS method to examine the nanocrystalline nickel films prepared by magnetron sputtering in a wide range of working gas pressure (0.33 Pa to 1.33 Pa) and onto substrates held at temperatures ranging from room temperature to 973 K. The results (in conjunction/correlation with XRD results taken on the same films [1]) allowed us to identify a component/phase of the film causing/governing the enhancement of a catalytic hydrogen evolution reaction [2].
GISAXS measurements were performed at the ELETTRA synchrotron radiation source, at the SAXS beamline, using the X-ray beam energy of 8 keV (λ = 1.54 Å). Grazing incidence measurements were taken at different, fixed grazing angles on the sample, using a 2-dimensional CCD detector (1024 x 1024 pixels) at a fixed position perpendicular to the incident beam. The spectra were corrected for background intensity and detector response. The incident angle was 0.1º above the critical angle for nickel, which results in about 150 nm X-ray penetration depth.
The GISAXS patterns for three samples deposited at different substrate temperatures (room temperature, 150 °C and 400 °C) are shown in figure 1.

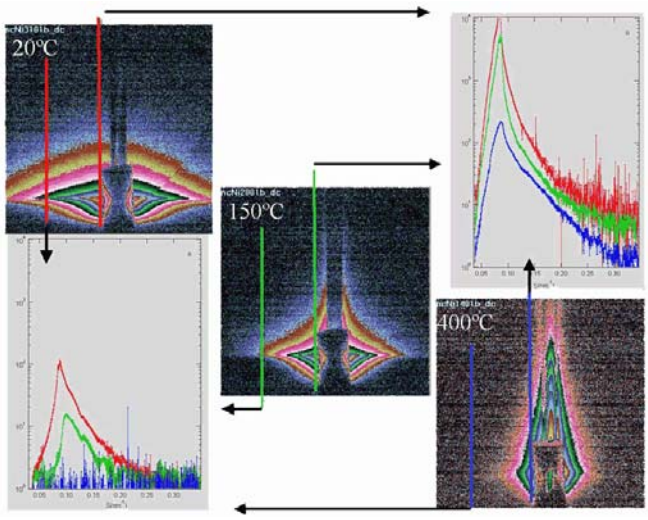

Figure 1. GISAXS patterns taken at 0.7º grazing angle for the nc-Ni samples deposited at different substrate temperatures as indicated in the figure. GISAXS intensities along $q_y = 0.20$ nm^{-1} (upper right corner) and $q_y = 0.75$ nm^{-1} (lower left corner) vs scattering angle for the nc-Ni samples deposited at different substrate temperatures (the upper curves correspond to 20 °C, the middle curves to 150 °C, and the lower curves to 400 °C).

Basically, the GISAXS patterns consist of two distinct parts whose relative intensity depends on the substrate temperature during deposition. At low temperatures (20 °C) isotropic scattering is dominating in the GISAXS pattern, while the scattering intensity is anisotropic and elongated along the specular plain at high substrate temperature (400 °C). The intermediate substrate temperature (150 °C) results in both contributions present at similar intensity levels.
In order to follow the evolution of the inhomogeneities with the substrate temperature, we show the intensities which were extracted from the 2-dim patterns along two different directions parallel to the specular plane, e.g. at $q_y = 0.75$ nm^{-1} and $q_y = 0.20$ nm^{-1} for the same substrate temperatures. The chosen cuts were convenient to separate the two distinct

contributions to the scattering, since there the isotropic/anisotropic contributions to the scattering are dominant, respectively.
Apart from the Porod (q^{-4}) type scattering above about $q_z = 1.2$ nm^{-1} (coming from the contrast between disordered part and larger nanocrystals that are embedded in the film), there is a particle-like scattering at smaller angles. A simple Guinier approximation was used in order to obtain the radius of gyration (R_G), e.g. typical size of the inhomogeneities as a function of temperature for both contributions to the GISAXS. The corrections for refraction (the bulk density of nickel was used for obtaining the electron density of nc-Ni), absorption and offset from the specular plane were included in the fitting function. Given the restricted angular range due to the refraction the obtained values of R_G serve as a reasonable approximation for the particle sizes and the influence of the sputtering temperature is clearly resolved. The results are presented in figure 2.

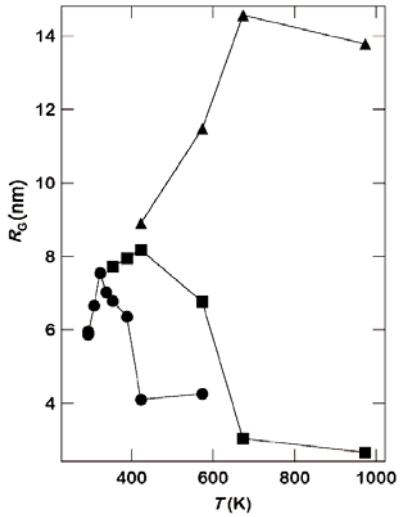

Figure 2. Size of the inhomogeneities in nc-Ni thin films: R_G was derived from GISAXS patterns for two kinds of inhomogeneities/"particles" - a) spherical (●), and b) platelet-like (■ and▲).

It was found that the nc-Ni films contain two kinds of. inhomogeneities - isotropic and platelet-like. The isotropic/round particles prevail up to about 100 °C, while above that temperature the platelet-like "particles" predominate
These inhomogeneities are ascribed to intergranular matter/ grain boundaries, since the grain size (as determined from the XRD patterns)
of the examined sample was found to increase from 12 nm in samples deposited at room temperature to about 90 nm in samples deposited at 150 °C, or higher temperatures.
A tentative explanation for the occurence (and competition between) the two kinds of inhomogeneities might be related to the incorporation of the residual gases as impurities into the intercrystalline matter.
In a separate investigation it was found that electrocatalytic activity of the nc-Ni films for the hydrogen evolution reaction (h.e.r.) significantly decreases (by more than 20 times) with the increasing deposition temperature and the increase of the Ni-grain size. Correspondingly, the catalytic activity of nanocrystalline nickel (nc-Ni) on the h.e.r. is markedly greater at larger fraction of the isotropic/spherical inhomogenities inside the film. This effect is especially strongly pronounced for the nc-Ni films prepared on the substrates at lower temperatures [2].

References:

[1] N. Radić, P. Dubček, S. Bernstorff, I. Djerdj, A. Tonejc, Journal of Applied Crystallography, 40, 377-382, 2007
[2] M. Metikoš-Huković, Z. Grubač, N. Radić, P. Dubček, I. Djerdj, Electrochemistry Communications 9, 299-302, 2007

ENHANCED BACKGROUND SCATTERING CAUSED BY DEFORMATION INDUCED VACANCIES: IN−SITU SYNCHROTRON WAXS, PART II: BODY CENTERED CUBIC METALS

E. Schafler[1], M. Kerber[1], L. Balogh[2], G. Ribárik[2],T. Ungàr[2], S. Bernstorff[3] and M. J. Zehetbauer[1]

1.) Institute of Materials Physics, University of Vienna, A-1090 Wien, Austria
2.) Department of General Physics, Eötvös University Budapest, H-1518 Budapest, Hungary
3.) Sincrotrone ELETTRA, Basovizza, I-34012 Trieste, Italy

During plastic deformation point defects are generated in parallel to line defect as well as planar ones. By assuming certain mechanisms for point defect generation which all include some interaction of dislocations, several models predict different strain dependent evolution laws for vacancy generation which have never checked by experiment so far [3]. One difficulty was to keep the vacancies stabile in density and/or in arrangement: They either annealed out or at least rearranged immediately after plastic deformation so that neither the density nor the arrangement of vacancies measured in the "dead" unloaded sample was representative for the deformation process. The present investigations are first attemts to check whether it is possible to measure vacancy concentrations *in-situ* during deformation in order to receive reliable data which can be compared with the models mentioned.

In situ X-ray line profile measurements were carried out at the SAXS beamline at ELETTRA in Trieste. Polycrystalline Tantalum specimens have been deformed in compression by a compact test machine mounted x-z-translation table in order to compensate the shape change during the deformation process. The (110), (211), (220) and (310) peaks have been measured in reflection by 3 linear position-sensitive detector. The polycrystalline Tantalum specimen with ultra-fine grain size smaller than 1 μm (state after equal channel angular pressing (ECAP) at 200°C, 8 x route B_C) have been investigated in-situ with a very low strain rate of about 10^{-5} s^{-1}. The diffraction peaks were recorded in 60 to 120 seconds, in this time intervall the true strain ε was smaller than 10^{-3} ('dynamic' measurements). The resulting true stress-true strain curve is shown in Fig.1. The abrupt decay in stress followd by a steep re-increase of the stress originates from deformation stops and re-starts. During these stops 'static' profiles have been recorded. Due to the low noise of the detector, the increase of the background to peak ratio R is attributed to diffuse scattering caused by deformation induced point defects, in particular by vacancies and/or vacancy clusters.

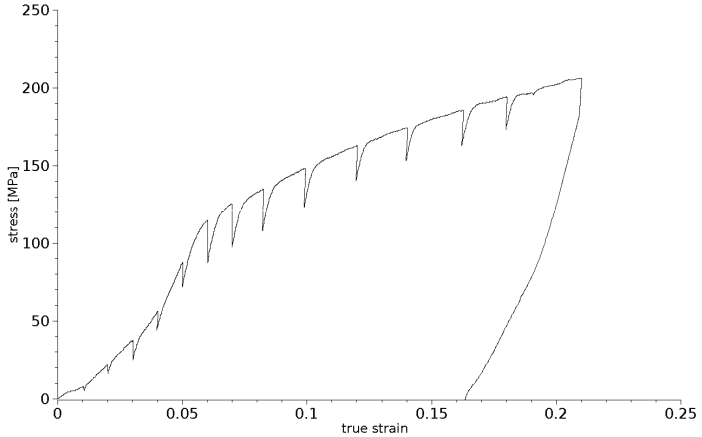

Figure 1. Stress-strain curve from the in-situ compression test of ultra-fine grained tantalum.

In the case of the undeformed specimens usually only a vanishing background intensity is observed. With increasing deformation the diffuse background intensity increased considerably. For the quantification of the diffuse background scattering, the ratio of the integrated background, A_{BG}, and the integrated peak intensity, A_{Peak}, has been introduced (see Figure1b) which is also a measure for the ratio between the densities of deformation induced vacancies and the dislocations [2]:

$$R = A_{BG}/A_{Peak} \quad (1)$$

The resulting deformation dependent evolution for the in-situ measurements of this ratio is presented in Figure 2. The extremly high value at the beginning of the deformation can be ascribed to a high vacancy concentration due the deformed state of the material – after this severe plastic deformation (ECAP) it has been shown that the deformation induced vacancy concentration is about a factor of 3 higher than compared to conventional deformation [3]

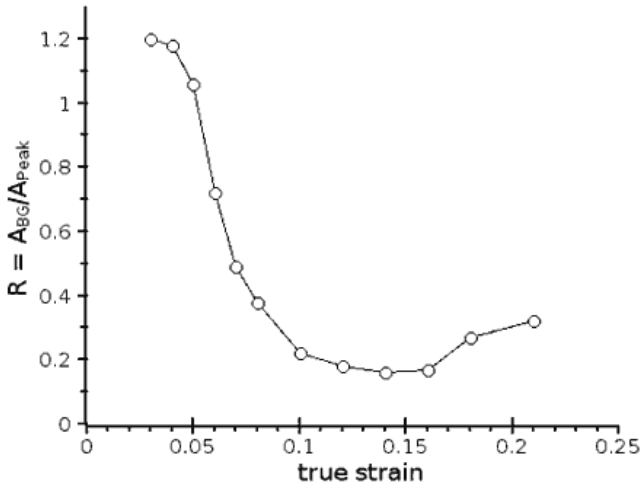

Figure 2. The ratios of the background to peak areas, *R*, for in-situ X-ray measurements of tantalum.

This evolution is rather surprising as the decrease of the value would mean a decrease of the vacancy concentration with increasing deformation. This can be interpreted as a loss of vacancies by increased annihilation of the already built in vacamcies in combination with the non-trivial deformation behaviour of bcc-metals at low homologous deformation temperatures. This assumption has to be investigated in more detail by additional X-ray as well as mechanical testing experiments.

References

[1] M. Zehetbauer, Key Eng. Mater. 97-98, 287 (1994).
[2] T. Ungár, E. Schafler, P. Hanák, S. Bernstorff, M. Zehetbauer, Mater. Sci. Eng. A 482, 398 (2007)
[3] E. Schafler, G. Steiner, E. Korznikova, M. Kerber, M. J. Zehetbauer, Mater. Sci. Eng. A 410-411, 169-173 (2005)

SAXS/DSC STUDY OF POLYMER ELECTROLYTE FOR NANOSTRUCTURED GALVANIC CELLS

A.Turković[1], M. Pavlović[1], P.Dubček[1], M. Lučić-Lavčević[2] and S. Bernstorff[3]

1.) Institute "Ruđer Bošković", P.O. Box 180, HR-10002 Zagreb, Croatia
2.) Department of Physics, Faculty of Chemical Technology, University of Split, Teslina 10/V, 21000 Split, Croatia
3.) Sincrotrone Trieste, S.S. 14, km 163.5 Basovizza, 34012 Trieste, Italy

$(PEO)_8ZnCl_2$ polymer electrolytes and nanocomposites were prepared using PEO γ-irradiated to a selected dose of 309 kGy and TiO_2 nanograins. The influence of the added nanosize TiO_2 grains to the polymer electrolytes and the effect of γ-radiation from a Co-60 source were studied by small-angle X-ray scattering (SAXS) simultaneously recorded with differential scanning calorimetry (DSC) at the SAXS-beamline of the synchrotron ELETTRA. Impedance spectroscopy (IS) was also performed. The above-mentioned treatments largely enhanced the conductivity of the polymer electrolyte.

SAXS/DSC of polymer electrolyte [PEO]8ZnCl2: Fig 1. is showing simultaneously performed SAXS and DSC of polymer electrolyte $(PEO)_8ZnCl_2$. In Figure 1a) the average grain sizes of a larger diameter are compared to DSC spectra. In a lamellar picture of PEO as presented in Baldrian et al. [1] the lamellar thickness for LP1 lamellae changes from 21 to 22 nm in the temperature range from 35 to 45˚C. This corresponds with our SAXS measurements for the grain sizes, which change from 19 to 20 nm in the same temperature range. In Figure 1b) the average grain sizes of a smaller diameter are compared to DSC spectra. These smaller grain sizes could be perceived as LP2 lamellae also combined with salt.

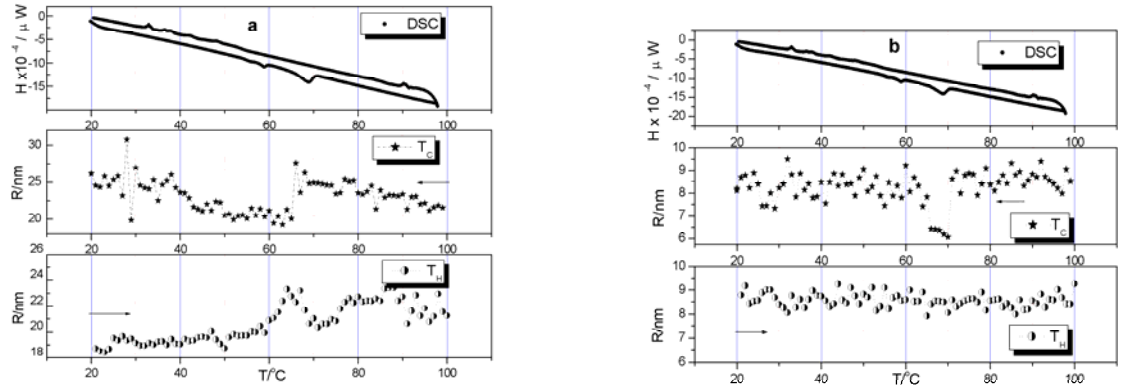

Figure 1. a) DSC and SAXS of $(PEO)_8ZnCl_2$ in the region of smaller grazing angle that is bigger average grain sizes, b) DSC and SAXS with smaller grain sizes.TH andTC refer to heating and cooling cycle, respectively).

SAXS/DSC of polymer electrolyte $(PEO)_8ZnCl_2$ nanocomposite with TiO_2: Heating and cooling cycles for larger nanosized structures, nanograins are shown in Fig 2a). Generally, their estimated average diameters (around 18 nm) are smaller than in pure polymer electrolyte. Smaller grains are shown in Fig 2b). The changes in size during the heating cycle confirm the complexity of this nanocomposite. The treatment of introducing nanograins of TiO_2 is reducing the size and number of the "spherulites", so it lowered their melting transition temperature. This we attribute to the influence of the TiO_2 nanograins on the polymer matrix.

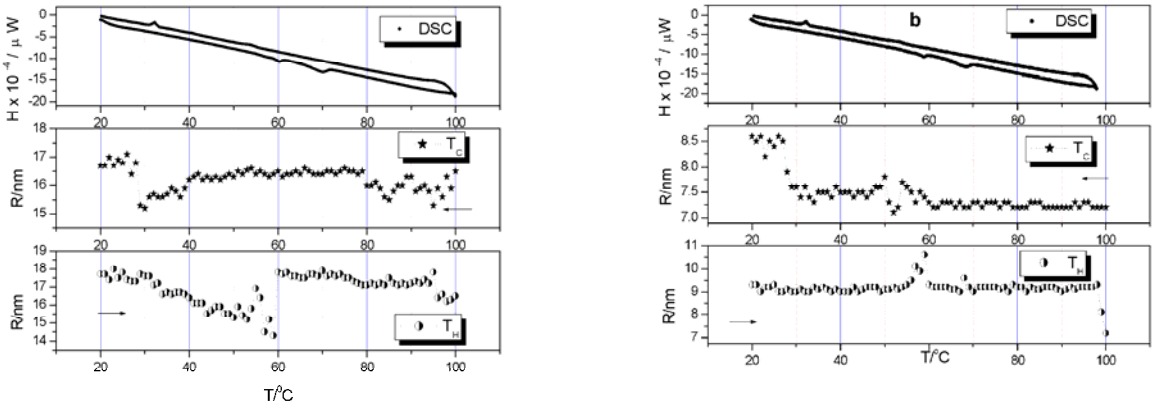

Figure 2. a) DSC and SAXS of $(PEO)_8ZnCl_2$ $+TiO_2$ in the region of smaller grazing angle that is bigger average grain sizes, b) DSC and SAXS with smaller grain sizes.T_H and T_C refer to heating and cooling cycle, respectively).

SAXS/DSC of γ-irradiated polymer electrolyte $(PEO)_8ZnCl_2$: Fig 3. is showing SAXS and DSC of material irradiated with γ-rays of 309 kGy. As a difference to the first two samples, which have a more disordered structure having two different grain sizes, this irradiated sample has only small grains. This is consistent with previous SAXS studies on irradiated PEO [2]. It was shown that irradiation with γ -rays mainly induces changes in the amorphous region and a decrease between crystalline and amorphous density [3]. Doses over 100 KGy result in melting of crystallites, which is applicable to our dose of 309 kGy. The amorphous phase becomes denser and causes a packing of the lamellar aggregates.

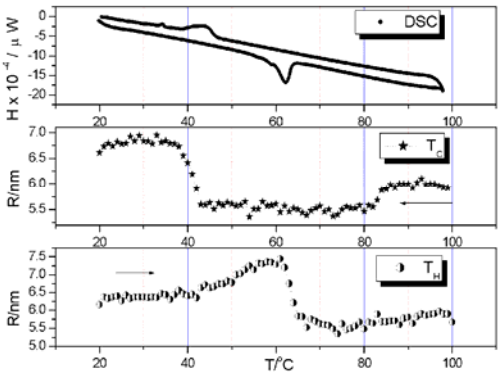

Figure 3. DSC and SAXS of $(PEO)_8ZnCl_2$ irradiated with γ-rays of 309 kGy.T_H andT_C referto heating and cooling cycle, respectively).

SAXS/DSC of γ-irradiated polymer electrolyte $(PEO)_8ZnCl_2$ nanocomposite with TiO_2: Fig 4. is showing SAXS and DSC of material irradiated with γ-rays of 309 kGy and nanocomposite with TiO_2 nanograins of 25 nm. As a difference to the first three samples, which are showing changes of grain sizes upon phase transition temperatures, this nanocomposite, irradiated sample has small grains, which are not changing upon the heating cycle. It was shown that irradiation with γ -rays mainly induces changes in the amorphous region and a decrease between crystalline and amorphous density [3]. Doses over 100 kGy result in melting of crystallites, which is applicable to this dose of 309 kGy. The amorphous phase becomes denser and causes of packing of the lamellar aggregates.

By means of combined DSC/SAXS measurements, we have shown that the nanostructure of polymer electrolyte $(PEO)_8ZnCl_2$ can be modified by two treatments applied during preparation of electrolytes: the irradiation with γ-rays and the addition of TiO_2 nanosize particles [4,5]. The significant role that the nano-dimensions of the electrolyte material play in Zn^{2+}-ion mobility, oxygen reduction in TiO_2 nanograins and cross-linking are discussed. Both treatments largely enhanced the conductivity of polymer electrolytes. SAXS information about the evolution of the average grain sizes during the phase transition gave insight into the nanomorphology, which influences ionic transport in nanocomposite polymer electrolyte. Further optimisations of electrolyte properties are in progress as nanostructured materials are very attractive for batteries or other types of electronic devices.

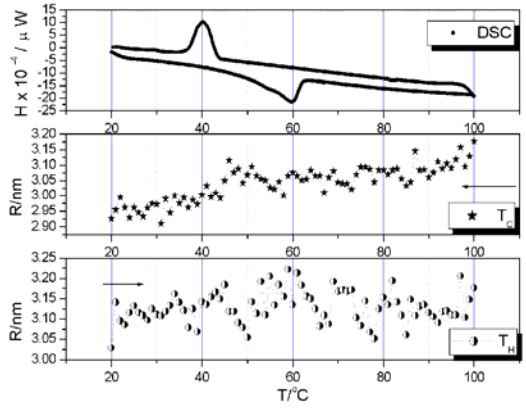

Figure 4. DSC and SAXS of $(PEO)_8ZnCl_2$ +TiO_2 irradiated with γ-rays of 309 kGy. (T_H and T_C refer to heating and cooling cycle, respectively).

References:

[1] J.Baldrian, M.Horky, M.Steinhart, H.Amenitsch and S.Bernstorff, Anuall Report 2000 Austrian SAX S Beamline at ELETTRA, 72 [2000].
[2] S.Tsvetkova and S.Tsvetkova, Radiat. Phys.Chem. 43(4) 397 [1994].
[3] S.Tsvetkova and S.Tsvetkova, Colloid & Polymer Science 272 903 [1994].
[4] A.Turković, M.Pavlović, P.Dubček, M.Lučić-Lavčević, B.Etlinger and S.Bernstorff, ECS Transactions 2 (20) 11 [2007].
[5] A.Turković, M.Pavlović, P.Dubček, M.Lučić-Lavčević, B.Etlinger and S.Bernstorff, Jornal of The electrochemical Society 154 (6) 1 [2007].

2. Life Science

DNA RELEASE FROM CATIONIC LIPOSOME/DNA COMPLEXES BY ANIONIC LIPIDS

G. Caracciolo[1], D. Pozzi[1], R. Caminiti[1], C. Marchini[2], M. Montani[2], A. Amici[2] and H. Amenitsch[3]

1.) Department of Chemistry, University of Rome "La Sapienza", P.le A. Moro 5, 00185 Rome, Italy
2.) Genetic Immunization Laboratory, Department of Molecular Cellular and Animal Biology, University of Camerino, Via Camerini 5, 62032 Camerino (MC), Italy.
3.) Institute of Biophysics and Nanosystems Research, Austrian Academy of Sciences, Schmiedelstrasse 6, A-8042 Graz, Austria

Cationic liposome/DNA complexes, named lipoplexes, currently account for the largest sector of non-viral gene delivery systems that are under clinical trials [1]. We have recently prepared multicomponent (MC) cationic liposome/DNA complexes (MC/DNA lipoplexes) [2,3]. With respect to usually employed lipoplexes, MC/DNA lipoplexes incorporate within the lipid bilayer a greater number (from three to six) of lipid molecules with different headgroups and a number of systematic variations in relevant physical-chemical parameters [2,3]. We have shown that such multicomponent systems may represent efficient gene vectors. Here we also show that, upon interaction of lipoplexes with anionic liposomes (model of cellular membranes), the highest the molar fraction of released DNA the lowest the transfection efficiency (TE) of lipoplexes. On the basis of our TE and structural results we claim that structural stability upon interaction with anionic lipids may be identified as a likely reason for why lipoplexes transfect cells with varying efficiency.

In the present study, we chose the well characterized DOTAP−DOPC and DC-Chol−DOPE binary liposomes, and the MC lipid system incorporating all the four lipid species simultaneously. TE of the above lipid formulations was investigated by performing transient transfection assay of two cell lines, namely a fibroblast cell line, NIH 3T3, a tumoral myofibroblast-like cell line, A17.

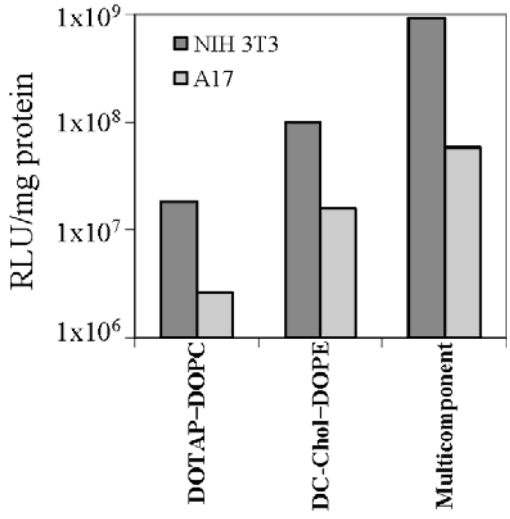

Figure 1. Transfection efficiency of DOTAP−DOPC/DNA, DC-Chol−DOPE/DNA and MC/DNA lipoplexes in mouse fibroblast (NIH 3T3; dark grey) and tumoral myofibroblast-like (A17; light grey) cell lines.

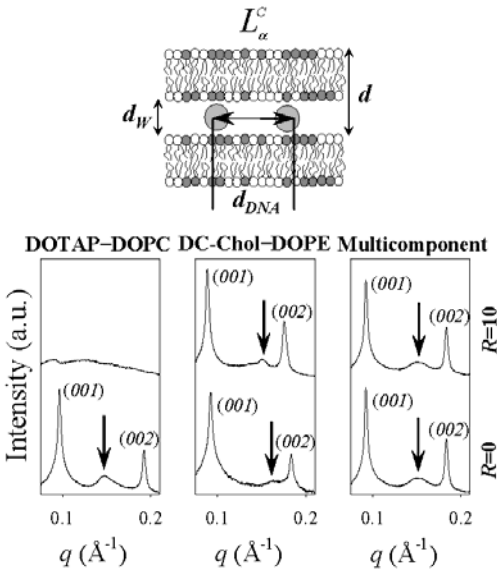

Figure 2. Synchrotron SAXD patterns of DOTAP−DOPC/DNA, DC-Chol−DOPE/DNA and MC/DNA lipoplexes as a function of the charge ratio, *R*=anionic charge/cationic charge

Figure 1 shows TE of the three lipid formulations with each bar representing an average value over at least three independent observations (standard deviation ≤10%). In both the cell lines, the TE of the formulations was in the following order: DOTAP−DOPC<DC-Chol−DOPE<MC. These results suggest potential utility of MC/DNA lipoplexes as efficient vector of genes. It has been recently shown that the structure of lipoplexes can be strongly modified, and even destroyed, by interaction with anionic lipids (such those the cellular membrane is rich in) and that such structural changes may critically affect the TE [4,5].
We therefore applied synchrotron small angle X-ray diffraction (SAXD) to study the structural changes of lipoplexes upon interaction with anionic liposomes (models of cellular membranes) prepared from diphosphatidylglycerol (DOPG), an anionic lipid common in mammalian cells, and added to lipoplexes. In the absence of anionic lipids (R=anionic charge/cationic charge=0), the SAXD patterns of Figure 2 show that DOTAP−DOPC/DNA, DC-Chol−DOPE/DNA and MC/DNA lipoplexes form highly-organized lamellar phases (L_α^C phase). The sharp periodically spaced peaks at q_{00n} are caused by alternating lipid bilayer-DNA monolayer structure with periodicity $d=2\pi/q_{001}$. The lamellar periodicity along the normal to lipid bilayer, d, is the sum of the lipid bilayer thickness (d_B) and the thickness of the water/DNA layer (d_W): $d=d_B+d_W=2\pi/q_{001}$. In Figure 2, the much broader peak (marked by an arrow) is the 'DNA peak' arising from the one-dimensional (1D) in plane lattice with repeat distance $d_{DNA}=2\pi/q_{DNA}$. From the synchrotron SAXD patterns of Figure 2 we calculated the electron density profiles along the normal to lipid bilayers from which, in turn, we routinely retrieved all the structural parameters of lipoplexes as listed in Table 1. In excess of anionic charge (R=10), the SAXD pattern of the less efficient DOTAP−DOPC/DNA lipoplexes changed remarkably and we could only detect a broad and weak first-order Bragg peak while there was no trace of higher order reflections and of the DNA peak. It means that DOTAP−DOPC/DNA lipoplexes were unstable against solubilisation by anionic DOPG and that the most part of delivered DNA was released. DC-Chol−DOPE/DNA lipoplexes were more stable than DOTAP−DOPC/DNA lipoplexes, but a part of the gene freight was released as shown by the enlargement in the DNA distance (Table 1).

	d (Å)	d_B (Å)	d_W (Å)	d_{DNA} (Å)
DOTAP-DOPC/DNA	64.6	38.4	26.2	42.6
DC-Chol-DOPE/DNA	67.9	41.6	26.2	38.1
MC/DNA	66.1	39.8	26.3	41.1

Table 1. Lamellar d-spacing, lipid bilayer thickness, d_B, water layer thickness, d_W, and DNA-DNA distance, d_{DNA}, of DOTAP−DOPC/DNA, DC-Chol−DOPE/DNA and MC/DNA lipoplexes (ρ=cationic lipid/DNA base=3.2) at R=0 calculated from the electron density profiles along the normal to lipid bilayers.

On the other side, the lamellar structure of the most efficient MC/DNA lipoplexes was absolutely not affected by interaction with anionic lipids. How are these findings related to the mechanism of transfection? Our SAXD experiments suggested possible events occurring at the early stages of internalization of lipoplex inside the cytoplasm. The less efficient binary lipoplexes might dissociate early in the cytoplasm where naked DNA is easily digested by enzymes the cytoplasm is rich in. Conversely, stable MC/DNA lipoplexes may protect the delivered DNA and may release their gene freight slowly in the cytoplasm. DNA release from lipoplexes is an essential step during lipofection and is believed to be the result of charge neutralization by cellular anionic lipids.
We have also presented a general formalism for calculating upper and lower limits of the molar fraction of DNA released from lamellar lipoplexes and of the molar fraction of anionic

lipid the lipoplex accommodate by using 1D DNA packing density as calculated by synchrotron SAXD patterns.

References:

[1] P. L. Felgner and G. M Ringold, Cationic liposome mediated transfection, Nature 331, 461-462 (1989).
[2] G. Caracciolo, D. Pozzi, R. Caminiti and H. Amenitsch, Lipid mixing upon deoxyribonucleic acid-induced liposomes fusion investigated by synchrotron small-angle x-ray scattering, Appl. Phys. Lett. 87, 133901-3 (2005).
[3] G. Caracciolo, D. Pozzi, H. Amenitsch and R. Caminiti, Multicomponent cationic lipid-DNA complex formation: role of lipid mixing, Langmuir 21, 11582-11587 (2005).
[4] R. Koynova, L. Wang, Y. Tarahovsky and R. C. MacDonald, Lipid Phase Control of DNA Delivery, Bioconjugate Chem. 16, 1335-1339 (2005).
[5] R. Koynova and R. C. MacDonald, Lipid transfer between cationic vesicles and lipid-DNA lipoplexes: effect of serum, Biochim Biophys Acta 1714, 63-70 (2005).

STRUCTURAL STABILITY AGAINST DISINTEGRATION BY ANIONIC LIPIDS RATIONALIZES THE EFFICIENCY OF CATIONIC LIPOSOME/DNA COMPLEXES

G. Caracciolo[1], D. Pozzi[1], R. Caminiti[1], C. Marchini[2], M. Montani[2], A. Amici[2] and H. Amenitsch[3]

1.) Department of Chemistry, University of Rome "La Sapienza", P.le A. Moro 5, 00185 Rome, Italy
2.) Genetic Immunization Laboratory, Department of Molecular Cellular and Animal Biology, University of Camerino, Via Camerini 5, 62032 Camerino (MC), Italy.
3.) Institute of Biophysics and Nanosystems Research, Austrian Academy of Sciences, Schmiedelstrasse 6, A-8042 Graz, Austria

We investigated the correlation between transfection efficiency (TE) and structural evolution of lipoplexes upon interaction with cellular (anionic) lipids. To this end, we used both binary and multicomponent (MC) lipoplexes [1,2]. We applied small angle synchrotron X-ray diffraction (SAXD) to study the structural correlates of the lipoplex formulations and their mixtures with anionic lipids. Electrophoresis experiments were carried out to measure the extent of DNA unbinding.

We were particularly interested in whether the structural changes in lipoplexes might correlate with the TE data. To this end, we mixed lipoplexes and anionic liposomes (models of cellular membranes) made of DOPG, an anionic lipid commonly found in mammalian cells. After the addition of negatively charged DOPG liposomes to the preformed lipoplexes, the structural organization of the membranes changed remarkably as a function of R=anionic/cationic charge ratio. Most importantly, we found evidence for the existence of three different stages.

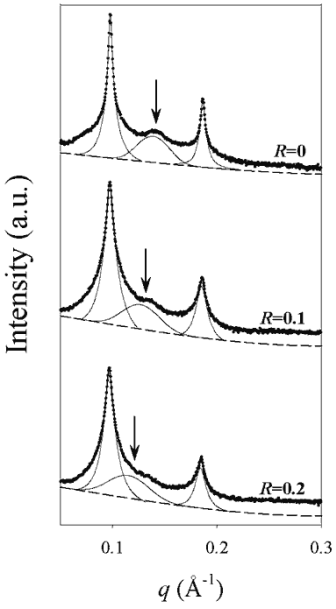

Figure 1. SAXD pattern of DOTAP–DOPC/DNA lipoplexes as a function of increasing anionic/cationic charge ratio, R ($0<R<0.2$).

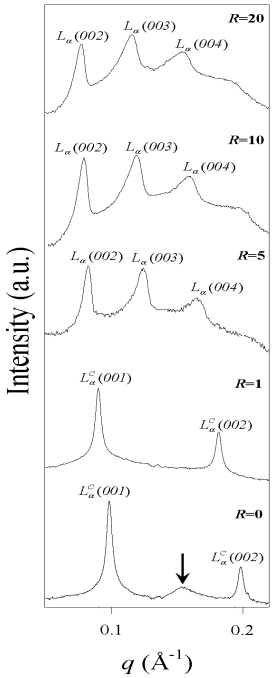

Figure 2. SAXD pattern of DOTAP–DOPC/DNA lipoplexes as a function of increasing anionic/cationic charge ratio, R.

In the first stage (0<*R*<1), SAXD patterns of lipoplexes changed, but the lamellar structure of lipoplexes was essentially preserved. Figure 1 shows the structural evolution of DOTAP–DOPC/DNA lipoplexes upon interaction with anionic lipids in the narrow range of anionic/cationic charge (0<*R*<0.2). SAXD measurements indicated that the DNA lattice was diluted by anionic lipids. This can be seen in SAXD scans where d_{DNA} changes from 42.6 Å at *R*=0 up to 51.4 Å at *R*=0.2. In the second stage, starting from *R*~1, a major reorganization of the initial multilamellar structure of lipoplexes subsequent to their interaction with anionic lipids was observed. Figure 2 shows SAXD patterns of DOTAP–DOPC/DNA lipoplexes as a function of *R*. Diffraction maxima of the L_{α}^{C} phase were visible up to *R*=1. For *R*>1, the system underwent a phase transition where disintegration of the initial structure of DOTAP–DOPC/DNA lipoplexes appeared. This was ascribed to the progressive disintegration of DOTAP–DOPC membranes by DOPG molecules. Structural changes induced by anionic lipids strictly depended on the lipid composition of lipoplexes. We defined R* as the anionic/cationic charge ratio at which disintegration of lamellar lipoplexes was completed.
Given the complexity of the lipoplex-AL system, it is remarkable that the data coalesced into a convex curve when plotted against R* (Figure 3). The new TE curve of Figure 3 exhibits three well-defined regimes of stability. Regime A, corresponding to unstable complexes, features an exponential increase in efficiency of over 2 orders of magnitude with increasing R*. Regime C, corresponding to highly stable complexes, is characterized by a decrease in efficiency with growing R*.

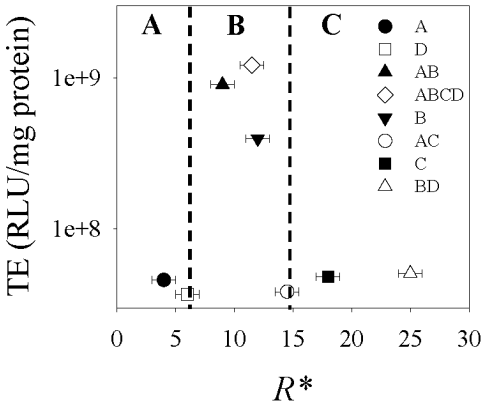

Figure 3. TE in RLU per mg/cellular protein plotted as a function of R* intended as the anionic/cationic charge ratio at which solubilisation of the lamellar phase of lipoplexes is complete.

Figure 3 also shows the existence of an intermediate regime (regime B) corresponding to the highest TE. This regime appeared to be like the region of optimal stability. Endocytosis is the dominant mechanism of entry of lamellar lipoplexes, as evident in recent work.52. After cellular uptake via endocytosis, lipoplexes must escape from endosomes in order for DNA to move toward the cell nucleus. As Figure 3 clearly shows, inefficient lipoplexes were unstable against disintegration by anionic lipids (regime A, Figure 13) and released DNA upon adhering to anionic vesicles. This may suggest that unstable lipoplexes fuse with the endosomal membrane and dissociate early in the cytoplasm, where naked DNA can be easily digested by enzymes in which the cytoplasm is rich. Rapid escape from the endosome might be unfavorable because it would prevent the complex from taking advantage of the trafficking of endosomes toward the nucleus. At high R*, lipoplexes were found to be inefficient, suggesting that high stability may also be an obstacle to successful DNA delivery by lamellar CL-DNA complexes. The maximum TE in the regime of optimal stability (regime B, Figure 13) is a sign of the compromise between opposing requirements: the structural instability of complexes may be disadvantageous because of the quick dissociation of complexes in the

cytoplasm whereas high stability may be at the origin of the endosomal entrapment of lipoplexes.

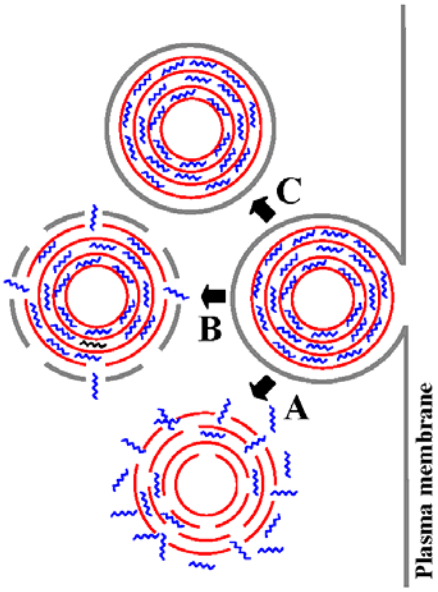

Figure 4. Proposed mechanism of the interaction of lipoplexes with the anionic plasma membrane of the cell. The less stable the lipoplexes, the earlier the dissociation of DNA in the cytoplasm (A). When naked, DNA may be easily digested by enzymes in which the cytoplasm is rich. Optimally stable lipoplexes (B) may release delivered DNAslowly into the cytoplasm, the event occurring through interactions with anionic proteins that readily form complexes with cationic vesicles. Lipoplexes that are too stable (C) do not fuse with the endosomes and do not allow for DNA release. Endosomal entrapment therefore results in a decrease in transfection efficiency.

Bearing in mind that for efficient delivery DNA must be retained until the lipoplex is in the vicinity of the nucleus, the stability of lipoplex structures is likely responsible for the successful transfer of DNA into the cell nucleus. Figure 4 summarizes a possible mechanism occurring in the early stages of internalization of the lipoplex within the cell. Electrostatic attractions let the lipoplex approach the anionic surface of the cell, and attachment is followed by endocytosis, resulting in endosomal entrapment. Our experiments suggest that the less stable lipoplexes dissociate early in the cytoplasm where naked DNA may be easily digested by enzymes in which the cytoplasm is rich. As a result, unstable lipoplexes are slightly efficient because the lipoplex might dissociate in the cytoplasm instead of in the nuclei.Optimally, stable lipoplexes may release delivered DNA slowly in the cytoplasm, with the event occurring through interactions with anionic proteins that readily form complexes with cationic vesicles. Overly stable lipoplexes remain trapped within endosomes and do not allow for complete DNA release, therefore resulting in a decrease in TE.

References:

[1] G. Caracciolo, D. Pozzi, R. Caminiti and H. Amenitsch, Appl. Phys. Lett. 87, 133901-3 (2005).
[2] G. Caracciolo, D. Pozzi, H. Amenitsch and R. Caminiti, Langmuir 21, 11582-11587 (2005).

NON-EQUILIBRIUM PHASE BEHAVIOUR FOR LIQUID CRYSTALS DURING HEATING AND COOLING

Y.D. Dong[1], H. Amenitsch[2], M. Rappolt[2], B. J Boyd[1]

1.) Department of Pharmaceutics, Victoria College of Pharmacy, Monash University, Parkville, VIC 3052, Australia
2.) Austrian Academy of Sciences, Institute of Biophysics and Nanosystems Research, Schmiedlstraße 6, A-8042 Graz, Austria

Introduction: Polar lipids, due to their amphiphilic molecular structure and insolubility in water often form nanostructured self-assembled systems such as lamellar (Lα), inverse cubic (Q_{II}), and inverse hexagonal (H_{II}) lyotropic liquid crystals in water. In some instances these liquid crystalline structures may be dispersed to form sub-micron particles, which retain the internal structure of the non-dispersed phase. The particles have been proposed to be useful as drug delivery vehicles, as drug release is dependent on phase structure, however the dynamic changes in the internal liquid crystal structure that can occur with temperature have been largely unexplored.
In these studies we used SAXS to determine whether the nanostructure of the liquid crystalline particles formed using phytantriol (PHYT), glyceryl monooleate (GMO), phytanyl glycerate (PG) and oleyl glycerate (OG) behave similarly to the parent bulk phase during heating and cooling. Both pure GMO and Myverol (an often utilised commercial form of GMO) were investigated. The impact of additives (oleic acid (OA) and vitamin E acetate (VitEA)), used to manipulate the transition temperatures between liquid crystalline phases in these systems with a view to their biological application, was also explored.

Results: In addition to gaining valuable information on the suppression of transition temperatures by VitEA and OA (Figure 1), there were three major new findings arising from these experiments that have consequences for the design and use of these systems in drug delivery applications;

i) significant supercooling can occur for the dispersed submicron particles as well as the bulk phase previously reported. In fact, the particles showed a propensity for greater supercooling than the parent LC phases,
ii) The phase progression on heating is not always obeyed on cooling, and
iii) The lattice spacing in some instances increases on heating immediately prior to a phase transition.

Supercooling: The bar charts in Figure 1 were derived from phase changes observed in the 3D intensity vs q vs temperature contour plots obtained for these systems (similar to Figure 3, but for different systems) when heated and cooled at 1°C/min using the DSC sample environment. Both GMO and PHYT based particle and bulk systems showed a significant super-cooling effect, in which the thermal phase transition boundaries were significantly lowered during cooling compared to heating. For example, the bottom pair of bar charts in Figure 1 show that for the non-dispersed bulk phytantriol-water system, the H_{II} (grey) to L_2 (black) phase transition occurred at 70°C on heating but at approximately 60°C on cooling. The dispersed form did not show the H_{II} phase in the absence of VitEA, and the L_2 phase persisted down to 40°C. While this may be in part due skipping the H_{II} phase in the particle system, the systems containing 3% and 5% VitEA showed significantly greater supercooling for the particle form compared to the bulk form.

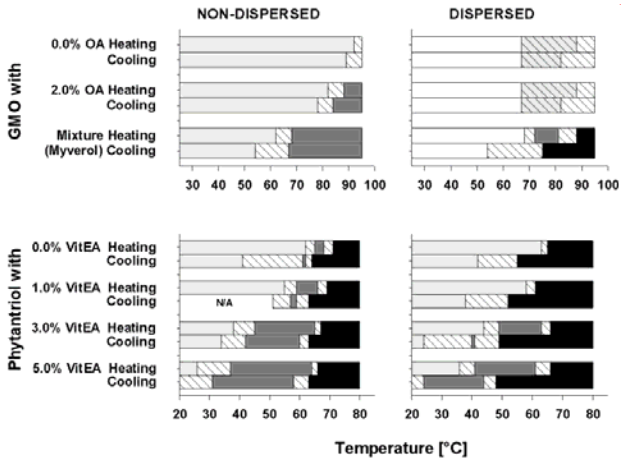

Figure 1. Comparison of phases formed during heating and cooling at 1 °C min^{-1} for non-dispersed and dispersed lyotropic systems in excess water, white = $Q_{II(Im3m)}$; light grey = $Q_{II(Pn3m)}$; dark grey = H_{II}; black = L_2; light grey diagonal stripes = $Q_{II(Im3m)}$ + $Q_{II(Pn3m)}$ co-existence; white diagonal stripes = transitional co-existence range between phases.

The exact reason for the difference in supercooling between the bulk and particle forms are not known at this time, but the limited number of unit cells in the submicron particles may lead to greater resistance to nucleation of new phases on cooling compared to the bulk phase. An even more dramatic supercooling phenomenon was observed with the phytanyl glycerate dispersion. The changes in phase structure and lattice parameter with heating (filled) and cooling (open) symbols are shown in Figure 2. This material transforms from H_{II} to L_2 phase at 65°C but on cooling retains the L_2 phase to below 30°C – this is an extreme example of the system avoiding the increase in packing frustration associated with the L_2 to H_{II} conversion described previously.[1]

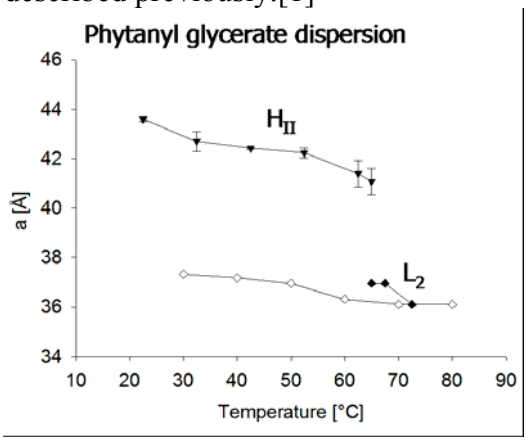

Figure 2. Phase structure and lattice parameter derived from I vs q plots at selected temperatures for phytanyl glycerate dispersion on heating (filled symbols) and cooling (open symbols).

Differences in Phase Progression: The intensity vs. q. vs. temperature contour plots for the Myverol and GMO dispersions are shown in Figure 3, and the phase sequence shows some interesting differences bringing into question the validity of substituting Myverol for GMO. Of particular interest is that for Myverol, on heating, the primitive cubic phase (Q_{Im3m}) transforms to an H_{II} phase, then to the L_2 phase, in agreement with the equilibrium phase behaviour. [2] However, on cooling there is no H_{II} phase observed, and before reversion to the primitive cubic phase, a region of co-existing diamond (Q_{Pn3m}) and gyroid phase (Q_{Ia3d}) is observed. The gyroid phase only occurs at equilibrium at low water contents, indicating that the kinetics of movement of water into the lattice on cooling impacts on the phase behaviour, even for the submicron particles. Similar behaviour was observed in the phytantriol bulk and dispersed systems (Figure 4), where a gyroid cubic phase occurred on cooling, even for the PHYT particles.

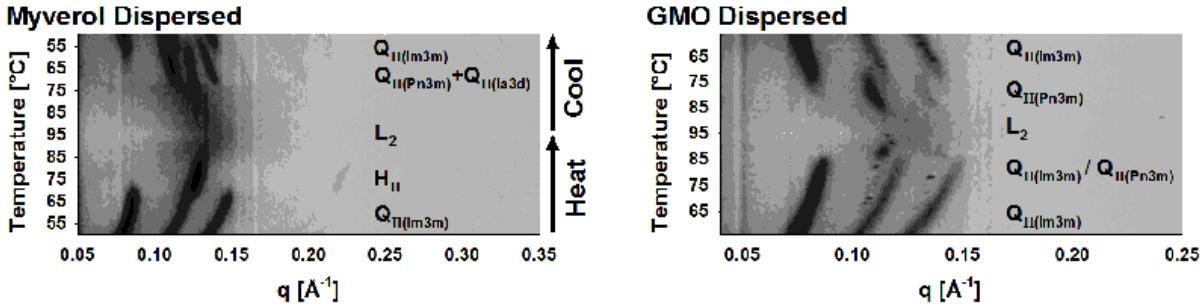

Figure 3. Contour plots (intensity vs q vs temperature) obtained for the Myverol and GMO dispersions on heating and cooling at 1°C/min with phase assignments indicated. Dark regions indicate increased scattering intensity.

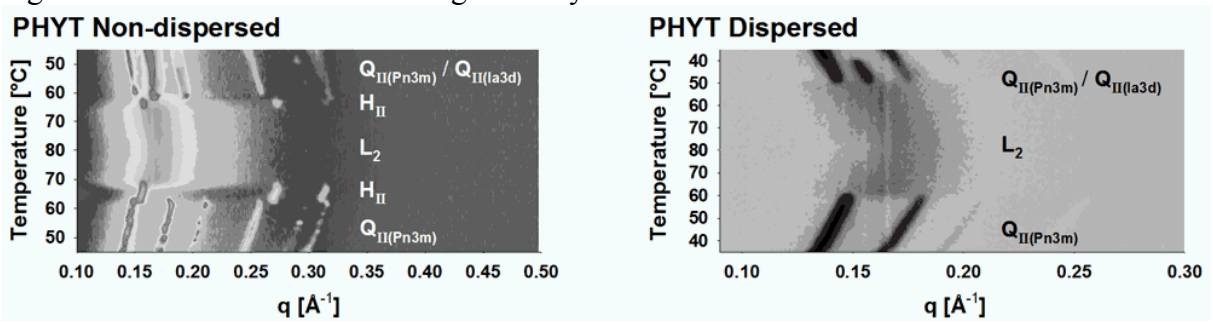

Figure 4. Contour plots (intensity vs q vs temperature) obtained for the phytantriol bulk phase and submicron dispersion on heating and cooling with phase assignments indicated. Dark regions indicate increased scattering intensity.

Lattice Expansion prior to Phase Change: All liquid crystalline systems investigated showed a continuous decrease in lattice spacing during heating, however in the case of some of the non-dispersed systems, there was an increase in the lattice spacing immediately before the transition boundary where the systems converted to H_{II} or L_2 phase. This is best illustrated using a plot of lattice spacing versus temperature in Figure 5, showing the slight upward inflexion in lattice parameter for the OG bulk phase at the transition boundaries. We believe this phenomenon to again be related to restrictions in the bulk movement of water through the lattice.

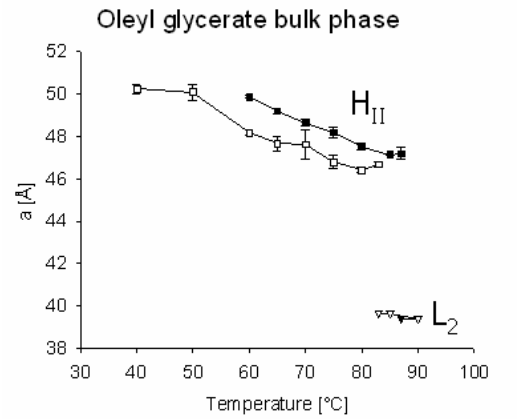

Figure 5. Phase structure and lattice parameter derived from I vs q plots at selected temperatures for oleyl glycerate bulk phase on heating (filled symbols) and cooling (open symbols).

Conclusion: Previous assumptions that the internal nanostructure of liquid crystalline particles closely follows the bulk phase behaviour and that the particles are in effective equilibrium with their surroundings have been challenged. We intend to next examine the kinetic aspects of these phase transitions in more detail.

References:

[1] de Campo, L., et al. Langmuir 2004, 20, 5254-5261
[2] Dong, Y. D., et al. Langmuir 2006, 22, 9512-9518

EFFECTS OF PLANT STEROLS ON STRUCTURE AND FLUCTUATIONS OF LIPID MEMBRANES

A. Hodzic, M. Rappolt, H. Amenitsch, P. Laggner, G. Pabst.

Institute of Biophysics and Nanosystems Research, Austrian Academy of Sciences, Schmiedlstr. 6, A-8042 Graz, Austria.

We have studied the concentration dependent influence of cholesterol, stigmasterol and sitosterol on the global structure and the bending fluctuations of fluid dimyristoyl phosphatidylcholine (DMPC) and palmitoyl oleoyl phosphatidylcholine (POPC) bilayers applying small-angle X-ray scattering. Applying a previously developed global X-ray data analysis technique [1,2] we find for both lipids that cholesterol is most efficient in increasing bilayer thickness and decreasing bilayer elasticity, followed by sitosterol and stigmasterol (Figs. 1-3).

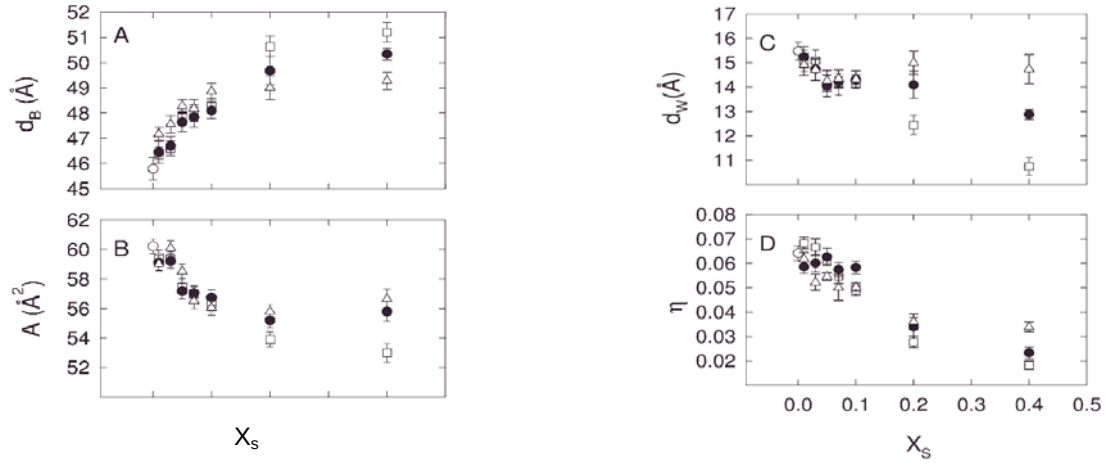

Figure 1. Global structural parameters of DMPC at 35°C in presence of cholesterol (□) sitosterol (●) and stigmasterol (Δ). (○)´s show results for the pure lipid. Panel **A** shows the concentration dependence of the membrane thickness, panel **B** lateral area per lipid, panel **C** the interstitial water layer, panel **D** Caille' parameter.

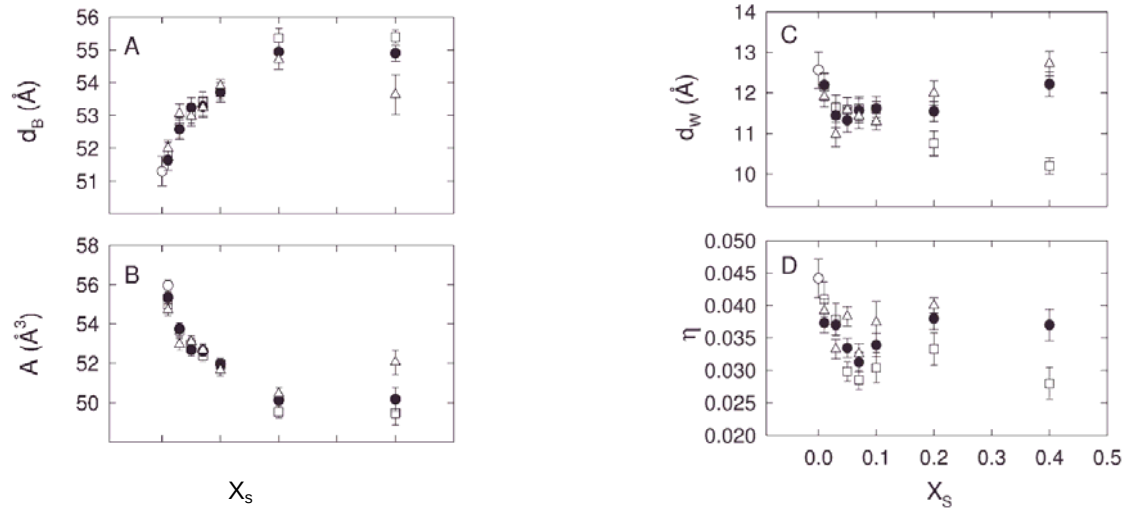

Figure 2. Global structural parameters of POPC (○) at 7°C in presence of cholesterol (□) sitosterol (●) and stigmasterol (Δ). (○)´s show results for the pure lipid. Panel **A** shows the concentration dependence of the membrane thickness, panel **B** lateral area per lipid, panel **C** the interstitial water layer, panel **D** Caille' parameter.

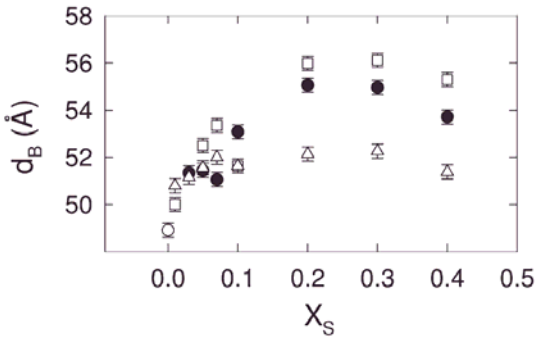

Figure 3. Global structural parameter of POPC (○) at 25°C in presence of cholesterol (□) sitosterol (●) and stigmasterol (Δ) at various concentrations. The diagram shows the concentration dependence of the membrane thickness, d_B.

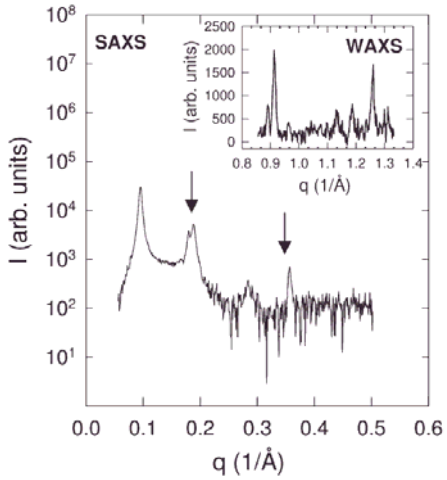

Figure 4. SWAXS patterns of fully hydrated POPC vesicles with 40 mol % of stigmasterol at 7°C. Arrows indicate the first and second order reflection of stigmasterol monohydrate (d = 34Å).

SWAXS data are showing a phase separation only in mixture of POPC and stigmasterol at 40 mol% concentration (Fig. 4), although lipids and sterols were prepared in the same way. Additional ethyl groups and double bonds of stigma- and sitosterol cause less solubility within the bilayer, which is most pronounced for POPC at high temperatures (Fig. 3). We agree with a previous study, which suggests that the double bond at carbon C_{22} gives stigmasterol a lower ability to interact with lipid bilayer [3]. Hence, it appears that some flexibility of the sterol hydrocarbon chain is needed in order to accommodate within the lipid bilayer. In addition, we do not observe two populations of membranes within the nominal liquid-ordered/liquid-disordered phase coexistence regime of binary sterol/lipid mixtures but a uniform phase. This lends further support to the idea of compositional fluctuations recently brought up by fluorescence microscopy experiments [4], which contrasts the formation of stable domains within the miscibility gap.

Acknowledgement: This work was supported by the Austrian Science Fund (Grant No. P17112-B10 to GP)

References

[1] Pabst, G., M. Rappolt, H. Amenitsch, and P. Laggner. 2000. Phys. Rev. E 62:4000-4009.
[2] Pabst, G., R. Koschuch, B. Pozo-Navas, M. Rappolt, K. Lohner, and P. Laggner. 2003. J.Appl. Crystallogr. 63:1378-1388.
[3] Hallig, K.K.,and J.P. Slotte, 2004. Biochim. Biophys. Acta 1664:161-171
[4] Veatch, S.L., K. Gawrisch, and Keller, S.L. 2006. Biophysical Journal 90:4428-4436.

SOLID SUPPORTED MEMBRANES MEASURED BY HIGH-PRESSURE GISAXS

M. Kriechbaum[1], M. Steinhart[2], H. Amenitsch.[1], M. Rappolt[1], B. Sartori[1], B. Marmiroli[1], S. Bernstorff[3] and P. Laggner[1]

1.) Institute of Biophysics and Nanosystems Research, Austrian Academy of Sciences, Graz, Austria.
2.) Institute of Macromolecular Chemistry, Czech Academy of Sciences, Prague, Czech Republic.
3.) Sincrotrone ELETTRA, Basovizza, TS, Italy.

Lipid bilayers as the universal structural matrix of biological membranes show a big variety of mesophases as a function of temperature, pressure or hydration. Their supramolecular structures (long- and short-range order) and phase transitions have already been studied extensively by small-angle X-ray diffraction. So far, most of these studies have been performed on lipids in bulk solutions where the lamellar lipid multi-layers or other higher-dimensional phases (hexagonal or cubic phases) are randomly oriented and dispersed as multi-lamellar liposomes in the aqueous bulk solution.
In order to gain more structural information other than in these bulk solution studies we have performed surface SAXS experiments on these membrane lipids aligned and oriented by a controlled deposition (about 100 bilayers) on a solid support (Si-wafer) and placed in a temperature-controlled SAXS high-pressure cell. The pressure cell itself was mounted in a Grazing-Incidence Small-Angle X-ray Scattering (GISAXS) setup allowing to perform 2D surface diffraction with a CCD detector or an image plate system, respectively, to obtain structural information in-plane as well as out-plane. That way we have applied temperature and pressure changes on the system to drive it through various phase transitions From our experiments we expect to answer the following fundamental questions: Will hydrostatic pressure perturb the orientational order of the supramolecular lipid structure on the solid support or will it just convert them into non-oriented multilayer liposomes? Will it be possible to access phases by pressure which are not accessible for certain lipids by temperature (except by low temperatures below 0°C) – like the lamellar crystalline L_c phase – and will the structure then still be ordered and oriented?
Fig. 1 shows the results of a successful experiment obtained at the SAXS-beamline at ELETTRA: Applying consecutive altrnating changes of temperature and pressure on a surface-aligned system of lipids (mono-elaidin) drives the system through thermotropic and barotropic phase-transitions (see red arrow in the p-T phase diagram) while preserving the orientational alignment in the respective new phase (see 2D-Xray diffraction pictures). These findings might be of technological relevance when using such surface-aligned membrane lipids as nanostructural chemo- or bio-sensors.

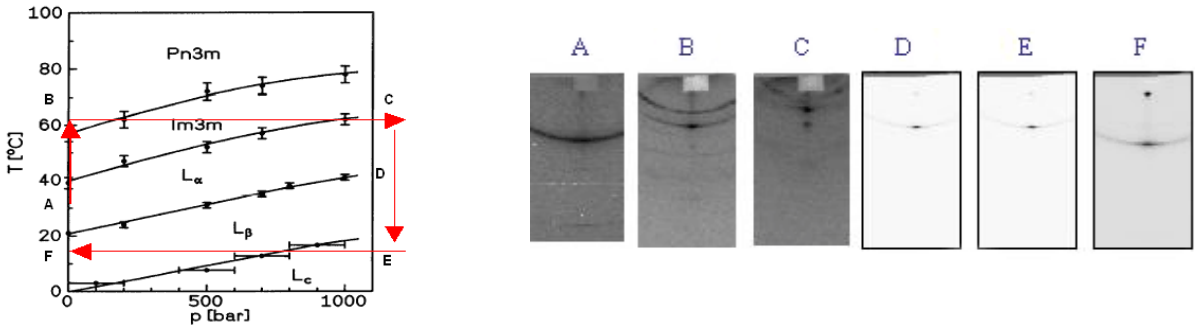

Figure 1. Left: Pressure-temperature phase diagram of the glycerolipid mono-elaidin in excess water containing three lamellar phases (L_c, L_β , L_α) and two cubic phases (Pn3m and Im3m). Applying pressure and temperature changes, 2D diffraction patterns (to the right) of the surface aligned lipid were taken at certain sampling points (indicated in the sequential

order A to E) showing clearly that the alignment (in-plane and out-of-plane) is preserved in all phases. From: ”Non-lamellar phases of solid supported phospholipids studied by high-pressure GISAXD”, H. Amenitsch, Internat. Conference on Small-Angle Scattering, Kyoto, 2006.

ADSORPTION OF BSA AND HEPATITIS-A VACCINE BY SBA-15 MESOPOROUS SILICA

T. Martins[1], C.V. Teixeira[2], H. Amenitsch[3], M.C.A.Fantini[1]

1.) Institute of Physics, University of Sao Paulo, CP 66318, 05315-970, Sao Paulo, SP, Brazil
2.) Unity of Biophysics, Faculty of Medicine, Autonomous University of Barcelona, Bellaterra, 08193, Spain
3.) Institute of Biophysics and Nanosystems Research, Austrian Academy of Sciences, Schmiedelstrasse, 6, 8043, Graz, Austria

One the several applications of the mesoporous materials is their use as drug delivery systems [1]. However, their ability to adsorb drugs is still a point that needs much investigation. The aim of the present experiment is to study the adsorption capacity of bovinum serum albuminum (BSA) and the hepatitis-A virus vaccine in SBA-15. BSA was used for the liability of application of the SBA-15 materials in chromatographic separation and purification of biomolecules [2]. The experiments consisted in adding either BSA solution or vaccine solution (both at pH 7) to SBA-15 powder in their final state, i.e., after hydrothermal treatment and calcination, at different additive:SBA-15 concentrations. The mixtures were put in glass capillaries and scattering curves were obtained at the SAXS Elettra beamline. A Mar180 Image plate was used and the curves were collected in an average time of 2 minutes. Comparison was made between pure SBA-15 powder, SBA-15 in buffer solution, SBA-15 with BSA and SBA-15 with the vaccine. Figure 1 shows the scattering curve of the SBA-15 powder with buffer compared with one sample of SBA-15/BSA and SBA-15/vaccine. The intensities of all curves are very close, so the curve of SBA-15 with vaccine was shifted downwards for better visualization. In a eye inspection, no apparent changes in the curves could be observed, however, the values of cell parameter and the ratio between the (200)/(110) reflections present some differences and are shown in Table 1. The cell parameters obtained are very close to each other, but the values obtained for the samples in buffer solution, with BSA and with vaccine are slightly, but systematically, higher than the value obtained for the pure SBA-15. This indicates that the solutions penetrate the silica structure, making it swell. The ratio between the (200)/(110) reflections also increases with the addition of the solutions, and this is related to the change between the pore/wall thicknesses ratio. However, no significant difference was observed between the different BSA concentrations, the pure buffer solution and the vaccine solutions. Most probably just after the addition of the solutions the time was not enough for the BSA or vaccine adhere to the pore walls. Therefore, two samples were further prepared and a solution of BSA at a ratio 1480 μg/3800 μg BSA/SBA-15 was added to each of them. In one of them the solvent was filtered and for the other, it was evaporated. N_2-adsoprtion measurements were performed and the data is presented in Table 2. The results show that the BET surface area, pore volume and mean pore size decrease after the solvent has been removed, in comparison to the pure SBA-15. This result proves that the BSA has been adsorbed inside the pores. The smaller values for the surface area, pore volume and pore size obtained for the sample evaporated in comparison to the filtered one shows that the adsorption of the BSA is quite slow. This might be the reason why no difference of the SAXS data was observed between the different concentrations of both vaccine and BSA in comparison with the pure buffer in SBA-15. Further SAXS measurements on the filtered and evaporated samples could probably show changes in the pore/wall thickness ratio.

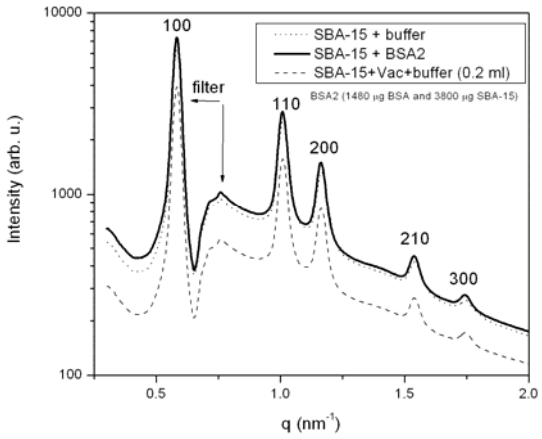

Figure 1. SAXS curves of SBA-15 in buffer solution, with BSA solution at 1480 μg/3800 μg BSA/SBA-15 and vaccine solution at 0.2 ml vaccine/3800 μg SBA-15.

Table 1. Cell parameter and (200)/(110) reflections ratio for the different samples. The mass of BSA and volume of vaccine presented are the volumes used for 3800 μg of SBA-15.

Sample	Cell parameter (nm)	(200)/(110) ratio
Pure SBA-15	12.37	0.429
SBA-15+buffer	12.42	0.508
SBA-15 + 370 μg BSA	12.49	0.479
SBA-15 + 740 μg BSA	12.46	0.500
SBA-15 + 1480 μg BSA	12.46	0.457
SBA-15 + 2960 μg BSA	12.47	0.470
SBA-15 + 0.05 ml vaccine	12.47	0.487
SBA-15 + 0.1 ml vaccine	12.47	0.484
SBA-15 + 0.2 ml vaccine	12.48	0.488

Table 2. Parameters obtained by N_2-adsorption for the samples with pure SBA-15 and after addition of 1480 μg BSA per 3800 μg SBA-15, and elimination of the solvent by filtration or evaporation.

Sample	BET Surface Area (m^2/g)	Pore Volume (cm^3/g)	Mean pore size (nm)
SBA-15	624	0.9	10.96
BSA2-Filtered	148	0.3	10.58
BSA2-Evaporated	72	0.2	10.01

Acknowledgments: Thanks are due to Dr. J.R. Matos, Dr. L.P. Mercuri and Dr. O.A.B. Sant'Anna for fruitful discussions.

References:

[1] J.B. Li,H. Moehwald, Z.H. An and G. Lu; Soft Matter. 1, 259 (2005); M. Hartmann, Chem. Mat., 17, 4577 (2005)
[2] A.Katiyar, S. Yadav, P.G. Smirniotis and N.G. Pinto; J. Chromatography 1122, 13 (2006)

EFFECTS OF PRESSURE AND PH ON LYSOZYME IN SOLUTION

M.G. Ortore[1], R. Sinibaldi[1], F. Spinozzi[1] and P. Mariani[1]

1.) Dipartimento di Scienze Applicate ai Sistemi Complessi, Università Politecnica delle Marche, Via Brecce Bianche 60131, Ancona, Italy

Pressure is a good tool for exploring and comprehending biological function. Even though pressure is apparently a non-biological parameter in the frame of our daily experiences, this view really disregards the existing internal pressures in liquids, solids and molecules which are often much larger than external perturbations by ambient pressure.
High pressure effects on protein structure and interactions have been studied by our group already involved in Small Angle Scattering experiments under pressure [1,2].
During the last decades much attention has been paid to the unfolding effect of pressure on proteins in solution [3], as to the oligomerization effect due to the presence of protein equilibria in solution [2]. Nonetheless the role played by pressure in protein-protein interactions has been considered only in a very few cases.
We performed a high pressure SAXS experiment on hen egg white lysozyme (Sigma Aldrich) in solution at different values of pH. The isotopic effect of deuterated solutions has been also investigated. The values of the investigated pressure range between ambient and 1.8 kbar, since it is known that lysozyme unfolding occurs after 3 kbar [4].
In order to study protein-protein interactions we chose high protein concentrations (c_p=100mg/ml); in these conditions a prominent interference peak appears, as shown in Fig.1.
Increasing the pH in solution, the lysozyme charge decreases (lysozyme pI=11.5), the interference peak is less evident and moves toward lower Q-values. Nonetheless it is not intuitive to imagine that decreasing the repulsion between particles, their average distance increases and this effect can be due to high protein concentration resulting in a large presence of counter ions.

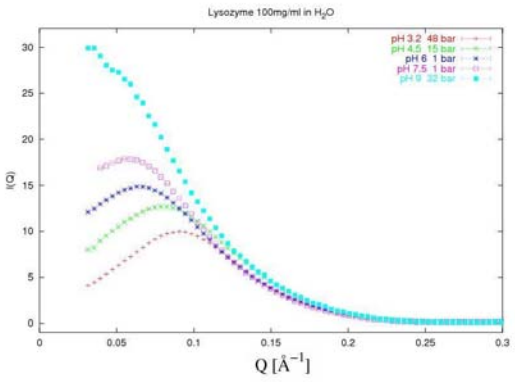

Figure 1. X-ray scattering pattern of lysozyme in different pH conditions.

The most interesting point of the experiment is that the effect of pressure on lysozyme interactions in solution strongly depends on the pH. We adopted the master equation $I(Q) = n_p \Delta\rho^2 S(Q) P(Q)$, where n_p is the number particle density, Δρ is the contrast between protein and solvent, *S(Q)* is the structure factor and *P(Q)* is the lysozyme form factor. We calculated on the basis of the PDB structure by means of the Montecarlo method the theoretical lysozyme form factor (*P(Q)*). Considering that the contrast changes under the pressure effect according to the literature, the experimental SAXS spectra have been divided by $n_p \Delta\rho^2 P(Q)$. Hence, we obtained the structure factors relative to each pressure condition, as reported in Fig.2.

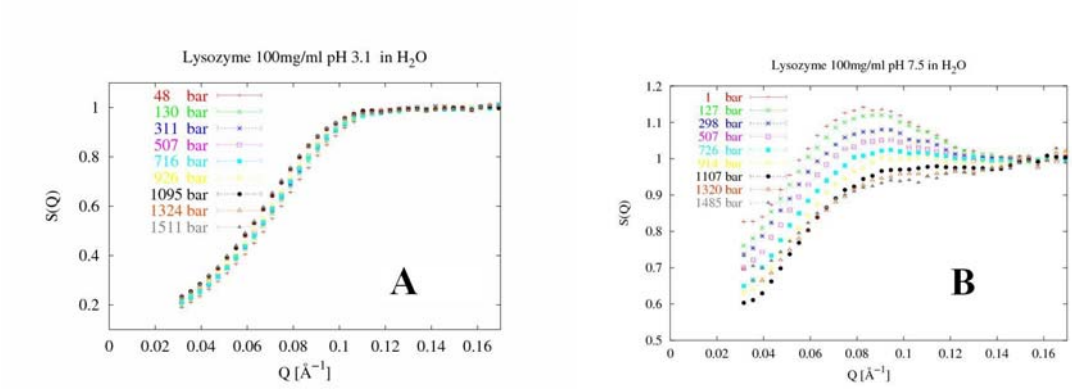

Figure 2. Effective structure factors obtained for two set of experiments **A**: pH 3.1 ; **B**: pH 7.5.

It can be observed that the pressure effect on the protein-protein interactions is more effective at higher pH values, i.e. at lower protein charge. While at higher protein charge (pH 3.1) the pressure seems to push the particles closer to each other (low effect), at lower protein charge (pH 7.5) the pressure increases the protein-protein repulsion (strong effect).
We can conclude that our experiments validate the prospective of the important role played by pressure in protein-protein interactions.

References:

[1] Ortore M.G., Carsughi F., Mariani P., Sinibaldi R., Spinozzi F., Onori G. 2005, *FEBS Journal* 272, [C6028P] (2005)
[2] Ortore M.G., Spinozzi F., Carsughi F., Mariani P., Bonetti M., Onori G. 2006, Chem. Phys. Lett. 418, 342–346 (2006)
[3] Refaee, M.,Tezuka, T.,Akasaka, K., Williamson, M,. J. Mol. Biol. 327, 857 (2003)
[4] Smeller L., Meersman F., Heremans K., B.B.A. 1764(3), 497-505 (2006)

HEXAGONAL MESOPHASE OF THE ANTICANCER DRUG GEMCITABINE SQUALENE EVIDENCED BY COUPLING DSC AND SAXS

B. Pili[1], C. Bourgaux[1], L. Harivardhan Reddy[1], H. Amenitsch[2], P. Couvreur[1], M. Ollivon[1]

1.) Physico-Chimie, Pharmacotechnie, Biopharmacie, UMR 8612, Univ. Paris-Sud, 5 rue JB Clément, Chatenay, France
2.) Institute of Biophysics and Nanosystems Research, Austrian Academy of Sciences, Graz, Austria

The self aggregation of a lipidic derivative of gemcitabine (GemSq), obtained by squalenization of gemcitabine reaction through squalenic acid as synthesis intermediate, was examined at small angles (SAXS) after ultracentrifugation of nanoparticles. GemSq nanoparticles exhibit an internal organization corresponding to hexagonal packing with a = 8.8 nm parameter.

Introduction Gemcitabine belongs to the class of nucleoside analogues that exhibits significant anticancer or antiviral properties. Gemcitabine is a drug that has been demonstrated to be active against a wide range of solid tumors, including colon, lung, pancreatic, breast, bladder, and ovarian cancers. However, like most of these molecules it possess some serious limitations that often restrict their use, such as short plasma half-life, rapid metabolism, induction of resistance, and/or the advent of severe side effects. Furthermore, some of these molecules are poorly absorbed after oral administration. Coupling of gemcitabine to the acyclic isoprenoid chain of squalene, a precursor in the sterol biosynthesis, is a new strategy that increase the therapeutic index of this molecule and allows its more efficient administration (Figure 1)[1]. Such coupling to a squalene moiety renders the molecule amphiphilic and able to form spherical nanoparticles ($\varnothing \leq 200$ nm) allowing its intravenous administration. In this administration form, the squalenoyl gemcitabine exhibited superior anticancer activity in vitro in human cancer cells and gemcitabine resistant murine leukemia cells, and in vivo in experimental leukemia both after intravenous and oral administration.

Experimental methods Nanoparticles of GemSq were obtained by nanoprecipitation using the technique of direct injection in water of its alcoholic solution. In this condition, it has been shown that the linkage of nucleoside analogue to squalene leads to amphiphilic molecules that self-organize in water as nanoassemblies of diameter 100-300 nm irrespective of the nucleoside analogue used [1]. The structural properties of GemSq nanoassemblies were examined at T = 20°C on the SAXS beamline of Elettra synchrotron using the Differential Scanning Calorimeter (DSC) (Microcalix) as a sample holder [2].

Results and discussion The preparation of GemSq from gemcitabine and squalene is shown Figure 1 [1]. The concentrated nanoparticles of GemSq obtained by nanoprecipitation have been centrifuged again at low speed in the quartz capillary used for calorimetry to concentrate the sample in the tube bottom. Figure 2 shows the SAXS diffraction pattern of GemSq nanoassembly such as recorded at 20°C. Molecular volume evaluations for both amphiphile moieties has lead us to propose the internal structure of particles schematized Figure 3. Squalene moieties of GemSq are surrounding the gemcitabine polar group that are located in water columns. Investigation of the thermal and structural behaviour of GemSq nanoparticles is under way using Microcalix.

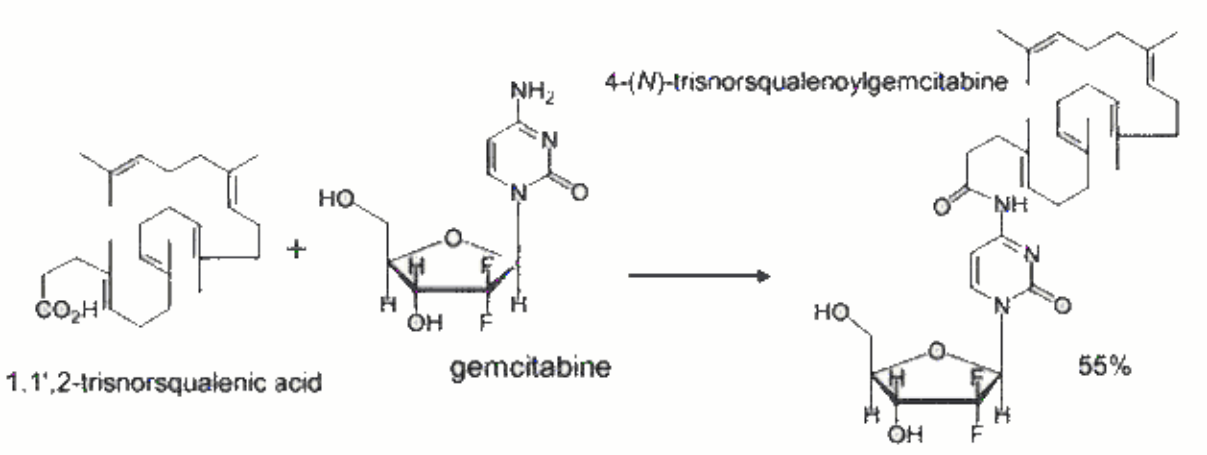

Figure 1. Synthesis of GemSq from squalenic acid and gemcitabine (yield) from ref 1

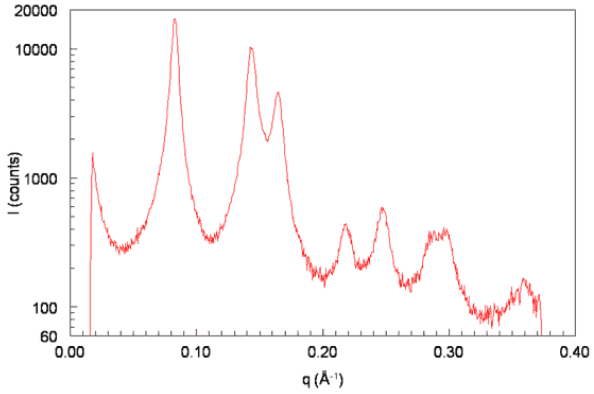

Figure 2. SAXS diffraction pattern of GemSq nanoassembly recorded at 20°C

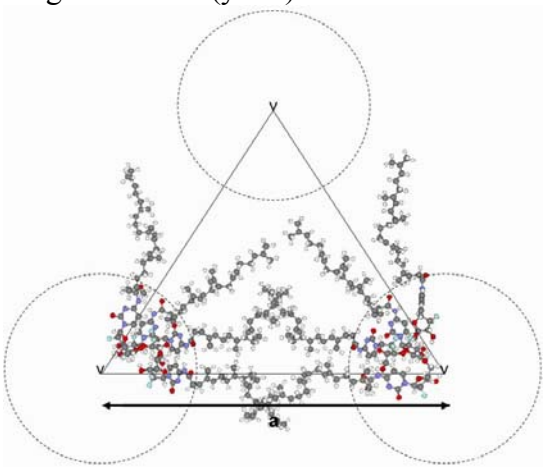

Figure 3. Schematic drawing of GemSq packing corresponding to the SAXS pattern presented figure 1.

Conclusion This study clearly demonstrates that the internal organization at supramolecular scale of the nanoparticles of GemSq at room temperature is hexagonal with a parameter a = 8.8 nm between hydrophilic columns. To our knowledge this is the first demonstration of occurrence of hexagonal phase organization with squalene derivative (3). While the squalenoylation is an original technology platform for generating more potent anticancer and antiviral nanomedicines, relationship of its drug efficiency with internal structuration of particles has to be investigated.

References

[1] Couvreur P. et al. Squalenoyl nanomedicines as potential therapeutics. Nano Letters, 6, 2544-2548 (2006).
[2] M. Ollivon, G. Keller, C. Bourgaux, D. Kalnin, P. Villeneuve and P. Lesieur, DSC and high resolution X-ray diffraction coupling, J. Thermal Anal. and Calor., 85 (2006) 219–224.
[3] Couvreur P. et al., submitted

LAMELLAR TO GYROID TO DIAMOND PHASE TRANSITIONS IN MONOOLEIN FILMS

M. Rappolt, B. Sartori, and H. Amenitsch

Institute of Biophysics and Nanosystems Research, Schmiedlstr. 6, 8042 Graz, Austria

Time-resolved grazing incidence small-angle X-ray diffraction experiments have been carried out to investigate the transformation from the L_α to the cubic gyroid *Ia*3*d* (G-phase) to the cubic diamond *Pn*3*m* phase (D-phase) in aligned monoolein films. The transition was induced by increasing the relative humidity from initially 98 % to nearly 100 %. Complete hydration of the lipid films was then achieved by subsequently decreasing the sample temperature from 26 °C to just above the dew point.

Of special interest was to investigate the epitaxial relationship of the two cubic phases of monoolein. In a recent letter [1] we proposed for the near equilibrium conditions, a direct transformation of the cubic phases involving the (220)-planes of the G-phase and the (111)-planes of the D-phase. In Fig. 1 the 2D-image of the gyroid cubic phase of an aligned monoolein film can be seen. Clearly, we observed also a coexistence regime of both cubic phase (data not shown), but for first conclusions further data analysis is necessary.

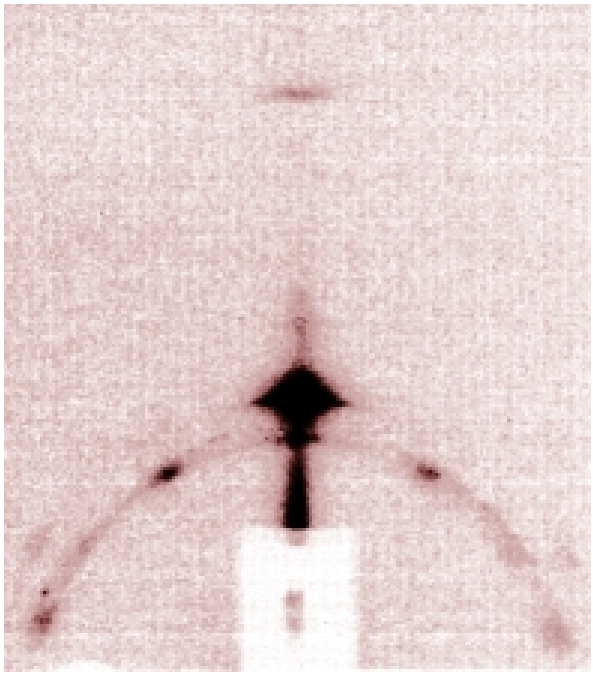

Figure 1. 2D-diffraction pattern of *Ia3d*-phase of monoolein film at room temperature.

Reference:

[1] M. Rappolt, G.M. Di Gregorio, M. Almgren, H. Amenitsch, G. Pabst, P. Laggner and P. Mariani, P. (2006): Non-equilibrium formation of the cubic Pn3m phase in a monoolein/water system. *Europhys. Letters* 75: 267-273.

BIDIRECTIONAL TENSILE TESTING ON HUMAN ARTERIES

F.Schmid[1], F.Cacho[2], M.Rappolt[1], P.Laggner[1], P.Regitnig[3], G.A.Holzapfel[4], H.Amenitsch[1]

1.) Institute of Biophysics and Nanosystem Research, Austrian Academy of Sciences, Schmiedlstraße 6, Graz, Austria
2.) Graz University of Technology, Institute for Structural Analysis – Computational Biomechanics, Graz, Austria,
3.) Medical University Graz, Institute of Pathology, Graz, Austria.
4.) Royal Institute of Technology, Department of Solid Mechanics, Stockholm, Sweden,

Cardiovascular diseases are the major cause of death in the western world. Their treatment has become more and more sophisticated, but also costly. Extraordinary scientific efforts are put into the understanding of the mechanics of arteries to improve existing treatments (e.g. balloon angioplasty), stent development or tissue engineering.
Collagen fibres are a found just about anywhere in animal tissue, where strength and flexibility are demanded. In particular, they are a mechanically important constituent of arteries, and their angular distribution is considered a key factor to the overall mechanical properties of the tissue.
In this fibre diffraction study we subjected individual layer stripes of different human arteries to tensile load – measuring force and geometrical distortion – during the acquisition of SAXS images to identify the angular fibre distribution. This enables a comparison of macro- and nanoscopic behaviour of the tissue. Recently we have developed a 2 dimensional stretching device improving the overall performance of the setup.
First experiments have been successfully accomplished. In contrast to commonly applied 1D stretching [1, 2], stress is applied more homogenously to better resemble the in-vivo situation of the tissue. For the first time two major directions of angular distribution of the collagen fibres could be determined by SAXD (Fig.1). These results will help to refine existing modelling [3] and to define realistic boundary conditions.

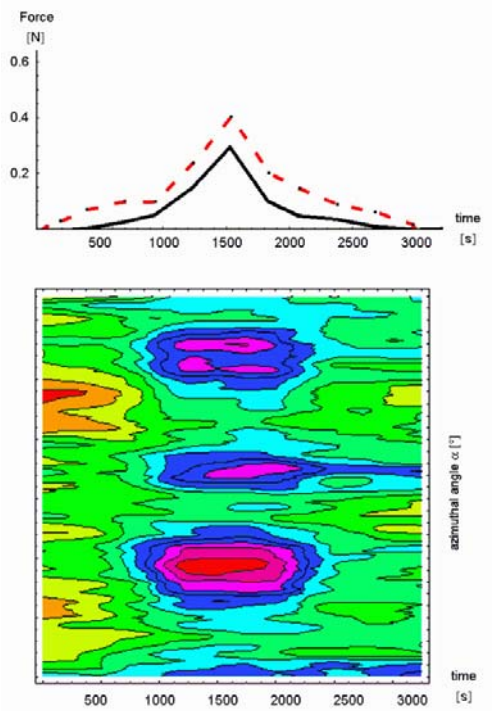

Figure 1. Equi-biaxial stretching experiment on an adventitial layer of a human artery. The change in azimuthal intensity distribution with increasing load can be clearly seen. The rise of these "peaks" shows the increased orientation of collagen fibres in the tissue**.**

References:

[1] Schmid, F., G.Sommer, M.Rappolt, P.Regitnig, G.Holzapfel, P.Laggner, and H.Amenitsch. 2006, NIMB 246, 262-268.
[2] Schmid,F., G.Sommer, M.Rappolt, C.A.J.Schulze-Bauer, P.Regitnig, G.A.Holzapfel, P.Laggner, and H.Amenitsch. 2005, Journal of Synchrotron Radiation 12, 727-733.
[3] Holzapfel,G.A. 2006, Journal of Theroetical Biology 238, 290-302.

EFFECT OF THE HUMAN ANTIMICROBIAL PEPTIDE LL-37 ON BACTERIAL MODEL MEMBRANES

E. Sevcsik, G. Deutsch, H. Amenitsch and K. Lohner

Austrian Academy of Sciences, Institute of Biophysics and Nanosystems Research, Schmiedlstraße 6, A-8042 Graz, Austria

Antimicrobial peptides are a class of substances that are thought to become an alternative to conventional antibiotics, which are often not effective anymore due to bacterial resistances. These peptides distinguish between foreign, e.g., bacterial and host cells based on differences in the composition of the cell membrane, however, the molecular mechanism of membrane disruption is still not clear [1]. The aim of our project was to study the interaction of the human antimicrobial peptide LL-37 with bacterial model membranes. DSC data showing a low-temperature phase transition at 29°C (Figure 1B) in conjunction with laboratory X-ray data indicated that LL-37 induces a ripple phase above 29°C in such membranes.

High resolution X-ray measurements and temperature scans were performed to allow us to further characterize this new phase thereby gaining information on the mode of interaction of LL-37 with bacterial membranes. This knowledge, in turn, will allow the design of novel peptide antibiotics killing their target cells by destruction of their phospholipid membrane integrity.

Specifically, the experiments were performed with mixtures of the negatively charged lipid dipalmitoyl-phosphatidylglycerol (DPPG) and the zwitterionic lipid dipalmitoyl-phosphatidylethanolamine (DPPE), which are the major components of cytoplasmic bacterial membranes. Liposomes of these lipids were prepared in the absence and presence of the peptide LL-37 and time-resolved scattering pattern were recorded following a defined temperature program. We succeeded in recording the SAXS and WAXS patterns as a function of temperature during a heating cycle, giving us detailed information of the low-temperature transition from the lamellar phase with a d spacing of 84 Å into the one with 124 Å (Figure 1A). Furthermore, high-resolution scattering pattern of the two phases were recorded that were analyzed with a global, full-q-range fitting model [2]. Parallel to the increase of the d spacing, also the phosphate-phosphate distance increases from 46.2Å to 50.4Å, which is an indication of a reorientation of the peptide in the lipid bilayer possibly involving the formation of a ripple phase. However, the second part of the project, identification of the ripple phase, was not as successful. Further experiments on oriented samples are planned to address this point.

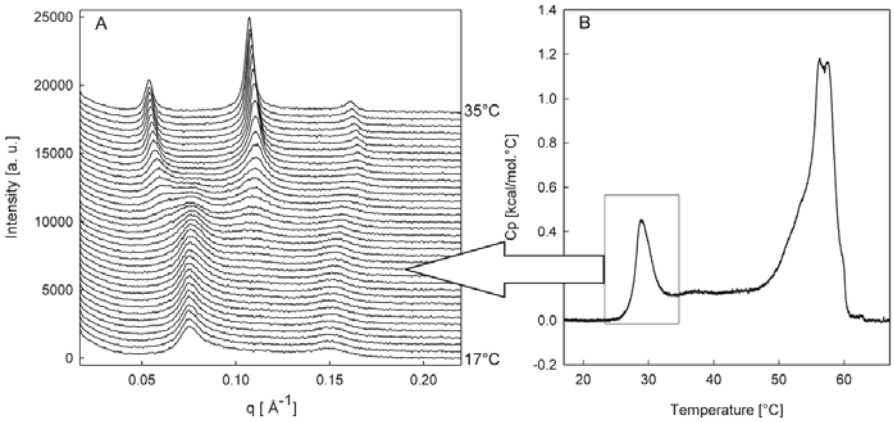

Figure 1. (A) Time-resolved SAXS patterns of the low-temperature transition observed for DPPE/DPPG 1/1 in the presence of 4 mol% LL-37. Exposure time was 60s for each frame.

(B) Differential scanning calorimetry data of DPPE/DPPG 1/1 in the presence of 4 mol% LL-37. Scans were recorded at 30°/h.

References:

[1] B. Bechinger, K. Lohner, Biochim.Biophys.Acta 1758, 1529-1539 (2006)
[2] G. Pabst, R. Koschuch, B. Pozo-Navas, M. Rappolt, K. Lohner, P. Laggner, J.Appl.Crystallogr. 63, 1378-1388 (2003)

3. Chemistry

STRUCTURAL INVESTIGATIONS OF MESOPOROUS THIN FILMS GROWN WITHIN CONFINED ARCHITECTURES.

D. C. Arnold[1], J. M. O'Callaghan[1], N. Petkov[1], H. Amenitsch[2], Michael A. Morris[1] and J. D. Holmes[1]

1.) Materials and Supercritical Fluids Group, Department of Chemistry, University College Cork, Cork, Ireland
2.) Institute for Biophysics and Nanosystems Research, Austrian Academy of Sciences, Schmiedlstraße 6, 8042, Graz, Austria

In recent years considerable attention has focused on nanoporous materials primarily due to their potential application as building blocks for constructing nanoscale architectures. In particular surfactant templated mesostructured materials, with pore-sizes between 2 and 10 nm, have been utilised as catalyst supports, nano-reactors for a variety of chemical reactions and as hosts for nano-structured materials with appealing properties. [1-3] If these materials are to be truly utilized for the potential construction of nanoelectronic and optoelectronic device architectures, the synthesis of preferentially aligned ordered arrays of mesoporous materials with controllable dimensions is crucial. At UCC our research has centred on the synthesis of highly aligned mesoporous silica thin (MTF) films, grown on etched silicon substrates and periodic mesoporous organosilica (PMO) materials formed within the pores of anodic aluminium oxide (AAO) membranes, which act as hierarchical templates for the assembly of such highly ordered porous structure.

Experiments conducted on the SAX beamline at Elettra have focussed on investigating the structure and hence the degree of order of mesoporous silica thin films prepared in our laboratories on etched silicon substrates. Electron microscopy analysis (figure 1) clearly demonstrates the hexagonal arrangement of the pores and the superior ordering achieved within the confining architectures of the etched channel. [4] GI-SAX investigations further confirmed the highly preferential alignment of pores across the substrate as indicated by the appearance of diffraction spots as apposed to arcs of intensity as shown in figure 1(a). In addition these patterns can be readily indexed to the P6mm 2D hexagonal structure with the pores lying parallel to the substrate surface and in a direction parallel to the x-ray plane. Moreover, the lattice spacing observed are consistent with those observed using conventional Bragg - Brentano laboratory based equipment.

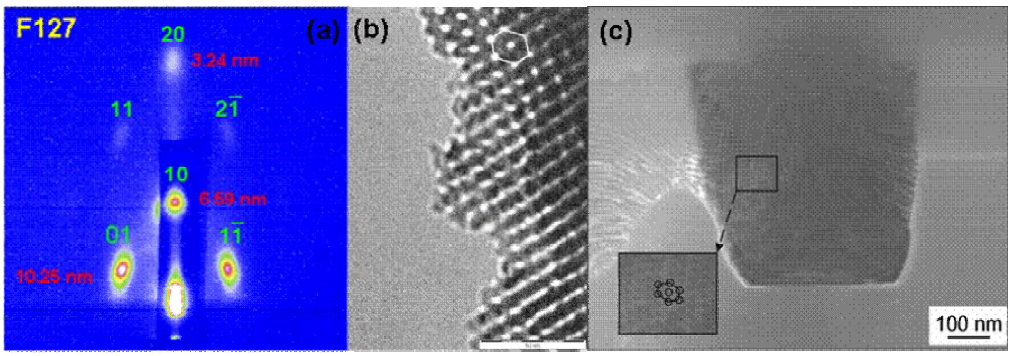

Figure 1. (a) SAX pattern collected for an ordered mesoporous silica thin film deposited onto an etched silicon substrate. (b) Transmission electron microscopy image showing the hexagonal arrangement of the mesopores and (c) Cross sectional high resolution scanning electron microscopy image collected showing the enhanced ordering of the mesopores achieved within the channel.

Confinement and environment effects have been further investigated through the growth of ethylene bridged PMO films within the confining architectures provided by the pores of AAO membranes. PMO materials were prepared with varying organic:silica ratios at various relative humidity's. Figure 2 shows typical SAX patterns collected for different organic ratio's of 50%, 75% and 100 % organic thin films respectively grown within the AAO membrane pores at a relative humidity of 30 %. It is clear from these data that the structure changes relative to the amount of organic present in the framework which is further confirmed by transmission electron microscopy (TEM) analysis. These preliminary results clearly indicate that not only is the PMO structure highly dependent upon the organic:silica ratio but also that the relative humidity is a crucial factor in controlling the PMO pore orientation, either parallel or perpendicular to the pore of the AAO membrane. It is suggested that both the organic:silica ratio and the environmental conditions effect the evaporation induced self assembly (EISA) mechanism and thus the pore ordering.

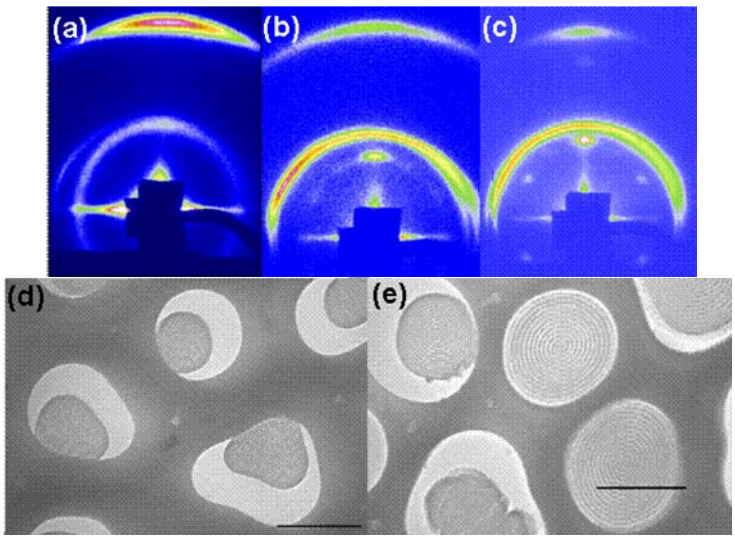

Figure 2. Typical SAX patterns collected for (a) 75:25, (b) 50:50 and (c) 100:0 organic:silica ratio thin films grown within the pores of an AAO membrane. (d) Transmission electron microscopy image showing the parallel pore arrangement of the mesopores and (e) Transmission electron microscopy image showing the perpendicular/lamellar pore arrangement of the mesopores. Scale bars represent 200 nm.

In summary GI-SAX has proved an essential tool for the analysis of mesoporous materials. Preliminary results collected for both mesoporous silica and PMO thin films indicate that the use of confining architectures acts to promote the ordering of the mesopores providing highly ordered porous templates for possible future device applications. GI-SAX has allowed us to probe the structural arrangement as a function of both humidity and organic:inorganic ratio in the case of the PMO materials and allowed us to index the higher pore order of MTF materials afforded by the etched channels in silicon substrates.

References:

[1] J. S. Beck, J. C. Vartuli, W. J. Roth, M. E. Leonowicz, C. T. Kresge, K. D. Schmitt, C. T. W. Chu, D. H. Olson, E. W. Sheppard, S. B. McCullen, J. B. Higgins and J. L. Schlenker; A New Family of Mesoporous Molecular Sieves Prepared with Liquid Crystal Templates; J. Am. Chem. Soc. 114, 10834-10843 (1992)

[2] A. P. Wright and M. E. Davis; Design and Preparation of Organic-Inorganic Hybrid Catalysts; Chem. Rev. 102,

[3] B. J. Scott, G. Wirnsberger and G. D. Stucky; Mesoporous and Mesostrucured Materials for Optical applications; Chem. Mater. 13, 3140-3150 (2001)

[4] R. L. Rice, D. C. Arnold, M. T. Shaw, D. Iacopina, A. J. Quinn, H. Amenitsch, J. D. Holmes and M. A. Morris; Ordered Mesoporous Silicate Structures as Potential Templates for Nanowire Growth; Adv. Func. Mater. 17, 133-141 (2007)

STRUCTURAL CHANGE INDUCED BY TEMPERATURE INCREASE IN MONOSACCHARIDE GEL

S. Bernstorff[1], H. Grigoriew[2], D. Chmielewska[2]

1.) Sincrotrone Elettra, Basovizza, Trieste, Italy
2.) Institute of Nuclear Chemistry and Technology, Warsaw, Poland

Up to now, the ability of the monosaccharides to induce gelation of organic solvents, also with very low concentration, is not well understandable, because of the small size of the sugar molecules, no possibility to join them by chemical bonds and the very weak gelator-solvent interactions. Monosaccharides are of potential application in industry, mainly as materials for immobilizing dangerous organic solvents.

The aim of the experiment was to check the structural change of the monosaccharide gel caused by temperature increase, from room temperature up to higher than T_g (gelation temperature). Then the gel dissolves to the liquid phase (sol). The monosaccharide gels belong to a class of physical gels, which are reversible [1], and this was confirmed for these gels [2]. Therefore such a change can be treated also as equivalent to a reverse process-gelation.

The studied gel was synthetized from methyl-4,6-O-benzylidene-a-D-galactopyranoside as a gelator with diphenyl ether as a solvent. The gelator concentration was 1% [g/mL]. The SAXS measurements were performed in time-resolved mode during the temperature increase. The measurement range was 0.007 – 0.4 [s], where $s=2\pi/\lambda\sin(\theta)$ [nm^{-1}]. The rate of temperature change was 0.5°C/min, and the measurement time per frame was 10 minutes.

A typical set of intensity I(s) curves, after initial treatment, is visible in Fig. 1. Beginning from room temperature, for subsequent measurements, the I(s) curves become weaker and of monotonously changed shape, through the T_g (55°C) and further, up to about 70°C. It can suggest that the observed I(s) change is caused by the structural change responsible for gelation. Beginning from 70°C no change of I(s) is detected for higher temperatures, so the remaining structure is stable in the sol (liquid) state.

Due to the additive properties of the scattered intensity, we subtracted the intensity curve of the highest temperature (I_h (s)) from the curve of room temperature (I_r (s)), and obtained (I_d (s)), i.e. the curve generated by structural change during the gel dissolution. The I_d (s) curve, visible in Fig. 2 in log-log scale, is a typical fractal structure, and from the slopes of the curves fitted to its straight-line segments, we obtained the mass fractal dimension, d_m =1.97, and the surface fractal dimension d_s = 2.96. The curve bend between the two fitted lines (Porod bend [3]) corresponding to the primary aggregate size, was determined to be about 21 nm. The determined mass fractal dimension corresponds to the DLCA (diffusion-limited cluster aggregation) mechanism of the gel structure formation [1], and the surface dimension equals about 3 - to rough surface of the average gel aggregate .

From the calculated FT of the I_d(s), we obtained the p(r) function (Fig.3). The p(r) curve consists of two broad peaks, the first at about 10 nm and the second at about 20nm, which form together a broad halo. Such a shape is typical for a disk with a hollow [4]. Simultaneously the R_g = 14.6 nm was calculated, which for the simplest case (spheres) corresponds to R=19 nm.

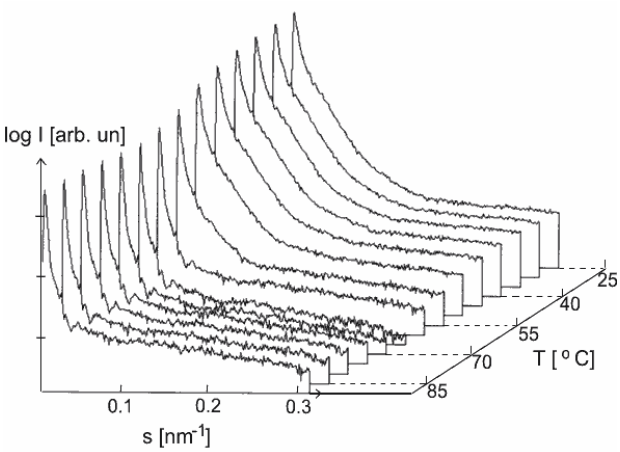

Figure 1. Set of SAXS curves, I(s), obtained during the temperature increase, after their initial treatment.

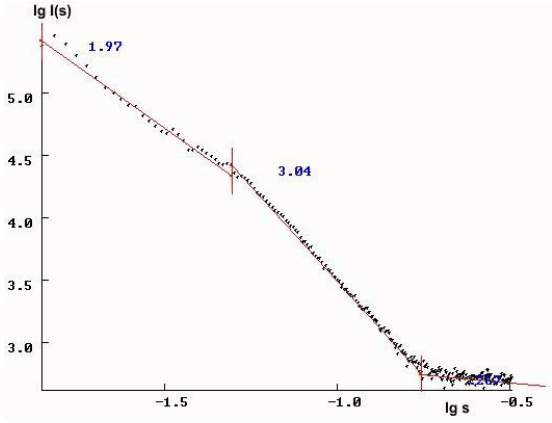

Figure 2. Difference between gel and sol curve, I_d (s), in fractal i.e. log-log scale. Fitted to the curve straight-line segments and their slopes are visible.

These results suggest that for gelation of a liquid sol is responsible the formation of a great population (due to the big intensity increase) of fractal-like aggregates in a previous, completely different sol structure.

The I(s) curves shape for sol (Fig 4), invariable for some high-temperature measurements, signals the existence of large aggregates of smooth surface, but the range of the SAXS measurements is here insufficient, which requires further measurements to smaller scattering angles. They are planned as SANS measurements in June 2007. Further data elaboration is in progress.

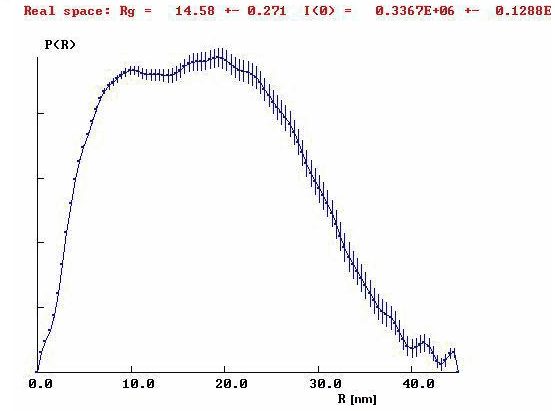

Figure 3. Fourier transform of the I_d(s). The R_g value calculated in this procedure is detected.

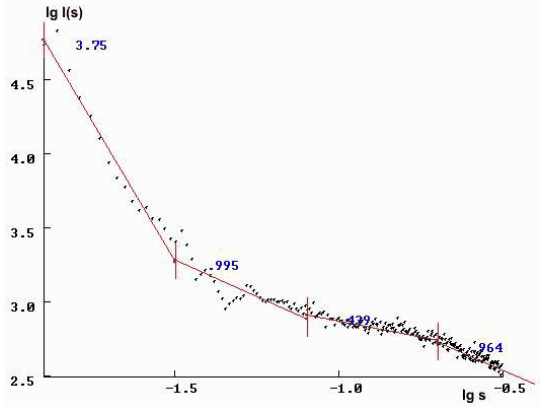

Figure 4. Log-log of the SAXS curve I_h(s), measured in the highest temperature.

References:

[1] C.J.Brinker, G.W.Scherer "Sol-Gel Science. The Physics and Chemistry of Sol-Gel Processing" Academic Press, Boston MA, 1990.
[2] K.Sakurai, Y.Jeong, K.Koumoto, A.Friggeri, S.Okamoto, K.Innoue, Shinkai, Langmuir 19 (2003) 8211
[3] G.Porod, Colloid Z., 124 (1951), 83
[4] K.Kajiwara,Y.Hiragi in "Application of Synchrotron Radiation to Material Analysis",Chapter 6, p.368, ed.by H.Saisho and Y.Gohshi, Elsevier, Amsterdam, 1996.

GISAXS ON MICROPHASE SEPARATED NANOPARTICLES/POLYMER FILMS

W. H. Binder[1], M. Josipovic[1], R. Sachsenhofer[1], H. Peterlik[2], S. Bernstorff[3]

1.) Martin-Luther University Halle-Wittenberg, Institute of Chemistry / Macromolecular Chemistry, Heinrich-Damerowstrasse 4 / TGZ III, D-06120 Halle, Germany
2.) University of Vienna, Institute of Experimental Physics, Physics Department, Austria
3.) Sincrotrone Trieste, in AREA Science Park, Strada Statale 14 km 163.5, 34012 Basovizza, Italy

The incorporation of nanoparticles (NPs) into materials is an important issue in modern nanotechnology science.[1] Among the many factors, which determine the distribution and possibility of incorproation of NPs into materials, the interaction between NP-surface and material is the most important. The underlying surface-interaction energy can stronlgy determine, whether a NP binds to a material in a stable form, or is expulsed from the material due to unfavorable interactions. The same holds true for the eventual ordering of the NP within the matrix, which is an important prerequesite for exerting the function of the NP.
In the present set of experiments we have investigated thin films, consisting of a microphase separating block copolymer (BCP) [2] and nanoparticles (CdSe-nanoparticles, sized ~4 nm) [3] with either a selective interacting interface between the nanoparticle and one block of the BCP or a nonselective interacting interface between the nanoparticle surface and the blocks of the BCP (see Figure 1).

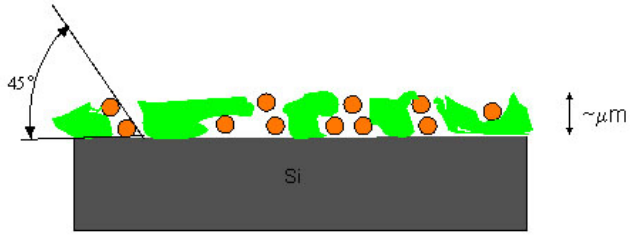

Figure 1. Schematic drawing of the generation of nanoparticle(NP)-polymer composites on the surface of a silicon wafer, after being applied via a solution-dipping process

The following issues were proposed to be studied via the GISAXS-experiments :
(a) the critical film-thickness required to achieve a sufficiently strong scattering signal of the beam, as to be able to detect the scattered beam. Since there do not exist any data on the necessary thickness of the films studied, this question was of uttermost significance. (b) the orientation and microphase separation of the films, and the possible orientation of the microphase-separated structure within the surface. In all cases, nanoparticles were incorporated into the film in amounts ranging from 1 w% until 15 w%. The samples were prepared from solution, by applying a chloroform solution of the respective nanoparticle/polymer mixture (approximately 10% solution, containing about 1w% NP to ~15 w% NP). The samples were then dried, leaving a film thickness of several microns. Thinner films were prepared by spin-coating methods, yielding films with thicknesses of about ~20 nm as determined by ellipsoidal measurements.
The primary GISAXS-pattern of a film of micron-sized thickness is shown in Figure 2. The incident beam was investigated between 0.2 and 0.7° - the strongest scattering was observed at an angle of 0.3° - these measurements are shown here.

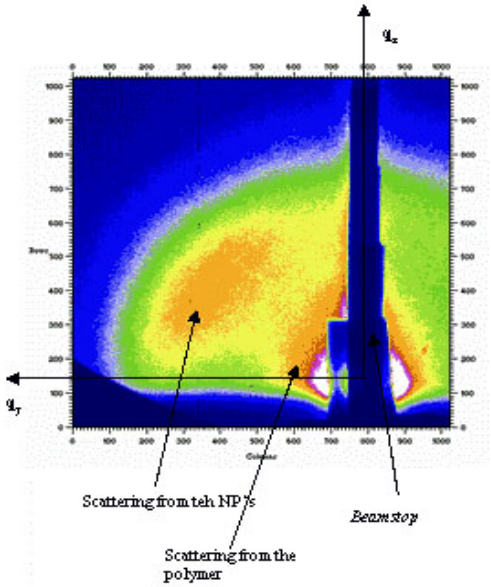

Figure 2. GISAXS-pattern of a NP/polymer composite (10 mol% interacting block plus 15 w% of selectively interacting nanoparticles).

The contributions from the polymer-scattering and the respective nanoparticle scattering are clearly seen. Several samples with variations of the content of the nanoaprticles (interacting and noninteracting, with 5 w% and 15 w% of NP) as well as the molar concentration of the interacting block (without, 1 mol%, 10 mol% and 50 mol%) are given in Figure 3a – d. The results clearly show the following features. (a) a close ordering of the nanoparticles due to the broad scattering peak at ~5 nm, corresponding to the size of the NP's. (b) a preferred orientation of the nanoparticles in an angle of 45° relative to the silicon-surface, a feature which may be explained by evaporation effects during the sample preparation. (c) a preferred ordering of the noninteracting nanoparticles at the interface of the microphase separated polymer, whereas the interacting nanoaprticles are enriched at the center of the microphase separated domains of the block copolymer. Summed up, the results demonstrate, that (1) a relative thick film of the sample is needed in order to achieve a scattering within this experimental setup, (2) a preferred orientation at about 45° takes place, presumably due to orientation effects during the evaporation of the solvent and (3) that a preferred location of the NP's in the polymer films can be achieved, depending on the nature of the interfacial interaction between the NP_surface and the BCP-interface and block structure.

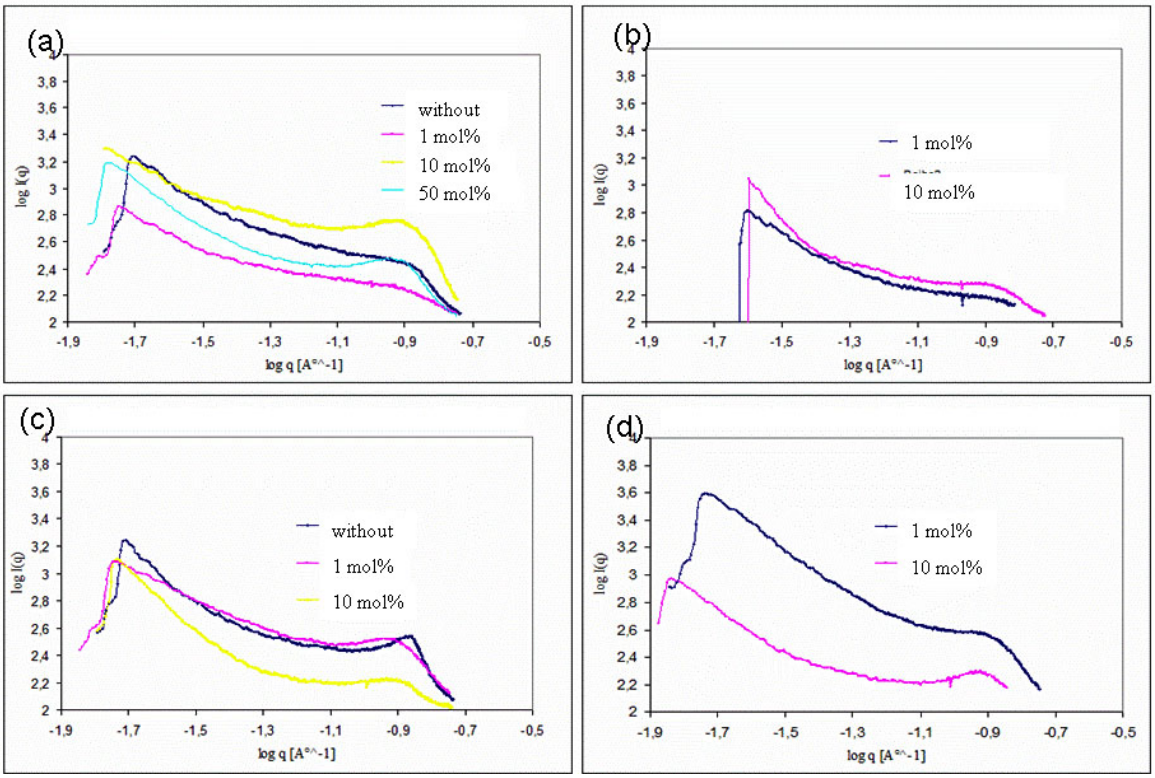

Figure 3. Integrated GISAXS-patterns for samples with (a) 15 w% interacting nanoaprticles in a polymer with 0 mol%, 1 mol%, 10 mol% and 50 mol% interacting block (b) 5 w% interacting nanoparticles in a polymer with 1 mol% and 10 mol% interacting block. (c) 15 w% of noninteracting nanoparticles in a polymer with 0 mol%, 1 mol% and 10 mol% interacting block. (d) 5 w% of noninteracting nanoparticles in a polymer with 1 mol% and 10 mol% interacting block.

References:

[1] A. Haryono, W. H. Binder, Controlled Arrangement of Nanoparticle Arrays in Block-Copolymer Domains; *Small* 2, 5, 600 – 611 (2006).

[2] (a) W. H. Binder, C. Kluger, C. J. Straif, G. Friedbacher, Directed Nanoparticle Binding onto Microphase Separated Block Copolymer Thin Films, *Macromolecules* 38, 9405 – 9410 (2005) (b) W. H. Binder, C. Kluger, M. Josipovic, C. J. Straif, G. Friedbacher, Directing Supramolecular Nanoparticle Binding onto Polymer Films : Film Formation and Influence of Receptor Density on Binding Densities, *Macromolecules* 39, 8092 – 8101 (2006).

[3] W. H. Binder, R. Sachsenhofer, C. J. Straif, R. Zirbs, Surface-modified Nanoparticles via Thermal and Cu(I)-mediated "click" chemistry : Generation of Luminescent CdSe-nanoparticles with Polyr Ligands Guiding Supramolecular Recognition *J. Mater. Chem*. 17, ASAP (2007)

IN SITU SAXS STUDY OF THE DEPOSITION OF ORDERED MESOPOROUS SILICA IN COMPOSITE MATERIALS FOR DRUG DELIVERY

G. Croce[1], D. Viterbo[1], M. Milanesio[1], B. Onida[2], V. Cauda[2], S. Fiorilli[2]

1.) DISTA, Università degli Studi del Piemonte Orientale, Via Bellini 25/g, Alessandria, Italy
2.) DISMIC, Politecnico di Torino, Corso Duca degli Abruzzi 24, Torino, Italy

Ordered mesoporous materials, because of their periodic array of uniform pores, are being proposed for hosting and further delivering molecules of pharmaceutical interest. Drug delivery systems generally consist of polymeric matrices or polymer-based composites containing different materials such as bioactive glasses or ceramics [1]. Silica xerogels have also been studied as carriers for controlled drugs release [2]. With all these disordered systems, it is difficult to ensure a homogeneous distribution of the guest species throughout the matrix, and this may affect the release rate. Ordered mesoporous matrices, where all pores show uniform size, arranged in a periodic array, represent suitable candidates for this application. J. Perez-Pariente et al. have carried out a pioneering study on the use of MCM-41 as ibuprofen delivery system [3], showing its feasibility and opening a new investigation area. A marked improvement in this field could come from combining the release properties shown by the ordered mesoporous systems with the bioactivity and biocompatibility of materials employed to fabricate implants. This achievement would provide systems able not only to promote successful integration of the implanted prostheses, but also to prevent infections by drug release. The only study concerning the coating of a bioactive glass with mesoporous silica thin films has been reported by Gomez-Vega et al. [4]

Recently B. Onida et al. [5] reported the synthesis of an ordered silica mesophase inside the macroporous structure of a bioactive glass-ceramic scaffold, in order to combine the bioactivity of the latter with the release properties of ordered mesoporous systems. These composite materials for drug delivery are prepared starting from a scaffold of bioactive glass, which shows interconnected macropores in the range 200-600 μm and is then used as a substrate for the growth of a crystalline mesoporous SBA phase. To this aim a solution of the triblock copolymer P123 is prepared in acidic media, followed by the addition of tetraethylorthosilicate (TEOS). After TEOS addition, the synthesis solution is stirred for 15 min to promote the hydrolysis of the silica precursor. The scaffold disk is soaked in the silica synthesis batch, under continuous stirring. After 15 min, the disk is separated from the solution, and aged in a closed vessel following different procedures.

SEM analysis reveals the presence of silica grains with hexagonal symmetry anchored to the porous scaffold. The SAXS patterns, obtained for the as-synthesized and calcined composites with different ageing, are consistent with the presence of an ordered hexagonal mesophase of the SBA type (figure 1). The *a* edge of this hexagonal phase varies from 12.8 nm of the as-synthesized sample to 12.4 nm of the calcined composite. Besides, the collected data permitted us to estimate the dimensions of the pores of the SBA phase, which vary from 8.4 nm of the as-synthesized SBA phase to 7.7 nm of the calcined one.

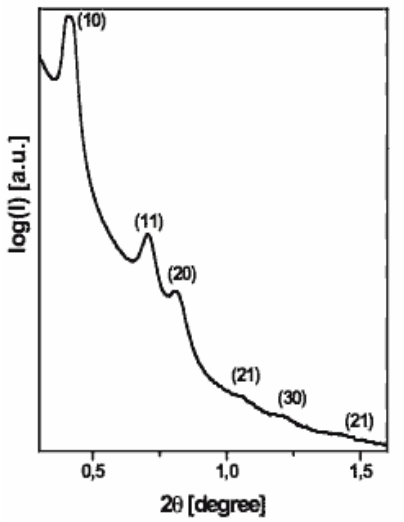

Figure 1. X-ray diffraction pattern of a calcined scaffold sample

The obtained results also revealed that the growth and the condensation of the SBA mesophase is correlated to the soaking time of the scaffold and the ageing procedure of the composites. In order to understand the mechanism of formation of the mesophase silica inside the scaffold macropores, we carried out an *in-situ* SAXS experiment aiming at investigating the structural features of the mesoporous phase growing under different conditions. In particular we were interested in studying the first steps of condensation of the silica network at different soaking times and ageing temperatures, in order to identify the most efficient synthetic method to achieve a well ordered mesophase.

Figure 2 shows the preliminary data analyses, which suggest that the ageing at 60°C is more efficient in obtaining an ordered mesophase and that the temperature promotes the complete condensation of the silica network, favoring the formation of the ordered mesostructure as described in the literature [6].

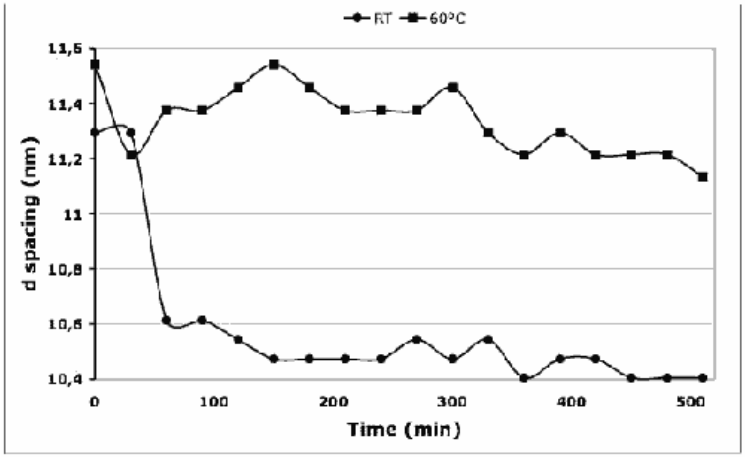

Figure 2. Time evolution of the d spacing of the scaffolds ageing at RT and at 60°C.

References:

[1] D. Arcos, C.V. Ragel, M. Vallet-Regi; Biomaterials 22, 701, (2001)
[2] M.S. Ahola, P. Kortesuo, I. Kangasniemi, J.Kiesvaara, A.U.O. Yli-Urpo; International J. Pharmaceutics 195, 219, (2000)
[3] M. Vallet-Regi, A. Ramila, R. P. del Real and J. Pérez-Pariente; Chem. Mater 13, 308, (2001)
[4] J.M. Gomez-Vega, A. Hozumi, E. Saiz, A.P.Tomsia, H. Sugimura, O.Takai, J.; Biomedical Mat. Research 56 (3), 382, (2001)
[5] Onida B., Cauda V., Fiorilli S., Vernè E., Vitale Brovarone C. Viterbo D., Croce Gianluca, Milanesio M., Garrone E.; Stud. Surf. Sci. Catal. 158, 2027, (2005)
[6] H.Yang, Q.Shi, B. Tian, S. Xie, F. Zhang, Y. Yan, B. Tu, D.Zhao ; Chem. Mater. 15(2), 536, 2003

IN-SITU MEASUREMENT OF BUBBLE NUCLEATION DURING FOAMING OF POLYMERS

T. Francis[1], P. Lopes[1,2], J. Rieger[1], P. Schuler[1], A. Moreira[1], M. Rüllmann[1], S. Behrens[3]

1.) BASF Aktiengesellschaft, Germany
2.) University of Porto, Portugal
3.) Department of Chemical and Biomolecular Engineering, Georgia Tech, USA

Background

In this study we were interested in improving the insulation performance of polymer foams used for insulation, by decreasing the average cell size of the foam. As the average cell size in a foam structure approaches the mean free path of gas molecules in air, the "Knudsen" effect begins to play an important role in determining the thermal insulation properties of foams[1]. When the cell size of a foam is small enough, the thermal properties of the foam in air are comparable to the thermal properties of the foam in a vacuum. To make a solid polymer nanofoams three requirements must be satisfied, first a high bubble nucleation rate is required, second limiting the growth of the bubble size is necessary to retain a nanostructure, and third the nanostructured foam must be stable. In order to achieve the first two goals an understanding of the early stages of bubble nucleation and growth is required. The specific questions to be answered in the study are: What is the number density of nucleating centers? Does the nucleation and growth approach apply in our cases? If so, what is the critical nucleation radius of a bubble? And what is the growth rate of bubbles in the early stages of growth?

Experimental

A high-pressure Chamber for Optical and X-ray In-situ Bubble Observation (COXIBO), capable of a rapid pressure release was designed and built, in order to study the early stages of bubble nucleation during the foaming of a gas-impregnated polymer melt.

The high-pressure cell used in this study was designed and built specifically for this work. The following design factors were considered in the design of the cell:

i) The ability to rapidly expand a gas impregnated polymer melt.
ii) The ability to refill the optical cell without complete disassembly of the cell.
iii) The ability to perform in-situ scattering experiments with a high time resolution.

These three design considerations resulted in the following; i) Rapid expansion of the gas-impregnated melt was accomplished by incorporating two opposed pistons into the cell. In this case the pistons put into use were vertically aligned. ii) In order to be able to refill the optical cell with polymer without disassembling the entire system a large piston acting as a reservoir for fresh, gas-impregnated polymer was attached to the cell. When filling the cell with fresh polymer, the fresh polymer would flow into the cell horizontally. iii) In-situ scattering experiments with a high time resolution are currently only possible using x-ray scattering at a synchrotron source. To reduce the attenuation of x-rays as they pass through the window material, diamond was chosen as the window material and the windows were as thin as possible. A schematic of the COXIBO system is shown in Figure 1.

The experiments were carried out at the ELETTRA synchrotron light scattering facility in Trieste, Italy on the BL 5.2L beamline. The reason for choosing this beamline is that a high-speed detector is available, which enables extremely high-speed SAXS measurements.

Results

Two systems were studied; foaming of polystyrene saturated with CO2 and a simpler phase transition, the nucleation of bubbles from a pure liquid CO2 phase. The first experiments attempted were the foaming of polystyrene + CO_2. In these experiments a dust-free polystyrene was loaded with 6,7% CO_2 by weight. The polystyrene was allowed to reach a homogeneous state at 185 bar and 200 °C, by equilibration for several hours. Data was

collected for ten expansions of the PS+CO_2 system, but the data did not show a high degree of repeatability and could therefore not be analyzed. The cause of the irreproducibility stemmed from several factors; the flow pattern of the foaming polymer during the expansion was irregular and the valves attached directly to the optical cell developed a small leak.

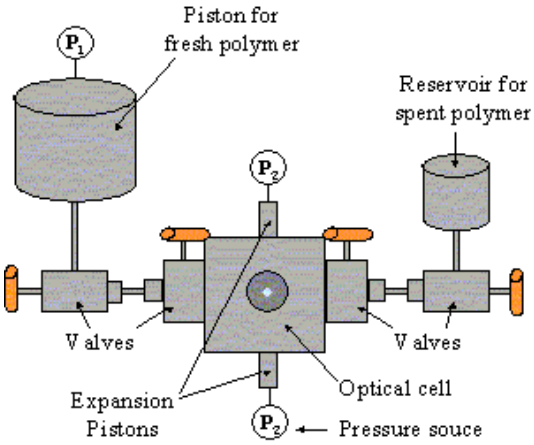

Figure 1. A schematic of the important parts of the COXIBO device.

The irregular flow patterns were caused by unequal movement of the expansion pistons when the backpressure holding the pistons in place was released. The uneven movement of the expansion pistons was influenced by the high viscosity of the polymer melt, as this uneven expansion was not observed in the case of the liquid to gas transition of pure carbon dioxide. The leak in the valves next to the cell was and unforeseen possibility and no replacement o-rings were available, so that all further experiments had a leak, so that the pressure at the beginning of the experiment was not reproducible.
Following the work with the PS+CO2 system, the experimentally simpler phase transition of liquid to gaseous CO2 was measured with similar results.

Conclusions

Several conclusions can be drawn from the experimental work:

i) Time-resolved SAXS measurements with an adequate time resolution are possible.
ii) The repeatability of the attempted foaming experiments was not adequate. In order to obtain usable data the foaming process must be repeatable on the millisecond level.
iii) The experimental cycle time for each measurement was too long. This was due to the manual nature of the experiments. Measurements should be automated so that a single trigger signal can be used to trigger the foaming process, data collection followed by bringing sample conditions back to the initial state, ready for the next triggering.
iv) A new detector that never reaches saturation will be soon available at the Elettra Synchrotron beamline, and will make possible to use the full power of the x-ray source. The use of higher incident intensity will reduce the number of measurements to average.

Future work to address these issues would require a re-designed high-pressure optical cell, which addresses issues specific to working with nucleation in polymers and to the synchrotron beamline.

Acknowledgement

The authours would also like to thank Bernd Sowart and Angelika Kühnle for their important contributions to this work.

References

[1] J. C. Harper; A. F. El Sahrigi;Thermal condictivity of gas filled porous solids; I & EC Fundamentals 3, 318 (1964).

IN-SITU INVESTIGATION ON THE FORMATION OF PERIODICALLY ORDERED MESOSTRUCTURES IN SILICA AND ORGANOSILICA GELS SYNTHESIZED WITH GLYCOL-MODIFIED SILANES AND ORGANOSILANES

C. Fritscher[1], N. Hüsing[2], S. Bernstorff[3], D. Brandhuber[4], T. Koch[1], S. Puchegger[5], S. Geist[2], J. Geserick[2], S. Hartmann[2], S. Seidler[1] and H. C. Lichtenegger[1]

1.) Institute of Materials Science and Technology, Vienna University of Technology, Favoritenstrasse 9-11/308, A-1040 Vienna, Austria
2.) Institute of Inorganic Chemistry I, Ulm University, Albert-Einstein-Allee 11, 89069 Ulm, Germany
3.) Sincrotrone Trieste, Strada Statale 14, Km. 163.5, in AREA Science Park 34012 Basovizza/Trieste, Italy
4.) Institute of Materials Chemistry, Vienna University of Technology, Getreidemarkt 9/165, A-1060 Vienna, Austria
5.) Faculty of Physic, Scattering and Spectroscopy, University of Vienna, Strudlhofgasse 4, A-1090 Vienna, Austria

Ethylene glycol modified silane (tetrakis(2-hydroxyethyl)orthosilicate, denoted as EGMS) [1, 2] and ethylene glycol modified phenylene bridged organosilane (1,4-bis(tris-(2-hydroxyethoxy)silyl)benzene, denoted as bPhGMS) [3] were used as precursor in the presence of the amphiphilic block copolymer Pluronic P123 as structure directing agent. The modification of the precursors with ethylene glycol allows for gel formation in purely aqueous media, resulting in highly porous materials with a bimodal pore arrangement and monolithic structure. Evolution of the periodic arrangement of the surfactant micelles forming the mesopores, as well as sol-gel transition were monitored *in-situ* with SAXS and WAXS.

The formation of periodically ordered mesostructures [4], and in the case of phenylene-bridged silica materials also the formation of lamellar arrangements of organic and inorganic moieties within the pore walls [5] has already been studied for powder synthesis with conventional ethoxy- or methoxy precursors by time-resolved SAXS/WAXS measurements. Powder formation from conventional alkoxysilanes starts from very dilute acidic ethanol/water solutions of the surfactant (~2.5 wt%) and silane (~5 wt%). In our case, we start with a lyotropic liquid crystalline (LLC) phase of surfactant in purely aqueous (acidic) medium resulting in very high concentrations of surfactant (15-20 wt%) and ethylene glycol-modified (organo-) silane (32-45 wt%). This is only possible due to the water solubility of the modified silanes and their very good compatibility with lyotropic liquid crystalline surfactant phases in water [1]. The aim of this SAXS study was to follow the formation of the inorganic and hybrid network formation, respectively, and to gain insight into – what should be – a "true" liquid crystalline templating approach.

The combined SAXS/WAXS measurements were carried out with the sample kept constantly at 40 °C, beginning as soon as the LLC phase and precursor were completely homogenized (6-15 min). A temperature of 40 °C is important for the optimal self assembly of the copolymer molecules.

In Figure 1 the SAXS pattern of an EGMS- (Fig. 1 a) and a bPhGMS- (Fig. 1 b) derived mesoporous material are shown as a function of time, starting with the homogenized sol and following the processes even after gelation and mesostructure evolution have been accomplished. Both systems start with a liquid crystalline phase of 30% (w/w) P123 in 10^{-2} M HCl, which consists of a mixture of cubic and hexagonally closed packed spheres. At the beginning of the measurements, after addition of the silane, some structural order of the LLC phase is still observed in the scattering pattern, especially in the case of the organically bridged precursor. Results for the fitted (10) reflection are depicted in Fig. 1c for both systems. At this pH (2.5) gelation takes place after approximately 4 h, although a significant increase in viscosity could be observed in the EGMS system already after the first 60-70 minutes. A colour change from transparent to turbid, denoting phase separation occurs parallel to gelation. The periodic mesostructure starts to form, which is visible in the EGMS-system in the rise of intensity and decrease of FWHM of the (10) reflection at q=0.429 nm^{-1}

and the appearance of the (20) reflection. In the bPhGMS system, the intensity of the (10) reflection at q=0.45 nm^{-1} starts to increase after 250 min. Shortly afterwards, two additional distinct Bragg peaks emerge, corresponding to (11) and (21) of a periodic structure of hexagonally arranged cylinders. The detailed development of the peak intensities for the bPhGMS-system can bee seen in Fig. 1d. After 460 min the (20) reflection becomes visible and overtakes the (11) reflection after 540 min, due to the progression of the walls thickness of the mesopores.

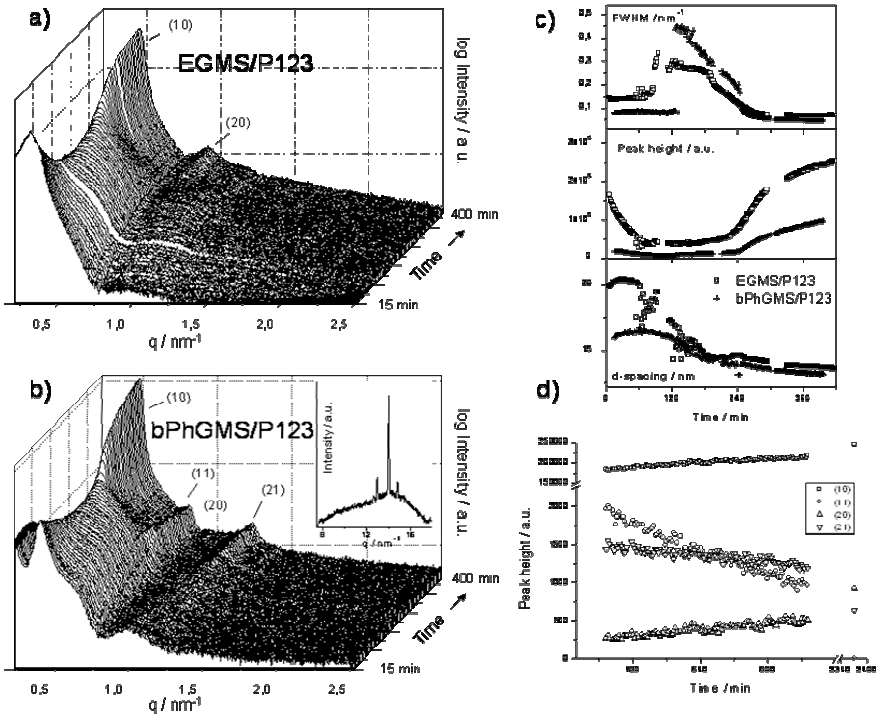

Figure 1. a) In-situ measurement of the sol-gel transition using ethylene glycol modified silane (EGMS) and b) ethylene glycol modified, phenylene bridged organosilane (bPhGMS) as precursor. In both cases, a mixture of 30% (w/w) Pluronic P123 in 10^{-2} M HCl was applied as structure directing liquid crystalline phase to obtain periodic mesopores. The insert in Fig. 1b shows the WAXS region at an early stage of the synthesis. c) The evolution of the observed peaks as a function of time, described by the full width at half maximum (FWHM), the intensity and the d-spacing ($d=2\pi/q$). d) Further evolution of the Bragg intensities of the bPhGMS system.

In the case of the phenylene-bridged precursor, three sharp peaks can be observed in the WAXS region at the start of the process. Those reflections can be ascribed to d-spacings of 0.43 nm, 0.45 nm and 0.48 nm. However, the intensities of all 3 peaks decrease continually until they vanish prior to the formation of the periodic mesostructure. This effect was only observed for two different *in-situ* measurements of the phenylene bridged organosilane and always with the same, rather high, concentration of organosilane. A possible explanation lies in the preparation of the bridged precursor. The glycol modification implies a removal of ethanol, resulting in a solid material consisting of grains, which are partly crystalline. The vanishing of the sharp peaks correlates to a consummation of residual precursor grains in the synthesis and was not observed in a more diluted system. During further progress of the gelation, no other change in the WAXS-pattern could be observed which would confirm a formation of periodic order within the walls of the hybrid mesophase parallel to the formation

of the mesostructure, as was reported by Morell et al [5]. Since the final material exhibits lamellar ordering in the walls [3], the ordering effect was either too small to be observed in the WAXS data or takes place at a later stage.

References:

[1] K. Sattler, M. Gradzielski, K. Mortensen, and H. Hoffmann; Influence of surfactant on the gelation of novel ethylene glycol esters of silicic acid; Berichte der Bunsen-Gesellschaft 102, 1544 (1998)

[2] N. Hüsing, C. Raab, V. Torma, A. Roig, and H. Peterlik; Periodically Mesostructured Silica Monoliths from Diol-Modified Silanes; Chem. Mater. 15, 2690 (2003)

[3] D. Brandhuber, H. Peterlik, and N. Huesing; Facile Self-Assembly Processes to Phenylene-bridged Silica Monoliths with Four Levels; Small 2(4), 503-506 (2006)

[4] K. Flodstrom, V. Teixeira Cilaine, H. Amenitsch, V. Alfredsson, and M. Linden; In situ synchrotron small-angle X-ray scattering/X-ray diffraction study of the formation of SBA-15 mesoporous silica; Langmuir 20, 4885 (2004)

[5] J. Morell, C. V. Teixeira, M. Cornelius, V. Rebbin, M. Tiemann, H. Amenitsch, M. Fröba, and M. Lindén; In situ Synchrotron SAXS/XRD Study on the Formation of Ordered Mesoscopic Hybrid Materials with Crystal-Like Walls; Chem. Mater. 16, 5564 (2004)

TIME-RESOLVED SIMULTANEOUS DETECTION OF STRUCTURAL AND CHEMICAL CHANGES DURING SELF-ASSEMBLY OF MESOSTRUCTURED FILMS

L. Malfatti[1], T. Kidchob[1], S. Costacurta[1,2], P. Falcaro[3], M. Piccinini[4,5], A. Marcelli[5], P. Morini[6], D. Sali[6], H. Amenitsch[7], P. Innocenzi[1]

1.) Laboratorio di Scienza dei Materiali e Nanotecnologie, Dipartimento di Architettura e Pianificazione, Università di Sassari, CR-INSTM, Palazzo Pou Salid, Piazza Duomo 6, 07041 Alghero (SS), Italy
2.) Dipartimento di Ingegneria Meccanica, Settore Materiali, Via Marzolo 9, 35131 Padova, Italy
3.) Associazione CIVEN – Nano Fabrication Facility, Via delle Industrie 9, 30175 Marghera, Venezia, Italy
4.) Laboratori Nazionali di Frascati – INFN, Via E. Fermi 40, 00044 Frascati (Roma), Italy
5.) Dipartimento di Scienze Geologiche, Università Roma Tre, Largo S. Leonardo Murialdo 1, 00146 Rome, Italy
6.) Bruker Optics s.r.l., Via Pascoli 70/3, 20133 Milano, Italy
7.) Institute of Biophysics and Nanosystems Research, Austrian Academy of Sciences, Schmiedlstraße 6, A-8042 Graz, Austria

We have performed at the Austrian SAXS beamline in Elettra simultaneous FTIR and SAXS in situ time-resolved experiment. We have designed the experimental equipment to perform simultaneous measurements using X-rays from synchrotron radiation (grazing incidence small angle X-ray scattering, GISAXS) and infrared light (Fourier transform infrared spectroscopy, FTIR) from a conventional source (Figure 1). This novel technique has been applied to the study of self-assembling mesostructured films during dip-coating: this combined analytical approach enabled us to get a direct correlation between chemical processes and structural changes occurring in the as-deposited film before, during and after mesostructure formation. Even if a very high number of articles has been dedicated to study the organization in mesoporous films during dip-coating [1-4] this is the first time a direct correlation can be done.

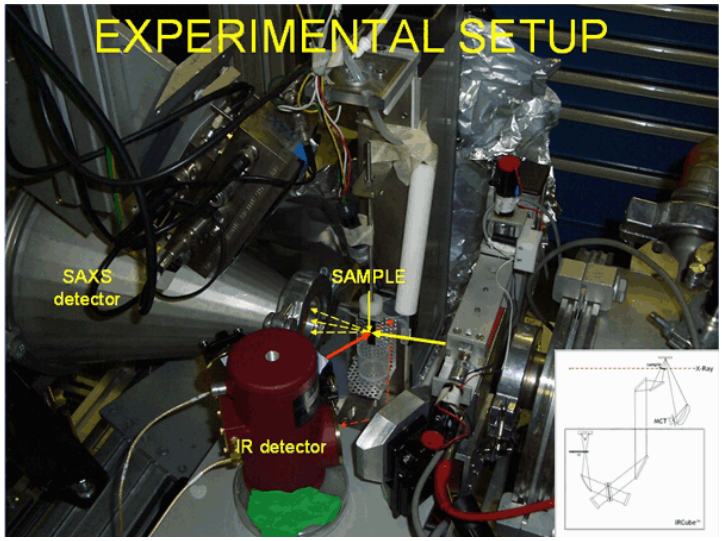

Figure 1. Schematic drawing of the experimental set-up used for the simultaneous SAXS – FTIR time-resolved experiments. The SAXS analysis is performed in grazing incidence and the infrared measure in transmission mode. A system of mirrors allows collecting the infrared light to the MCT detector. Inset: picture of the experimental set-up mounted at the SAXS Austrian beam-line at Elettra

A precursor solution was prepared using methyltriethoxysilane (MTES), tetraethylorthosilicate (TEOS), ethanol (EtOH), and block copolymer Pluronic F127 as the templating agent. Silicon wafers were employed as the substrates because they are transparent in the mid-IR range used for this measurement. The dip-coating system was a home-made device customized for this in situ experiment, in which the sample remains at a fixed position in order to ensure that the same area is investigated by the probing beams. The whole experimental apparatus was enclosed into a plastic cabinet, so that dry air could be fluxed in in order to maintain relative humidity as constant as possible (typically ≈10%). GISAXS measurements were performed in grazing incidence mode. FTIR measurements were performed using the optical system of the IRCube™ interferometer, a very compact

commercial spectrometer for middle infrared (Mid-IR) spectroscopy produced by Bruker Optics, a Ge/KBr beam-splitter and a Globar source. Data were collected with a liquid nitrogen-cooled PC-MCT detector by averaging 16 interferograms collected at a resolution of 8 cm^{-1}, consecutive IR spectra were collected at a time interval of 2 seconds.
Figure 2 shows the time-resolved SAXS two-dimensional patterns recorded at intervals of two seconds. The first significant snapshots are shown, from t = 0 to t = 20 sec; another SAXS snapshot, recorded after 20 minutes, is also reported for reference. The GISAXS and FTIR spectra were recorded for times as long as 40 minutes.

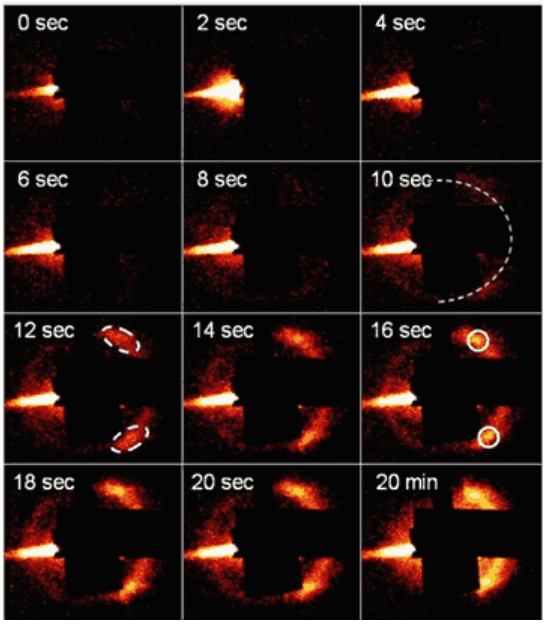

Figure 2. SAXS images recorded at different times after the dip-coating

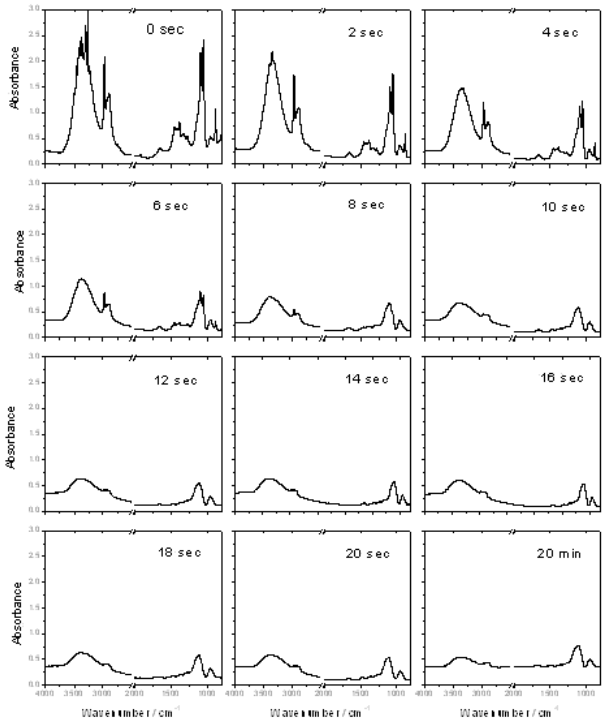

Figure 4. Change in the area of the 1640 cm^{-1} band of water and 880 cm^{-1} band of ethanol as a function of the time after dip-coating

Within this time frame the experimental conditions inside the deposition chamber are maintained stable e.g., RH and temperature were maintained constant at 10% and 22°C, respectively, both within ±5%. The GISAXS patterns show that after 10 seconds the presence of a ring (dotted line in the figure) indicates that organization is starting, even though a mesophase is still not well-defined. At 12 seconds the detection of well defined spots reveals the presence of an ordered mesostructure and while these spots increase in definition and intensity with time negligible changes are observed at times longer than 20 seconds.

The simultaneous FTIR and GISAXS measurements allow getting a direct correlation between the chemical processes and the structural changes occurring in the film. More in detail, what is detected by time-resolved FTIR is the kinetics of solvent and water evaporation, which can be correlated with structural data on mesophase ordering obtained from SAXS measurements (Figure 3). At the first stages the FTIR spectra are dominated by the signature of ethanol.
The intense signals at 2973, 2927, 2885 cm^{-1}, at 1460-1270 cm^{-1}, at 1088 and 1050 cm^{-1}, and at 880 cm^{-1} allow following solvent evaporation with the time. After about 8 seconds this

process is considered to be completed. It is important to note that in the SAXS patterns corresponding to the first 8 seconds of the process no mesophase order is observed. Two specific absorption bands that are well resolved and not overlapped with other vibrational modes were used to monitor the changes in water and alcohol content: the 1640 and 880 cm^{-1} band for water and ethanol, respectively. Figure 4 shows the change in ethanol and water content within the film as a function of time after dip-coating. The area of the two bands was used for the calculation, assuming the areas at t = 0 to account for 100% of water and ethanol. The evaporation of ethanol is fast and follows a linear trend, whereas the evaporation of water has a three-stage trend: a fast initial evaporation is followed by an intermediate stage of slower evaporation, fast evaporation again. The second stage (slower evaporation) is attributed to water enrichment in the system, due to polycondensation reactions. This behaviour agrees with our previous findings in time-resolved experiments on self-assembled cast films [1,5]. The appearance of the ν_{as}(Si-O-Si) band, around 1100 cm^{-1}, is an indication that after 10-12 an interconnected silica network is formed. At this stage, however, the silica film is still compliant enough to allow the re-organization of the micelles.

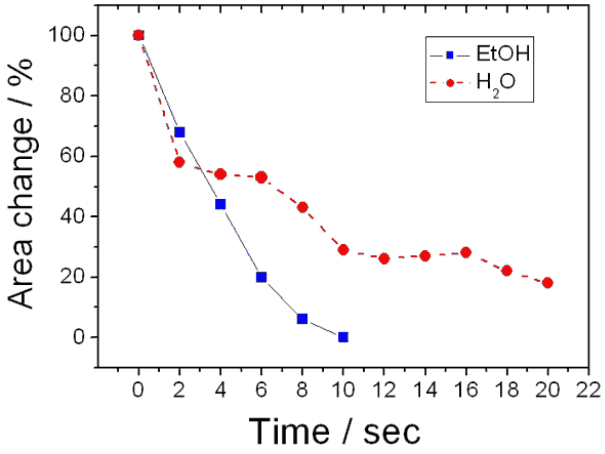

Figure 3. Transmission FTIR absorption spectra recorded at different times after the dip-coating. Silicon was used as the substrate

By SAXS measurements, it is observed that organization starts only after ≈10 seconds, after ethanol evaporation is completed and 70% of the water content is decreased in the film: the diffraction spot intensity increases showing a sigmoidal trend with time. It is reasonable to assume, in fact, that *cmc* is reached only after the first evaporation stage: no experimental evidence of micelle formation at an earlier stage is at the moment reported in the literature to our knowledge. The data show that organization starts only after solvent evaporation which represents the critical step in self-assembly. After this stage the micelles are formed even if we can only observe their organization at a later moment.

The main advantage in applying this simultaneous FTIR and SAXS analysis is the possibility to discriminate between the evaporation rates of ethanol (or any other solvent) and water, and to obtain semiquantitative data that can be examined in the light of the structural data provided by SAXS. It has been demonstrated that the formation of an organized mesophase occurs after all ethanol and 70% of water have evaporated. At this stage, the presence of water in the film can be estimated as $h = [H_2O]/[Si] = 1.56$ (i.e. 30% of h in the precursor solution), which is close to the values obtained through other in situ experimental techniques such as Karl-Fischer titration [3]. However, this new technique is not invasive, can be applied to thin films instead of thick films, cast drops or solutions, and does not require altering the chemistry of the self-assembling system. It also takes into account the presence of atmospheric water, because a reference background is acquired prior to each FTIR measurement session. Finally, from analysis of the FTIR spectra, other information can be inferred, for example the amount of free water, the degree of condensation of the inorganic walls.

References

[1] P. Falcaro, S. Costacurta, G. Mattei, H. Amenitsch, A. Marcelli, M. Cestelli Guidi, M. Piccinini, A. Nucara, A., L. Malfatti, T. Kidchob, P. Innocenzi; J. Am. Chem. Soc.; 127, 3838-3846 (2005).

[2] D. A. Doshi, A. Gibaud, N. Liu, D. Sturmayr, A. P. Malanoski, D. R. Dunphy, H. Chen, S. Narayan, A. MacPhee, J. Wang, S. T. Reed, A. J. Hurd, F. Van Swol, C. J. Brinker; J. Phys. Chem. B; 107, 7683-7688 (2003).

[3] F. Cagnol, D. Grosso, G. J. A. A. Soler-Illia, E. L. Crepaldi, F. Babonneau, H. Amenitsch, C. J. Sanchez; J. Mater. Chem., 13, 61-66 (2003).

[4] Innocenzi, P.; Malfatti, L.; Kidchob, T.; Falcaro, P.; Costacurta, S.; Guglielmi, M.; Mattei, G.; Amenitsch, H.; J. Synchr. Radiation; 12, 734-738 (2005).

[5] P. Innocenzi, L. Malfatti, T. Kidchob, P. Falcaro, M. Cestelli Guidi, M. Piccinini, A. Marcelli; Chem. Comm.; 2384-2386 (2005).

SAXS STUDY OF THE FDU-1 CUBIC MESOPOROUS SILICA GROWTH KINETICS

T. Martins[1], C.V. Teixeira[2], H. Amenitsch[3], M.C.A. Fantini[1]

1.) Institute of Physics, University of Sao Paulo, CP 66318, 05315-970, Sao Paulo, SP, Brazil
2.) Unity of Biophysics, Faculty of Medicine, Autonomous University of Barcelona, Bellaterra, 08193, Spain
3.) Institute of Biophysics and Nanosystems Research, Austrian Academy of Sciences, Schmiedelstrasse, 6, 8043, Graz, Austria

Cubic FDU-1 silica, templated with B50-6600 (EO_{39}-BO_{47}-EO_{39}), Dow Chemical Co., triblock copolymer, was successfully prepared by means of microwave hydrothermal treatment [1]. Recently, the same synthesis was successfully reproduced by using a new Dow Chemical Co. triblock copolymer, Vorasurf 504 (EO_x-BO_y-EO_x), in HCl solution [2]. Vorasurf 540 is more hydrophilic and less viscous than the former, with longer EO and shorter BO chains, but with the same molecular weight. In this experiment we follow the kinetics assembling of mesoporous silica with this new polymer, comparing the effect of HCl with HBr in the initial surfactant solution. The surfactant was dissolved in a HCl(HBr)/ethanol solution and then tetraethyl orthosilicate (TEOS) was added to the solution. The SAXS measurement started at the time of TEOS addition.
Time-resolved SAXS curves were obtained every 2 minutes, and are shown in Figure 1.

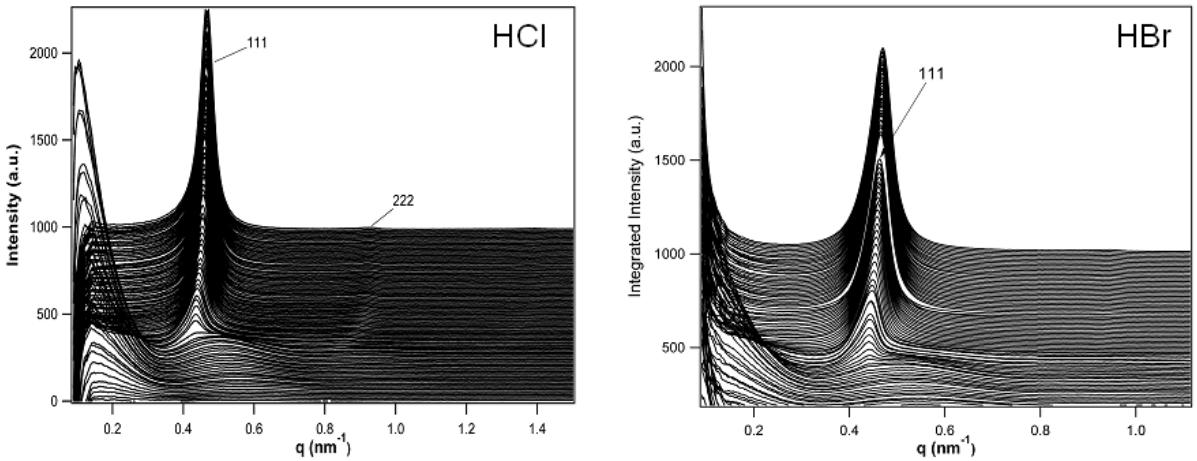

Figure 1. Time-resolved SAXS patterns of the FDU-1 system for the synthesis made with HCl and HBr.

At the beginning of the reaction, the presence of micelles in the solution is observed. The micellar scattering increases as the silica condenses in the hydrophilic layer. After 70 minutes into the reaction the ordered phase is formed and the Bragg reflections start to increase.
The variation of the cell parameter and integrated intensity with time is shown in Figure 2. The integrated intensities follow the same trend with both acids, indicating the same kinetics of reaction and, as expected, the cell parameter shrinks as the silica condenses. However, the cubic phase is formed at the same time for both salts, and this is surprising, as Cl^- is supposed to make the surfactant more hydrophobic than Br^- and the ordered phase was expected to be formed earlier for HCl [3]. But some differences were observed on the time of all the micellar scattering disappear, being longer for HBr.
From the peak positions both samples were indexed as having a FCC structure. Figure 3 shows a comparison between the scattering curves obtained at 100 minutes for both samples. Not all peaks corresponding to the FCC symmetry are present in both samples. Neither the (220) nor the (420) reflections are present in the sample synthesized with HCl.

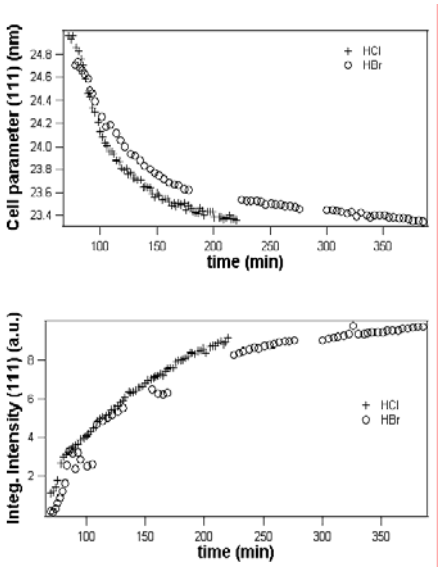

Figure 2. Variation of cell parameter and integrated intensity with time for the FDU-1 system synthesized with HCl and HBr.

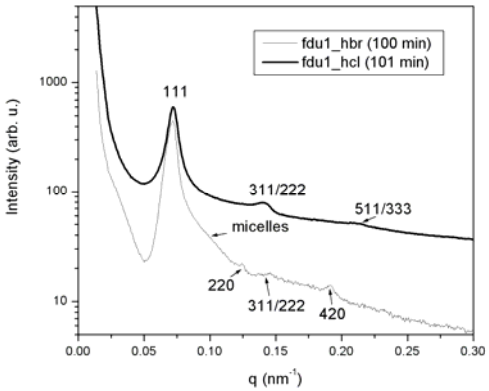

Figure 3. Scattering curves of FDU-1 system synthesized with HCl and HBr. Curves obtained at a reaction time of 100 minute.

Besides, the sample with HBr still has a strong micellar scattering, whereas in the sample with HCl there is no influence of the micellar scattering in the curve at this reaction time. This shows that, although the cubic phase is formed at the same time for both salts, the organization process is slightly different for both. This result points that with HCl the system becomes more ordered at intermediate times than with HBr, as the Bragg reflections hide the micellar scattering in the first case. This can be understood, as in the case of the SBA-15 [3], as an effect of the salting-out behaviour of the Cl^-.

The last point observed in Figure 3 is that the high order peaks are very broad and poorly defined, so that not all reflections can be well resolved, as in the case of the (311) and (222) reflections. This can be caused by a three-dimensional hexagonal intergrowth in addition to the cubic phase, already observed for this system [4].

After the samples were dried and the solvent removed by ethanol extraction, the cell parameter obtained was 21.2 nm and 21.3 nm for HCl and HBr samples, respectively. This is smaller than the value previously obtained for the FDU-1 synthesized with B50-6600 and calcined (23.6 nm). However, as the new surfactant has a smaller hydrophobic core than the former, this difference could be expected.

Acknowledgments: Thanks are due to Dr. J.R. Matos for fruitful discussions.

References:

[1] M.C.A.Fantini, J.R.Matos, L.C.C Silva, L.P.Mercuri, G.O., Chiereci, E.B.Celer and M.Jaroniec,; Mat. Sci. Eng. B 112, 106-110 (2004)
[2] L.C.C. da Silva et al., manuscript in preparation.
[3] C.V. Teixeira, V.Alfredsson, H. Amenitsch, P. Linton, M. Lindén, manuscript in preparation
[4] J.R. Matos, M. Kruk, L.P.Mercuri, M. Jaroniec, L. Zhao, T. Kamiyama, O. Terasaki, T.J. Pinnavaia and Y. Liu; J. Am. Chem. Soc., 125, 821 (2003); M.C.A. Fantini, J.R. Matos, L.C.C. Silva, L.P. Mercuri, G.O. Chiereci, E.B. Celer and M. Jarioniec; Mat. Sci. Eng. B, 112, 106 (2004)

MESOPOROUS ALUMINOPHOSPHATE THIN FILMS WITH TUNABLE CUBIC AND HEXAGONAL PORE ARRANGEMENT

M. Mazaj[1], S. Costacurta[2], N. Zabukovec Logar[1], G. Mali[1], N. Novak Tusar[1], P. Innocenzi[2], L. Malfatti[2], F. Thibault-Starzyk[3], H. Amenitsch[4], V. Kaučič[2], G.J.A.A. Soler-Illia[5]

1.) National Institute of Chemistry, Hajdrihova 19, 1000 Ljubljana, Slovenia.
2.) Laboratorio di Scienza dei Materiali e Nanotecnologie, Dipartimento di Architettura e Pianificazione, Università di Sassari, INSTM, Palazzo Pou Salid, Piazza Duomo 6, 07041 Alghero (SS), Italy
3.) Laboratoire Catalyse et Spectrochimie, ISMRA-CNRS,14050 Caen CEDEX, France
4.) Institute of Biophysics and Nanosystems Research, Austrian Academy of Sciences, Schmiedelstraße 6, A-8042 Graz, Austria.
5.) Unidad de Actividad Quimica, Av. Gral Paz 1499 (1650) San Martín, Buenos Aires, Argentina.

Abstract: highly ordered large-pore cubic mesoporous aluminophosphate thin films with controlled pore arrays presenting 3D cubic ($Im\bar{3}m$) or 2D hexagonal (p6mm) symmetry were synthesised using block copolymer nonionic surfactants F127, F108 and Brij56 nonionic templates. The films retain their ordered mesostructure up to 620 K. In-situ SAXS shows the formation of a hybrid ordered mesostructure upon the dip-coating process. A transition from an amorphous aluminophosphate gel to a well-defined phosphate with 4-coordinated Al centres was observed by TEM, FTIR and MAS-NMR.

Mesoporous aluminophosphates (AlPOs) with large, intercommunicated pore systems are becoming increasingly important for catalytic processes where larger molecules are involved, or molecule diffusion should be improved.[1] Thermally unstable lamellar mesostructured AlPOs were first synthesised using diaminoalkanes ($H_2N(CH_2)nNH_2$) as the structure directing agents; thermal stability was improved by preparing hexagonal mesoporous AlPOs using cationic surfactant (CTACl) templates.[2] A general route based on the "acid-base pair" concept was recently developed.[3] We report the detailed preparation and structural characterisation of large-pore 2D hexagonal and, for the first time, cubic AlPO thin films.
Films were made up by dip-coating into $AlCl_3/H_3PO_4$/ethanol solutions, containing block copolymer surfactants F127, F108 or Brij 56. s=polymer/Al mole ratio was set to 0.005 for F127 and F108-templated films; s=0.016 for Brij 56-templated films. Dip-coating was performed at constant humidity of 40 % and withdrawing speed of 14 $cm \cdot min^{-1}$. The dip-coater was inserted in the beam path so in situ diffraction patterns of the AlPO film could be acquired. Mesostructure symmetry was determined by Grazing Incidence Small Angle X-ray Scattering (GISAXS). The instrumental grazing angle was set slightly above the critical angle of the film (λ=1.54 Å). The sample-to-detector distance and beam centre were calculated from the diffraction pattern of a silver behenate calibration standard powder in a capillary glass. GI SAXS was crossed with FTIR, NMR, TGA/DSC, WAXS, and TEM/EDS, in order to obtain a full characterization from the local and mesoscopic structural domains. An [Al]/[P]=1 molar ratio was determined by EDS for as-deposited and template-free thin films.
Figure 1 shows typical GISAXS patterns after deposition. For the F127-templated sample, spots can be assigned to a body-centred arrangement of spherical micelles (space group ($Im\bar{3}m$), with the (110) plane oriented perpendicular to the substrate, with a cell parameter a = 17.5 nm. Films treated at 373 K for 2 hours show a uniaxial contraction of the d_{110} parameter perpendicular to the substrate d_{110} = 11.03 nm (d_{110} = 12.37 nm for the in-plane reflections).

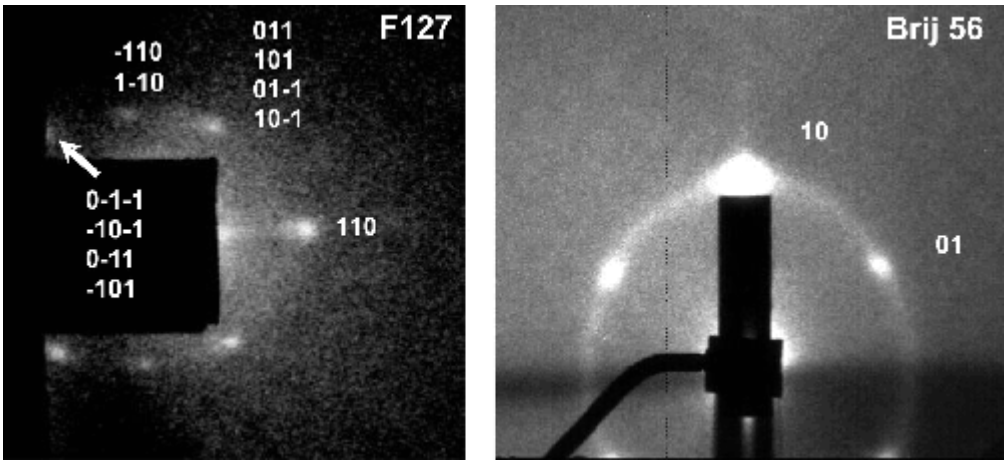

Figure 1. GISAXS patterns of as-deposited F127- and Brij-56 templated AlPO thin films with corresponding indexation.

The thermal behaviour of the AlPO-based thin films was followed by XRD and in-situ FTIR for dip-coated films, and TGA and MAS-NMR for cast films. XRD shows that samples thermally treated at 623 K retained their structure. Peaks are shifted towards higher 2θ angles due to the out-of-plane contraction of the unit cell. Thermogravimetric analysis show a total weight loss between 55 and 70 wt% up to 623 K, depending on the template used. FTIR and NMR studies show that a robust AlPO framework is formed upon thermal treatment.
Figure 2 shows TEM micrographs of highly ordered cubic pore arrangements of template-free F127-templated thin film samples. along [111], [100] and [110] directions, respectively. The estimated TEM distances are in excellent agreement with the SAXS measurement.

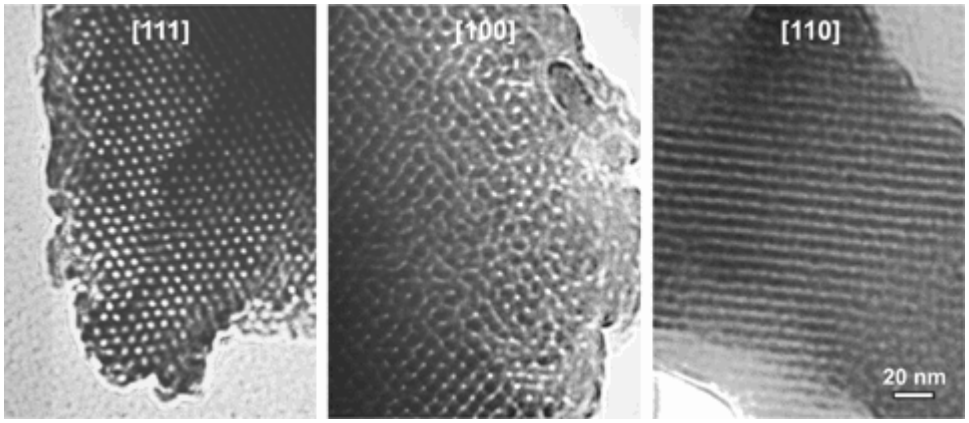

Figure 2. Transmission electron micrographs of template-free AlPO thin film treated at 623 K along (111), (100) and (110) directions.

In conclusion, large-pore mesoporous 1:1 aluminophosphate-based framework with cubic and hexagonal symmetries were successfully produced by dip-coating. The pore arrangement symmetry can be controlled by changing the template. For the first time, it has been shown that these films are stable to thermal treatment, and that there is an evolution in the inorganic framework, according to FTIR and NMR. The percentage of tetrahedrally coordinated aluminium in AlPO samples increases when raising the temperature of sample treatment. Transition metal-modified AlPO films are expected to be produced under similar conditions, which are interesting for catalytic applications.

References

[1] A. Corma, Chem. Rev. 97, 2373 (1997). G. J. A. A. Soler-Illia, C. Sanchez, B. Lebeau, J. Patarin, Chem. Rev. 102, 4093 (2002). G. J. A. A. Soler-Illia, E. L. Crepaldi, D. Grosso, C. Sanchez, Curr. Opin. Colloid Interface Sci. 8, 109, (2003). D. Grosso, et al. Adv. Funct. Mater. 14, 309, (2004).

[2] B. Kraushaar-Czarnetzki, W.H.J. Stork and R.J. Dogterom, Inorg. Chem., 93, 5029 (1993). D. Zhao, Z. Luan and L. Kevan, Chem. Commun., 11, 1009 (1997). P. Selvam and S.K. Mohapatra, Micropor. Mesopor. Mater., 73, 137 (2004). P. Selvam and S.K. Mohapatra, J. Catal., 238, 88 (2006).

[3] B. Tian, X. Liu, B. Tu, C. Yu, J. Fan, L. Wang, S. Xie, G. D. Stucky, D. Y. Zhao, Nat. Mater. 2, 159 (2003). Y. Nishiyama, S. Tanaka, H. W. Hillhouse, N. Nishiyama, Y. Egashira, K. Ueyama, Langmuir, 22, 9469 (2006).

DETERMINATION OF THE PHASE DIAGRAM OF DIBLOCK COPOLYMERS IN IMMISCIBLE SELECTIVE SOLVENTS

P.Štěpánek[1], M. Steinhart[1], H. Amenitsch[2]

1.) Institute of Macromolecular Chemistry, A.S. CR, Heyrovsky Sq.2, 162 06 Prague, Czech Republic
2.) Institute of Biophysics and Nanosystem Research, A.A.S., Schmiedlstrasse 6, 8010 Graz, Austria

The purpose of the study was to perform SAXS experiments on solutions of four diblock copolymers with variable ratio of A and B block lengths, at polymer concentrations and solvent compositions where a homogeneous system exists either in the disordered or self-organized phase and to investigate the morphology of the ordered structures in various regions of the phase diagram.

We have examined 2 diblock copolymers of polystyrene and poly(ethylene propylene) in a mixture of partially miscible solvents cyclohexane (CX) and dimethylformamide (DMF) that have an upper critical solution temperature of 45°C at a critical composition of 38% DMF. The measurements were performed at a temperature of 25°C. A typical accumulation time needed to produce good-quality difractograms was 3 minutes. This indicates that the contrast of the polymer solvent system was appropriate. Series of measurements have been made as a function of polymer concentration and as a function of solvent composition. Totally, we have investigated 98 samples.
At certain low concentrations and low content of the minority solvent, DMF, the scattering curves were featureless, as expected for solutions that at room temperature are above the order-disorder transition. For higher concentrations a form factor or a structure factor appeared. In certain favorable circumstances both are visible in a single scattering curve, when the scattering objects are small and organized in a lattice with a large characteristic distance. This makes the form factor and the structure factor well separated on the q-scale. Figure 1 shows an example where both types of information appear simultaneously. Given the large number of samples examined, complete analysis of all experimental data is still under progress.

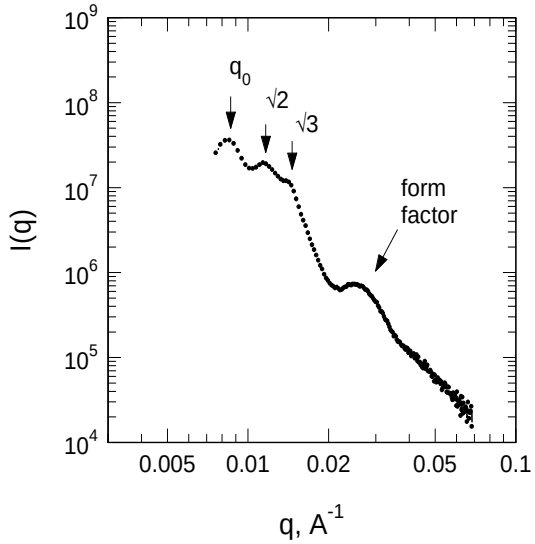

Figure 1. Scattering curve obtained on a self-organized solution of a diblock copolymer polystyrene-*b*-poly(ethylene propylene) at polymer concentration c = 4% and solvent composition 88% cyclohexane/12% dimethylformamide, at temperature 25 °C

IONIC LIQUID CRYSTAL TEMPLATE FOR SILVER NANOPARTICLE SUPERSTRUCTURES

L. Suber[1], G. Campi[2], A. Pifferi[2]

1.) Istituto di Struttura della Materia, via Salaria Km 29,300, Monterotondo Roma, Italy
2.) Istituto di Cristallografia, via Salaria Km 29,300, Monterotondo Roma, Italy

Nanostructured noble metals are of special interest, since their physicochemical properties have many applications in fields as diverse as photovoltaic, catalysis , electronic and magnetic devices, etc [1]. A range of chemical methods have been used to prepare nanosize noble metals, and several of these are based on self-assembled templates. As regards preparation of silver particles, a well known chemical method is reduction of silver ions with ascorbic acid in the presence of a dispersant agent (necessary to avoid particle aggregation). We have used as dispersant agent a aqueous solution of a commercial product known as Daxad 19, a condensation product of naphthalene sulfonic acid. Surprisingly, mainly depending upon slight changes in a mild range (10°C-60°C) of reaction temperature, the reaction has shown an extreme versatility producing silver platelets and stripes [2]. In this work we used in solution Small Angle X ray Scattering (SAXS) to study the role that the dispersant agent Daxad has in the formation of silver superstructures.

The SAXS measurements were conducted at the Austrian SAXS beamline at ELETTRA synchrotron, Trieste, utilizing linear position sensitive detector; the SAXS camera was set to a length of 1.5 m and to a photon energy of 8 KeV. Typically the aqueous solutions in glass capillaries were heated up to 60°C with a rate of 1°C /55sec. SAXS patterns were recorded continuously during the heating. The data were normalized for the intensity of the incident beam and detector efficiencies. The scattering data from the water inside capillaries were also collected, allowing us to assess and subtract backgrounds. Furthermore, in order to investigate the kinetic of the reaction when ascorbic acid is used to reduce the silver ions, we extended our study to in situ formation of silver nanoparticles by using a stopped flow apparatus. A drop of 80 µl of ascorbic acid was added in the aqueous solutions of Daxad with $AgNO_3$ with a rate of 1drop/100sec and each SAXS pattern was collected in 10 sec.

The 10% daxad aqueous solution scattering pattern didn't show any peak in the Q range of 0.03-0.6 nm^{-1}, indicating the absence of ordered structures in the solution. The data, shown in Figure 1 (a) have been modelled by using the unified exponential approach [3] with two levels of related polydisperse nanostructures and the G1 and G2 parameters, proportional to the particle number for the two structural levels and the correspondent radius of gyration Rg1 and Rg2 are reported in Table 1. The introduction of silver nitrate led to a modification of the two levels of the nanoparticle structures, as shown in Figure 1 (b). The values of G1, G2, Rg1, Rg2, reported in Table 1 indicate that the main effect of the added silver nitrate is to increase the volume and the fraction (Rg1 and G1) of the largest structural aggregate. No temperature dependence was observed for all measured samples. A new feature appears in the powder Daxad pattern (Figure 1 (c)), due to a peak at Q ~ 0.47 nm^{-1} consistent with a coexisting lamellar phase.
The influence of added ascorbic acid on the kinetics of formation of the nanoparticles is studied as a function of time; we used a stopped flow apparatus in order to control the amount of ascorbic acid to add to the 0.5% and 5% aqueous solutions of Daxad with silver nitrate. The first stage results are showed in Figure 2 where the integrated intensity of the SAXS patterns are plotted as a function of time. We can observe the enhancement of the scattering following the addition of the ascorbic acid. This analysis is still in progress.

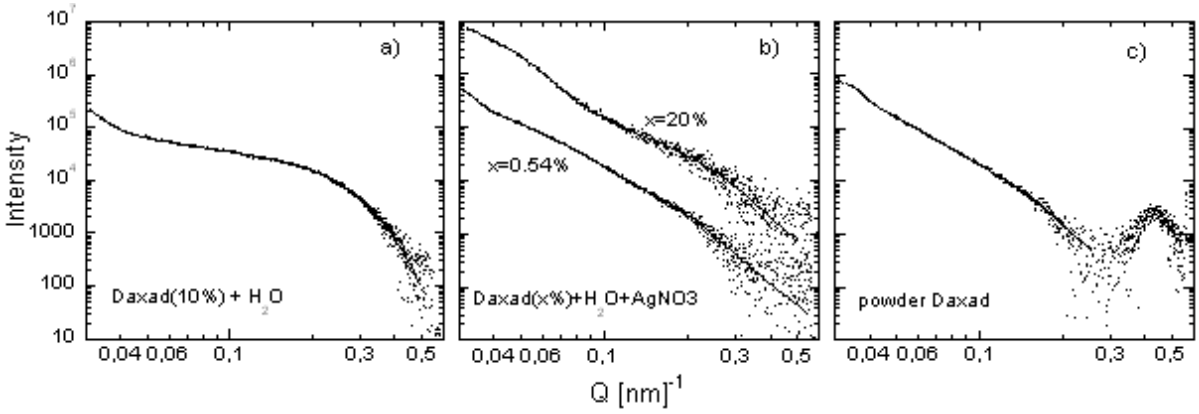

Figure 1. Small angle X ray profiles measured at T = 5°C of (*a*) the 10% aqueous solution of Daxad, of (*b*) the 0.54% and 20% of aqueous solution of Daxad with $AgNO_3$, (c) the powdered Daxad.

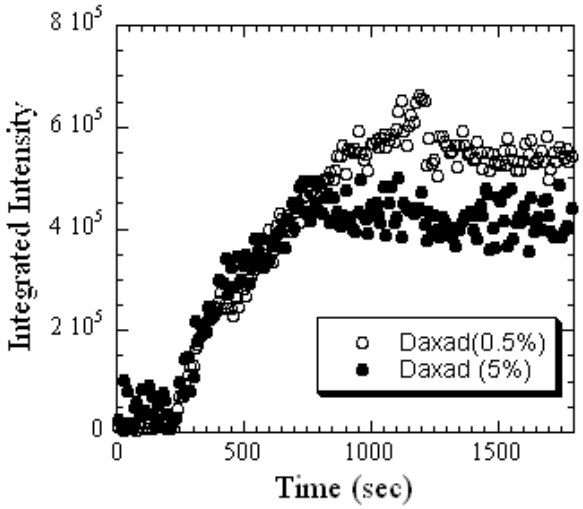

Figure 2. Integrated intensity of the SAXS pattern measured at T=40°C as a function of time for 0.5% and 5% of aqueous solution of Daxad with $AgNO_3$ during the addition of ascorbic acid.

Table 1. G1, R_g1, G2, R_g2 values obtained by fitting data with the unified exponential approach [3].

Sample	G1	R_g1 (nm)	G2	R_g2 (nm)
Daxad(10%)	36976 ± 2.12e+03	28.903 ± 0.714	40946 ± 185	8.7434 ± 0
Daxad(0.54%)+AgNO3	1.8899e+05 ± 6.3e+03	30.964 ± 0.595	11634 ± 2.03e+03	12.191 ± 0.825
Daxad(20%)+AgNO3	1.4398e+07 ± 1.19e+06	49.908 ± 0.404	78143 ± 8.28e+03	9.5515 ± 0.686
Daxad powder	3.656e+05 ± 3.24e+04	39.237 ± 1.43	38016 ± 6.43e+03	17.645 ± 0.913

References:

[1] G. Schmid; Nanoparticles: From Theory to Application, Wiley-VCH, Weinheim, 2004
[2] L. Suber, I. Sondi, E. Matijevic and Dan V. Goia; Preparation and the mechanism of formation of silver particles of different morphologies in homogeneous solutions; Journal of Colloid and Interface Science **288**, 489-495 (2005)
[3] G. Beaucage; Approximations Leading to a Unified Exponential/Power-Law Approach to Small-Angle scattering

FORMATION OF HELICAL SELF-ASSEMBLED NANOTUBES STUDIED BY IN-SITU SAXS

C.V Teixeira[1], H. Amenitsch[2], M. Lindén[1]

1.) Department of Physical Chemistry, Abo Akademi University, Porthansgatan, 3,2, FI-20500, Turku, Finland
2.) Institute of Biophysics and Nanosystems Research, Austrian Academy of Sciences, Schmiedelstrasse, 6, 8043, Graz, Austria

The self-assembly of amphiphilic precursors is a highly promising route towards a rational design of nanotubes (NT).[1] Typically, these nanotubes are formed upon cooling an isotropic precursor solution to a temperature which is below the gel-to-liquid crystalline phase transition temperature. Recently, Aida and collaborators reported the formation of helical arrays of a stacked graphene molecule, using the amphiphilic hexa-peri-hexabenzocoronene (HBC) as the precursor, by slowly cooling a solution of HBC in tetrahydrofurane (THF) followed by aging under ambient conditions.[2] A nanotubular graphitic structure was then formed, where the graphene sheets were stacked in axial direction. The wall thickness was 3 nm, which suggests that the wall consists of a bilayer of HBC. The overall structure consisted of a uniform, smooth, 14-nanometer-wide, open-ended hollow space with an aspect ratio greater than 1000. The radius is an order of magnitude larger than those of conventional carbon NTs.
We have studied the assembly and disintegration of the HBC nanotubes by means of in situ SAXS at ELETTRA, [3] and this is the first structural assignment of HBC nanotubes in solution. Time-resolved measurements were performed at an energy of 8 KeV and with a sample to detector distance of 2317 mm. A Mar180 Imageplate was used to record 2-D images every 160 s, which, after correction for detector inhomogeneity and efficiency, were integrated and corrected for background. 5 mg/ml of HBC was dissolved in THF at 50^{o}C, and an aliquot was filled in a pre-heated quartz capillary which was immediately sealed. The capillary was then cooled to room temperature at a rate of 1^{o}C/min, and subsequently aged for 10 h. The SAXS curve measured for the aged sample is shown in Figure 1.

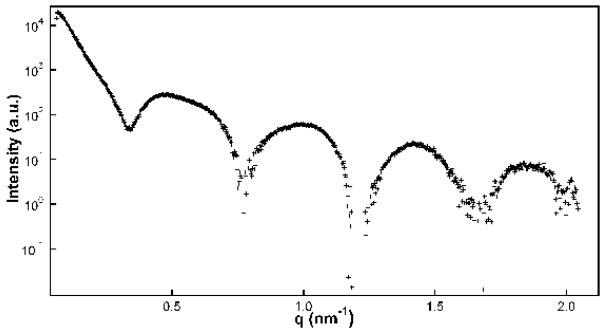

Figure 1. Scattered intensity of a sample after equilibrium of 10 hours, at 20 °C

The scattering curve exhibits 5 distinct minima within the angular resolution range studied ($0.07 < q < 2.10$ nm^{-1}), which indicates that the scattering objects have an extremely narrow size distribution. The fine structure observed mainly in the first two side maxima is not compatible with the form factor of cylinders, indicating the presence of helices in solution. In a further experiment, heating and cooling cycles were performed.
Selected curves during both processes are presented in Figures 2 and 3 respectively. The total scattered intensity gradually decreases upon heating and increases upon cooling, corresponding to the disintegration and re-assembly of the nanotubes, respectively. The

position of the main oscillations does not change, indicating that the radius of the tubes present in solution remains unchanged during both processes.

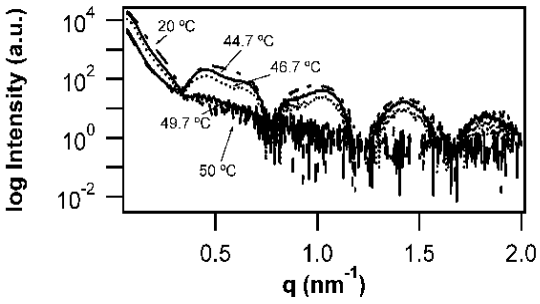

Figure 2. Scattering curves obtained at different times (and temperatures) while heating up, from 20°C to 50°C at a heating rate of 1°C/min, a sample that was at 20°C for 10 hours.

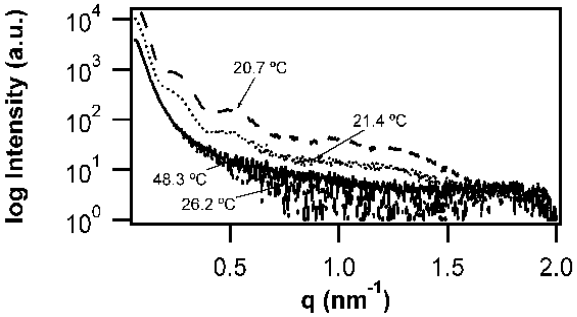

Figure 3. Scattering curves obtained at different times (and temperatures) while cooling down from 50°C to 20°C at a cooling rate of 1°C/min.

However, at intermediate temperatures the peaks become highly asymmetric. This asymmetry can be related to coexistence of aggregates of different symmetries, like helices and bilayer tapes, for instance. At 50°C the scattered curve is featureless, which means that the nanotubes are totally molten. The integrated intensities measured during the heating from 20 to 50°C and subsequent cooling of the sample from 50 to 20°C are shown in Figure 4. There is a clear hysteresis in the curves: during the heating cycle, the integrated intensity starts decreasing after 35°C whereas upon cooling a pronounced increase in the scattered intensity is not observed before the temperature has reached 24°C. However, at 21°C, the total scattered intensity reaches the same level as for the aged sample, indicating that the concentration of nanotubes is similar in both cases. Nevertheless, the scattering curves do not have the same level of fine-structure, which underlines the need for an aging period in order to achieve a high level of monodispersity and closure of the helix ribbons.

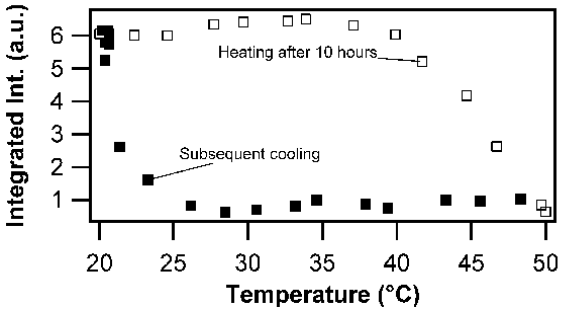

Figure 4. Variation of the integrated intensity with temperature, for heating and cooling (1°C/min each). Heating performed after 10 hours resting at 20°C.

References:

[1] T. Shimizu, M. Masuda, H. Minamikawa;; Chem Rev., 105, 1401-1443 (2005); P. Terech. A. De Geyer, B. Struth, Y. Talmon, Adv. Mater., 14, 495 (2002).

[2] J.P.Hill, W.Jin, A.Kosaka, T.Fukushima, H.Ichihara, T.Shimomura, K.Ito, T.Hashizume, N.Ishii, T.Aida; Science, 304, 1481 (2004).

[3] H.Amenitsch, M.Rappolt, M.Kriechbaum, H.Mio, P.Laggner, S.Bernstorff, J. Synchrotron Radiat., 5, 506 (1998).

12CB AND 8CB LIQUID CRYSTALS CONFINED TO CPG GLASSES

A. Zidanšek[1]

1.) J. Stefan Institute and J. Stefan International Postgraduate School, Jamova 39, 1000 Ljubljana, Slovenia

12CB and 8CB liquid crystals confined to CPG pores represent an interesting system, which reflects the interplay between elastic, surface interaction forces and finite size effects. Randomly curved and interconnected pores introduce some kind of randomness into the system. For this reason one often considers such systems as a testing ground for the statistical physics of disorder [1, 2].

Temperature dependence of the small angle X-ray scattering smectic peak was measured in smectic phase of the 12CB and 8CB liquid crystals confined to CPG glasses of various pore diameters. The results confirmed our hypothesis that confinement to CPG pores has qualitatively different effect on 8CB versus 12 CB liquid crystal.

In this experiment we focused on the influence of confinement in CPG glasses on temperature dependence of smectic ordering in the ranges of CPG diameter between 37 nm and 292 nm. The 8CB liquid crystal exhibits at high temperatures the isotropic (I) phase, crossing the nematic (N) phase, until strong smectic A (SmA) ordering is established at low temperatures, while in 12CB the nematic phase is absent and the transition is directly from the isotropic into the smectic A phase.

Results of this experiment can be explained in terms of the Landau-Ginzburg-de Gennes type phenomenological model. A typical result of the SAXS experiment is shown in Fig. 1.

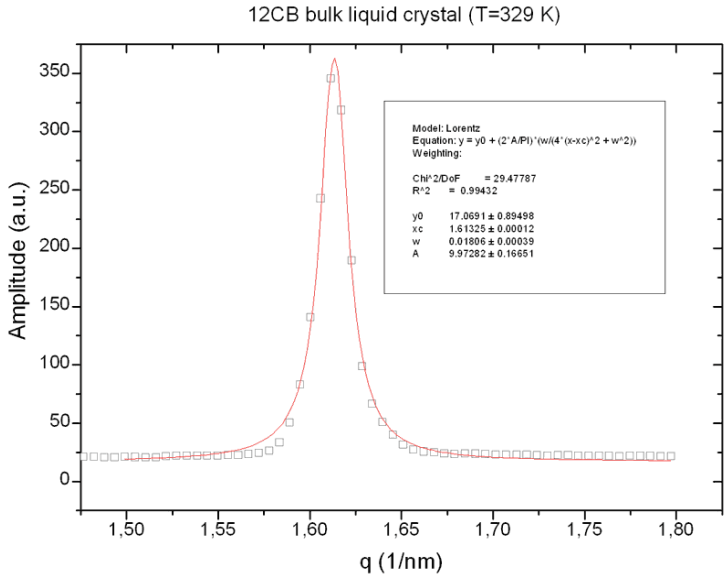

Figure 1. Typical X-ray scattering pattern of the 12CB liquid crystal confined to CPG glass

A more comprehensive review is under preparation for publication in Physical Review E.

References:

[1] Kancler A, Lahajnar G, Kralj S, Zidansek A, Amenitsch H, Bernstorff S; Molecular Crystals And Liquid Crystals 439: 1899-1908 (2005)

[2] Zidansek A, Kralj S, Repnik R, Lahajnar G, Rappolt M, Amenitsch H, Bernstorff S, Journal of Physics-Condensed Matter 12: A431-A436 (2000)

Publications

Publications in Journals and Reviewed Proceedings 2006

H. Amenitsch, F. Schmid, G. Sommer, M. Rappolt, P. Regitnig, G. Holzapfel & P. Laggner
Time-resolved fibre diffraction on human arteries during tensile testing and nanostructure correlation to mechanical behavior
Acta Cryst. A62, abstract s41 (dec. 2006)

V. K. Aswal, J. Kohlbrecher, P. S. Goyal, H. Amenitsch, S. Bernstorff
Counterion condensation on charged micelles in an aqueous electrolyte solution as studied with combined small-angle neutron scattering and small-angle x-ray scattering
Journal of Physics-Condensed Matter 18, 11399-11410 (2006)

S. Bernstorff, P. Dubcek, B. Pivac, I. Kovacevic, A. Sassella, and A. Borghesi
XRR and GISAXS study of silicon oxynitride films
Applied Surface Science 253, 33-37 (2006)

I. Beurroies, P. Agren, G. Buchel, J.B. Rosenholm, H. Amenitsch, R. Denoyel, M. Linden
?Detailed in Situ XRD and Calorimetric Study of the Formation of Silicate/Mixed Surfactant Mesophases under Alkaline Conditions. Influence of Surfactant Chain Length and Synthesis Temperature
J. Phys. Chem. B. 110(33), 16254-16260 (2006)

C. Boissiere, L. Nicole, C. Gervais, F. Babonneau, M. Antonietti, H. Amenitsch, C. Sanchez, and D. Grosso
Nanocrystalline mesoporous gamma-alumina powders "UPMC1 material" gathers thermal and chemical stability with high surface area
Chemistry of Materials 18, 5238-5243 (2006)

T. Brezesinski, M. Groenewolt, N. Pinna, H. Amenitsch, M. Antonietti, B. Smarsly
Surfactant-mediated Generation of Iso-oriented Dense and Mesoporous Crystalline Metal Oxide Layers
Adv. Mater. 18, 1827 (2006)

G. Caracciolo, D. Pozzi, H. Amenitsch, . Caminiti
One-Dimensional Thermotropic Dilatation Area of Lipid Headgroups within Lamellar Lipid/DNA Complexes
Langmuir 22(9), 4267-73 (April 25, 2006)

G. Caracciolo, D. Pozzi, R. Caminiti, H. Amenitsch
Formation of overcharged cationic lipid/DNA complexes
Chemical Physics Letters, 429, 250-254 (2006)

G. Caracciolo, D. Pozzi, R. Caminiti and H. Amenitsch
Two-dimensional lipid mixing entropy regulates the formation of multi-component lipoplexes
Journal of Physical Chemistry B 110, 20829 - 20835 (2006)

G. Caracciolo, D. Pozzi, R. Caminiti, C. Marchini, M. Montani, A. Amici and H. Amenitsch.
DNA release from cationic liposome/DNA complexes by anionic lipids
Applied Physics Letters 89, 233903-(1-3) (2006) (3 pages)

D. Cojoc, E. Ferrari, V. Garbin, E. Di Fabrizio, H. Amenitsch, M. Rappolt, B. Sartori, C. Riekel, M. Burghammer
Combined laser trapping and small-angle X-ray scattering experiment for the study of liposome colloidal microparticles
Proc. of SPIE, Vol. 6326: 63261M1-6 (2006)

I.D. Desnica-Frankovic, P. Dubcek, U.V. Desnica, S. Bernstorff, M.C. Ridgway and C.J. Glover
GISAXS studies of structural modifications in ion-beam amorphized Ge
Nucl. Instr. Methods Phys. Res. B 249, Issues 1-2, pp 114-117 (Aug 2006)

U.V. Desnica, M. Buljan, P. Dubcek, Z. Sikatic, I. Bogdanovic Radovic, S. Bernstorff, U. Serincan and R. Turan
Ion beam synthesis and characterization of Ge nanocrystals in SiO2
Nim B 249 (2006) 843-846

A.B. Dros, D. Grosso, C. Boissière, G.J.A.A. Soler-Illia, P.-A. Albouy, H. Amenitsch and C. Sanchez
Niobia-stabilised anatase TiO2 highly porous mesostructured thin films
Microporous and Mesoporous Materials 94, Issues 1-3, 208-213 (8 September 2006)

P. Dubcek, B. Pivac, S. Bernstorff, F. Corni, R. Tonini, and G. Ottaviani
X-ray reflectivity study of hydrogen implanted silicon
Applied Surface Science 253, 283-286 (2006)

J. I. Flege, Th. Schmidt, V. Aleksandrovic, G. Alexe, T. Clausen, B. Gehl, A. Kornowski, S. Bernstorff, H. Weller, J. Falta
Grazing-incidence small-angle X-ray scattering investigation of spin-coated CoPt3 nanoparticle films
Nuclear Inst. and Methods in Physics Research, B Volume: 246, Issue: 1, May, 2006, pp. 25-29

D. Gracin, K. Juraic, P. Dubcek, A. Gajovic and S. Bernstorff
The nano-structural properties of hydrogenated a-Si and Si-C thin films alloys by GISAXS and vibrational spectroscopy
Applied Surface Science, Volume 252, Issue 15, 30 May 2006, 5598-5601

P. J. Griffiths, M.A. Bagni, B. Colombini, H. Amenitsch, S. Bernstorff, S. Funari, A. C Christopher and G. Cecchi
Effects of the number of actin-bound S1 and axial force on X-ray patterns of intact skeletal muscle
Biophysical Journal 90, 975-984 (2006)

P. Kenesei, G. Horváth, S. Bernstorff, T. Ungár, J. Lendvai
Early stages of nucleation and growth of Guinier–Preston zones in Al–Zn–Mg and Al–Zn–Mg–Cu alloys
Zeitschrift fuer Metallkunde 97 (2006) 315-320

M. Kerber, E. Schafler, P. Hanak, G. Ribàrik, S. Bernstorff, T. Ungàr, M. Zehetbauer
Spatial fluctuations of the microstructure during deformation in Cu Single Crystals
Z. Krist. Suppl. 23, 105 (2006)
Zeitschrift fuer Kristallographie, Vol. Suppl23, pp. 105-6 (2006)

E. Korznikova, E. Schafler, G. Steiner, M. Zehetbauer
Measurements of Vacancy type Defects in SPD deformed Nickel
Proc. 2006 TMS Annual Meeting, San Antonio, 4th Int. Symp. on ultrafine grained materials, ed. Y.T. Zhu et al., TMS publications, Warrendale, 97-102 (2006)

I. Kovacevic, B. Pivac, P. Dubcek, N. Radic, S. Bernstorff, and A. Slaoui
A GISAXS study of SiO/SiO2 superlattice
Thin Solid Films 511-512, 463-467 (2006)

R. Krishnaswamy, G. Pabst, M. Rappolt, V. A. Raghunathan, A. K. Sood
Structure of DNA-CTAB-hexanol complexes
Physical Review E 73, 031904: 1-8 (2006)

L. Malfatti, P. Falcaro, H. Amenitsch, S. Caramori, R. Argazzi, C.A. Bignozzi, S. Enzo, M. Maggini, and P. Innocenzi
Mesostructured self-assembled titania films for photovoltaic applications
Microporous and Mesoporous Materials 88 (1-3), pp. 304-311 (2006)

L. Malfatti, T. Kidchob, S. Costacurta, P. Falcaro, P. Schiavuta, H. Amenitsch, P. Innocenzi
Highly ordered self-assembled mesostructured hafnia thin films: an entropy driven rewritable mesostructure
Chem. Mater. 18, 4553-4560, 2006

G. Pabst
Global properties of biomimetic membranes: perspectives on molecular features
Biophysical Reviews and Letters, Vol.1, No.1 (2006) 57 –84

J. Pereira-Lachtaignerais, R. Pons, H. Amenitsch, M. Rappolt, B. Sartori, and O. Lopez
Effect of sodium dodecyl sulfate at different hydration conditions on dioleoyl phosphatidylcholine bilayers studied by grazing incidence X-ray diffraction
Langmuir 22, 5256-5260, (2006)

B. Pivac, P. Dubcek, I. Kovacevic, S. Bernstorff, R. Mu, M. Wu, A. Ueda, B. Vlahovic
GISAXS study of gold implanted fused silica
Scripta Materialia 55, 135-138 (2006)

B. Pivac, I. Kovacevic, P. Dubcek, N. Radic, S. Bernstorff, and A. Slaoui
Self-organized growth of Ge islands on Si(100) substrates
Thin Solid Films 511-512, 153-156 (2006)

B. Pivac, I. Kovacevic, P. Dubcek, N. Radic and S. Bernstorff
GISAXS study of Si nanocrystals formation in SiO2 thin films
Thin Solid Films, 515, 756-758 (2006)

D. Pozzi, H. Amenitsch, R. Caminiti and G. Caracciolo,
How lipid hydration and temperature affect the structure of DC-Chol-DOPE/DNA lipoplexes
Chemical Physics Letters, Volume 422, Issues 4-6, 10 May 2006, Pages 439-445

N. Radic, B. Pivac, P. Dubcek, I. Kovacevic, and S. Bernstorff
Growth of Ge islands on Si substrates
Thin Solid Films 515 (Issue 2), 752-755 (25 October 2006)

M. Rappolt, G.M. Di Gregorio, M. Almgren, H. Amenitsch, G. Pabst, P. Laggner and P. Mariani
Non-equilibrium formation of the cubic Pn3m phase in a monoolein/water system
Europhysics Letters, 75, 267-273 (2006)

E. Schafler, K. Nyilas, S. Bernstorff, L. Zeipper, M. Zehetbauer, T. Ungàr
Microstructure of post deformed ECAP-Ti investigated by Multiple X-Ray Line Profile Analysis
Zeitschrift fuer Kristallographie, Vol. Suppl. 23, pp. 129-134 (2006)

Schmid, F., Sommer, G., Rappolt, M., Regitnig, P., Holzapfel, G.A., Laggner, P., Amenitsch, H.
Bidirectional tensile testing cell for in situ small angle X-ray scattering investigations of soft tissue
Nuclear Inst. Meth. B246, pp. 262-268 (May 2006)

F. Spinozzi, P. Mariani, F. Rustichelli, H. Amenitsch, F. Bennardini, G. M. Mura, A. Coi, M. L. Ganadu
Temperature dependence of chaperone-like activity and oligomeric state of alphaB-crystalline
Biochim Biophys Acta 1764(4), 677-687 (Apr. 2006)

R. Supplit, N. Hüsing, H. Bertagnolli, M. Bauer, V. Kessler, G.A. Seisenbaeva, S. Bernstorff and S. Gross
Synthesis and characterization of orthorhombic, 2d-centered rectangular and lamellar iron oxide doped silica films
Journal of Materials Chemistry 16, pp. 4443-4453 (2006)

A. Turkovic, M. Pavlovic, M. Ivanda, M. Gaberšček, Z. Crnjak Orel
Influence of Intercalated Lithium on Structural and Electrical Properties of V_2O_5, Mixed V/Ce Oxide and Fe_2O_3
Journal of the Electrochemical Society (JES), 153, 1; A122-A126 (2006)

M. J. Zehetbauer, G. Steiner, E. Schafler, A. Korznikov, E. Korznikova
Deformation induced vacancies with Severe Plastic Deformation: Measurements and Modelling
Mater.Sci.Forum 503-504, 57-64 (2006)

Publications during January - June 2007

H. Amenitsch, D. Cojoc, M. Rappolt, B. Sartori, P. Laggner, E. Ferrari, V. Garbin, M. Burghammer, Ch. Riekel, and E. Di Fabrizio
Optical Tweezers for Sample Fixing in Micro-Diffraction Experiments
AIPConfProc 879, pp. 1287-1290 (Jan 2007)

S. Bernstorff, P. Dubcek, I. Kovacevic, N. Radic, B. Pivac
Si nanocrystals in SiO2 films analyzed by small angle X-ray scattering
Thin Solid Films 515, 5637 – 5640 (2007)

G. Caracciolo, C. Marchini, D. Pozzi, R. Caminiti, H. Amenitsch, M. Montani, A. Amici
Structural stability against disintegration by anionic lipids rationalizes the efficiency of cationic liposome/DNA complexes
Langmuir 23 (8), 4498-4508 (2007)

Y. Castro, B. Julian, C. Boissiere, B. Viana, H. Amenitsch, D. Grosso, and C. Sanchez
Synthesis, characterization and optical properties of Eu2O3 mesoporous thin films
Nanotechnology 18 (5), p.055705 1-7 (2007)

G. Croce, D. Viterbo, M. Milanesio, H. Amenitsch
Mesoporous pattern created by nature in spicules from Thetya Aurantium sponge
Biophysical Journal 92 (1), 2007, 288-292

R. A. Farrell, K. Cherkaoui, N. Petkov, H. Amenitsch, J. D. Holmes, P. K. Hurley and M. A. Morris
Physical and Electrical Properties of Low Dielectric Constant Self Assembled Mesoporous Silica Thin Films
Microelectronics Reliability 47, 759-763 (2007)

D. Gracin, S. Bernstorff, P. Dubcek, A. Gajovic and K. Juraic
Study of amorphous nanocrystalline thin silicon films by grazing-incidence small-angle X-ray scattering
J. Appl. Cryst. 40 (2007) s373–s376

D. Gracin, S. Bernstorff, P. Dubcek, A. Gajovic, K. Juraic
The influence of substrate morphology on the growth of thin silicon films: a GISAXS study
Thin Solid Films 515, 5615 – 5619 (2007)

D. Grozdanic, B. Rakvin, B. Pivac, P. Dubcek, N. Radic, S. Bernstorff
Structural characterization of thin amorphous Si films
Thin Solid Films 515, 5620 – 5623 (2007)

P. Gupta, A. Gupta, G. Principi, A. Maddalena, S. Bernstorff, and H. Amenitsch
Effect of annealing current density on the microstructure of nanocrystalline FeCuNbSiB alloy
J. Appl. Phys. 101 (5), 053907 (2007) (5 pages 0539071-5)

P. Innocenzi, L. Malfatti, T. Kidchob, S. Costacurta, P. Falcaro, M. Piccinini, A. Marcelli, P. Morini, D. Sali, H. Amenitsch
Time-Resolved Simultaneous Detection of Structural and Chemical Changes during Self-Assembly of Mesostructured Films
Journal of Physical Chemistry C 111, 5345-5350, 2007

I. Kovacevic, B. Pivac, P. Dubcek, H. Zorc, N. Radic, S. Bernstorff, M. Campione, and A. Sassella
Formation of Ge islands from a Ge layer on Si substrateduring post-growth annealing
Applied Surface Science 253, 3034-3040 (2007)

I. Kovacevic, P. Dubcek, S. Duguay, H. Zorc, N. Radic, B. Pivac, A. Slaoui, S. Bernstorff
Silicon nanoparticles formation in annealed SiO/SiO2 multilayers
Physica E38, 50–53 (2007)

M. Lucic-Lavcevic, P. Dubcek, A. Turkovic, Z. Crnjak Orel, S. Bernstorff
Nanostructural Depth-Profile of Vanadium/Cerium Oxide Film as a Host for Lithium Ions
Solar Energy Materials & Solar Cells 91 (7), 616-620 (2007)

M. Lucic Lavcevic, A. Turkovic, P. Dubcek, S. Bernstorff
Nanostructured CeO2 thin films: a SAXS study of the interface between grains and pores
Thin Solid Films 515 (2007) pp. 5624 – 5626

G. A. Maier, G. M. Wallner, R. W. Lang, J. Keckes, H. Amenitsch and P. Fratzl
Fracture of poly(vinylidene fluoride): a combined synchrotron and laboratory in-situ X-ray scattering study
J. Appl. Cryst. 40 (2007), 564-567

A.G. Marangoni, S.H.J. Idziak, C. Vega, H. Batte, M. Ollivon, P.S. Jantzi, J.W.E. Rush
Encapsulation-stucturing of edible oil attenuates acute elevation of blood lipids and insulin in humans
Soft Matter 3, 183-187 (2007)

Metikoš-Hukovic, Mirjana; Grubac, Zoran; Radic, Nikola; Dubcek, Pavo; Djerdj, Igor
The influence of local structure of nanocrystalline Ni films on the catalytic activity
Electrochemistry Communications 9, 299–302, 2007

H.Peterlik, H.Renhofer, V.Torma, U.Bauer, M.Puchberger, N.Hüsing, S.Bernstorff, and U.Schubert:
Structural investigation of alumina silica mixed oxide gels prepared from organically modified precursors
Journal of Non-Crystalline Solids 353 (2007) 1635–1644

N. Radic, P. Dubcek, S. Bernstorff, I. Djerdj and A. M. Tonejc
Structural study of nanocrystalline nickel thin films
J.Appl. Cryst. 40, 377–382 (2007)

M. Rappolt
The biologically relevant lipid mesophases as "seen" by X-rays
Elsevier book series "Advances in Planar Lipid Bilayers and Liposomes", Vol. 5 (ed. by A. Leitmannova, Monte Carlo, New York, Elsevier Inc, Academic Press, USA),
chapter 9, page 253-284 (2007)

R. L. Rice, D. C. Arnold, M. T. Shaw, D. Iacopina, A. J. Quinn, H. Amenitsch, J. D. Holmes and M. A. Morris
Ordered Mesoporous Silicate Structures as Potential Templates for Nanowire Growth
Adv. Func. Mater. 17, 133-141 (2007)

C. Sinturel, M. Vayer, R. Erre, H. Amenitsch
Nanostructured Polymers Obtained from Polyethylene-block-poly(ethylene oxide) Block Copolymer in Unsaturated Polyester
Macromolecules Vol. 40 - 7, pp. 2532-7 (2007)

F. Spinozzi, P. Mariani, L. Saturni, F. Carsughi, S. Bernstorff, S. Cinelli, and G. Onori
Met-myoglobin association in dilute solution during pressure-induced denaturation: an analysis at pH 4.5 by high-pressure small-angle X-ray scattering
Journal Physical Chemistry B111, 3822-3830 (2007)

A. Turkovic, M. Pavlovic, P. Dubcek, M. Lucic-Lavcevic, B. Etlinger, and S. Bernstorff
SAXS/DSC Study of Polymer Electrolyte for Zn Rechargeable Nanostructured Galvanic Cells
ECS Transactions, 2 (20) 11-23 (2007)

A. Turkovic, M. Pavlovic, P. Dubcek, M. Lucic-Lavcevic, B. Etlinger, and S. Bernstorff
SAXS/DSC Study of Polymer Electrolyte for Zn Rechargeable Nanostructured Galvanic Cells
Journal of The Electrochemical Society 154, A554-A560 (2007)
and also:
Virtual Journal of Nanoscale Science & Technology, Volume 15, Issue 17, April 30, 2007

T. Ungár, E. Schafler, P. Hanák, S. Bernstorff, M. Zehetbauer
Vacancy Production During Plastic Deformation in Copper Determined by In-situ X-ray Diffraction
Mater. Sci. Eng. A 462, 398-401 (2007)

R. Viswanatha, H. Amenitsch and D.D. Sarma
Growth Kinetics of ZnO Nanocrystals: A Few Surprises
Journal of the American Chemical Society 129(14), 4470-4475 (2007)

A. Yaghmur, P. Laggner, S. Zhang, M. Rappolt
Tuning Curvature and Stability of Monoolein Bilayers by Designer Lipid-Like Peptide Surfactants
PLoS ONE, 2 (5), e479, May 2007

M. Zehetbauer, E. Schafler, T. Ungár
Non-microscopic methods for characterisation of microstructures and properties of UFG metals
Int. J. Mater. Res. (ex Z. Metallk.) 98, 290-298 (2007)

International Conferences and Workshops in 2006

W. Amara-Dali, M. Ollivon et al.
Thermal and Structural Behaviors of Anhydrous Goat's Milk Fat, Characterization of ingredients and foods session
IUFOST, Nantes, France, 17-21 September 2006 (poster)

H. Amenitsch
Austrian SAXS beamline at ELETTRA: from biology to material sciences
Dept. Physical Chemistry, Abo Akademi University, Turku, Finland, 05.04.06

H. Amenitsch
Self-assembly processes of molecules to nanoparticles as seen by small angle X-ray scattering
3rd National Conference on Nanoscience and Nanotechnology: "The molecular approach", SISSA Conference Room, Trieste, Italy, May 22-24, 2006 (talk)

H. Amenitsch
SAXS in solution and under extreme conditions
School on Synchrotron Radiation and Applications, ICTP, Trieste, Italy, 8.-26.5.2006 (lecture)

H. Amenitsch, Y. Diawara, R. Menk, S. Bernstorff, P. Laggner and M. Rappolt
Microsecond time resolution with the VANTEC-1 detector: first results
XIIIth International Conference on Small-Angle Scattering SAS06, Kyoto, Japan, 9-13 July 2006 (poster IM-P20b)

H. Amenitsch, B. Sartori, M. Rappolt, G. Pabst, D. Grosso, P. Laggner
Evaporation induced self-assembly of phospholipids forming lamellar and non-lamellar phases studied with GISAXD
XIIIth International Conference on Small-Angle Scattering SAS06, Kyoto, Japan, 9-13 July 2006 (poster GI-P017b)

H. Amenitsch, D. Cojoc, M. Rappolt, E. Ferrari, V. Gabrin, E. Di Fabrizio, P. Laggner, M. Burghammer and Ch. Riekel
Optical Tweezers for fixing micrometer sized samples in microSAXS Experiments
XIIIth International Conference on Small-Angle Scattering SAS06, Kyoto, Japan, 9-13 July 2006 (poster Nm-P07c)

H. Amenitsch, M. Kriechbaum, B. Sartori, M. Rappolt and P. Laggner
Non-lamellar phases of solid supported phospholipids studied by high pressure GISAXD
XIIIth International Conference on Small-Angle Scattering SAS06, Kyoto, Japan, 9-13 July 2006 (poster SI-P17b)

H. Amenitsch, M. Kriechbaum, B. Sartori, M. Rappolt and P. Laggner
Self assembly and high pressure behavior of non-lamellar phospholipid phases on solid supports studied with GISAXD
9th International Conference on Surface X-ray and Neutron Scattering 9SXNS, Taipei, Taiwan, 16-20 July 2006 (talk)

H. Amenitsch, D. Cojoc, M. Rappolt, B. Sartori, P. Laggner, E. Ferrari, V. Garbin, M. Burghammer, Ch. Riekel, and E. Di Fabrizio
Optical Tweezers for Sample Fixing in Micro-Diffraction Experiments
Ninth International Conference on Synchrotron Radiation Instrumentation, Daegu (Korea), 28 May-2 June 2006 (talk)

H. Amenitsch, P. Laggner, O. Konovalov, C. Riekel, J. Perez, J.G. Grossman, S. Hasnain, M. Petoukhov, M. Roessle, D. Svergun
SAXS at high brilliance European synchrotrons for bio- and nano-technology (project SAXIER)
Ninth International Conference on Synchrotron Radiation Instrumentation, Daegu (Korea), 28 May-2 June 2006

H. Amenitsch
Self assembly processes of nanoparticles studied by small angle scattering
First Workshop SILS on "Nanoparticle spectroscopy by synchrotron radiation", Palazzo Feltrinelli, lago di Garda, Gargnano (Brescia), Italy, 2-3 march 2006 (lecture)

H. Amenitsch
Status and future development of the Austrian SAXS beamline
International Symposium on "SAXS on Nanosystems – Science and Technology", Trieste, Italy, November 23-24, 2006 (talk)

H. Amenitsch, B. Sartori, G. Pabst, M. Rappolt, P. Laggner
Self-assembly of phospholipids on surfaces
International Symposium on "SAXS on Nanosystems – Science and Technology", Trieste, Italy, November 23-24, 2006 (poster)

H. Amenitsch, D. Cojoc, M. Rappolt, B.Sartori, E. Ferrari, V. Gabrin, E. DiFabrizio, P. Laggner, M. Burghammer, Ch. Riekel
Optical tweezers for fixing micrometer sized samples in μSAXS Experiments
International Symposium on "SAXS on Nanosystems – Science and Technology", Trieste, Italy, November 23-24, 2006 (poster)

H. Amenitsch, Y. Diawara, R. Menk, S. Bernstorff, P. Laggner, M. Rappolt
Microsecond Time Resolution with the VANTEC-1 Detector: First Results
International Symposium on "SAXS on Nanosystems – Science and Technology", Trieste, Italy, November 23-24, 2006 (poster)

H. Amenitsch, F. Schmid, G. Sommer, M. Rappolt, P. Regitnig, G. Holzapfel & P. Laggner
Time-resolved fibre diffraction on human arteries during tensile testing and nanostructure correlation to mechanical behavior
23rd European Crystallography Meeting, Leuven, Belgium, August 2006

M. Angeloni, L. Moretti, V. Mocella, L. De Stefano, L. Rotiroti, I. Rea and S. Bernstorff
In-situ investigation of capillary condensation phenomena in porous silicon nanostructures by means of GISAXS and SAXS measurements
E-MRS Spring Meeting 2006, Nice, France, May 29 - June 2, 2006, poster U/PI.20

D. C. Arnold, B. Daly, J. S. Kulkarni, R. L. Rice, M. T. Shaw, M. A. Morris and J. D. Holmes
Porous Materials as Templates for the Growth of Nanowire Arrays
Japan – UK Joint Symposium on Chemistry of Coordination Space, London, UK, 12 – 13 July 2006 (Poster)

Niki Baccile
Study of organic/inorganic interactions at nanostructured silica interface. A solid state NMR contribution
May 9th – May 11th 2006: GDR meeting on interfaces, La Grande Motte (France) (talk)

N. Baccile, F. Babonneau, C.V. Teixeira, H. Amenitsch and M. Lindén
Time-resolved in-situ SAXS of the formation of cubic surfactant-templated silica
XIIIth International Conference on Small-Angle Scattering SAS06, Kyoto, Japan, 9-13 July 2006 (poster CS-P068a)

J. Baldrian, M. Steinhart, H. Amenitsch and S. Bernstorff
Self-Assembled Nanostuctures in Block Copolymer Blends
International Symposium on "SAXS on Nanosystems – Science and Technology", Trieste, Italy, November 23-24, 2006 (poster)

S. Bernstorff, M. Buljan, P. Dubcek, U.V. Desnica, N. Radic, K. Salamon
Controlling of Ge nanocrystal properties in SiO_2 substrate by magnetron sputtering deposition conditions – a GISAXS study
XIIIth International Conference on Small-Angle Scattering SAS06, Kyoto, Japan, 9-13 July 2006 (poster GI-P019a)

S. Bernstorff, P. Dubcek, I. Kovacevic, N. Radic, B. Pivac
Si nanocrystals in SiO_2 films analyzed by small angle X-ray scattering
9th International Conference on Surface X-ray and Neutron Scattering 9SXNS, Taipei, Taiwan, 16-20 July 2006 (poster)

S. Bernstorff
Nanostructures Studied by SAXS with Synchrotron Light
50th IUVSTA workshop "Toward Novel Nano-structure Based Devices: Nanostructured Materials Fabrication, Characterization and Assembly for Novel Devices", Dubrovnik, Croatia, 22.-26.10.2006 (invited lecture)

S. Bernstorff. P. Dubcek, I. Kovacevic, N. Radic, B. Pivac
Si nanostructures in SiO_2 films studied by GISAXS
XIV Elettra Users' Meeting 2006, Trieste, Italy, 21.11.2006 (poster)

S. Bernstorff, M. Buljan, P. Dubcek, U. Desnica and N. Radic
Controlling of Ge nanocrystals properties in SiO_2 sustrate by magnetron sputtering deposition conditions - a GISAXS study
XIV Elettra Users' Meeting 2006, Trieste, Italy, 21.11.2006 (poster)

S. Bernstorff, P. Dubcek, I. Kovacevic, N. Radic, B. Pivac
Si nancrystals in SiO_2 films studied by GISAXS
International Symposium on "SAXS on Nanosystems – Science and Technology", Trieste, Italy, November 23-24, 2006 (poster)

Maja Buljan
Self-Organization of Ge nanoparticles in 3D superlattice within amorphous matrix
Annual Meeting of Croatian Vacuum Society, Zagreb, Croatia, February 23, 2006 (introductory talk)

M. Buljan, V. Desnica, G. Dražic, M. Ivanda, N. Radic, P. Dubcek, K. Salamon, S. Bernstorff
Formation of three-dimensional Ge quantum dot superlattices with post-deposition controllable properties in amorphous SiO_2 matrix
10th Brijuni Conference: Exploring the fundamental problems in science, Brijuni 2006: Imaging in Space and Time, Brijuni Island, Croatia, 27. 08 – 01- 09. 2006 (poster)

M. Buljan, U.V. Desnica, M. Ivanda, P. Dubcek, I. Bogdanovic-Radovic, Z. Siketic, K. Salamon, N. Radic, S. Bernstorff
Samoorganizacija Ge nanocestica u 3D superrešetke
13th Int. Meeting on "Vacuum Science and Technology", Koprivnica, Croatia, Jun 13, 2006 (poster)

John O'Callaghan
Characterization and use of Thin Films in Nano-Templating
Post-graduate research seminar, CRANN (Centre for Research on Adaptive Nanostructures and Nanodevices), Trinity College Dublin, Dublin, Ireland, 24.8.2006

Capan, Ivana; Dubcek, Pavo; Duguay, S.; Zorc, Hrvoje; Radic, Nikola; Pivac, Branko; Slaoui, A.; Bernstorff, S.
Silicon nanoparticles formation in annealed SiO/SiO_2 multilayers
13. Medunarodni sastanak Vakuumska znanost i tehnika, Zagreb, Croatia, 2006

G. Caracciolo, D. Pozzi, H. Amenitsch, Cristina Marchini, Augusto Amici, Maura Montani and R. Caminiti
Structural Stability of Transfection Efficient Lipid/DNA Complexes
XIV Congresso della Società Italiana di Luce di Sincrotrone (SILS), Napoli, 6-8.7.2006

G. Caracciolo
Structural Stability of Transfection Efficient Cationic Liposome/DNA Complexes
XIV Elettra Users' Meeting 2006, Trieste, Italy, 21.11.2006 (invited talk as winner of the "Luciano Fonda and Paolo Maria Fasella Award" which is assigned each year to a young scientist for outstanding experiments performed with Elettra synchrotron light)

G. Caracciolo, D. Pozzi, H. Amenitsch, Cristina Marchini, Maura Montani, Augusto Amici and R. Caminiti
Multi-component cationic liposome/DNA complexes: efficient vectors for gene delivery
10th Anniversary Symposium on "SAXS on Nanosystems – Science and Technology", Trieste, Italy, November 23-24, 2006 (poster)

G. Caracciolo, D. Pozzi, R. Caminiti, , Cristina Marchini,Augusto Amici, Maura Montani, H. Amenitsch
Lipoplessi a multi-componenti per la terapia genica
XXII Congresso Nazionale della SCI, Florence, Italy, 10-15 September 2006 (talk)

G. Caracciolo, D. Pozzi, H. Amenitsch, R. Caminiti
L'ultima frontiera della terapia genica: lipoplessi a multi-componenti
II Convegno Giovani Chimici, Dipartimento di Chimica, Università degli Studi di Roma "La Sapienza", June 2006 (poster)

A. Carbini, S. Mazzoni, F. Spinozzi and P. Mariani
SAXS analysis for evaluating candidate models in protein structure prediction
SIBPA Meeting, Palermo, Italy, 18 September 2006 (poster)

S. Chattopadhyay, D. Erdemir, L. Guo, J. Ilavsky, H. Amenitsch, C.U. Segre and A.S. Myerson
Nucleation of glycine polymorphs examined by SAXS
XIIIth International Conference on Small-Angle Scattering SAS06, Kyoto, Japan, 9-13 July 2006 (poster BS-P004a)

Mark P. Copley, John P. Hanrahan, John M. O' Callaghan, Nikolay Petkov, Trevor R. Spalding, Justin D. Holmes, Michael A. Morris, David Stetyler, Milos Steinhart and Heinz Amenitsch
Small Angle X-ray Scattering and Neutron Studies of Hexagonally Ordered Mesoporous Silica
The 4th International TRI/Princeton Workshop, Princeton, NJ, USA, 21 – 23 June 2006. (Poster)

Stefano Costacurta
Highly organized self-assembled mesostructured membranes
Italian Workshop on Sol-Gel 2006, Milan, Italy, 22-23 June 2006 (Oral contribution)

Z. Crnjak Orel, and A. Turkovic
Novel counter electrode based on mixed vanadium cerium oxides: preparation and characterization
World renewable energy congress IX, Florence, Italy, 19-25 August 2006 (invited talk)

Gianluca Croce, Marco Milanesio, DavideViterbo, Heinz Amenitsch
A mesoporous pattern created by nature in siliceous spicules from marine sponges
XIIIth International Conference on Small-Angle Scattering SAS06, Kyoto, Japan, 9-13 July 2006 (oral, talk FD-3)

Gianluca Croce, Davide Viterbo, Marco Milanesio, Barbara Onida, Enrica Verné
Structural characterization of bioactive glasses
XXIII European Crystallographic Meeting, Leuven, Belgium, 6-11 August 2006, (poster)

G. Croce, M. Milanesio, D.Viterbo and H. Amenitsch
A Mesoporous Pattern Created by Nature in Siliceous Spicules from Marine Sponges
International Symposium on "SAXS on Nanosystems – Science and Technology", Trieste, Italy, November 23-24, 2006 (poster)

I.D. Desnica-Frankovic, P. Dubcek, M. Buljan, U.V. Desnica, S Bernstorff
Vacancy-clusters imaging
10th Brijuni Conference: Exploring the fundamental problems in science, Brijuni 2006: Imaging in Space and Time, Brijuni Island, Croatia, 27. 08 – 01- 09. 2006 (poster)

I. D. Desnica-Frankovic, P. Dubcek, M. Buljan, U. V. Desnica, S. Bernstorff, Mark C. Ridgway, Cris J. Glower
Ion-irradiation-induced amorphization and porosity of Germanium: GISAXS studies of structural modifications and relaxation:
15th Int. Conf. on "Ion Beam Modification of Materials", Taormina, Italy, 18-22.09.2006 (poster P - 293)

U.V. Desnica, M. Buljan, P. Dubcek, I.D. Desnica Frankovic, N. Radic, Z. Siketic, I. Bogdanovic-Radovic, M. Ivanda, K. Salamon , S. Bernstorff
Ge nanocrystals formed SiO_2 in (Ge+SiO_2)/SiO_2 multilayers deposited by magnetron sputtering and post-position thermal treatment
13th Int. Meeting on Vacuum Science and Technology, Koprivnica, Croatia, Jun 13, 2006 (poster)

U.V. Desnica, M. Buljan, P. Dubcek, G. Dražic, I.D. Desnica Frankovic, N. Radic, M. Ivanda, Z. Siketic, I. Bogdanovic-Radovic, K. Salamon, S. Bernstorff
Imaging of Quantum Dots in 2D and 3D Space
10th Brijuni Conference: Exploring the fundamental problems in science, Brijuni 2006: Imaging in Space and Time, Brijuni Island, Croatia, 27. 08 – 01- 09. 2006 (poster)

U. Desnica, I. D. Desnica Frankovic, P. Dubcek, K. Furic, S. Bernstorff
Ion beam synthesis of CdSe QDs studied by GISAXS and Raman spectroscopy
15th Int. Conf. on "Ion Beam Modification of Materials", Taormina, Italy, 18-22. 09. 2006 (oral)

G. Deutsch, D. Zweytick, S.E. Blondelle, D. Monreal, J. Leiva, K. Lohner
Modulation of membrane perturbation by N-acylated peptides derived from a human lactoferrin fragment
International Symposium on "SAXS on Nanosystems – Science and Technology", Trieste, Italy, November 23-24, 2006 (poster)

I. Djerdj, A. Tonejc, M. Bijelic, V. Vraneša, A. Turkovic
Transmission Electron Microscopy Studies of Nanostructured TiO2 Films on Various Substrates
2nd Croatian Congress on Microscopy with International Participation, Topusko May 18-21, 2006 (Invited lecture)

P. Dubcek, B. Pivac, I. Kovacevic, S. Bernstorff, R. Mu, M. Wu, A. Ueda and B. Vlahovic
GISAXS study of gold implanted glass
International Symposium on "SAXS on Nanosystems – Science and Technology", Trieste, Italy, November 23-24, 2006 (poster)

P. Dubcek, N. Radic, S. Bernstorff, I. Djerdj
Struktura neuredene faze u nanokristalnom niklu
13. Medunarodni sastanak Vakuumska znanost i tehnika, Koprivnica, Croatia, 13 June 2006

C. Fritscher
Entwicklung der Mesostruktur bei Pluronic P123-Gelen; Mechanische Eigenschaften der getrockneten Gele
Seminar, Institute of Materials Chemistry, Vienna University of Technology, Austria, 18th May 2006 (oral)

C. Fritscher, H. C. Lichtenegger, J. Stampfl, N. Huesing, R. Liska, R. Inführ, T. Koch, S. Seidler
3-Dimensional Mesoporous Silica Monoliths and their Structural and Mechanical Properties
Polymerwerkstoffe 2006, Halle/Saale, Germany, 27-29 September 2006 (oral)

C. Fritscher, H. C. Lichtenegger, J. Stampfl, N. Huesing, R. Liska, R. Inführ, T. Koch, S. Seidler
Hierarchisch strukturiertes Siliziumdioxid und seine mechanischen Eigenschaften
2. Wiener Biomaterialsymposium, Vienna, Austria, 22-24 November 2006 (oral)

Bernhard Gehl, Jan-Ingo Flege, Vesna Aleksandrovic, Thomas Schmidt, Sigrid Bernstorff, Jens Falta, Horst Weller, Marcus Bäumer
Plasma modified bimetallic nanocolloid arrays – a model system for structural and order effects in particle catalysis
Spring meeting of the Deutsche Physikalische Gesellschaft (DPG), Abteilung Festkörperphysik, Regensburg, Germany, 26-30.03.2007 (talk O57.11)

D.Gracin, S. Bernstorff, P.Dubcek, A.Gajovic, K.Juraic
Study of mixtures of amorphous-nanocrystalline thin silicon films by GISAXS
XIIIth International Conference on Small-Angle Scattering SAS06, Kyoto, Japan, 9-13 July 2006 (poster GI-P018c)

D. Gracin, S. Bernstorff, P. Dubcek, A. Gajovic, K. Juraic
The influence of substrate morphology on the growth of thin silicon films: a GISAXS study
9th International Conference on Surface X-ray and Neutron Scattering 9SXNS, Taipei, Taiwan, 16-20 July 2006 (poster)

D. Gracin, K.Juraic, A. Gajovic, P. Dubcek, C. Devilee, H.J. Muffler, W.J. Soppe, S. Bernstorff
The structural ordering of thin silicon films at the amorphous to nano-crystalline phase transition by GISAXS and Raman spectroscopy
E-MRS Spring Meeting 2006, Nice, France, May 29 - June 2, 2006 (talk)

D.Gracin, B.Etlinger, K.Juraic, A.Gajovic, P.Dubcek, S.Bernstorff
The DC conductivity and structural ordering of thin silicon films at the amorphous to nano-crystalline phase transition
11th Joint Vacuum Conference, Prague, Czech Republic, Sept 24-28, 2006

D.Gracin, K.Juraic, A.Gajovic, P.Dubcek, I.Djerdj, N.Tomasic, S.Bernstorff
The influence of post deposition plasma treatment on SnO_x structural properties
11th Joint Vacuum Conference, Prague, Czech Republic, Sept 24-28, 2006

D. Grosso, C. Boissiere, L. Nicole, P.A. Albouy, H. Amenitsch and C. Sanchez
In situ time-resolved SAXS investigations of mesoporous thin film formation and treatment
XIIIth International Conference on Small-Angle Scattering SAS06, Kyoto, Japan, 9-13 July 2006 (talk IM3-4)

D. Grozdanic, B. Rakvin, B. Pivac, P. Dubcek, N. Radic, S. Bernstorff
Structural characterization of thin amorphous Si films
9th International Conference on Surface X-ray and Neutron Scattering 9SXNS, Taipei, Taiwan, 16-20 July 2006 (poster)

A. Hodzic, M. Rappolt, H. Amenitsch, P. Laggner and G. Pabst
Effects of plant sterols on structure and fluctuations of lipid membranes
International Symposium on "SAXS on Nanosystems – Science and Technology", Trieste, Italy, November 23-24, 2006 (poster)

S. Ibrahimkutty, M. Rappolt, P. Laggner, H. Amenitsch
Small angle study of aerosol particles in gas phase
International Symposium on "SAXS on Nanosystems – Science and Technology", Trieste, Italy, November 23-24, 2006 (poster)

Plinio Innocenzi
Highly Ordered Self-Assembled Mesostructured Hafnia Thin Films
Italian Workshop on Sol-Gel 2006, Milan, Italy, 22-23 June 2006 (Oral contribution)

P. Innocenzi, L. Malfatt, T. Kidchob, P. Falcaro, S. Costacurta, M. Piccininic, A. Marcelli, P. Morini, D. Sali, H. Amenitsch
Time resolved simultaneous detection of structural and chemical changes during self-assembly of mesostructured films by in-situ SAXS and FTIR
International Symposium on "SAXS on Nanosystems – Science and Technology", Trieste, Italy, November 23-24, 2006 (poster)

M. Kerber, E. Schafler, P. Hanak, G. Ribàrik, S. Bernstorff, T. Ungàr, M. Zehetbauer
Spatial fluctuations of the microstructure during deformation in Cu single crystals
10th Aniversary Symposium "SAXS on Nanosystem – Science and Technology", Trieste, Italy, November 2006 (poster)

E. Korznikova, E. Schafler, G. Steiner, M. Zehetbauer
Measurements of Vacancy type Defects in SPD deformed Nickel
Lecture at the 2006 TMS Annual Meeting, 4th Int. Symp. on ultrafine grained materials, San Antonio, USA, March 2006

I. Kovacevic, P. Dubcek, S. Duguay, N. Radic, B. Pivac, A. Slaoui, S. Bernstorff
Si nanostructures formation in SiO/SiO_2 multilayers
E-MRS Spring Meeting 2006, Nice, France, May 29 - June 2, 2006, poster C P1 16

M. Kriechbaum, B. Sartori, M. Steinhart, H. Amenitsch, M. Rappolt, S. Bernstorff, P. Laggner
Barotropic phase transitions of binary mixtures of POPC and sterols (cholesterol and plant sterols) studied by SAXS
XIIIth International Conference on Small-Angle Scattering SAS06, Kyoto, Japan, 9-13 July 2006 (poster CS-P035b)

M. Kriechbaum, B. Sartori, M. Steinhart, H. Amenitsch, M. Rappolt, S. Bernstorff and P. Laggner
Pressure - Scanning SAXS of Lipid/Sterol Mixtures
International Symposium on "SAXS on Nanosystems – Science and Technology", Trieste, Italy, November 23-24, 2006 (poster)

P. Laggner
Bridging the Nano gap: From symchrotron to bench-top SAXS
Center for Bits & Atoms, Massachusetts Institute of Technology, Cambridge, MA, USA, 11.5.2006

P. Laggner
From structural proteomics to integrated nanosystems. Recent advances by X-ray and neutron scattering
Paul Scherrer Institute, Villingen, Swiss, 21.4.06

P. Laggner
Nano-Systemforschung mit Roentgenstrahlen
Physikalisches Institut, TU Graz, Austria, 2.5.06

P. Laggner
Simultaneous SAXS and WAXS to study changes in the molecular mobility in amorphous systems
Dept. Pharmaceutics, University of Minnesota, Minneapolis, MN, US 9.10.06

P. Laggner
X-ray instrumentation for nanoanalytics – from benchtop to synchrotron source
Austrian Russian Science Day, Russisches Kulturinstitut, Wien, Austria, 16.10.06

P. Laggner
The elusive joy of SAXS: X-ray structure without crystals
Max F. Perutz Laboratories, Department for Biomolecular Structural Chemistry, University Departments at the Vienna Biocenter, 9.11.06

P. Laggner
From structural proteomics to integrated nanosystems
National Institute for Research and Development in Microtechnologies, IMT-Bukarest, Romania, 6.12.06

P. Laggner, M. Kriechbaum, L. Volpe, M. Rappolt and H. Amenitsch
How crystals are born: novel insight from Small- and Wide-Angel X-Ray Scattering
XIIIth International Conference on Small-Angle Scattering SAS06, Kyoto, Japan, 9-13 July 2006 (poster IA-P01c)

C. Lopez, C. Bourgaux, P. Lesieur, A. Riaublanc, M. Ollivon
Cristallization and polymorphism in fat globules elucidated at a molecular level using coupled time-resolved synchrotron X-ray diffraction and DSC
Symposium on Dairy Science and Technology, Shanghai, October 2006 (invited lecture)

M. Lucic Lavcevic, P. Dubcek, A. Turkovic, S. Bernstorff, Z. Crnjak Orel
Nanostructural characteristics of Vanadium/Cerium Oxide film as a host for Lithium ions
E-MRS Spring Meeting 2006, Nice, France, May 29 - June 2, 2006, (poster)

M. Lucic Lavcevic, A. Turkovic, P. Dubcek, S. Bernstorff
Nanostructured CeO_2 thin films: a GISAXS study of the interface between grains and pores
9th International Conference on Surface X-ray and Neutron Scattering 9SXNS, Taipei, Taiwan, 16-20 July 2006 (poster)

M. Lucic-Lavcevic, A.Turkovic, P. Dubcek, S. Bernstorff, Z. Crnjak Orel
GISAXS on Nanostructured Vanadium Cerium Oxide Films Intercalated by Lithium
Joint vacuum conference JVC 11, Prague, Czech Republic, 24-28 September 2006 (poster)

Paolo Mariani
High-pressure synchrotron X-ray scattering experiments on lyotropic phases: a different way to learn about structural mechanical properties of biological systems
SILS XIV Congress, Facoltà di Ingegneria – Università di Napoli "Federico II", Napoli, Italy, 6-8 July 2006 (talk)

Paolo Mariani
Structural studies on lyotropic polymorphism, stability and energetics of guanosine four stranded helices
ESF Exploratory workshop "Self-assembly of guanosine derivatives: from quadruplex DNA to biomolecular devices", Bled, Slovenia, 12 - 15 September 2006 (talk)

B. Marmiroli, H. Amenitsch, G. Grenci, L. Businaro, D. Cojoc, B. Sartori, A. Gosparini
Microfluidics for SAXS Experiments
International Symposium on "SAXS on Nanosystems – Science and Technology", Trieste, Italy, November 23-24, 2006 (poster)

B.M. Misof, P. Roschger, H. Amenitsch, S. Bernstorff, K. Klaushofer, and P. Fratzl
The maturation of the mineral particles in bone tissue from healthy individuals and cases of coeliac sprue and Paget's disease
33rd European Symposium on Calcified Tissues, Prague, Czech Republic 10-14 May, 2006

L. Moretti, V. Mocella, M. Angeloni, L. De Stefano, L. Rotiroti, I. Rea, P. Dardano, C. Ferrero, S. Bernstorff
Investigation of the structural features of porous silicon multilayers by means of GISAXS measurements
SILS XIV Congress, Facoltà di Ingegneria – Università di Napoli "Federico II", Napoli, Italy, 6-8 July 2006 (talk)

M. Ollivon
New tools for monitoring the structural evolution of oral lipid-based drug delivery systems at the molecular and supramolecular levels
3rd International conference of the European Drug Absorption Network (EDAN), Leuwen, Belgium, March 19-21, 2006 (invited lecture)

M. Ollivon, C. Bourgaux, W. Amara, H. Gliguem and G. Keller
Analysis of lipid containing foods by coupled time-resolved X-ray diffraction and DSC
'Food Structure and Functionality Forum' of the 97th meeting and exhibition of the American Oil Chemists' Society (AOCS) in the session 'New Techniques/Methods for Food Structure & Functionality'. April 30- May 3, 2006, St Louis, MO, USA (invited opening lecture)

M. Ollivon
"Hand bags, Skirts, Pores, Channels, Globules, Crystals, Cigars, Peanuts : How to characterize the numerous structures made by lipids?"
Invitation by John Hancock, Chairman of the Oils and Fats Group of Society of Chemical Industry. Hilditch Memorial Lecture Award, plenary lecture presented at the Euro Fed Lipid Congress "Oils, Fats and Lipids for a Healthier Future" Madrid, Spain, 1-4 October 2006

Maria Grazia Ortore
Interaction and dissociation in ß -lactoglobulin in solution
Italian Physics Society Meeting, Torino, Italy, 22 September 2006 (talk)

M. G. Ortore, R. Sinibaldi, F. Spinozzi, F. Carsughi and P. Mariani
Understanding interaction properties of ß-lactoglobulin in solution
SISN Meeting, Sirolo, Italy, 30 June 2006 (grant as best poster)

M. G. Ortore, R. Sinibaldi, F. Spinozzi and P. Mariani
Interaction and dissociation in ß-lactoglobulin in solution
SIBPA Meeting, Palermo, Italy, 18 September 2006 (poster)

M. G. Ortore, F. Spinozzi, F. Carsughi, M. Bonetti, G. Onori and P. Mariani
High pressure Small-Angle Neutron scattering study of the aggregation state of ß-lactoglobulin in water and in water / ethylene-glycol solutions
SAS 2006, Kyoto, Japan, 12 June 2006 (poster)

G. Pabst
Biological model membranes – From cells to vesicles and solid supported bilayers
Institut fuer Experimentalphysik, TU Graz, Graz, Austia, 1.6.06

G. Pabst, H. Amenitsch, M. Rappolt, P. Laggner, J. Katsaras, K. Lohner, A. Hickel
Effect of chain length on the lateral organization of charged lipid membranes
EMRS conference, Strassbourg, France

Georg Pabst
GAP - A Tool for the Global Analysis of Diffraction Data from Lamellar Phases
International Symposium on "SAXS on Nanosystems – Science and Technology", Trieste, Italy, November 23-24, 2006 (poster)

O. Paris
Scanning SAXS/WAXS of hierarchical nanocomposites: A story that began at the ELETTRA SAXS beamline
International Symposium on "SAXS on Nanosystems – Science and Technology", Trieste, Italy, November 23-24, 2006 (talk)

M. Pavlovic, A. Turkovic, P. Dubcek, M. Lucic-Lavcevic, B. Etlinger, S. Bernstorff
Istraživanja $(PEO)_8ZnCl_2$ Polimernih Elektrolita Pomocu SAXS I DSC Mjerenja
13. Medunarodni sastanak Vakuumska znanost i tehnika, held in Koprivnica, Hrvatska, Croatia, 13 June 2006 (poster)

B. Pivac, I. Kovacevic, P. Dubcek, N. Radic, S. Bernstorff
GISAXS study of Si nanoclusters formation in SiO/SiO2 layers
XIII International Conference on Small-Angle Scattering (SAS-06), Kyoto, Japan, July 9-13, 2006

B. Pivac, I. Kovacevic, P. Dubcek, N. Radic, S. Bernstorff, A. Slaoui
Self-organized growth of Ge islands on Si(100) substrates
International Symposium on "SAXS on Nanosystems – Science and Technology", Trieste, Italy, November 23-24, 2006 (poster)

B. Pivac, I. Kovacevic, P. Dubcek, N. Radic, S. Bernstorff
GISAXS Study of Si Nanoclusters in SiO/SiO2 Layers
JVC11 Joint Vacuum Conference, Prag, Czech Republic, 2006

S. Puchegger, H. Rennhofer, D. Loidl, P. Zioupos, S. Bernstorff and H. Peterlik
Relaxation of human bone at the nanoscale
International Symposium on "SAXS on Nanosystems – Science and Technology", Trieste, Italy, November 23-24, 2006 (poster)

N. Radic, P. Dubcek, S. Bernstorff, I. Djerdj and A. M. Tonejc
Structural study of nanocrystalline nickel thin films
XIIIth International Conference on Small-Angle Scattering SAS06, Kyoto, Japan, 9-13 July 2006 (poster GI-P020b)

N. Radic, P. Dubcek, S. Bernstorff, I. Djerdj, U. Kreissig, M. Metikoš-Hukovic, Z. Grubac
Structure and Catalytic Activity of Nanocrystalline Nickel Thin Films
E-MRS 2006 Fall Meeting, Warsaw, Poland, 3-9 September 2006

N. Radic, P. Dubcek, S. Bernstorff, I. Djerdj, A. M. Tonejc
Structural Study of Nanocrystalline Nickel Thin Films
XIV Elettra Users' Meeting 2006, Trieste, Italy, 21.11.2006 (poster)

M. Rappolt
Bicontinuous Cubic Phases: Basic Tools
IBN, Graz, Austria, 17.05.2006

M. Rappolt
Elevator pitch: The biologically relevant lipid mesophases as "seen" by X-rays.
IBN-Brainstorming Workshop 2006, Schloss-Seggau, Austria, 19.-20.04.06

M. Rappolt
The biologically relevant lipid mesophases as "seen" by X-rays
International Symposium on "SAXS on Nanosystems – Science and Technology", Trieste, Italy, November 23-24, 2006 (poster)

H. Reynaers, K. Bongaerts, F. Cuppo, S. Bernstorff, S. Paoletti
On the confirmation of κ-carrageenan in aqueous solution: a SR-SAXS and WALLS study
XIIIth International Conference on Small-Angle Scattering SAS06, Kyoto, Japan, 9-13 July 2006 (poster PO-P107b, letzte Seite late contribution)

H. Reynaers, F. Cuppo, K. Bongaerts, G. Evmenenko H. Amenitsch, S. Bernstorff, A. Gamini, S. Paoletti
On the conformation of κ-carrageenan in aqueous solution: A WALLS and SR-SAXS study
International Symposium on "SAXS on Nanosystems – Science and Technology", Trieste, Italy, November 23-24, 2006 (poster)

E. Schafler, G. Steiner, E. Korznikova, H. Schindler, M. Kerber, M. J. Zehetbauer
Lattice defect analysis in severely plastically deformed Ni
Frühjahrstagung der Deutschen Physikalischen Gesellschaft/Festkörperphysik, Dresden, Deutschland, März 2006 (lecture)

E. Schafler, M. Zehetbauer
Lattice Defects in SPD Nanometals: Analysis and Importance for Mechanical Properties
Int. Conf. On Processing & Manufacturing of Advanced Materials – THERMEC 2006, Vancouver, Canada, July 2006 (lecture)

E. Schafler, M. Zehetbauer, T. Ungar
Characterisation of deformation induced lattice defects by X-ray diffraction with high lateral/time resolution
International Symposium (10th Anniversary Symposium) on "SAXS on Nanosystems – Science and Technology", Trieste, Italy, November 23-24, 2006 (poster)

F. Schmid, G. Sommer, M. Rappolt, C.A. Schulze-Bauer, P. Regitnig, G.A. Holzapfel, P. Laggner and H. Amenitsch
Layer Specific Collagen Orientation in Human Arteries During Tensile Testing and Correlation to Mechanical Behaviour
13th International Conference on Small-Angle Scattering SAS2006, Kyoto, Japan, 9.-13.7.2006 (lecture)

F. Schmid, G. Sommer, M. Rappolt, C.A.J. Schulze-Bauer, P. Regitnig, G. Holzapfel, P. Laggner, H. Amenitsch
Layer Specific Collagen Orientation in Human Arteries During Tensile Testing and Correlation to Mechanical Behavior
International Symposium on "SAXS on Nanosystems – Science and Technology", Trieste, Italy, November 23-24, 2006 (poster)

F. Schmid, G. Sommer, M. Rappolt, P. Regitnig, C.A. Schulze-Bauer, G.A. Holzapfel, H. Amenitsch, P. Laggner
Zeitaufgeloeste Aenderung der Kollagenfaserrichtung in menschlichen Arterien im Zugtest und Korrelation des mechanischen Verhaltens
2. Wiener Biomaterialsymposium, Vienna, Austria, 22.-24.11.2006 (lecture)

Thomas Schmidt
Semiconductor nanostructures: From self-assembly to self-ordering
Spring meeting of the Deutsche Physikalische Gesellschaft (DPG), Abteilung Festkörperphysik, Regensburg, Germany, 26-30.03.2007 (invited talk O48.1)

E. Sevcsik, G. Pabst, A. Jilek, and K. Lohner
Lipid discrimination of LL-37, a human multifunctional peptide
International Symposium on "SAXS on Nanosystems – Science and Technology", Trieste, Italy, November 23-24, 2006 (poster)

C. Sinturel, M. Vayer, H. Amenitsch, R. Erre
Self organization of block-copolymer in reactive blends studied by real-time SAXS, WAXS, DSC
"Journées Soleil Région Centre 5" Orléans, France, 13-14.3.2006 (poster)

C. Sinturel, M. Vayer, H. Amenitsch, R. Erre
Self-organisation of block copolymer: nanostructured polymer and organised mesoporous polymer.
CRMD, Orléans, France, 14 april 2006 (seminar)

C. Sinturel, M. Vayer, H. Amenitsch, R. Erre
Polymères nanostructurés obtenus par exfoliation de copolymères à blocs lamellaires dans des résines thermodurcissables.
"Matériaux 2002" Dijon, 13-17 november 2006 (talk)

M. Šlouf, H. Synková, J. Baldrian, A. Marek, J. Kovárová, P. Schmidt, H. Dorschner, M. Stephan, U. Gohs
Nanostructure Changes of UHMWPE after e-Beam Irradiation and Thermal Treatment
International Symposium on "SAXS on Nanosystems – Science and Technology", Trieste, Italy, November 23-24, 2006 (poster)

Francesco Spinozzi, Maria Grazia Ortore, Raffaele Sinibaldi, Sigrid Bernstorff, Paolo Mariani, Franco Rustichelli
Gracing-incidence small-angle X-Ray scattering applied to the characterization of plasma deposited proteins
XVIII Congresso Nazionale della Società Italiana di Biofisica Pura e Applicata (SIBPA), Palermo, Italy, 17-21 September 2006 (talk)

F. Spinozzi, R. Sinibaldi, F. Carsughi, M.G. Ortore, G. Onori, S. Cinelli and P. Mariani
The hydration shell of lysozyme in water/glycerol mixtures
SAS 2006, Kyoto, Japan, 12 June 2006 (poster)

M. Steinhart
10 years of high-pressure measurements at ELETTRA
International Symposium on “SAXS on Nanosystems – Science and Technology”, Trieste, Italy, November 23-24, 2006 (talk)

C.V. Teixeira, M. Lindén, H. Amenitsch, V. Alfredsson and P. Linton
The role played by salts of the Hofmeister series in the formation of SBA-15
XIIIth International Conference on Small-Angle Scattering SAS06, Kyoto, Japan, 9-13 July 2006 (talk P01-4)

A. Turkovic, P. Dubcek, N. Fox, M. Lucic-Lavcevic, M. Pavlovic and S. Bernstorff
SAXS/DSC Study of Polymer Electrolyte for Zn Rechargeable Nanostructured Galvanic Cells
Monday, May 8, 2006 at 11:00 in the Symposium "Nanotechnology"
209th Meeting of The Electrochemical Society, Colorado, USA, May 7 - 12, 2006 (talk)

A. Turkovic, P. Dubcek, M. Pavlovic, M. Lucic-Lavcevic and S. Bernstorff
Study of (PEO)8ZnCl2 polymer electrolytes via SAXS and DSC techniques
Anniversary Symposium, 10 Years Austrian SAXS Station at ELETTRA on "SAXS on Nanosystems- Science and Technology", Trieste, Italy, November 23-24, 2006 (poster)

A. Turkovic, P. Dubcek, M. Pavlovic, M. Lucic-Lavcevic, Z. Crnjak Orel and S. Bernstorff
Study of temperature evolution in nanostructured CeVO4 films via GISAXS techniques
Anniversary Symposium, 10 Years Austrian SAXS Station at ELETTRA on "SAXS on Nanosystems- Science and Technology", Trieste, Italy, November 23-24, 2006 (poster)

A. Turkovic, M. Lucic lavcevic, P.Dubcek and S. Bernstorff
SAXS Study of the Interface Between Grains and Pores in CeO_2 Thin Films
Joint vacuum conference JVC 11, Prague, Czech Republic, 24-28 September 2006 (poster)

R. Vishwanatha, Heinz Amenitsch, D.D. Sarma
Study of Growth Mechanism in Cadmium Sulfide Nanocrystals
International Symposium on “SAXS on Nanosystems – Science and Technology”, Trieste, Italy, November 23-24, 2006 (poster)

A. Yaghmur
Reversible phase transitions of nanostructured lipid systems in confined geometry
IBN, Graz, Austria, 15.02.2006

A. Yaghmur, M. Rappolt, P. Laggner and S. Zhang
Effect of charged surfactant-like peptides on the monoolein-based cubic phase Pn3m
Workshop der Oesterr. Netzwerke fuer Nanowissenschaften und Nanotechnologie, Krems, Austria, 21.-22.11.2006 (poster)

A. Yaghmur, M. Rappolt, P. Laggner and S. Zhang
Effect of charged surfactant-like peptides on the monoolein-based cubic phase Pn3m
SAXS on Nanosystems – Science and Technology, Trieste, Italy, 23.-24.11.2006 (poster)

M. Zehetbauer, E. Schafler, T. Ungár
Non-microscopic methods for characterisation of microstructures and properties of UFG metals
Int. Conf. On Ultrafine Grained Materials-From Basics to Application – UFG 2006, Kloster Irrsee, Germany, September 2006 (lecture)

D. Zweytick, G. Deutsch, D. Monreal, and K. Lohner
Biophysical Studies on the Effect of Derivatives of Human Lactoferricin on Model Membrane Systems
International Symposium on "SAXS on Nanosystems – Science and Technology", Trieste, Italy, November 23-24, 2006 (poster)

ELETTRA Highlights 2005-2006

W. H. Binder, C. Kluger, M. Kunz, L. Petraru and S. Bernstorff
Polymeric materials built via supra-molecular assembly: studies by in-situ SAXS, revealing modulative behavior
Elettra Research Highlight, pp. 24-26 (2006)

G. Caracciolo, D. Pozzi, R. Caminiti and H. Amenitsch
Multi-Component cationic liposome/DNA complexes for gene delivery
Elettra Research Highlight, pp. 27-30 (2006)

Anniversary Symposium: 10 Years of SAXS-Station at ELETTRA

A symposium on „SAXS on Nanosystems – Science and Technology" was held at the Abdus Salam International Centre for Theoretical Physics (Trieste, Italy) during 23.-24.11.2006 in order to celebrate the first 10 Years of the SAXS-Station at ELETTRA. Organized by P. Laggner, H. Amenitsch, S. Bernstorff, B. Sartori.

SAXS training courses

In March 2006, H. Amenitsch, S. Bernstorff, M. Rappolt and Barbara Sartori participated at the international school "HERCULES", organized by the university "Joseph Fourier" (Grenoble, France) and the National Polytechniche Institute of Grenoble with the help of ERSF, ILL, ELETTRA, LLB, CEA and CNRS. They gave 7 tutorials and 4 hours, including hands-on experience for the students during the measurements performed in the SAXS-lab and at the Austrian SAXS-beamline, and during the corresponding data treatment.

On May 15, 2006, the SAXS group participated at the "International ICTP School for Synchrotron Radiation", organized by the International Center for Theoretical Physics in Trieste, Italy. They gave 1 lecture (H. Amenitsch, "SAXS in solution and under extreme conditions") and 1 half-day tutorial (S. Bernstorff, M. Rappolt and S. Ibrahimkutty, "Small Angle X-ray Scattering Analysis")

Luciano Fonda and Paolo Maria Fasella Award

During the XIV ELETTRA Users' Meeting (Trieste, November 20-22, 2006) our user dr. Giulio Caracciolo (from the Department of Chemica, University "La Sapienza", Rome, Italy) received the ELETTRA Award in Memory of Luciano Fonda and Paolo Maria Fasella, which is assigned each year to a young scientist for outstanding experiments performed with Elettra synchrotron light. Dr. Giulio Caracciolo won this price for his studies concerning the "Structural Stability of Transfection Efficient Cationic Liposome/DNA Complexes". The experiments were performed at the small-angle x-ray scattering (SAXS) beamline in close cooperation with the local research staff.

Habilitation Thesis 2006

G. Pabst
Global properties of biological model membranes
Thesis 2006, Technical University Graz

PhD Thesis 2006

Niki Baccile
Contribution to the study of surfactant/silica interactions in mesostructured silica powders
Chimie de la Matière Condensée, Université Pierre et Marie Curie, Paris, France, September 18th, 2006

Mark Patrick Copley
Syntheses, Modification and Applications of Hexagonally Ordered Mesoporous Silica
University College Cork, Ireland, 2006

G. Deutsch
Modulation of membrane perturbation by N-acylated peptides derived from a human lactoferrin fragment
Technical University Graz, Austria, 2006

C. Kluger
Supramolecular Materials and Surfaces from Functionalized Poly(oxynorbornenes)
TU Wien, Austria, 2006

Maria Grazia Ortore
Studio SAS dell'equilibrio monomero-dimero della B-lattoglobulina in soluzione
Dottorato in Fisica, Ciclo XVIII, Università degli Studi di Perugia, Italy, 24/01/2006

Lydia Paccamiccio
Proprietà strutturali di sistemi lipidici di interesse biologico: analisi mediante la tecnica di diffrazione dei raggi X
Thesis in Biomolecular Science, Ancona, Italy 2006

E. Sevcsik
Hemolytic and antimicrobial activity of LL-37 is based on diverse modes of membrane pertubation
Technical University Graz, Austria, 2006

Raffaele Sinibaldi
Studio dell'idratazione proteica in miscele acquose: esperimenti SAS
Thesis in Biomolecular Science, Ancona, Italy, 2006

Authors Index